

EARTHQUAKE RESPONSE OF FIXED OFFSHORE STRUCTURES

Owen Major Kirkley

Library
Naval Postgraduate School
Monterey, California 93940

EARTHQUAKE RESPONSE OF FIXED OFFSHORE STRUCTURES

BY

OWEN MAJOR KIRKLEY

B.S., United States Naval Academy, 1958
B.C.E., Rensselaer Polytechnic Institute, 1960
M.S., University of Illinois, 1968

THESIS

Submitted in partial fulfillment of the requirements
for the degree of Doctor of Philosophy in Civil Engineering
in the Graduate College of the
University of Illinois at Urbana-Champaign, 1973

Urbana, Illinois

T152 651

EARTHQUAKE RESPONSE OF FIXED OFFSHORE STRUCTURES

BY

OWEN MAJOR KIRKLEY

B.S., United States Naval Academy, 1958

B.C.E., Rensselaer Polytechnic Institute, 1960

M.S., University of Illinois, 1968

THESIS

Submitted in partial fulfillment of the requirements
for the degree of Doctor of Philosophy in Civil Engineering
in the Graduate College of the
University of Illinois at Urbana-Champaign, 1973

Urbana, Illinois

Thesis
K 516

ACKNOWLEDGMENT

The author wishes to thank his advisor, Professor J. P. Murtha, for his invaluable suggestions, encouragement, and advice throughout the course of this research. Acknowledgment is extended to the Department of the Navy for the opportunity to conduct the research, and to the Computing Services Office for the use of computer facilities. The author wishes to express his most sincere thanks and appreciation to his wife, Jean, for her patience, encouragement, and understanding, without which this work would not have been done.

TABLE OF CONTENTS

Chapter		Page
1	INTRODUCTION	1
	1.1 General	1
	1.2 Description of the Problem.	2
	1.3 Summary of Previous Research	8
	1.4 Objective and Scope	11
	1.5 Related Topics.	12
	1.6 Notation.	16
2	SINGLE DEGREE OF FREEDOM OSCILLATOR	20
	2.1 General	20
	2.2 Elastic Deformation Response Spectra	21
	2.3 Linearization of the Drag Force	27
	2.4 Linear Hydraulic Damping	34
	2.5 Idealized Elastic Deformation Response Spectrum.	37
	2.6 Hydrodynamic Parameters.	40
	2.7 Idealized Elastic Hydrodynamic Parameter Response Spectra.	43
	2.8 Inelastic Response Spectra.	46
3	MULTI-DEGREE OF FREEDOM SYSTEMS.	51
	3.1 General	51
	3.2 Approximate Solution of the Nonlinear Equations of Motion.	51
	3.3 Idealized Elastic Deformation Response Spectra	70
	3.4 Hydrodynamic Parameters.	72
	3.5 Idealized Elastic Hydrodynamic Parameter Response Spectra.	79
4	APPLICATIONS	80
	4.1 General	80
	4.2 Displacement Response	81
	4.3 Hydrodynamic Parameters.	83
5	CONCLUSIONS AND RECOMMENDATIONS FOR FURTHER STUDY.	85
	5.1 Conclusions.	85
	5.2 Recommendations for Further Study	88



Page

LIST OF REFERENCES	91
VITA.	215



LIST OF TABLES

Table		Page
1.1	Characteristics of Earthquakes Used	93
2.1	Characteristics of Series Representation of Base Acceleration	95
2.2	Comparison of Estimated $ Z _{\max}$ With $ Z _{\max}$ Computed at High Frequencies by Numerical Integration	96
2.3	Distribution of Total Damping Between Structural and Hydraulic for Comparison Purposes	97
2.4	Elastic Deformation Spectrum Amplification Factors	97
2.5	Elastic Hydrodynamic Parameter Spectrum Amplification Factors.	98
2.6	Actual and Approximate Reduction Factors for the High Frequency Region of Inelastic Response Spectra. El Centro Earthquake $\beta_s = 0.02$, $\frac{K \ddot{x}_{Dg \max}}{K} = 0.50$	100
3.1	Relative Values of Mass, Stiffness, and Drag Factor for 5 Degree of Freedom Systems	101
3.2	Response of System 1L to El Centro Earthquake, 1940, N-S Component. Direct Integration Solution. $\beta_s = .01$	102
3.3	Response of System 1L to El Centro Earthquake, 1940, N-S Component. Direct Integration Solution. $\beta_s = .05$	103
3.4	Response of System 1M to El Centro Earthquake, 1940, N-S Component. Direct Integration Solution. $\beta_s = .01$	104
3.5	Response of System 1M to El Centro Earthquake, 1940, N-S Component. Direct Integration Solution. $\beta_s = .05$	105

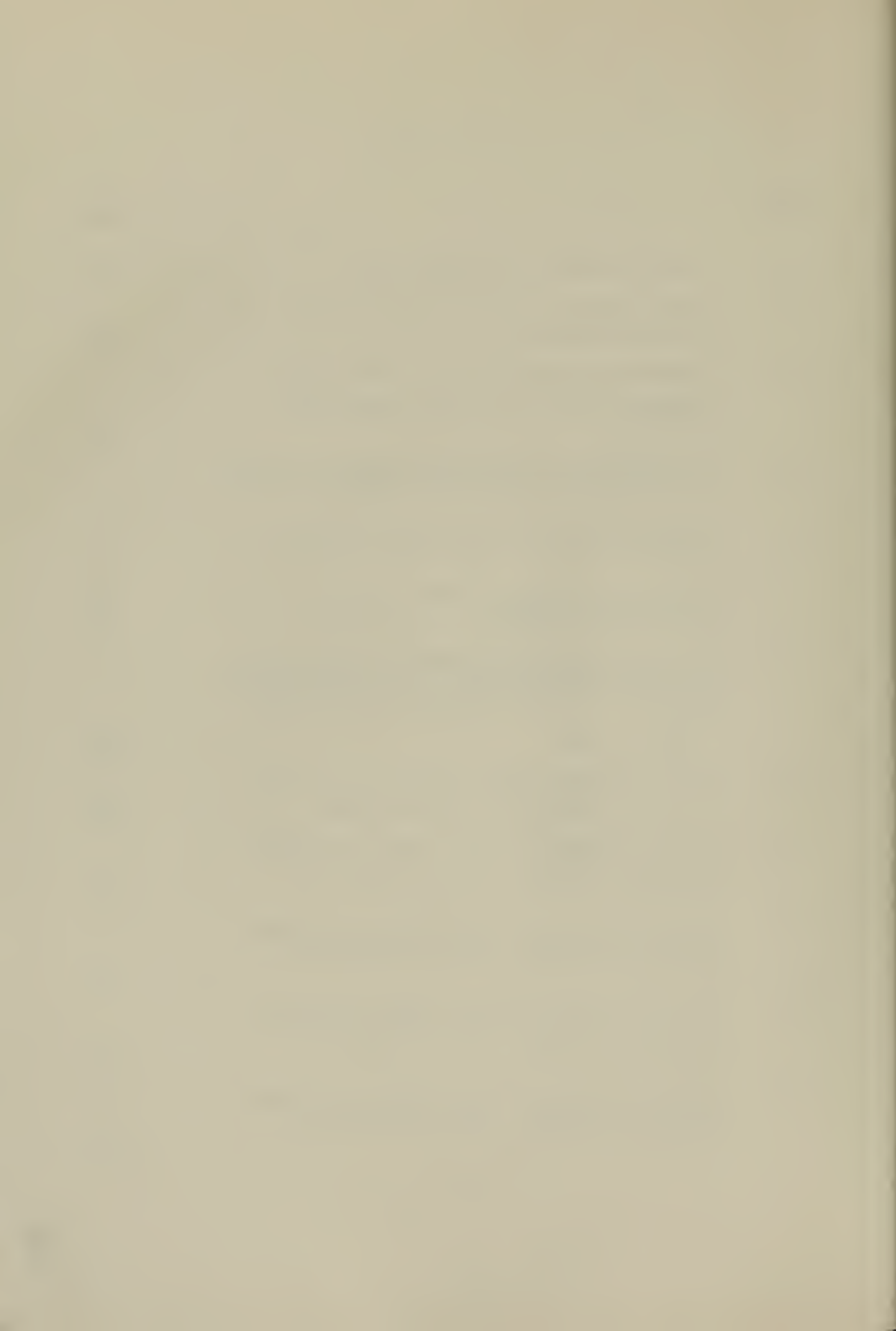
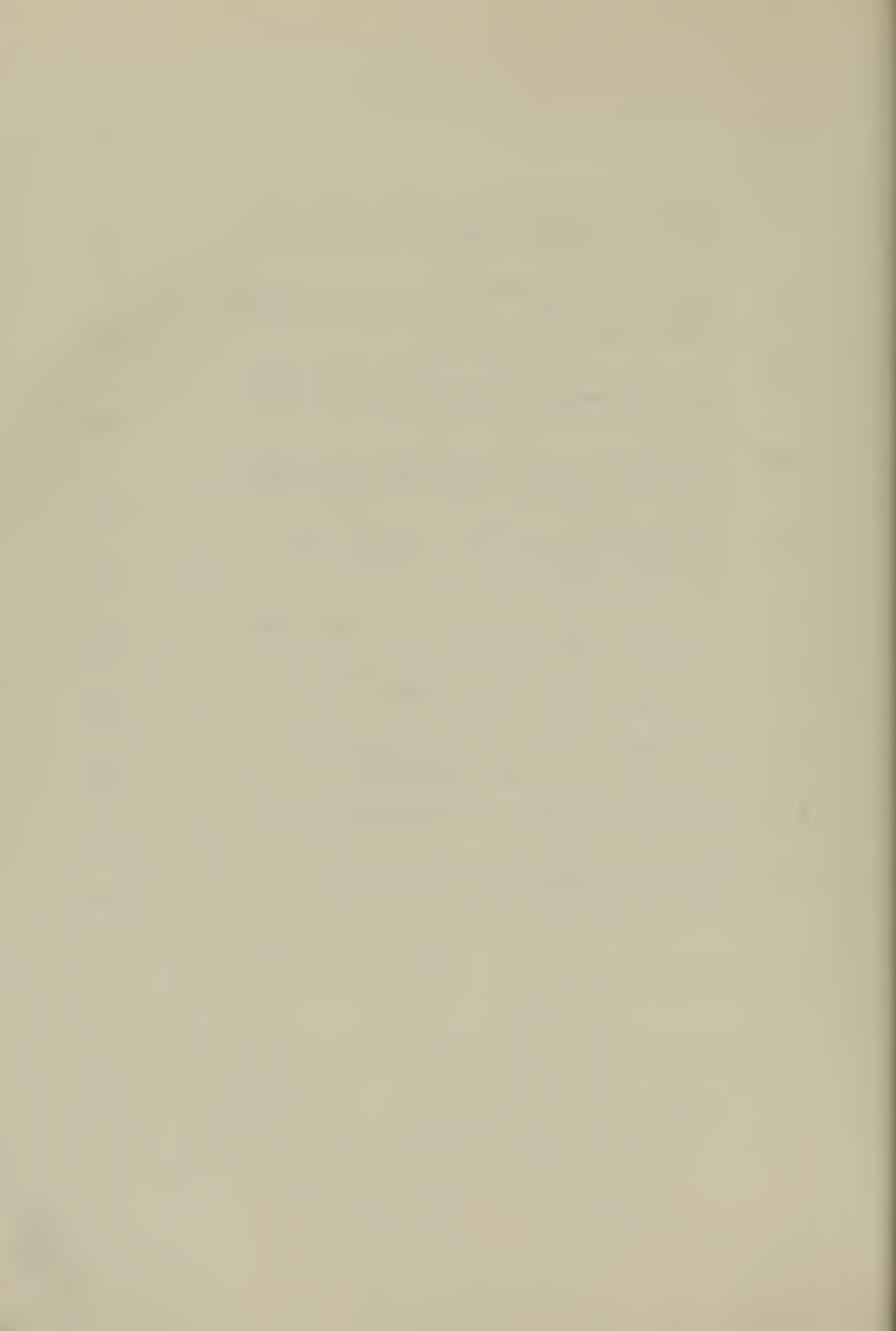


Table		Page
3.6	Response of System 2L to El Centro Earthquake, 1940, N-S Component. Direct Integration Solution. $\beta_S = .01$	106
3.7	Response of System 2L to El Centro Earthquake, 1940, N-S Component. Direct Integration Solution. $\beta_S = .05$	107
3.8	Response of System 2M to El Centro Earthquake, 1940, N-S Component. Direct Integration Solution. $\beta_S = .01$	108
3.9	Response of System 2M to El Centro Earthquake, 1940, N-S Component. Direct Integration Solution. $\beta_S = .05$	109
3.10	Response of System 3L to El Centro Earthquake, 1940, N-S Component. Direct Integration Solution. $\beta_S = .01$	110
3.11	Response of System 3L to El Centro Earthquake, 1940, N-S Component. Direct Integration Solution. $\beta_S = .05$	111
3.12	Response of System 4L to El Centro Earthquake, 1940, N-S Component. Direct Integration Solution. $\beta_S = .01$	112
3.13	Response of System 4L to El Centro Earthquake, 1940, N-S Component. Direct Integration Solution. $\beta_S = .05$	113
3.14	Response of System 4M to El Centro Earthquake, 1940, N-S Component. Direct Integration Solution. $\beta_S = .01$	114
3.15	Response of System 4M to El Centro Earthquake, 1940, N-S Component. Direct Integration Solution. $\beta_S = .05$	115
3.16	Response of System 4H to El Centro Earthquake, 1940, N-S Component. Direct Integration Solution. $\beta_S = .01$	116
3.17	Response of System 4H to El Centro Earthquake, 1940, N-S Component. Direct Integration Solution. $\beta_S = .05$	117

Table		Page
3.18	Response of System 5H to El Centro Earthquake, 1940, N-S Component. Direct Integration Solution. $\beta_s = .01$	118
3.19	Response of System 5H to El Centro Earthquake, 1940, N-S Component. Direct Integration Solution. $\beta_s = .05$	119
3.20	Response of System 6M to El Centro Earthquake, 1940, N-S Component. Direct Integration Solution. $\beta_s = .01$	120
3.21	Response of System 6M to El Centro Earthquake, 1940, N-S Component. Direct Integration Solution. $\beta_s = .05$	121
3.22	Response of System 6H to El Centro Earthquake, 1940, N-S Component. Direct Integration Solution. $\beta_s = .01$	122
3.23	Response of System 6H to El Centro Earthquake, 1940, N-S Component. Direct Integration Solution. $\beta_s = .05$	123
3.24	Response of System 7M to El Centro Earthquake, 1940, N-S Component. Direct Integration Solution. $\beta_s = .01$	124
3.25	Response of System 7M to El Centro Earthquake, 1940, N-S Component. Direct Integration Solution. $\beta_s = .05$	125
3.26	Response of System 7H to El Centro Earthquake, 1940, N-S Component. Direct Integration Solution. $\beta_s = .01$	126
3.27	Response of System 7H to El Centro Earthquake, 1940, N-S Component. Direct Integration Solution. $\beta_s = .05$	127
3.28	Response of System 1L to El Centro Earthquake, 1940, N-S Component. Modal Superposition and Direct Integration Solutions. $\beta_s = .01$	128
3.29	Response of System 1L to El Centro Earthquake, 1940, N-S Component. Modal Superposition and Direct Integration Solutions. $\beta_s = .05$	129

Table		Page
3.30	Response of System 4M to El Centro Earthquake, 1940, N-S Component. Modal Superposition and Direct Integration Solutions. $\beta_s = .01$	130
3.31	Response of System 4M to El Centro Earthquake, 1940, N-S Component. Modal Superposition and Direct Integration Solutions. $\beta_s = .05$	131
3.32	Response of System 7H to El Centro Earthquake, 1940, N-S Component. Modal Superposition and Direct Integration Solutions. $\beta_s = .01$	132
3.33	Response of System 7H to El Centro Earthquake, 1940, N-S Component. Modal Superposition and Direct Integration Solutions. $\beta_s = .05$	133
3.34	Hydrodynamic Parameters for System 4, Mid-Frequency Range. El Centro Earthquake. $\beta_s = .02$ in Each Mode	134
4.1	Structural Properties ($\beta_s = .01$ in Each Mode) of Towers A, B, C, and D ^s	135
4.2	Estimated Linear Hydraulic Damping Ratios for Towers A, B, C, and D.	139
4.3	Contributions of Each Mode to the Maximum Base Shear. Σ ABS Modal Combination	139
4.4	Properties of System 4M, Mid-Frequency Range. $\beta_s = .02$ in Each Mode	140
4.5	Hydrodynamic Parameters for System 4M. El Centro Earthquake	142



LIST OF FIGURES

Figure		Page
1.1	Schematic Diagram of Typical Offshore Structure and Lumped Parameter Model	143
1.2	Elastic Deformation Response Spectra for El Centro Earthquake	144
1.3	Ground Acceleration, Velocity, and Displacement of El Centro Earthquake, 1940, N-S Component	145
1.4	Ground Acceleration, Velocity, and Displacement of Taft Earthquake, 1952, N-21-E Component	146
1.5	Ground Acceleration, Velocity, and Displacement of Ferndale Earthquake, 1954, N-44-E Component.	147
1.6	Ground Acceleration, Velocity, and Displacement of San Fernando Earthquake (Pacoima Dam Record), 1971, S-16-E Component.	148
2.1	Elastic Deformation Response Spectra for $\ddot{x}_g = 16.1 \sin 2 \pi t$ (ft/sec ²). $\beta_s = 0.01$	149
2.2	Elastic Deformation Response Spectra for $\ddot{x}_g = 16.1 \sin 2 \pi t$ (ft/sec ²). $\beta_s = 0.05$	150
2.3	Elastic Deformation Response Spectra for Six Term Series Base Acceleration Record. $\beta_s = 0.01$	151
2.4	Elastic Deformation Response Spectra for Six Term Series Base Acceleration Record. $\beta_s = 0.05$	152
2.5	Elastic Deformation Response Spectra. El Centro Earthquake. $\beta_s = .00$	153
2.6	Elastic Deformation Response Spectra. El Centro Earthquake. $\beta_s = .02$	154
2.7	Elastic Deformation Response Spectra. El Centro Earthquake. $\beta_s = .05$	155



Figure		Page
2.8	Comparison of Elastic Deformation Response Spectra With Linear and Nonlinear Drag for Series Representation of Base Disturbance. $\beta_s = 0.01$, $K_D \ddot{x}_{g \max} / K = 0.20$	156
2.9	Comparison of Elastic Deformation Response Spectra With Linear and Nonlinear Drag for Series Representation of Base Disturbance. $\beta_s = 0.05$, $K_D \ddot{x}_{g \max} / K = 0.20$	157
2.10	Comparison of Elastic Deformation Response Spectra With Linear and Nonlinear Drag for El Centro Earthquake. $\beta_s = 0.02$, $K_D \ddot{x}_{g \max} / K = 0.50$	158
2.11	Comparison of Linear and Nonlinear Solution. (Linearized by Oscillator Velocity) El Centro Earthquake. $\beta_s = .00$	159
2.12	Comparison of Linear and Nonlinear Solution. (Linearized by Oscillator Velocity) El Centro Earthquake. $\beta_s = .02$	160
2.13	Comparison of Linear and Nonlinear Solution. (Linearized by Oscillator Velocity) El Centro Earthquake. $\beta_s = .05$	161
2.14	Linearizing Parameter for Single Degree of Freedom Oscillator. El Centro Earthquake. $\beta_s = .00$	162
2.15	Linearizing Parameter for Single Degree of Freedom Oscillator. El Centro Earthquake. $\beta_s = .02$	163
2.16	Linearizing Parameter for Single Degree of Freedom Oscillator. El Centro Earthquake. $\beta_s = .05$	164
2.17	Comparison of Nonlinear Drag Spectrum With Linear Drag Spectrum (Linearized by Ground Velocity). El Centro Earthquake. $\beta_s = 0.02$, $K_D \ddot{x}_{g \max} / K = 0.006$	165
2.18	Comparison of Nonlinear Drag Spectrum With Linear Drag Spectrum (Linearized by Ground Velocity). El Centro Earthquake. $\beta_s = 0.02$, $K_D \ddot{x}_{g \max} / K = 0.08$	166

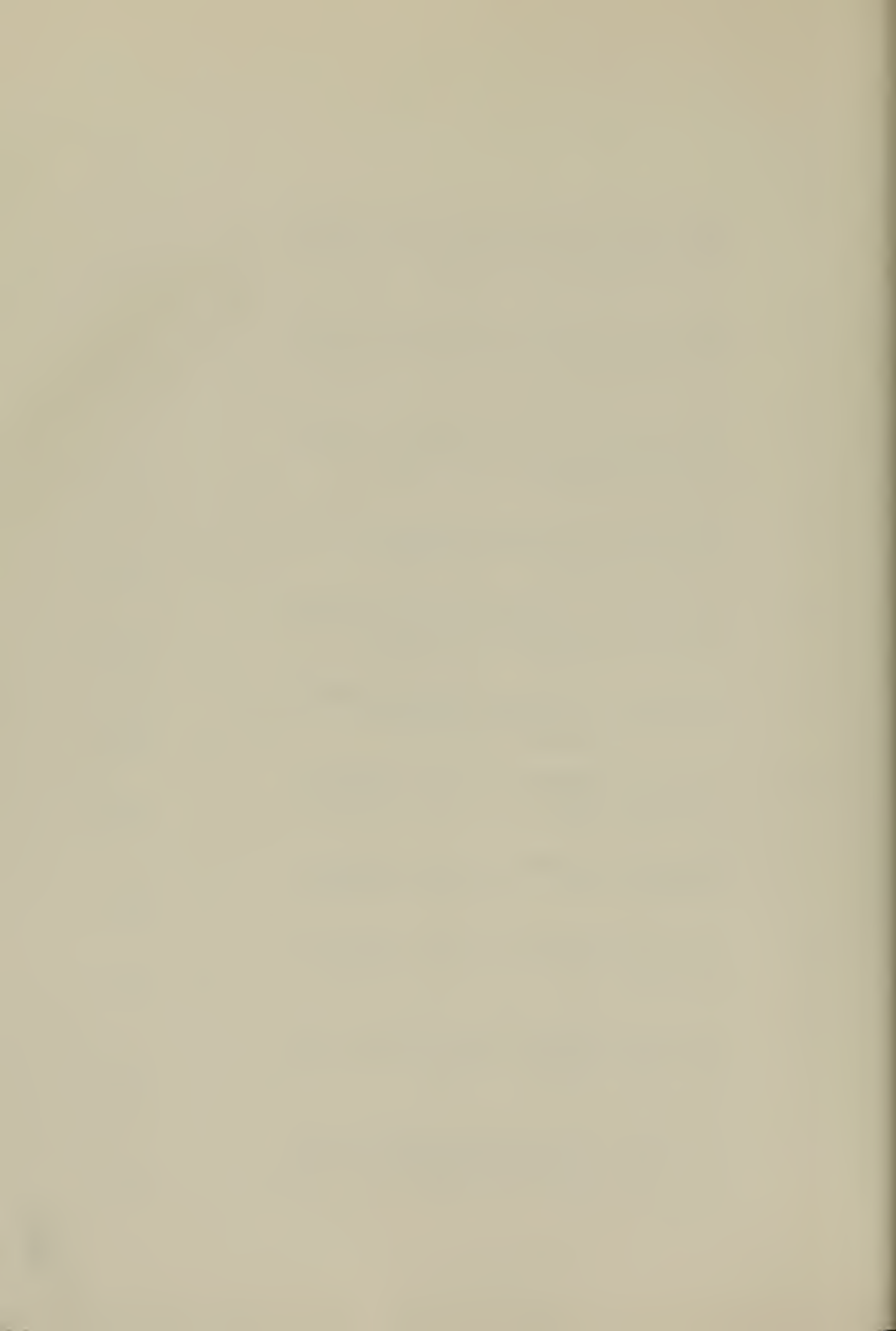


Figure	Page
2.19 Comparison of Nonlinear Drag Spectrum With Linear Drag Spectrum (Linearized by Ground Velocity). El Centro Earthquake. $\beta_s = 0.02$, $K_D \ddot{x}_{g \max} / K = 0.50$	167
2.20 Comparison of Linear and Nonlinear Solution (Linearized by Ground Velocity). El Centro Earthquake. $\beta_s = 0.02$	168
2.21 Elastic Deformation Response Spectra for El Centro Earthquake	169
2.22 Elastic Deformation Response Spectra for Taft Earthquake.	171
2.23 Elastic Deformation Response Spectra for Ferndale Earthquake	173
2.24 Elastic Deformation Response Spectra for San Fernando Earthquake	175
2.25 Comparison of Spectra for Two Distributions of Total Damping Ratio. Ferndale Earthquake. $\beta_{total} = .07$	177
2.26 Construction of Idealized Elastic Deformation Response Spectrum	178
2.27 Elastic Hydrodynamic Parameter Response Spectra. El Centro Earthquake. $\beta_{total} = 0, 1, 2, 5, 10\%$	179
2.28 Elastic Hydrodynamic Parameter Response Spectra. Taft Earthquake. $\beta_{total} = 0, 1, 2, 5, 10\%$	181
2.29 Elastic Hydrodynamic Parameter Response Spectra. Ferndale Earthquake. $\beta_{total} = 0, 1, 2, 5, 10\%$	183
2.30 Elastic Hydrodynamic Parameter Response Spectra. San Fernando Earthquake. $\beta_{total} = 0, 1, 2, 5, 10\%$	185
2.31 Construction of Idealized Hydrodynamic Parameter Response Spectrum for a Displacement Parameter	187
2.32 Construction of Idealized Hydrodynamic Parameter Response Spectrum for a Velocity Parameter.	188
2.33 Elasto-Plastic Resistance-Deformation Relationship	189

Figure		Page
2.34	Inelastic (Elasto-Plastic) Response Spectra, El Centro Earthquake, $\beta_s = .02$, $K_D \ddot{x}_{g \max} / K = 0.00$	190
2.35	Inelastic (Elasto-Plastic) Response Spectra, El Centro Earthquake, $\beta_s = .02$, $K_D \ddot{x}_{g \max} / K = 0.006$	191
2.36	Inelastic (Elasto-Plastic) Response Spectra, El Centro Earthquake, $\beta_s = .02$, $K_D \ddot{x}_{g \max} / K = 0.08$	192
2.37	Inelastic (Elasto-Plastic) Response Spectra, El Centro Earthquake, $\beta_s = .02$, $K_D \ddot{x}_{g \max} / K = 0.50$	193
2.38	Inelastic (Elasto-Plastic) Response Spectra, El Centro Earthquake, $\beta_s = .02$, $\mu = 1.5$	194
2.39	Inelastic (Elasto-Plastic) Response Spectra, El Centro Earthquake, $\beta_s = .02$, $\mu = 2.0$	195
2.40	Inelastic (Elasto-Plastic) Response Spectra, El Centro Earthquake, $\beta_s = .02$, $\mu = 4.0$	196
3.1	Comparison of Linear Drag Solution (Linearized by Ground Velocity) and Nonlinear Drag Solution. System 1L. El Centro Earthquake, 1940, N-S Component.	197
3.2	Comparison of Linear Drag Solution (Linearized by Ground Velocity) and Nonlinear Drag Solution. System 1M. El Centro Earthquake, 1940, N-S Component.	198
3.3	Comparison of Linear Drag Solution (Linearized by Ground Velocity) and Nonlinear Drag Solution. System 2L. El Centro Earthquake, 1940, N-S Component.	199
3.4	Comparison of Linear Drag Solution (Linearized by Ground Velocity) and Nonlinear Drag Solution. System 2M. El Centro Earthquake, 1940, N-S Component.	200

Figure		Page
3.5	Comparison of Linear Drag Solution (Linearized by Ground Velocity) and Nonlinear Drag Solution. System 3L. El Centro Earthquake, 1940, N-S Component.	201
3.6	Comparison of Linear Drag Solution (Linearized by Ground Velocity) and Nonlinear Drag Solution. System 4L. El Centro Earthquake, 1940, N-S Component.	202
3.7	Comparison of Linear Drag Solution (Linearized by Ground Velocity) and Nonlinear Drag Solution. System 4M. El Centro Earthquake, 1940, N-S Component.	203
3.8	Comparison of Linear Drag Solution (Linearized by Ground Velocity) and Nonlinear Drag Solution. System 4H. El Centro Earthquake, 1940, N-S Component.	204
3.9	Comparison of Linear Drag Solution (Linearized by Ground Velocity) and Nonlinear Drag Solution. System 5H. El Centro Earthquake, 1940, N-S Component.	205
3.10	Comparison of Linear Drag Solution (Linearized by Ground Velocity) and Nonlinear Drag Solution. System 6M. El Centro Earthquake, 1940, N-S Component.	206
3.11	Comparison of Linear Drag Solution (Linearized by Ground Velocity) and Nonlinear Drag Solution. System 6H. El Centro Earthquake, 1940, N-S Component.	207
3.12	Comparison of Linear Drag Solution (Linearized by Ground Velocity) and Nonlinear Drag Solution. System 7M. El Centro Earthquake, 1940, N-S Component.	208
3.13	Comparison of Linear Drag Solution (Linearized by Ground Velocity) and Nonlinear Drag Solution. System 7H. El Centro Earthquake, 1940, N-S Component.	209
4.1	Response of Towers A, B, C, and D to El Centro Earthquake, 1940, N-S Component. $\beta_s = 0.01$	210

Figure		Page
4.2	Idealized Elastic Deformation Response Spectra for the First Five Modes of Tower C. $\beta_s = .01$ in Each Mode.	212
4.3	Response of Towers A, B, C, and D Using Idealized Spectra	213

EARTHQUAKE RESPONSE OF FIXED OFFSHORE STRUCTURES

Owen Major Kirkley, Ph.D.
Department of Civil Engineering
University of Illinois at Urbana-Champaign, 1973

The response of fixed offshore structures, such as those used for oil drilling and production purposes, to earthquake excitation is investigated. An approximate method of computing maximum response quantities in the structure is developed. The approximate method uses superposition of classical normal mode responses as determined by response spectrum techniques. The structure is modeled as a lumped parameter system, the earthquake is represented by the deterministic time history record of the ground acceleration, and the hydrodynamic forces are considered to be those computed from Morison's equation.

A single degree of freedom oscillator with nonlinear drag characteristics is subjected to various representations of ground motion, including earthquake motions. The existence of a high frequency tail in the response spectrum is shown, and a method for linearizing the nonlinear hydrodynamic drag force is developed and shown to be satisfactory. A method is developed for conservatively estimating the magnitude of equivalent linear hydraulic damping in the system based on velocity characteristics of the ground motion. Rules are developed for the construction of idealized response spectra for several different response quantities. The effects of the nonlinear hydrodynamic drag force on the inelastic response of the single degree of freedom oscillator are investigated.

The principles and approximate methods developed during the study of the single degree of freedom system are applied to the multi-degree of

freedom model of the actual structure. The linearization technique is extended to the multi-degree of freedom system in such a manner as to insure the existence of classical normal modes in the equations of motion. A series of multi-degree of freedom systems is subjected to one of the earthquake records and the linearization technique is shown to be satisfactory in computing the response quantities of interest. The response of a series of offshore towers to an earthquake record is computed by the superposition of modal responses as determined by both exact spectra and idealized spectra. The approximate method considers the effects of the structure-fluid interaction by conservatively estimating the amount of linear hydraulic damping developed as a result of this interaction.

CHAPTER 1

INTRODUCTION

1.1 General

The design of fixed offshore structures is frequently based on the static forces resulting from the loads imposed on the structure by wind, waves, ocean currents, and earthquakes. Design on the basis of static forces is satisfactory when the response of the structure is not magnified by the dynamic nature of the loads. However, the characteristics of the structure and the forces acting upon it are often such that the response of the structure to wind, waves, currents, and earthquakes is dynamic and magnified greatly over the static response. In these cases, design should properly be based on the dynamic response of the structure. Various methods are available for calculating the dynamic response of a land-based structure to earthquake forces, but similar calculations for offshore structures are complicated by the presence of nonlinear hydrodynamic forces acting on submerged portions of the structure. Further, these nonlinear forces are dependent not only on the physical characteristics of the structure, but also on the actual response of the structure to the forces acting on it.

Many offshore structures are currently in use, with the most notable use being that of oil drilling and production platforms. While platforms in water depths of up to 300 feet are fairly common now, the search for new sources of oil and gas may result in many offshore structures situated in greater water depths. The location of oil resources off the coast of California, in the Gulf of Alaska, and other portions of the circumpacific earthquake belt

as well as other regions of seismic activity emphasizes the need to be able to predict the response of offshore structures to earthquake motions. Drilling and production platforms represent a very large investment in cost, and large numbers of personnel are involved in the operation of such a structure. Failure of one of these platforms could result in many lives being lost as well as the loss of investment both from the cost of the platform and the loss of production time.

1.2 Description of the Problem

An offshore structure of the type mentioned in the preceding section is shown schematically in Fig. 1.1(a) and is a continuous system with an infinite number of degrees of freedom. Such structures are space frames composed of circular pipe sections generally welded together, with diagonal bracing as shown in the figure. The top portion of the structure may consist of more than one level and contains the heavy equipment necessary for oil drilling and production and often contains facilities for berthing and messing of the crew. The operating and production portion of the structure is generally quite heavy. The research reported in this thesis is based on a lumped parameter model^{1*} of the structure with mass, stiffness, forces and other characteristics of the structure lumped into a discrete number of nodes, as shown in Fig. 1.1(b).

The equations of motion for the system shown in Fig. 1.1(b), subjected to ground motion in quiescent water, are, in matrix form:

$$[m]\{\ddot{x}_s\} + [C_s]\{\dot{x}_s - \dot{x}_g\} + [K]\{x_s - x_g\} = \{P\} \quad (1.1)$$

*

Numbers refer to List of References at end of text.

where

- $[m]$ = mass matrix of the system
- $[C_s]$ = structural damping matrix of the system
- $[K]$ = stiffness matrix of the system
- \ddot{x}_{sj} = absolute acceleration of node j
- \dot{x}_{sj} = absolute velocity of node j
- x_{sj} = absolute displacement of node j
- \dot{x}_g = ground velocity
- x_g = ground displacement

The symbol $[\quad]$ denotes a matrix in which the off-diagonal elements are zero. No structural dampers are shown on the model, but the damping matrix $[C_s]$ can take a variety of forms as will be discussed in a later chapter.

The hydrodynamic forces acting at each node of the system are considered to be those computed from Morison's equation² for circular cylinders as:

$$\{P\} = - [m'] \{\ddot{x}_s\} - [K_D] \{\dot{x}_s | \dot{x}_s|\} \quad (1.2)$$

where

- $[m']$ = added mass matrix³ = $\rho [C_I V]$
- ρ = mass density of the fluid surrounding the structure
- C_{Ij} = empirical inertia coefficient at node j
- V_j = enclosed volume at node j
- $[K_D]$ = drag factor matrix = $\frac{1}{2} \rho [C_D A]$

C_{Dj} = empirical drag coefficient at node j

A_j = projected area at node j

If the coordinate transformation, $\{Z\} = \{x_s - x_g\}$, is made, where $\{Z\}$ is a vector of a motion quantity of a node relative to that of the ground, Eqs. 1.1 and 1.2 can be combined to yield:

$$[M]\{\ddot{Z}\} + [C_s]\{\dot{Z}\} + [K]\{Z\} = -[M]\{\ddot{x}_g\} - [K_D]\{\dot{x}_s|\dot{x}_s|\} \quad (1.3)$$

where

$[M]$ = virtual (or total) mass matrix = $[m] + [m']$

\ddot{x}_g = ground acceleration

Equation 1.3 differs from the equations of motion for a land-based structure subjected to earthquake forces in two important aspects. First, the presence of the added mass term causes the structure to possess natural frequencies and mode shapes which are different from those of a structure with the same stiffness and only the structural mass $[m]$. Secondly, the hydrodynamic force term $[K_D]\{\dot{x}_s|\dot{x}_s|\}$ is not present in the conventional land-based earthquake problem, and this nonlinear hydrodynamic force causes the major difficulty in solving Eq. 1.3.

If the nonlinear hydrodynamic force $[K_D]\{\dot{x}_s|\dot{x}_s|\}$ can be converted into an "equivalent" linear hydrodynamic force, say $[K_{DL}]\{\dot{x}_s\}$, Eq. 1.3 can be written as

$$[M]\{\ddot{Z}\} + [C_s]\{\dot{Z}\} + [K]\{Z\} = -[M]\{\ddot{x}_g\} - [K_{DL}]\{\dot{x}_s\} \quad (1.4)$$

Since $\{Z\} = \{x_s - x_g\}$, Eq. 1.4 can be rewritten as

$$\begin{aligned}
& [M]\{\ddot{Z}\} + [C_s]\{\dot{Z}\} + [K_{DL}]\{\dot{Z}\} + [K]\{Z\} \\
& = -[M]\{\ddot{x}_g\} - [K_{DL}]\{\dot{x}_g\}
\end{aligned} \tag{1.5}$$

Equation 1.5 differs from the equations of motions for a land-based multi-degree of freedom damped structure of mass $[M]$, subjected to a base excitation, in the linear drag force $[K_{DL}]\{\dot{x}_g\}$.

One well-known and convenient method of solving simultaneous linear differential equations of motion is the normal mode method.¹ In the normal mode method, the vector of a response quantity expressed in one coordinate system, such as the relative displacement between each node and the base $\{Z\}$, is transformed into the "normal" coordinate system by the relation

$$\{Z\} = [\phi]\{Y\} \tag{1.6}$$

where

$[\phi]$ = a matrix of the natural mode shapes of the system with the i th column in the matrix representing the deflected shape of the i th mode of the system.

and $\{Y\}$ = a vector of modal response quantities with the i th element in the vector representing the modal response quantity in the i th mode.

Thus, Eq. 1.6 expresses the response at each node in the model as a combination of the responses at that node in each of the natural modes of vibration in the system. The natural mode shapes in the modal matrix $[\phi]$ are orthogonal¹, with respect to $[M]$ and $[K]$ and will be orthogonal with $[C_s]$ if the elements of $[C_s]$ are specified in a certain way.²¹ Substitution of Eq. 1.6 into Eq. 1.5 yields,

$$\begin{aligned}
& [\Gamma M \Gamma][\phi]\{\ddot{Y}\} + [C_s][\phi]\{\dot{Y}\} + [\Gamma K_{DL} \Gamma][\phi]\{\dot{Y}\} + [K][\phi]\{Y\} \\
& = -[\Gamma M \Gamma]\{\ddot{x}_g\} - [\Gamma K_{DL} \Gamma]\{\dot{x}_g\}
\end{aligned} \tag{1.7}$$

Pre-multiplying Eq. 1.7 by $[\phi]^T$ yields,

$$\begin{aligned}
& [\phi]^T [\Gamma M \Gamma][\phi]\{\ddot{Y}\} + [\phi]^T [C_s][\phi]\{\dot{Y}\} + [\phi]^T [\Gamma K_{DL} \Gamma][\phi]\{\dot{Y}\} \\
& + [\phi]^T [K][\phi]\{Y\} = -[\phi]^T [\Gamma M \Gamma]\{\ddot{x}_g\} - [\phi]^T [\Gamma K_{DL} \Gamma]\{\dot{x}_g\}
\end{aligned} \tag{1.8}$$

Recognizing the orthogonal relationships between the modal matrix $[\phi]$ and other matrices in Eq. 1.8, the following matrices are defined:

$$\begin{aligned}
[\Gamma M^* \Gamma] &= [\phi]^T [\Gamma M \Gamma][\phi] && = \text{a diagonal modal mass matrix} \\
[\Gamma C_s^* \Gamma] &= [\phi]^T [C_s][\phi] && = \text{a diagonal modal structural damping} \\
&&& \text{matrix. The form of } [C_s] \text{ which permits} \\
&&& \text{this is discussed later.} \\
[\Gamma K^* \Gamma] &= [\phi]^T [K][\phi] && = \text{a diagonal modal stiffness matrix} \\
[\tilde{K}_{DL}] &= [\phi]^T [\Gamma K_{DL} \Gamma][\phi] && = \text{a modal linear hydraulic damping matrix} \\
&&& \text{which is not necessarily diagonal} \\
[\Gamma \omega^2 \Gamma] &= [\Gamma M^* \Gamma]^{-1} [\Gamma K^* \Gamma] && = \text{a matrix of circular natural frequencies} \\
&&& \text{of the system}
\end{aligned}$$

Using these quantities, Eq. 1.8 becomes

$$\begin{aligned}
& [\Gamma M^* \Gamma]\{\ddot{Y}\} + [\Gamma C_s^* \Gamma]\{\dot{Y}\} + [\tilde{K}_{DL}]\{\dot{Y}\} + [\Gamma K^* \Gamma]\{Y\} \\
& = -[\phi]^T [\Gamma M \Gamma]\{\ddot{x}_g\} - [\phi]^T [\Gamma K_{DL} \Gamma]\{\dot{x}_g\}
\end{aligned} \tag{1.9}$$

If the modal linear hydraulic damping matrix $[\tilde{K}_{DL}]$ can be made diagonal, then the set of simultaneous differential equations of motion represented by Eq. 1.9 will be completely uncoupled. Suppose that the nondiagonal matrix $[\tilde{K}_{DL}]$ can, in some satisfactory manner, be converted into a diagonal matrix, say $[K_{DL}^*]$. Then Eq. 1.9 can be written

$$\begin{aligned} [M^*]\{\ddot{Y}\} + [C_s^*]\{\dot{Y}\} + [K_{DL}^*]\{\dot{Y}\} + [K^*]\{Y\} \\ = -[\phi]^T[M]\{\ddot{x}_g\} - [\phi]^T[K_{DL}]\{\dot{x}_g\} \end{aligned} \quad (1.10)$$

Or, for the i th mode,

$$\begin{aligned} M_{ii}^* \ddot{Y}_i + C_{s_{ii}}^* \dot{Y}_i + K_{DL_{ii}}^* \dot{Y}_i + K_{ii}^* Y_i \\ = - \left(\sum_{j=1}^{nn} \phi_{ji} M_{jj} \right) (\ddot{x}_g) - \left(\sum_{j=1}^{nn} \phi_{ji} K_{DL_{jj}} \right) (\dot{x}_g) \end{aligned} \quad (1.11)$$

where

$$nn = \text{number of nodes in the model}$$

Equation 1.11 can also be written as

$$\begin{aligned} \ddot{Y}_i + 2\beta_{s_i} \omega_{ii} \dot{Y}_i + 2\beta_{h_i} \omega_{ii} \dot{Y}_i + \omega_{ii}^2 Y_i \\ = - \left(\frac{\sum_{j=1}^{nn} \phi_{ji} M_{jj}}{M_{ii}^*} \right) (\ddot{x}_g) - \left(\frac{\sum_{j=1}^{nn} \phi_{ji} K_{DL_{jj}}}{M_{ii}^*} \right) (\dot{x}_g) \end{aligned} \quad (1.12)$$

where

$$\beta_{s_i} = \frac{C_{s_{ii}}^*}{2M_{ii}^* \omega_{ii}} = \text{structural damping ratio in the } i\text{th mode}$$

$$\beta_{hi} = \frac{K_{DL_{ii}}^*}{2M_{ii}^*\omega_{ii}} = \text{linear hydraulic damping ratio in the } i\text{th mode}$$

If the modal response quantity of interest, Y , \dot{Y} , or \ddot{Y} can be obtained from Eq. 1.12 for each mode, then the total response of the structure can be obtained by using the relationship given in Eq. 1.6. The modal response quantities vary with time, and the time variation is different for each mode, so an exact calculation of the total response of the structure can only be made if the exact time histories of the modal responses are known and superimposed on one another. Generally, the maximum response quantity at each node of the model is desired, but the modal maxima do not necessarily occur at the same time. An approximation to the actual maximum response at each node of the model can be made by determining the maximum response in each mode and then combining the modal responses in some fashion. The response spectrum is a convenient way to determine the maximum modal response.¹¹⁻¹³

1.3 Summary of Previous Research

Equation 1.3, or a similar form, has been solved by other investigators using various methods. Much of the existing work in this area has been devoted to the response of offshore structures to wave forces, but the nonlinear difficulties are somewhat similar for wave forces and earthquake forces acting on submerged or partially submerged structures. Further, the bulk of recent investigations has been devoted to the use of stochastic representations of wave and earthquake motions.

Burke and Tighe⁴ integrate the equations of motion directly for a series of towers subjected to different deterministic ground acceleration

records by using an iterative technique which computes the response quantities of interest at step-by-step time points throughout the earthquake record. For a tower in 800 feet of water subjected to four accelerograms (normalized to the intensity of the 1940 El Centro earthquake), the effect of the water-structure interaction was found to reduce the maximum base shear and the maximum overturning moment by about 33 percent from the values found when the water-structure interaction was not included in the solution. This method, while permitting the direct use of the structural properties of the system, including the nonlinear drag force, requires the use of a digital computer and the availability of actual or simulated earthquake records. For purposes of preliminary design of a structure for a "design" earthquake of the designer's choice, however, the step-by-step technique is costly, time consuming, and requires that a time history of the "design" earthquake be available. Preliminary design would best be served by a rapid, approximate method of solution which permits the use of selected parameters for the design earthquake and accounts for the effects of the nonlinear drag forces, yet yields satisfactory results.

Penzien, in association with other investigators,⁶⁻⁸ linearizes the drag forces in Eq. 1.3 by replacing the nonlinear force vector with a linear force vector which performs the same amount of work during the history of the response. This linearization results in an "equivalent" linear hydraulic damping matrix acting on the system in much the same manner as the structural damping matrix acts. The linear equations of motion are then transformed into a normal coordinate system and solved by the normal mode method of superposition.¹ Unfortunately, the linear hydraulic damping matrix does not uncouple when the

equations are transformed into the normal coordinate system. As a result, an uncoupling (or diagonalizing) technique, similar to the original linearizing technique, must be employed in order to separate the equations into the desired modal equations. The linearizing and diagonalizing are accomplished by an iterative process which uses actual response quantities of the system as they are developed, and the procedure is time consuming and requires great care in its formulation and use. For towers subjected to a stochastic representation of the ground motion, equivalent linear hydraulic damping ratios on the order of 9 percent of critical are reported for the first two modes of towers in deep water, with "very much smaller" hydraulic damping ratios for the tower in shallow water.⁶

Foster⁹ solves the problem of an offshore tower subjected to stochastic representation of wave forces by linearizing the drag force, then, recognizing that nonproportional hydraulic damping may result, solving the linear equations of motion using complex eigenvalues and eigenvectors. This procedure recognizes that, unless the linearization of the drag force is done in a certain way, classical normal modes may not necessarily exist in the equations, thus the normal mode method of superposition is not a rigorously correct approach.

Nath and Harleman¹⁰ conclude that, for large diameter cylinders in deep water waves, the nonlinear drag force can be neglected, and, since shallow water structures are relatively stiff, and therefore the dynamic response to waves is not greatly magnified over the static response, design of shallow water structures can proceed on a static basis. These conclusions, however, were arrived at by considering the response of structures to waves, which generally have much longer period components of motion than do earthquakes.

1.4 Objective and Scope

The objective of this thesis is to investigate the effects of the nonlinear hydrodynamic drag force on the earthquake response of single degree of freedom and multi-degree of freedom systems and to develop a satisfactory method of linearizing this force in order that conventional methods of solving linear differential equations may be employed in the solution of the equations of motion.

A further objective is to develop an approximate method for the solution of Eq. 1.3 by the superposition of normal mode responses, using response spectra to estimate the modal response quantities necessary. A rapid, yet fairly accurate method of solution is desirable in the preliminary stages of the design of an offshore structure in order that the designer may have an estimate of the response of a tentative design to one or more design earthquakes of his specification. It should be kept in mind that the approximate solution developed in this thesis is no substitute for a more detailed analysis of the structure once the design is in its final stages.

In Chapter 2, the effects of the nonlinear hydrodynamic drag force on the response of a single degree of freedom oscillator are explored. A reasonable method of linearizing the drag force and a method for conservatively predicting the resultant linear drag effects are developed and shown. A method is developed for estimating certain response quantities of the oscillator in order to determine more accurately the range of hydraulic drag and inertia coefficients which should be used in the force equation. The response of the oscillator in the inelastic region, assuming elasto-plastic force-displacement

characteristics of the spring, is shown. Finally, the construction of idealized response spectra, which include the effects of hydraulic drag, is shown.

The concepts developed in Chapter 2 for the single degree of freedom system are extended to the multi-degree of freedom system in Chapter 3. The nonlinear drag force is linearized in such a manner as to insure the existence of classical normal modes in the equations of motion in order that normal mode superposition may be used as an approximate solution to the problem. The method of linearization is shown to be accurate for a series of five degree of freedom systems which are representative of the type of structure being investigated. A means of estimating the amount of equivalent linear hydraulic damping, using ground motion velocity characteristics, is developed and is shown to yield good results. The construction of an idealized response spectrum for each mode of the multi-degree of freedom system is discussed and described, and sample problems are solved by the superposition of normal mode responses.

The application of the approximate method to a series of actual offshore towers is demonstrated, and the results of calculations of the response of these towers are discussed in Chapter 4.

1.5 Related Topics

In this section, several topics of general interest in the field of earthquake engineering are briefly discussed in order that the reader may more fully understand the display of results by the use of response spectra, the numerical method of integrating the equations of motion, and the characteristics of the earthquake records used in the research.

1.5.1 Response Spectra

The equation of motion for a damped, single degree of freedom oscillator in air, subjected to a base disturbance is

$$m\ddot{x}_s + C_s(\dot{x}_s - \dot{x}_g) + K(x_s - x_g) = 0 \quad (1.13)$$

By making the transformation $Z = x_s - x_g$, Eq. 1.13 becomes

$$m\ddot{Z} + C_s\dot{Z} + KZ = -m\ddot{x}_g \quad (1.14)$$

Or, in an alternate form

$$\ddot{Z} + 2\beta_s\omega\dot{Z} + \omega^2 Z = -\ddot{x}_g \quad (1.15)$$

The solution of Eq. 1.15 depends on the characteristics of the ground motion function, the amount of damping in the system as represented by the dimensionless parameter β_s , and the natural frequency of the system, ω . The frequency parameter enters into the solution as a dimensionless product of ω and a characteristic time of the base motion.¹³

A plot of the maximum value of a response quantity, without regard to sign, as computed from Eqs. 1.13, 1.14 or 1.15, as a function of the frequency of the system is called a response spectrum for that quantity. The response spectrum is a convenient way to represent various maximum response quantities of interest as a function of the variables involved in the solution. The response quantity of greatest interest is usually the maximum spring distortion, $|Z|_{\max}$, which occurs during the response history of the oscillator, although other response quantities are sometimes of interest.¹³

The response spectrum is conveniently shown on tripartite logarithmic

graph paper as shown in Fig. 1.2. The grid of this representation is constructed such that the abscissa represents the frequency of the oscillator, the ordinate represents velocity units of response, the diagonal lines sloping up to the right are lines of constant displacement units, and the lines sloping down to the right are lines of constant acceleration units. In this thesis, unless otherwise indicated, the response spectra shown are deformation response spectra in which the pseudo-velocity, $\omega|Z|_{\max}$ is plotted against the undamped frequency of the system. The displacement quantity shown is the maximum spring deformation, $|Z|_{\max}$, and the acceleration quantity is the pseudo-acceleration, $\omega^2|Z|_{\max}$. Response spectra for a damped single degree of freedom oscillator, in air, are shown in Fig. 1.2 for the El Centro earthquake. The shape of the spectra is typical for strong motion earthquakes of the type used in this thesis. More detailed information on response spectra can be found in the literature.¹¹⁻¹⁴

Since the response spectra for strong motion earthquakes exhibit the characteristic shape shown in Fig. 1.2, the spectra can be idealized by straight line segments. Amplification factors, which relate the idealized spectrum to the ground motion quantities $x_{g \max}$, $\dot{x}_{g \max}$, and $\ddot{x}_{g \max}$, have been developed for a range of damping ratios.¹⁴ The ability to construct an idealized representation of the response spectrum for a given set of conditions permits an estimate of the response to be made without having an actual earthquake record available.

1.5.2 Numerical Integration of the Equations of Motion

The equations of motion for a system subjected to a base disturbance

can be solved by numerical integration. In this thesis, numerical integration of the equations of motion is performed by the Newmark "Beta Method."⁵ In the calculations, β is set to be equal to $1/6$, thus representing the ground response acceleration as linear between adjacent time points. The time interval used is $1/20$ of the natural period for frequencies up to 10 cps and $1/40$ of the natural period for frequencies equal to, or greater than 10 cps. These time increments insure good accuracy, stability and convergence in the solution. Convergence of the solution at any time point is assumed to have occurred if two successive iterations yield values of acceleration which are within 0.1 percent. In the case of multi-degree of freedom equations of motion, the time increment is based on the shortest natural period in the system, and iteration is carried out until the computed acceleration at each node is within 0.1 percent of the value computed on the previous cycle. In all cases, the integration of the equations of motion is carried out for a period of time equal to one-half the natural period (the longest natural period in the case of multi-degree of freedom systems) after the base disturbance ends.

1.5.3 Earthquake Records Considered

Four actual earthquake records are used in this thesis. The records are described numerically in Table 1.1 and the time history of the ground acceleration, velocity, and displacement for each record is shown in Figs. 1.3 through 1.6. In each earthquake record, a very small (less than .005g) artificial acceleration point has been generated near the end of the record so that the velocity of the base motion is zero at the end of the record.

Although a parabolic baseline correction¹⁶ had previously been applied to the acceleration records, a slight residual velocity still remained at the end of the record and it is this residual velocity which is removed by the artificial acceleration point. The four records chosen are considered to be representative of strong motion earthquakes on firm soil.

1.6 Notation

As much as possible, the same symbols are used for both the single degree of freedom oscillator and the multi-degree of freedom system, with matrix and vector notation indicating the multi-degree of freedom system. Symbols are defined as they first appear in the text. For ease of reference the symbols used are summarized in this section.

$\lceil A \rceil$	projected area matrix
C_D	empirical dimensionless drag coefficient
C_I	empirical dimensionless inertia coefficient
$[C_S]$	structural damping coefficient matrix
$\lceil C_S^* \rceil$	modal damping coefficient matrix = $[\phi]^T [C_S] [\phi]$
D	diameter of a single degree of freedom oscillator
$\{HDPF\}$	vector of participation factors for hydrodynamic parameter response quantities $\{HDPF\} = \lceil K^* \rceil^{-1} [\phi]^T [K] \{I\}$
$\{I\}$	unit vector

$[K]$	structure stiffness matrix
$[K^*]$	modal stiffness matrix = $[\phi]^T [K] [\phi]$
$[K_D]$	drag factor matrix = $\frac{1}{2} \rho [C_D A]$
$\{K_D^*\}$	modal drag factor vector for very high frequency system = $[M^*]^{-1} [\phi]^T [K_D] \{I\}$
$[K_{DL}]$	linear drag factor matrix
$[K_{DL}^*]$	modal linear drag factor matrix = $[\phi]^T [K_{DL}] [\phi]$
$\frac{K_D \ddot{x}_{g \max}}{K}$	dimensionless drag parameter
$[M]$	total structure dynamic mass matrix = $[m] + [m']$
$[M^*]$	modal mass matrix = $[\phi]^T [M] [\phi]$
$\{P\}$	hydrodynamic force vector
$\{PF\}$	participation factor vector for displacement response = $[M^*]^{-1} [\phi]^T [M] \{I\}$
$[V]$	enclosed volume matrix
$\{Y\}, \{\dot{Y}\}, \{\ddot{Y}\}$ $\{Q\}, \{\dot{Q}\}, \{\ddot{Q}\}$	displacement, velocity, and acceleration vectors in normal coordinates
$\{Z\}, \{\dot{Z}\}, \{\ddot{Z}\}$	vectors of displacement, velocity, and acceleration of the structure relative to the base
Z_y	deformation at which yielding occurs

a	relative acceleration between fluid and a single degree of freedom oscillator
i	subscripts indicating mode number
j	subscripts indicating node number
$[m]$	structural mass matrix
$[m']$	added mass matrix = $\rho[C_I V]$
nm	number of modes in the multi-degree of freedom system
nn	number of nodes in the lumped parameter model
$p(t)$	hydrodynamic force acting on the single degree of freedom oscillator
v	relative velocity between fluid and a single degree of freedom oscillator
$\{x_g\}, \{\dot{x}_g\}, \{\ddot{x}_g\}$	ground displacement, velocity and acceleration vectors
$x_{g \max}, \dot{x}_{g \max}, \ddot{x}_{g \max}$	maximum displacement, velocity, and acceleration in the ground motion record
$\{x_s\}, \{\dot{x}_s\}, \{\ddot{x}_s\}$	vectors of structure displacement, velocity, and acceleration
$y_i, \dot{y}_i, \ddot{y}_i$ $q_i, \dot{q}_i, \ddot{q}_i$	displacement, velocity, and acceleration of the i th mode single degree of freedom equation of motion after the modal participation factor has been taken out. Expressed in normal coordinates

α	constant of proportionality between the linear drag factor matrix and the total mass matrix $[K_{DL}]$ $= \alpha [M]$
β_{h_i}	linear hydraulic damping ratio in the i th mode
β_{s_i}	structural damping ratio in the i th mode $\beta_{s_i} = \frac{C_{s_{ii}}^*}{2M_{ii}^* \omega_{ii}}$
$\{\gamma\}$	vector of modal stiffness factors $\{\gamma\} = [\phi]^T [K] \{I\}$
μ	ductility factor for inelastic response $= \frac{ Z _{\max}}{Z_y}$
$[\phi]$	mode shape matrix
ρ	mass density of the fluid
ω_{ii}	circular natural frequency of the i th mode $[\omega^2] = [M^*]^{-1} [K^*]$

CHAPTER 2

SINGLE DEGREE OF FREEDOM OSCILLATOR

2.1 General

The normal mode method of solving Eq. 1.3 requires the solution of single degree of freedom equations of motion. For this reason, and to understand more fully the effects of the nonlinear hydrodynamic drag force on the response of a simple system, Chapter 2 is devoted to the investigation of the effects of the hydrodynamic drag force on the response of a single degree of freedom oscillator.

In the investigation of the response of the oscillator with nonlinear drag characteristics it is shown that the response of the oscillator in the very high frequency region can be estimated if the drag properties of the system are known and if the maximum velocity of the base motion is known. The nonlinear drag force is linearized by equating the work done by a fictitious linear force with the work done by the real, nonlinear force. This method of linearization is shown to be accurate until the high frequency region of the spectrum is reached. It is shown that the linear drag force is equivalent to a linear hydraulic damper in which the force is dependent upon the velocity of the mass, and that the magnitude of the hydraulic damping coefficient is dependent upon the amount of structural damping in the system. A means of estimating the amount of linear hydraulic damping is developed for earthquake motions, and the estimate is shown to be conservative except in the low frequency range. The maximum response of the system in the mid-frequency range to earthquake excitation is shown to be dependent upon the

total amount of linear damping present, and not upon the ratio in which the damping is distributed between structural and hydraulic.

Response quantities which may be used in order to select reasonable values of the inertia and drag coefficients, C_I and C_D , are explored, and a method of estimating these response quantities is developed. The inelastic response of an oscillator with elasto-plastic force-displacement characteristics of the spring is investigated and the results are shown in the form of response spectra.

The construction of idealized elastic response spectra which include the effects of the nonlinear hydrodynamic forces is demonstrated in this chapter.

2.2 Elastic Deformation Response Spectra

The equation of motion can be written for the single degree of freedom oscillator as

$$M\ddot{Z} + C_S\dot{Z} + KZ = -M\ddot{x}_g - K_D\dot{x}_S|\dot{x}_S| \quad (2.1)$$

or

$$\ddot{Z} + 2\beta_S\omega_S\dot{Z} + \omega_S^2Z = -\ddot{x}_g - \frac{K_D}{M}\dot{x}_S|\dot{x}_S| \quad (2.2)$$

or

$$\ddot{Z} + 2\beta_S\omega_S\dot{Z} + \omega_S^2Z = -\ddot{x}_g - \left(\frac{K_D}{K}\frac{\ddot{x}_{g \max}}{\ddot{x}_{g \max}}\right)\left(\frac{\omega_S^2}{\ddot{x}_{g \max}}\right)\dot{x}_S|\dot{x}_S| \quad (2.3)$$

As pointed out in Chapter 1, the solution of the equation of motion for a land-based single degree of freedom oscillator (Eq. 2.1 without the nonlinear

hydrodynamic drag force $K_D \dot{x}_s |\dot{x}_s|$) depends on the characteristics of the ground motion, the amount of damping in the system as represented by the dimensionless parameter β_s , and the natural frequency of the system, ω . The solution of Eq. 2.1 depends on the magnitude of K_D in addition to these parameters. A dimensional analysis of Eq. 2.1 yields the dimensionless drag parameter

$$\frac{K_D \ddot{x}_{g \max}}{K}$$

as one of the parameters on which the response of the oscillator depends. When using a maximum ground acceleration of 0.5 g, values of 0.01, 0.2, and 0.6 represent a reasonable range over which to vary the dimensionless drag parameter. For the maximum ground acceleration in the El Centro earthquake record (0.312 g), values of 0.006, 0.08, and 0.50 for the parameter yield slightly greater variations in the magnitude of K_D . Obviously, a zero value of the drag parameter represents a "no-drag" system and increasing values of the parameter represent increasing magnitudes of K_D in the system for fixed values of K and $\ddot{x}_{g \max}$.

Equation 2.1 is solved numerically for the steady-state maximum response of the oscillator when the base acceleration is

$$\ddot{x}_g = 16.1 \sin 2\pi t$$

where

$$\ddot{x}_g \text{ is in ft/sec}^2$$

$$t \text{ is in seconds}$$

Deformation response spectra (in which $\omega |Z|_{\max}$ is plotted against frequency) are plotted in Figs. 2.1 and 2.2 to show the results of the calculations.

In order to investigate the response of the oscillator to a slightly more complicated representation of the base disturbance, the base acceleration is represented as a six term cosine series. The numerical characteristics of the series used in the response calculations are shown in Table 2.1. The series has the features of zero acceleration, velocity, and displacement at the beginning and end of the base motion. Equation 2.1 is solved numerically for the maximum response of the oscillator when subjected to five cycles of this base disturbance, and the results are shown in the form of deformation response spectra in Figs. 2.3 and 2.4.

Equation 2.1 is solved numerically for the maximum response of the oscillator when subjected to the El Centro earthquake record. The results are shown in the form of deformation response spectra in Figs. 2.5 through 2.7.

A study of the spectra presented in Figs. 2.1 through 2.7 reveals several interesting characteristics which are best discussed in terms of frequency ranges of the oscillator.

In the low frequency region, the maximum spring deformation, $|Z|_{\max}$, approaches that for the case of $K_D \ddot{x}_{g \max} / K = 0$, regardless of the amount of hydrodynamic drag in the system for the range of drag parameter used. This is reasonable to expect, since the magnitude of the drag force is a function of the oscillator velocity, \dot{x}_s , and very soft (low frequency) systems exhibit little velocity response of the mass (\dot{x}_s).

In the mid-frequency region, where spectra for the conventional "no-drag" oscillator show an amplification of the pseudo-velocity over the maximum ground velocity, the spectra for systems with drag also show an amplification of the pseudo-velocity over the maximum ground velocity. However,

the presence of the nonlinear hydrodynamic drag force causes a reduction in the response of the oscillator from the response of the "no-drag" oscillator. The amount of reduction is greater for greater values of the drag parameter up to some frequency. This reduction would suggest that, in the mid-frequency range of the spectrum, the nonlinear hydrodynamic force can be replaced by an equivalent linear hydrodynamic force which will effect the response in much the same manner as the presence of structural damping effects the response. The amount of reduction in response caused by the drag force is also seen from the spectra to be dependent upon the amount of structural damping in the system. This is easily noted by comparing Figs. 2.5 and 2.6. In Fig. 2.5, the system has no structural damping, and a slight amount of drag (represented by $K_D \ddot{x}_{g \max} / K = 0.006$) is seen to reduce significantly the maximum response of the oscillator in the frequency range of about 1 to 10 cps. In Fig 2.6 the system has 2 percent structural damping, and the drag parameter of 0.006 is seen to cause very little reduction in the response spectrum between 1 and 10 cps. The effects of structural damping on the amount of reduction in response caused by the hydrodynamic drag are to be expected, since the drag force is a function of the oscillator velocity, \dot{x}_s , and this velocity is a function of the amount of structural damping in the system.

In the high frequency region, response spectra for "no-drag" oscillators typically show the pseudo-acceleration approaching the maximum ground acceleration, $\ddot{x}_{g \max}$. Response spectra in the high frequency region for the oscillators with nonlinear hydrodynamic force exhibit entirely different characteristics, however. In all the response spectra shown, a frequency is reached at which the maximum response quantity $|Z|_{\max}$ for the oscillator with

drag exceeds that for the "no-drag" oscillator. In fact, for the systems with larger values of the drag parameter, the quantity $|Z|_{\max}$ is seen to approach a relatively constant value. The magnitude of this high frequency "tail" in the spectrum can be estimated as follows:

Consider an undamped system with spring stiffness so great that

$$\dot{x}_s \approx \dot{x}_g \quad \ddot{x}_s \approx \ddot{x}_g$$

The forces on the oscillator are

$$F_{\text{spring}} = F_{\text{inertia}} + F_{\text{drag}}$$

$$F_{\text{spring}} = M\ddot{x}_s + K_D \dot{x}_s |\dot{x}_s|$$

or,

$$F_{\text{spring}} \approx M\ddot{x}_g \pm K_D (\dot{x}_g)^2$$

Since the drag parameter

$$\frac{K_D \ddot{x}_{g \max}}{K}$$

is held constant, K_D must increase as the spring stiffness K increases, so a frequency will be reached at which the inertia force can be neglected with respect to the drag force. If the inertia force is neglected, then

$$(F_{\text{spring}})_{\max} \approx K_D (\dot{x}_{g \max})^2$$

And

$$|Z|_{\max} = \frac{(F_{\text{spring}})_{\max}}{K} \approx \frac{K_D}{K} (\dot{x}_{g \max})^2 = \left(\frac{K_D \ddot{x}_{g \max}}{K} \right) \left(\frac{\dot{x}_{g \max}^2}{\ddot{x}_{g \max}} \right) \quad (2.4)$$

A comparison of $|Z|_{\max}$ obtained at high frequencies by the numerical integration of Eq. 2.1 with $|Z|_{\max}$ computed from Eq. 2.4 is shown in Table 2.2 for all systems and base disturbances considered. A study of the data presented in Table 2.2 shows that, particularly for the earthquake records, the high frequency tail of the deformation response spectrum can be satisfactorily estimated by the use of Eq. 2.4.

When an acceleration record is integrated numerically in order to obtain the velocity and displacement records, the integration is done from time point to time point in the record. This double integration yields the values of $\dot{x}_{g \max} = 12.79$ in./sec and $x_{g \max} = 8.24$ inches for the El Centro record as shown in Table 1.1. However, if the acceleration record is integrated to find the ground velocity and displacement at some time point which is between time points in the acceleration record, linear interpolation of the acceleration record must be performed in order to obtain the acceleration quantity necessary to compute the ground velocity and displacement at the intermediate time point. This interpolation introduces small errors into the acceleration, which in turn introduces slightly larger errors into the ground velocity which in turn introduces even larger errors into the ground displacement computed at the intermediate time point.¹⁶ It was found that, when using the very small time increments necessary for stability and convergence in the numerical integration of the equation of motion at high frequencies (above about 8 cps), the interpolation of the El Centro acceleration record introduced errors into the magnitude of \dot{x}_g such that $\dot{x}_{g \max}$ was found to be about 14.0 in./sec in lieu of the value 12.79 in./sec previously obtained, even though double precision was used in all calculations. In order

to achieve comparability of results in the comparison of $|Z|_{\max}$ estimated from Eq. 2.4 and $|Z|_{\max}$ obtained at high frequencies from the integration of the equation of motion, $\dot{x}_{g \max} = 14.0$ in./sec is used in Eq. 2.4 to obtain the results shown in Table 2.2 for $K_D \ddot{x}_{g \max} / K = 0.006$ and 0.08.

2.3 Linearization of the Drag Force

It was seen in Chapter 1 that the use of the normal mode method to solve Eq. 1.3 depends on the ability to linearize the nonlinear hydrodynamic force vector $[K_D] \{\dot{x}_s |\dot{x}_s|\}$ in a satisfactory manner. The linearization of the hydrodynamic drag force in the single degree of freedom system is investigated in this section. It is desirable to replace the nonlinear drag force, $K_D \dot{x}_s |\dot{x}_s|$, in Eq. 2.1 by a linear drag force, say, $K_{DL} \dot{x}_s$, which will yield the same maximum response in the system. Consider the work done by the two forces:¹⁵

$$\text{Work done by the nonlinear drag force over a period of time} = \int_0^t (K_D \dot{x}_s |\dot{x}_s|) (\dot{x}_s) dt$$

$$\text{Work done by a linear drag force over a period of time} = \int_0^t (K_{DL} \dot{x}_s) (\dot{x}_s) dt$$

Equating the amounts of work done,

$$\int_0^t K_D \dot{x}_s^2 |\dot{x}_s| dt = \int_0^t K_{DL} \dot{x}_s^2 dt$$

$$K_D \langle \dot{x}_s^2 |\dot{x}_s| \rangle = K_{DL} \langle \dot{x}_s^2 \rangle$$

$$K_{DL} = K_D \left(\frac{\langle \dot{x}_s^2 |\dot{x}_s| \rangle}{\langle \dot{x}_s^2 \rangle} \right) \quad (2.5)$$

(The symbol $\langle \rangle$ denotes the average value of the quantity enclosed over the time of the response of the oscillator.) This expression is the same expression used by other investigators⁶⁻⁹ to linearize a nonlinear force. With the nonlinear drag force replaced by an "equivalent" linear drag force, Eq. 2.1 becomes,

$$\begin{aligned} M\ddot{Z} + C_S\dot{Z} + KZ &= -M\ddot{x}_g - K_{DL}\dot{x}_s \\ M\ddot{Z} + C_S\dot{Z} + K_{DL}\dot{Z} + KZ &= -M\ddot{x}_g - K_{DL}\dot{x}_g \end{aligned} \quad (2.6)$$

or,

$$\ddot{Z} + 2\beta_S\omega\dot{Z} + 2\beta_h\omega\dot{Z} + \omega^2Z = -\ddot{x}_g - 2\beta_h\omega\dot{x}_g \quad (2.7)$$

where,

$$\beta_h = \frac{K_{DL}}{2M\omega} = \text{equivalent linear hydraulic damping ratio}$$

It now remains to investigate how the maximum response in the equivalent linear system compares with the maximum response in the actual nonlinear system.

Equation 2.6 is solved numerically for $|Z|_{\max}$ using a linear drag factor K_{DL} which is linearized in accordance with Eq. 2.5 for the single degree of freedom oscillator subjected to the series representation of the base disturbance. The quantities $\langle \dot{x}_s^2 | \dot{x}_s | \rangle$ and $\langle \dot{x}_s^2 \rangle$ necessary for the linearization were obtained from the integration of the nonlinear equation of motion for the same set of conditions. The results are plotted on Figs. 2.8 and 2.9, and it is seen that, for this base disturbance, the linearization is very good until the high frequency tail begins to appear. This might have been expected,

since a linearization of a weak nonlinearity would normally be better than a linearization of a strong nonlinearity, and the high frequency tail is the result of the nonlinear hydrodynamic drag force becoming quite strong and dominant in Eq. 2.1.

A similar set of calculations is made for the El Centro earthquake. The response spectra for K_D and K_{DL} are shown in Fig. 2.10 for $\beta_s = 0.02$ and $K_D \ddot{x}_{g \max} / K = 0.50$. It is seen from this figure that the linearization for the earthquake motion, while not quite as good as the linearization for the series representation of the base motion, is still reasonably good up until the high frequency tail of the spectrum is reached. A comparison of $|Z|_{\max}$ computed for the nonlinear drag system with $|Z|_{\max}$ for the linear drag system is shown in Figs. 2.11 through 2.13 for all of the variables considered. It is seen from a study of these figures that the maximum response of the linear system is close to the maximum response of the nonlinear system until the high frequency region is reached. The figures further indicate that the linearized response is slightly on the conservative side of the actual response until the high frequency region is reached. The accuracy of the linearization in the high frequency region is expected to become poor as the nonlinearity is becoming more and more dominant in the system, and thus the linearization becomes less and less equivalent. However, Eq. 2.4 permits a fairly good estimate to be made of the maximum relative displacement in the high frequency region.

Since the linearization of the drag force in Eq. 2.1 is seen to yield a slightly conservative maximum response at frequencies below the beginning of the high frequency tail in the response spectrum, a method of

estimating the linear drag factor K_{DL} from the known nonlinear drag factor K_D is now developed for earthquake motions. A study of Eq. 2.5 shows that two velocity quantities, $\langle \dot{x}_s^2 |\dot{x}_s| \rangle$ and $\langle \dot{x}_s^2 \rangle$ are necessary in order to linearize the drag force and, since these quantities are actual response quantities of the nonlinear system, they cannot be calculated a priori. A series of computations is made in which the quantity

$$\frac{\langle \dot{x}_s^2 |\dot{x}_s| \rangle}{\langle \dot{x}_s^2 \rangle}$$

is computed for the actual, nonlinear oscillator subjected to the El Centro earthquake. The results are shown in Figs. 2.14 through 2.16. From these figures it is seen that, for the range of variables studied, if the quantity

$$\frac{\langle \dot{x}_s^2 |\dot{x}_s| \rangle}{\langle \dot{x}_s^2 \rangle}$$

is estimated as

$$\frac{\langle \dot{x}_g^2 |\dot{x}_g| \rangle}{\langle \dot{x}_g^2 \rangle}$$

for the particular earthquake considered, then this estimated value will be less than the actual

$$\frac{\langle \dot{x}_s^2 |\dot{x}_s| \rangle}{\langle \dot{x}_s^2 \rangle}$$

for all frequencies except low frequencies. Using the value of

$$\frac{\langle \dot{x}_g^2 |\dot{x}_g| \rangle}{\langle \dot{x}_g^2 \rangle}$$

in Eq. 2.5 to linearize the drag term results in a value of K_{DL} which is less than the value of K_{DL} which would result from using the actual oscillator velocity quantities. When this lower value of K_{DL} is converted into the linear hydraulic damping ratio, β_h , shown in Eq. 2.7, the value of β_h is less than the actual value of β_h which would be computed had the actual oscillator velocity terms been available for use in Eq. 2.5. In other words, linearizing the drag term by using

$$\frac{\langle \dot{x}_g^2 |\dot{x}_g| \rangle}{\langle \dot{x}_g^2 \rangle}$$

in Eq. 2.5 leads to a conservative value of K_{DL} which, in turn, leads to a conservative value of the maximum response in all except the low frequency region and the high frequency tail region of the spectrum. The unconservative nature of K_{DL} in the low frequency region when computed from the ground velocity terms is reasonable to expect, however, as the amount of hydraulic damping is dependent on the velocity response of the oscillator, and very soft (low frequency) systems have little velocity response, so the amount of hydraulic damping should approach zero as the system becomes softer and softer. Figures 2.14 through 2.16 further show that, for a system with given drag characteristics, the linear drag factor K_{DL} estimated by using the quantity

$$\frac{\langle \dot{x}_g^2 |\dot{x}_g| \rangle}{\langle \dot{x}_g^2 \rangle}$$

becomes less conservative as the amount of structural damping increases and as the amount of nonlinear drag increases. The linear drag factor estimated in this manner does not become unconservative (except in the low frequency region) for the range of variables studied.

The amount of conservatism introduced by the use of

$$\frac{\langle \dot{x}_g^2 |\dot{x}_g| \rangle}{\langle \dot{x}_g^2 \rangle}$$

in linearizing the drag factor, K_D , is seen in Figs. 2.17 through 2.19. In these figures, the spectrum for the linear drag solution is seen to be conservative up until the high frequency tail begins. The linearized spectra were found to be slightly unconservative, as expected, in the low frequency region, but the scale of the figures is such that this unconservatism cannot easily be seen. The use of Eq. 2.4, repeated here for convenience,

$$|Z|_{\max} = \left(\frac{K_D}{K}\right)(\dot{x}_{g \max})^2 = \left(\frac{K_D \ddot{x}_{g \max}}{K}\right)\left(\frac{\dot{x}_{g \max}^2}{\ddot{x}_{g \max}}\right) \quad (2.4)$$

is also seen to provide a very good estimate of the nonlinear drag spectrum in the high frequency region. At the point in the spectrum at which the high frequency tail just begins to appear, the intersection of the linear drag spectrum with the estimate of the high frequency tail provided by Eq. 2.4 is seen to be slightly unconservative. The amount of unconservatism in this transition "saddle" to the high frequency tail is reduced as the amount of nonlinear drag in the system increases. It is seen from the figures that, while linearizing the drag force by the relation,

$$K_{DL} = K_D \left(\frac{\langle \dot{x}_g^2 |\dot{x}_g| \rangle}{\langle \dot{x}_g^2 \rangle} \right) \quad (2.8)$$

yields conservative results in the mid-frequency region of the spectrum, the degree of conservatism is not so great as to be considered too conservative.

The presence of the nonlinear hydrodynamic drag force has been seen to cause a reduction in $|Z|_{\max}$ from that computed for the "no-drag" oscillator at a given frequency, up until the high frequency tail region is reached. A measure of how much of this reduction is accounted for in the computation of $|Z|_{\max}$ for the system with linear drag (linearized by the ground velocity) is seen in Fig. 2.20. The ordinate in the figure is the ratio of the reduction (from the "no-drag" case) in $|Z|_{\max}$ when the actual nonlinear drag force is used to the reduction (again, from the "no-drag" case) in $|Z|_{\max}$ when the drag force has been linearized by the ground velocity terms. In Fig. 2.20, values of the ordinate greater than 1 represent unconservative results. The unconservative nature of the linearization in the low frequency region and the high frequency tail region is noted. While the linearization of low-drag systems is seen to account for less than 50 percent of the actual reduction in $|Z|_{\max}$ in many cases, the actual reduction for low-drag systems is quite small itself, as seen in Fig. 2.17. It is further seen from the figure that more of the reduction in $|Z|_{\max}$ is accounted for in the high-drag systems than in the low-drag systems.

Figures 2.17 through 2.20 show a measure of the amount of conservatism introduced in $|Z|_{\max}$ by using the ground velocity characteristics to linearize the drag force when the structural damping ratio, β_s , is 0.02. For systems with less structural damping, the amount of conservatism will be slightly greater, and for systems with more structural damping the amount of conservatism will be slightly less.

2.4 Linear Hydraulic Damping

The preceding section of this chapter has demonstrated that the drag factor K_D can be linearized in a manner which yields slightly conservative values of $|Z|_{\max}$ over a wide range of frequencies in the response spectrum. The linearized drag factor, K_{DL} , can be converted into a linear hydraulic damping ratio, β_h , as shown by Eq. 2.7, which is repeated here for convenience.

$$\ddot{Z} + 2\beta_s \omega \dot{Z} + 2\beta_h \omega \dot{Z} + \omega^2 Z = -\ddot{x}_g - 2\beta_h \omega \dot{x}_g \quad (2.7)$$

Equation 2.7 is seen to have the same form as Eq. 1.12 with the exception of the coefficients of the forces on the right side of the equation. Since the solution of Eq. 1.12 was shown in Chapter 1 to be necessary in order to use the normal mode method of solution for the response of the multi-degree of freedom model, the effects of β_h on the solution of Eq. 2.7 will now be investigated.

Equation 2.7 is solved numerically for $|Z|_{\max}$ for all four earthquakes with values of β_s ranging from 0 to 0.10 and values of β_h ranging from 0 to 0.10. These ranges of β_s and β_h are considered to be inclusive of all reasonable values of these variables for the type of structure considered in this thesis. The results of the computations are shown as response spectra in Figs. 2.21 through 2.24. These response spectra are seen to have the same general shape as spectra for an oscillator without hydraulic damping until the high frequency region is reached. It should be noted that a high frequency tail also appears in the spectra for systems with equivalent linear hydraulic damping. The magnitude of this tail can be shown to approach

$(\frac{2\beta_h}{\omega})(\dot{x}_{g \max})$ from above. However, since the equivalent linearization of the nonlinear hydrodynamic drag force has already been shown to break down as the drag force becomes more dominant in the solution at high frequencies, an estimate of $|Z|_{\max}$ in the high frequency tail region of the spectrum for a given system can best be made by the use of Eq. 2.4.

Newmark et al.^{11,13,14} construct an idealized representation of the single degree of freedom response spectrum for an oscillator without drag forces by using amplification factors for displacement, velocity, and acceleration. These amplification factors are multiplied by the corresponding maximum ground motion quantity in order to obtain an idealized spectrum for an earthquake motion of known (or assumed) values of $x_{g \max}$, $\dot{x}_{g \max}$, and $\ddot{x}_{g \max}$. If amplification factors can be developed for the response spectrum of the system with equivalent linear hydraulic damping when β_s and β_h are known, and the high frequency tail of the spectrum for the actual nonlinear system is estimated from Eq. 2.4, then an idealized response spectrum can be constructed for a given set of conditions for the oscillator with nonlinear hydrodynamic drag forces.

During the course of establishing the amplification factors necessary for the construction of idealized response spectra for systems with linear hydraulic damping ratios (Eq. 2.7), it was found that, within the range of variables studied, the amount of total linear damping, $\beta_s + \beta_h$, is the important factor controlling the response quantity $|Z|_{\max}$ throughout the spectrum except for the high frequency region. Comparisons of $|Z|_{\max}$ computed from Eq. 2.7 at 31 frequencies from 0.04 cps to 15 cps were made for all four

earthquake records for total damping ratios equal to .02, .05, .07, .10, .12, and .15 with the damping being distributed between structural and hydraulic as shown in Table 2.3. The comparison showed that, up to the beginning of the high frequency tail in the spectrum, for a given value of the total damping ratio, $|Z|_{\max}$ computed for the first distribution of β_s and β_h was within 5 percent of $|Z|_{\max}$ computed for the second distribution of β_s and β_h . Further, the great majority of the comparisons revealed a difference of less than 2 percent between $|Z|_{\max}$ computed for the two different distributions of damping at a given value of the total damping ratio. The ratio

$$\frac{|Z|_{\max} \text{ for } \beta_s = A, \beta_h = B}{|Z|_{\max} \text{ for } \beta_s = B, \beta_h = A}$$

was found to be sometimes greater than 1 and sometimes less than 1, indicating that at least a small part of the difference may be the result of the convergence criterion (0.1 percent) used in the numerical integration procedure.

A comparison of $|Z|_{\max}$ when $\beta_s = 0.00$ and $\beta_h = 0.15$ with $|Z|_{\max}$ when $\beta_s = 0.15$ and $\beta_h = 0.00$ was made for each of the four earthquakes considered. It was found that, for frequencies up to the beginning of the high frequency tail of the spectrum, the value of $|Z|_{\max}$ computed for the first distribution of total damping was not always within 5 percent of the value of $|Z|_{\max}$ computed for the second distribution of total damping. Most of the comparisons differed by less than 10 percent, but a few showed differences on the order of 15 percent.

The conclusion to be drawn is that, for frequencies up to the beginning of the high frequency tail region, $|Z|_{\max}$ computed from Eq. 2.7 is

dependent upon the total linear damping in the system, and not the distribution of damping between structural damping and equivalent linear hydraulic damping for values of β_h up to and including 0.10. Thus, the use of the amplification factors published in Ref. 14, and included in this thesis as Table 2.4, is a valid and proper method of constructing a portion of an idealized response spectrum for the single degree of freedom oscillator with drag characteristics.

The scale of the response spectra shown in Figs. 2.21 through 2.24 is so small that the conclusion is difficult to see from the figures. For illustrative purposes, a comparison of response spectra for $\beta_t = .07$ is shown in Fig. 2.25 for the Ferndale earthquake. It is readily seen from this figure that, up until the high frequency tail begins to appear, the spectral values are a function of the total amount of linear damping in the system, and the relative distribution of the total damping between structural and hydraulic has little effect.

2.5 Idealized Elastic Deformation Response Spectrum

It was mentioned in Section 1.5.1 that the characteristic shape of response spectra for earthquake motions has led to the development of amplification factors from which an idealized response spectrum can be constructed for a given set of conditions. The idealized spectrum permits an estimate to be made of the maximum response of the system. This response quantity may then be used as a modal response quantity for a particular mode of a multi-degree of freedom system, and the various modal response quantities may then be combined in some manner to yield an approximate solution for the multi-degree of freedom system as outlined in Chapter 1.

The principles and concepts developed in Sections 2.2 through 2.4

are summarized here for the reader in such a manner as to demonstrate the construction of an idealized response spectrum for a single degree of freedom system, with nonlinear hydrodynamic drag forces, subjected to a strong-motion earthquake of the type used in this thesis.

To construct an idealized deformation response spectrum for a given system:

1. For the system, compute the drag factor, K_D , and the undamped circular natural frequency of the system, ω .
2. Establish the structural damping ratio, β_s , to be used in the system. For the type of structure discussed in this thesis, a structural damping ratio of between 0.005 (when the stress is below one-quarter of the yield stress) and 0.05 (when the stress is at, or just below, the yield stress) is reasonable to assume.¹⁴
3. Select the values of $x_{g \max}$, $\dot{x}_{g \max}$, $\ddot{x}_{g \max}$ for which the spectrum is to be constructed.
4. Compute the quantity

$$\beta_h = \frac{K_D \left(\frac{\langle \dot{x}_g^2 |\dot{x}_g| \rangle}{\langle \dot{x}_g^2 \rangle} \right)}{2 M \omega}$$

It should be noted from Table 1.1 that the magnitude of

$$\frac{\langle \dot{x}_g^2 |\dot{x}_g| \rangle}{\langle \dot{x}_g^2 \rangle}$$

is approximately one-half the magnitude of $\dot{x}_{g \max}$ for the four earthquakes shown.

5. Enter Table 2.4 with the value of β_s expressed as a percent, obtain the displacement amplification factor, multiply the displacement amplification factor times $x_{g \max}$, and plot the result on tripartite logarithmic graph paper as a displacement line. This is shown as line 1 on Fig. 2.26. The method of linearizing the drag force by using ground velocity characteristics has been shown to be unconservative in the low frequency region. The use of β_s alone means that any hydraulic damping effects in the low frequency region are neglected. This is reasonable, however, because the small amount of velocity response in the low frequency region results in minor amounts of hydraulic damping. Further, as the frequency of the system becomes lower and lower, the amount of damping of any type has little effect on the maximum deformation.
6. Enter Table 2.4 with the amount of total damping ($\beta_s + \beta_h$ as computed above) and obtain velocity and acceleration amplification factors. Multiply the velocity amplification factor times $\dot{x}_{g \max}$ and plot the result as a horizontal line. Multiply the acceleration amplification factor times $\ddot{x}_{g \max}$ and plot the result as an acceleration line. These two lines are shown as lines 2 and 3 on Fig. 2.26.
7. Plot the quantity $(\frac{K_D}{K})(\dot{x}_{g \max})^2$ as a displacement line. This line is shown as line 4 on Fig. 2.26.
8. The envelope formed by the intersection of the four lines plotted is the idealized response spectrum for the system and conditions given.

With the idealized response spectrum constructed as described in (1) through (8) above, an estimate of the maximum response of the system is obtained by entering the figure with the natural frequency of the system and reading $|Z|_{\max}$, pseudo-velocity ($\omega|Z|_{\max}$), or pseudo-acceleration ($\omega^2|Z|_{\max}$). If the characteristics of the system are changed, a new response spectrum should be constructed.

Linear interpolation can be used to obtain amplification factors for values of damping not shown exactly in the table.

2.6 Hydrodynamic Parameters

The hydrodynamic force exerted by the fluid on the mass of the oscillator as it moves through the fluid is represented by Morison's formula, Eq. 1.2 as described in Section 1.2. This force expression contains two dimensionless, empirical coefficients, C_I and C_D , which are dependent upon the response of the oscillator for their magnitude. Many investigators have undertaken studies to determine the value of these coefficients under various conditions. The results of some of these investigations are published and discussed in Refs. 17 and 18. Morison's investigations² show a variation of the drag coefficient C_D with Reynolds Number, which is related to the relative velocity between the mass and the fluid. Keulegan and Carpenter¹⁹ have shown a variation in both coefficients with a dimensionless period parameter which can be interpreted as the ratio of the relative displacement between the mass and the fluid to the pile diameter for forces against circular piles. Laird²⁰ has shown that the two coefficients may vary greatly for flexible oscillating cylinders. Evaluation of the two coefficients for oscillatory motion is further

complicated by turbulence associated with eddy formations on either side of the mass as it moves back and forth through the fluid.¹⁸ This thesis considers that the drag factor, K_D , and the added mass of the oscillator, m' , remain constant throughout the entire time history of the oscillator motion. The values of K_D and m' used in the calculations in this thesis do not presuppose any specific values for C_I and C_D , except as values were assigned to these coefficients by Burke⁴ in the formulation of properties of a series of offshore towers which are used as sample structures in a later chapter. However, the designer of an actual offshore structure, whose physical properties and dimensions will eventually be known, must have a means of estimating the coefficients C_I and C_D with reasonable accuracy in order to analyze the response of his structure. Further, investigators who are engaged in experimental research on the response of submerged or partially submerged bodies to earthquake excitation should have a method of estimating the coefficients in order that the experimental work may be conducted over a reasonable range of variables. Since C_I and C_D are most commonly considered to be dependent upon the relative motion between the mass and the fluid, x_s and \dot{x}_s in the case of the mass moving through the fluid at rest, a method is developed in this section for estimating the response quantities $|x_s|_{\max}$, $\langle |x_s| \rangle$, $|\dot{x}_s|_{\max}$, $\langle |\dot{x}_s| \rangle$ (hereinafter called hydrodynamic parameters) for strong motion earthquakes of the type considered in this thesis.

Consider the equations

$$M\ddot{Z} + C_S\dot{Z} + K_{DL}\dot{Z} + KZ = -M\ddot{x}_g - K_{DL}\dot{x}_g \quad (2.6)$$

and

$$\ddot{Z} + 2\beta_s \omega \dot{Z} + 2\beta_h \omega \dot{Z} + \omega^2 Z = -\ddot{x}_g - 2\beta_h \omega \dot{x}_g \quad (2.7)$$

is which the nonlinear drag term K_D has been linearized in the manner discussed previously. In the response computation, the quantities x_s and \dot{x}_s may be computed at each time point from the relations

$$x_s = Z + x_g$$

and

$$\dot{x}_s = \dot{Z} + \dot{x}_g$$

Equation 2.7 is solved numerically for values of β_s and β_h which are reasonable to expect for the type of system considered, and again it is found that the hydrodynamic parameters $|x_s|_{\max}$, $\langle |x_s| \rangle$, $|\dot{x}_s|_{\max}$, and $\langle |\dot{x}_s| \rangle$ are affected by the total amount of damping in the system and not by the distribution of damping between structural and hydraulic. Comparisons were made of the hydrodynamic parameters when the total amount of damping was equal to 2, 5, 7, 10, 12 and 15 percent of critical with the damping being distributed between β_s and β_h as shown in Table 2.3. The difference in a hydrodynamic parameter at a given value of total damping ratio is within two to five percent for the different distributions of damping between β_s and β_h , thus indicating that, if the amount of total damping can be estimated, the parameter can be estimated. The comparison holds true for all four hydrodynamic parameters.

Spectra for the hydrodynamic parameters $|x_s|_{\max}$, $\langle |x_s| \rangle$, $|\dot{x}_s|_{\max}$, and $\langle |\dot{x}_s| \rangle$ are shown in Figs. 2.27 through 2.30 for total damping ratios up to ten percent. The general shape of the spectra indicates that an idealized spectrum may be able to be constructed for a given set of conditions in much

the same manner as an idealized deformation response spectrum is constructed. Each hydrodynamic parameter spectrum was plotted, a smooth spectrum which approximated the actual spectrum was established by the author, and appropriate amplification factors were computed for each of the four earthquakes considered. These amplification factors were then averaged in a mean square sense to yield the amplification factors listed in Table 2.5. The use of these amplification factors to construct idealized spectra for the hydrodynamic parameters $|x_s|_{\max}$, $\langle |x_s| \rangle$, $|\dot{x}_s|_{\max}$, and $\langle |\dot{x}_s| \rangle$ is explained in the next section of this chapter.

2.7 Idealized Elastic Hydrodynamic Parameter Response Spectra

The construction of idealized response spectra for the hydrodynamic parameters discussed in Section 2.6 is very similar to the construction of an idealized elastic deformation response spectrum.

2.7.1 Displacement Parameter

To construct an approximate response spectrum for $|x_s|_{\max}$ (or $\langle |x_s| \rangle$) for a given system:

1. Determine the quantities K_D , ω , β_s , and β_h in the same manner as described in Section 2.5.
2. Enter the appropriate section of Table 2.5 with the value of β_s expressed as a percent and obtain the displacement amplification factor. Multiply this amplification factor times $x_{g \max}$ (or $\langle x_g \rangle$) and plot the result as a displacement line on tripartite logarithmic paper. This line is shown as line 1 on Fig. 2.31.

3. Enter the appropriate section of Table 2.5 with the amount of total damping ($\beta_s + \beta_h$) and obtain the velocity amplification factor. Multiply this amplification factor times $\dot{x}_{g \max}$ (or $\langle |\dot{x}_g| \rangle$) and plot the result as a velocity line as shown by line 2 on Fig. 2.31.
4. Plot the value $x_{g \max}$ (or $\langle |x_g| \rangle$) as a displacement line. This is shown as line 3 on Fig. 2.31.
5. The envelope formed by the intersection of these three lines is an idealized spectrum for $|x_s|_{\max}$ (or $\langle |x_s| \rangle$).

2.7.2 Velocity Parameter

To construct an idealized response spectrum for $|\dot{x}_s|_{\max}$ (or $\langle |\dot{x}_s| \rangle$) for a given system:

1. Obtain and use displacement and velocity amplification factors from the appropriate section of Table 2.5 exactly as described above for the construction of an idealized spectrum for a displacement hydrodynamic parameter. The resulting lines are shown as lines 1 and 2 on Fig. 2.32.
2. Enter the appropriate section of Table 2.5 with the amount of total damping ($\beta_s + \beta_h$) and obtain the acceleration amplification factor. Multiply this amplification factor times $\ddot{x}_{g \max}$ (or $\langle |\ddot{x}_g| \rangle$) and plot the result as an acceleration line. This is shown as line 3 on Fig. 2.32.
3. Plot the value of $\dot{x}_{g \max}$ (or $\langle |\dot{x}_g| \rangle$) as a velocity line as shown by line 4 on Fig. 2.32.

4. The envelope formed by the intersection of the four lines is an idealized response spectrum for $|\dot{x}_s|_{\max}$ (or $\langle |\dot{x}_s| \rangle$).

Linear interpolation can be used to obtain amplification factors for values of damping not shown exactly in the table.

Unfortunately, no reasonably consistent ratios were found to exist between $\langle |x_g| \rangle$, $\langle |\dot{x}_g| \rangle$, $\langle |\ddot{x}_g| \rangle$ and other ground motion quantities such as $x_{g \max}$, $\dot{x}_{g \max}$, $\ddot{x}_{g \max}$ for the four earthquakes considered. Thus, the designer of an offshore structure who wishes to estimate the hydrodynamic parameters $\langle |x_s| \rangle$ and $\langle |\dot{x}_s| \rangle$ will have to obtain the values of $\langle |x_g| \rangle$, $\langle |\dot{x}_g| \rangle$, and $\langle |\ddot{x}_g| \rangle$ from processing an actual earthquake record or estimating them using the values shown in Table 1.1 as a guide. The range of the ratios between $\langle |x_g| \rangle$, $\langle |\dot{x}_g| \rangle$, $\langle |\ddot{x}_g| \rangle$ and $x_{g \max}$, $\dot{x}_{g \max}$, $\ddot{x}_{g \max}$ are repeated here for the convenience of the reader.

<u>Ratio</u>	<u>Lowest Value</u>	<u>Highest Value</u>
$\frac{\langle x_g \rangle}{x_{g \max}}$	0.194	0.385
$\frac{\langle \dot{x}_g \rangle}{\dot{x}_{g \max}}$	0.124	0.167
$\frac{\langle \ddot{x}_g \rangle}{\ddot{x}_{g \max}}$	0.084	0.185

It should be noted that the idealized spectra for hydrodynamic parameters become less descriptive of the oscillator response at very low frequencies, about 0.08 cps and less for the four earthquakes used in the computations. This is to be expected, since the quantities $|x_s|_{\max}$, $\langle |x_s| \rangle$, $|\dot{x}_s|_{\max}$, and $\langle |\dot{x}_s| \rangle$ become quite small for very soft (low frequency) systems.

2.8 Inelastic Response Spectra

In this section, the effects of the nonlinear hydrodynamic drag force on the response of the oscillator in the inelastic range are investigated. Figure 2.33 shows the resistance-deformation relationship of the spring in a system with elasto-plastic spring characteristics. The characteristics of the elasto-plastic system are an initial elastic region, a constant plastic resistance limit, and an elastic unloading region. The unloading portion is considered to have the same slope as the initial elastic curve, and the unloading is elastic until yielding is reached in the opposite direction.¹² The yield point deformation is denoted by Z_y , and the absolute maximum displacement of the mass relative to the base is denoted by $|Z|_{\max}$. The yield resistance is denoted by R_y . The ductility factor, μ , is defined as

$$\mu = \frac{|Z|_{\max}}{Z_y} \quad (2.9)$$

and expresses the maximum deformation of the inelastic system in terms of its yield point deformation. With μ defined in this manner, the maximum deformation of the system is μZ_y , the maximum elastic deformation is Z_y , and the maximum inelastic deformation is $(\mu - 1)Z_y$. A variety of calculations of the response of inelastic systems has been made and reported in the literature.¹¹⁻¹⁴ The results of the calculations are conveniently displayed in the form of response spectra in much the same manner as response spectra for elastic systems are displayed. For elasto-plastic systems, response spectra can be plotted for constant values of the ductility factor, μ , and when the plot is made in terms of the elastic component of the displacement,

the accelerations are properly presented.¹² In this type of spectrum representation, the pseudo-velocity quantity plotted is ωZ_y . Elasto-plastic response spectra for systems with $\beta_s = 0.02$, $K_D \ddot{x}_{g \max} / K = 0.00$ (no drag), subjected to the El Centro earthquake are shown in Fig. 2.34 for values of $\mu = 1$ (elastic case) to $\mu = 4$. In these spectra, the total deformation of the system can be determined by reading the displacement quantity, which is Z_y , and then using the relationship

$$|Z|_{\max} = \mu Z_y$$

In the low frequency range of the spectra shown in Fig. 2.34, the total deformation is approximately the same for the elasto-plastic systems as for the elastic systems. In the high frequency region, the pseudo-acceleration is approximately the same for the elasto-plastic systems as for the elastic system. In the mid-frequency region, some generalizations have been made regarding the amount of reduction in yield level for different values of μ , but more detailed generalizations are still under study.¹²

Elasto-plastic deformation response spectra for systems with non-linear hydrodynamic drag forces subjected to the El Centro earthquake are shown in Figs. 2.35 through 2.37. Again, in the low frequency region, the total deformation is approximately the same for the elasto-plastic systems as for the elastic system. In the mid-frequency region, the spectra have the same general shape as do the elasto-plastic spectra for systems without the drag forces, but no quantification of the results has been made. Further study in the direction of establishing rules for the construction of idealized elasto-plastic response spectra in this frequency region is clearly indicated.

In the high frequency region, the elasto-plastic spectra for the systems with the lowest value of the drag parameter (0.006) approach approximately the same values in the high frequency tail as the elastic spectrum does. However, for the systems with the greatest value of the drag parameter (0.50), the high frequency tails of the elasto-plastic spectra approach values which are reduced by as much as 50 percent from the elastic case. In other words, there is a reduction in the magnitude of the elasto-plastic high frequency tail from that obtained in the elastic case, and the amount of the reduction is a function of the amount of nonlinear hydrodynamic drag in the system. In the systems with a small amount of drag, the reduction is very slight, and may not merit much consideration, but the reduction for high drag systems can be significant. A study of the numerical results obtained in this investigation revealed that, for the spectra with $\beta_s = 0.02$, $K_D \ddot{x}_{g \max} / K = 0.50$, values of μ up to 4 and the El Centro earthquake, the factor $\frac{\mu}{2\mu - 1}$ applied to the elastic case high frequency tail yields a satisfactory estimate of the elasto-plastic high frequency tail (see Table 2.6). The reader is cautioned that this expression for the reduction factor is applicable only to the specific systems and earthquake used, and is not to be extended to other conditions.

In order to compare the effects of the nonlinear hydrodynamic drag force on the elasto-plastic response spectra, spectra are plotted for given values of structural damping ratio, β_s , and ductility factor, μ , for systems with varying amounts of drag subjected to the El Centro earthquake. These comparisons are shown in Figs. 2.38 through 2.40. These figures show that, for a small ductility factor ($\mu = 1.5$), increasing amounts of nonlinear hydrodynamic drag reduce the value of the yield deformation, Z_y , for a range of

frequencies between low frequencies and the beginning of the high frequency tail. This means that the maximum response of the system with high drag forces is less than the maximum response of the system with lower drag forces, or, the drag forces tend to produce a damping effect on the maximum deformation of the spring in the mid-frequency region of the spectrum. For example, in Fig. 2.38, at a frequency of 1 cps, and the highest value of the dimensionless drag parameter used (0.50), Z_y is only about 50 percent of the value of Z_y for the system with no drag. However, as the ductility factor μ increases, the effects of the nonlinear hydrodynamic drag force become less and less noticeable in the mid-frequency range. In Fig. 2.40, with $\mu = 4$, the value of Z_y for the highest drag system is about 90 percent of the value of Z_y for the system with no drag at a frequency of 1 cps. This is reasonable to expect, since the velocity of the oscillator, \dot{x}_s , can be expected to be smaller during plastic deformation of the spring than during elastic deformation of the spring, and the magnitude of the drag force is a function of the oscillator velocity. It is also to be noted from Fig. 2.40 that it is possible for Z_y in the case of the system with drag to exceed slightly the value of Z_y for the system with no drag at the same frequency (note the response values at frequencies of 0.8 cps and 3.0 cps) in the mid-frequency range. This can result since the maximum response of the elasto-plastic system depends on the entire history of the deformation and the energy absorbed in the spring during plastic deformation as well as the energy dissipated by the damping effects of the fluid surrounding the oscillator.

The significant features of the elasto-plastic response spectra for systems with nonlinear hydrodynamic drag are:

1. The drag does not have much effect on the spectrum in the low frequency region;
2. A high frequency tail does exist, and large amounts of drag can cause significant reductions in Z_y for increasing values of the ductility factor (less significant reductions in Z_y with increasing values of μ for low drag systems);
3. The damping effects of the drag in the mid-frequency region of the spectrum become less pronounced as the ductility factor increases, even for the systems with high drag.

CHAPTER 3

MULTI-DEGREE OF FREEDOM SYSTEMS

3.1 General

In this chapter, the principles developed and discussed in Chapter 2 for the single degree of freedom oscillator are extended to the multi-degree of freedom system. The nonlinear drag forces are linearized in such a manner as to insure the existence of classical normal modes in the equations of motion in order that normal mode superposition may be used as an approximate solution to the problem. The method of linearization is shown to be accurate for a series of five degree of freedom systems which are representative of the type of structure being investigated. A means of estimating the amount of equivalent linear hydraulic damping, using ground motion velocity characteristics, is developed and is shown to yield good results. The construction of an idealized response spectrum for each mode of the multi-degree of freedom system is discussed and described, and sample problems are solved by the superposition of normal mode responses.

3.2 Approximate Solution of the Nonlinear Equations of Motion

In this section, an approximate method of solving the nonlinear equations of motion for the multi-degree of freedom system is developed and shown to yield satisfactory results. Various features of the solution, such as the formulation of the structural damping matrix, the linearization of the drag forces, the superposition of modal responses, and the response of very high frequency modes, are discussed. The transformation of the nonlinear

equations of motion into uncoupled linear modal equations, which was first shown in Chapter 1, is repeated in this section for the convenience of the reader.

3.2.1 Equations of Motion

The equations of motion for the lumped parameter model shown in Fig. 1.1(b) are written in matrix form as Eq. 1.3 and are repeated here to form the basis of the analytical discussion in this section.

$$[M]\{\ddot{Z}\} + [C_S]\{\dot{Z}\} + [K]\{Z\} = -[M]\{\ddot{x}_g\} - [K_D]\{\dot{x}_s|\dot{x}_s|\} \quad (3.1)$$

No structural dampers are shown on the model, but the damping matrix $[C_S]$ can take a variety of forms as will be discussed in later paragraphs. For a given structural system and known earthquake record, response quantities of interest may be obtained by the numerical integration of Eq. 3.1, but this procedure is costly and requires the use of a digital computer. If Eq. 3.1 can be satisfactorily approximated by a system of simultaneous linear differential equations of motion which possess classical normal modes, then a solution can be obtained by the superposition of normal mode solutions. A further approximation can be made by using response spectra to obtain the maximum response in each mode and then combining the modal maxima in some fashion, very much like the approximate modal techniques, using response spectra, which are reported in the literature¹¹⁻¹³ for land-based structures.

In the normal mode method, the vector of a response quantity expressed in one coordinate system, such as the relative displacement between

each node and the base, $\{Z\}$, is transformed into the "normal" coordinate system by the relation

$$\{Z\} = [\phi]\{Y\} \quad (3.2)$$

If the nonlinear drag force were not present, Eq. 3.2 and the orthogonality relationship between $[\phi]$ and $[M]$, $[K]$, and $[C_s]$ could be used to transform Eq. 3.1 into nm (number of modes) uncoupled single degree of freedom equations in the normal coordinate system. If the nonlinear drag force can be converted into an equivalent linear drag force, then the resulting linear differential equations of motion can be transformed into uncoupled single degree of freedom equations of motion in the normal coordinate system as follows: Consider that $[K_D] \{\dot{x}_s | \dot{x}_s|\}$ can be transformed into an equivalent linear force, $[K_{DL}] \{\dot{x}_s\}$ i.e.,

$$[K_D] \{\dot{x}_s | \dot{x}_s|\} \rightarrow [K_{DL}] \{\dot{x}_s\} \quad (3.3)$$

Substitution of Eq. 3.3 into Eq. 3.1 yields,

$$[M]\{\ddot{Z}\} + [C_s]\{\dot{Z}\} + [K]\{Z\} = -[M]\{\ddot{x}_g\} - [K_{DL}]\{\dot{x}_s\} \quad (3.4)$$

Since $\{\dot{Z}\} = \{\dot{x}_s\} - \{\dot{x}_g\}$, Eq. 3.4 can be rewritten as

$$\begin{aligned} [M]\{\ddot{Z}\} + [C_s]\{\dot{Z}\} + [K_{DL}]\{\dot{Z}\} + [K]\{Z\} \\ = -[M]\{\ddot{x}_g\} - [K_{DL}]\{\dot{x}_g\} \end{aligned} \quad (3.5)$$

Substitute Eq. 3.2 into Eq. 3.5 and premultiply the result by $[\phi]^T$

$$\begin{aligned}
[\phi]^T [\bar{M}] [\phi] \{\ddot{Y}\} + [\phi]^T [C_s] [\phi] \{\dot{Y}\} + [\phi]^T [\bar{K}_{DL}] [\phi] \{\dot{Y}\} + [\phi]^T [K] [\phi] \{Y\} \\
= -[\phi]^T [\bar{M}] \{\ddot{x}_g\} - [\phi]^T [\bar{K}_{DL}] \{\dot{x}_g\}
\end{aligned} \tag{3.6}$$

Recall the following definitions from Chapter 1:

$$[\bar{M}^*] = [\phi]^T [\bar{M}] [\phi] = \text{a diagonal modal mass matrix}$$

$$[\bar{C}_s^*] = [\phi]^T [C_s] [\phi] = \text{a diagonal modal structural damping matrix. The form of } [C_s] \text{ which permits this is discussed later.}$$

$$[\bar{K}^*] = [\phi]^T [K] [\phi] = \text{a diagonal modal stiffness matrix}$$

$$[\bar{K}_{DL}^*] = [\phi]^T [\bar{K}_{DL}] [\phi] = \text{a modal linear hydraulic damping matrix which is not necessarily diagonal}$$

$$[\omega^2] = [\bar{M}^*]^{-1} [\bar{K}^*] = \text{a matrix of circular natural frequencies of the system}$$

Substitution of these definitions into Eq. 3.6 yields

$$\begin{aligned}
[\bar{M}^*] \{\ddot{Y}\} + [\bar{C}_s^*] \{\dot{Y}\} + [\bar{K}_{DL}^*] \{\dot{Y}\} + [\bar{K}^*] \{Y\} \\
= -[\phi]^T [\bar{M}] \{\ddot{x}_g\} - [\phi]^T [\bar{K}_{DL}] \{\dot{x}_g\}
\end{aligned} \tag{3.7}$$

At this point, the formulation of the structural damping matrix, $[C_s]$, and the linearization of the drag factor, $[\bar{K}_D]$, will be discussed.

3.2.2 Structural Damping

If the structural damping matrix $[C_s]$ is proportional to the mass

matrix, then $[C_s^*]$ will be diagonal since the natural mode shapes are orthogonal with the mass matrix. This formulation of $[C_s]$ results in modal damping ratios which decrease with increasing natural frequency. This is shown as follows:

Let,

$$[C_s] = \xi [M]$$

then,

$$[\phi]^T [C_s] [\phi] = \xi [\phi]^T [M] [\phi] = \xi [M^*] = [C_s^*] \quad (3.8)$$

Define

$$[M^*]^{-1} [C_s^*] = [2\beta_s \omega] = \xi [I] \quad (3.9)$$

then,

$$\beta_{s_i} = \frac{\xi}{2\omega_{ii}} \quad (3.10)$$

where

β_{s_i} = structural damping ratio in the i th mode

ω_{ii} = circular natural frequency of the i th mode

In a similar manner, it can be shown that, if the structural damping matrix $[C_s]$ is proportional to the stiffness matrix $[K]$, then $[C_s^*]$ is a diagonal matrix in which the modal damping ratios β_{s_i} increase with increasing frequency.

The elements of the structural damping matrix $[C_s]$, can be selected to yield the same structural damping ratio in each mode. It is common practice to assume the same structural damping ratio in all modes in the dynamic

analysis of damped multi-degree of freedom systems.¹² If the modal matrix $[\phi]$ is normalized such that

$$[\phi]^T [M] [\phi] = [I] \quad (\text{a unit matrix}) \quad (3.11)$$

Then

$$[C_s] = [M] [\phi] [C_s^*] [\phi]^T [M] \quad (3.12)$$

And, since

$$[C_s^*] = [M^*] [2\beta_s \omega] \quad (3.13)$$

Equation 3.12 can be written as

$$[C_s] = [M] [\phi] [M^*] [2\beta_s \omega] [\phi]^T [M] \quad (3.14)$$

Thus, it is seen that $[C_s]$ can be formulated in such a manner as to yield modal structural damping ratios which are constant, which increase with increasing mode number, or which decrease with increasing mode number. In the computations reported in this thesis, the structural damping matrix $[C_s]$ is computed in such a way that β_s is the same in all modes.

3.2.3 Linearization of the Drag Force

Foster,⁹ and Malhotra and Penzien⁶ linearize the nonlinear drag forces, $[K_D] \{\dot{x}_s |\dot{x}_s|\}$ by replacing them with a velocity dependent linear force, $[K_{DL}] \{\dot{x}_s\}$ at each node which performs the same amount of work during a period of time as does the nonlinear force at that node. Foster then recognizes that the resulting $[K_{DL}]$ matrix is not orthogonal with the mode shapes and proceeds to solve the equations of motion by a nonclassical mode

approach using complex eigenvalues and eigenvectors. Malhotra and Penzien transform $[K_{DL}]$ into $[\tilde{K}_{DL}]$ and then force $[\tilde{K}_{DL}]$ to be diagonal by means of an iterative process that replaces the nondiagonal matrix with a diagonal matrix which dissipates the same amount of energy over a period of time.

The hydraulic drag forces, whether linear or nonlinear, may be considered to act as dampers, that is, they cause energy to be dissipated as the system oscillates through the fluid. In the approximate solution being developed in this section, the nonlinear dampers in the multi-degree of freedom system are replaced with linear dampers (except for very high frequency modes which are discussed in a later section) which dissipate the same amount of energy over the total system, but do not necessarily preserve the dissipation of energy at each node. Further, the resulting "equivalent" linear damper at each node is made to be proportional to the lumped mass of that node in order that the modal equations of motion will be uncoupled. For an offshore structure with a portion of the structure above the water line as shown in Fig. 1.1(a), this procedure results in a linear hydraulic damper being provided at the level of the top mass where, in fact, no nonlinear hydraulic damper really exists. With this exception, the proportioning of the linear hydraulic dampers in the same ratio as the mass is distributed is a reasonable approach for the type of structure being discussed, since the nonlinear damper is proportional to the projected area of the structure lumped at the node, and the magnitude of the mass at a given node will also be generally proportional to the projected area. The method of linearizing is as follows:

$$\begin{aligned}
 \text{Energy dissipated by nonlinear dampers} &= \sum_{j=1}^{nn} \int_0^t (K_{D_{jj}} \dot{x}_{s_j} |\dot{x}_{s_j}|) (\dot{x}_{s_j}) dt \\
 &= t \sum_{j=1}^{nn} K_{D_{jj}} \langle \dot{x}_{s_j}^2 |\dot{x}_{s_j}| \rangle
 \end{aligned} \tag{3.15}$$

$$\begin{aligned}
 \text{Energy dissipated by equivalent linear dampers} &= \sum_{j=1}^{nn} \int_0^t (K_{DL_{jj}} \dot{x}_{s_j}) (\dot{x}_{s_j}) dt \\
 &= t \sum_{j=1}^{nn} K_{DL_{jj}} \langle \dot{x}_{s_j}^2 \rangle
 \end{aligned} \tag{3.16}$$

where

nn = number of nodes in the system

j = j th node in the system

Equating the energy dissipated,

$$\sum_{j=1}^{nn} K_{D_{jj}} \langle \dot{x}_{s_j}^2 |\dot{x}_{s_j}| \rangle = \sum_{j=1}^{nn} K_{DL_{jj}} \langle \dot{x}_{s_j}^2 \rangle \tag{3.17}$$

It is noted that only the total energy dissipated is preserved and the distribution of the energy dissipation among nodes is not preserved. Now, by forcing the linear dampers to be proportional to the mass matrix,

$$[K_{DL}] = \alpha [M] \tag{3.18}$$

and substituting Eq. 3.18 into Eq. 3.17

$$\alpha = \frac{\sum_{j=1}^{nn} K_{Djj} \langle \dot{x}_{sj}^2 | \dot{x}_{sj} | \rangle}{\sum_{j=1}^{nn} M_{jj} \langle \dot{x}_{sj}^2 \rangle} \quad (3.19)$$

Recall that $[K_{DL}^{\sim}]$ was defined as $[\phi]^T [K_{DL}] [\phi]$. Substituting Eq. 3.18 into this definition,

$$[K_{DL}^{\sim}] = \alpha [\phi]^T [M] [\phi] = \alpha [M^*] \quad (3.20)$$

Substituting Eq. 3.20 into Eq. 3.7 yields

$$\begin{aligned} [M^*] \{\ddot{Y}\} + [C_S^*] \{\dot{Y}\} + \alpha [M^*] \{\dot{Y}\} + [K^*] \{Y\} \\ = [\phi]^T [M] \{-\ddot{x}_g - \alpha \dot{x}_g\} \end{aligned} \quad (3.21)$$

Equation 3.21 represents nn single degree of freedom uncoupled equations of motion in the normal coordinate system.

Before proceeding, the method of linearizing described by Eqs. 3.18 and 3.19 will be tested for accuracy in computing the response of multi-degree of freedom systems to earthquake excitation. A series of five degree of freedom systems, representative of offshore towers in mass, stiffness, and drag distribution, is developed in order to test the linearization technique.

Seven structural systems, consisting of different combinations of mass and stiffness distribution, are considered. Each system is further subdivided into one or more distributions of the drag factor, K_D , at each node. The characteristics of these systems are shown in Table 3.1. In the table, the values shown for the mass at each node are considered to be the total mass at that node, and include the added mass term. The different

distributions of drag factor are labeled L, M, and H in the table, and the column under each of these headings represents the relative magnitude of K_D at each node for the particular distribution shown. For example, drag factor distribution M represents the distribution of K_D at each node as 0, 1, 1, 2, 3 at nodes 1 through 5 respectively. The values of $\Sigma K_D / \Sigma m$ shown in the table for the distributions of drag factor are of sufficient range to span reasonable values of this quantity for actual offshore towers of the type being investigated. The quantity $\Sigma K_D / \Sigma m$ for the four towers reported by Burke and Tighe⁴ range from a low of 0.0034 inches⁻¹ to a high of 0.0054 inches⁻¹. The relative magnitudes of the undamped natural frequencies of the system, normalized to the fundamental frequency, are as shown. In the computations which are discussed in the following paragraphs, one of the natural frequencies is set to a desired value and the fundamental frequency is computed from the ratio of natural frequencies. The value of k_1 is computed from f_1 and the quantity $f_1 / \sqrt{k_1 / m_1}$, then the remaining spring stiffnesses are computed from k_1 and the distribution of k_2 through k_5 . The stiffness matrix $[K]$ for the entire system is then assembled and is a tri-diagonal matrix for the systems shown.

Each of the systems shown in Table 3.1 is subjected to the El Centro earthquake and response quantities are computed by the numerical integration of the equations of motion using the criteria for convergence and time interval described in Chapter 1. For each system, computations of maximum response are made for two values of β_s in each mode, 0.01 and 0.05, and three frequency ranges. The low frequency range, range number 1, is established by setting the fifth natural frequency equal to the frequency at which x_g max

and $\dot{x}_{g \max}$ intersect when plotted on tripartite logarithmic paper. The mid-frequency range, range number 2, is established by setting the fundamental frequency equal to the frequency at which $x_{g \max}$ and $\dot{x}_{g \max}$ intersect. The high frequency range, range number 3, is established by setting the fundamental frequency equal to the frequency at which $\dot{x}_{g \max}$ and $\ddot{x}_{g \max}$ intersect when plotted on tripartite logarithmic paper. The maximum displacement of each node relative to the base, $\{|Z|_{\max}\}$, is computed. The results of the computations are shown in Tables 3.2 through 3.27. The column in the tables titled "No Drag" shows the results of the computations when $[K_D]$ is set to zero. The column in the tables titled "Actual Drag" shows the results of the computations when $[K_D]$ is computed from the values shown in Table 3.1, thus nonlinear hydrodynamic drag forces, $[K_D]\{\dot{x}_s|\dot{x}_s|\}$, are acting on the structure. In the computations for the "Actual Drag" systems, the time averages $\{\langle \dot{x}_s^2 |\dot{x}_s| \rangle\}$ and $\{\langle \dot{x}_s^2 \rangle\}$ are collected. These time averages are then used to linearize the drag factor and set it to be proportional to the mass matrix as prescribed by Eqs. 3.18 and 3.19. Equation 3.4, using the linear drag factor matrix just computed, is then integrated numerically to obtain the response quantity $\{|Z|_{\max}\}$. The results of this integration are labeled "Case 1" in the tables of results. The column labeled "Case 1/Actual Drag" in Tables 3.2 through 3.27 represents the comparison of the solution of Eq. 3.1 with the solution of Eq. 3.4. A study of these results reveals that the linearization technique described by Eqs. 3.18 and 3.19 is extremely accurate. The difference between the linear and the nonlinear results is less than 6 percent (with one exception--system 1M, $\beta_s = 0.01$, node 3, mid-frequency range) and is less than 2 percent in the majority of the cases.

The maximum distortion between two adjacent nodes is also computed for both the linear and the nonlinear equations of motion. The results of the computations for the linear case in which the linearization is carried out according to Eqs 3.18 and 3.19 are not shown in this thesis, but the linear solution is as close to the nonlinear solution as for the response quantity $\{|Z|_{\max}\}$ shown in the tables. Thus, it is concluded that the method of linearizing the drag force described by Eqs. 3.18 and 3.19 yields satisfactory results.

The primary difficulty in using Eqs. 3.18 and 3.19 to linearize the drag force lies in the ability to determine the quantities $\{\langle \dot{x}_s^2 | \dot{x}_s | \rangle\}$ and $\{\langle \dot{x}_s^2 \rangle\}$ a priori. If these quantities can be estimated in some fashion, and if the estimate can be shown to be accurate in certain frequency ranges, then Eq. 3.1 can be linearized into Eq. 3.4, and Eq. 3.4 can be transformed into uncoupled, modal, single-degree of freedom equations in the normal coordinate system which can be solved by spectrum techniques. It was demonstrated in Chapter 2 that, for the single degree of freedom oscillator, the quantities $\langle \dot{x}_g^2 | \dot{x}_g | \rangle$ and $\langle \dot{x}_g^2 \rangle$ are conservative estimates of the oscillator velocity in all but the low frequency region of the spectrum. Since the major effects of hydraulic damping occur in the velocity amplification region of the spectrum, it seems reasonable to estimate the quantities $\{\langle \dot{x}_s^2 | \dot{x}_s | \rangle\}$ and $\{\langle \dot{x}_s^2 \rangle\}$ as $\{\langle \dot{x}_g^2 | \dot{x}_g | \rangle\}$ and $\{\langle \dot{x}_g^2 \rangle\}$ respectively. Using these quantities, Eq. 3.19 becomes

$$\alpha = \left(\frac{\sum_{j=1}^{nn} K_{Djj}}{\sum_{j=1}^{nn} M_{jj}} \right) \left(\frac{\langle \dot{x}_g^2 | \dot{x}_g | \rangle}{\langle \dot{x}_g^2 \rangle} \right) \quad (3.22)$$

A series of computations, labeled "Case 2" in Tables 3.2 through 3.27, is made in which the nonlinear drag factor is linearized in the manner prescribed by Eqs. 3.18 and 3.22. A study of the column labeled "Case 2/Actual Drag" shows that the linearization described by Eqs. 3.18 and 3.22 is, in general, conservative in the mid and high frequency ranges and is generally unconservative in the low frequency range. The degree of conservatism in the mid-frequency range is seen to be less than 5 percent in most cases, although one case is conservative by 12 percent. In the high frequency range, the results are seen to be conservative by as much as 20 percent in some cases, especially in the high drag systems, but many of the results are conservative by less than 10 percent in the high frequency range. The degree of unconservatism in the low frequency range is seen to be less than 10 percent in most cases, but can range as high as 23 percent. This unconservatism in the low frequency range is to be expected, since very soft (low frequency) systems can be expected to exhibit little velocity response at each node, and so the use of the ground velocity characteristics overestimates the velocity of each node. One further observation to be made from a study of the numerical results is that the use of the ground velocity to linearize the drag force is generally more conservative as the response is reduced to a greater degree by the actual nonlinear drag force. In those cases in which the Case 2 linearization is unconservative in frequency ranges 2 and 3, the degree of unconservatism is generally very slight (less than 1 percent).

The maximum deformation between adjacent nodes is also computed and a comparison of the linear drag response (linearized by the ground velocity characteristics) with the nonlinear drag response is shown in Figs. 3.1

through 3.13. These figures show that the maximum spring deformation computed when the drag force is linearized by the ground velocity characteristics is also conservative in the mid and high frequency ranges and generally unconservative in the low frequency range. It is concluded from these computations that the use of Eqs 3.18 and 3.22 is a reasonable way to linearize the drag force and yields slightly conservative results except in the low frequency range. The conservatism introduced by the linearization is seen from the figures to be generally less than 10 percent in the mid and high frequency ranges, with some of the results in the high frequency range being conservative by as much as 20 percent. The results of the low frequency range calculations are generally unconservative by less than 20 percent, but can be unconservative by as much as 25 percent.

The effect of structural damping on the response is quite apparent from the tables and figures. For example, the maximum relative displacement between the bottom node (mass number 5) and the ground for system 4M in frequency range 2 is reduced approximately 17 percent by the hydraulic drag when the structural damping ratio is 0.01 in each mode (see Table 3.14). Yet the response is reduced by less than 2 percent by the hydraulic drag when the structural damping ratio is 0.05 in each mode (see Table 3.15). Thus, the selection of structural damping ratios to use in the response computations is seen to be very important.

3.2.4 Modal Equations in Normal Coordinates

The use of Eqs. 3.18 and 3.22 to linearize the drag force has been shown to yield generally conservative results in the mid and high frequency

ranges, and unconservative results in the low frequency range. Since the linearization prescribed by Eqs. 3.18 and 3.22 insures that the equations of motion for the linearized system (Eq. 3.5) will possess classical normal modes, the discussion of the superposition of normal modes is resumed. Recall the uncoupled equations of motion in the normal coordinate system.

$$\begin{aligned} & \{M^*\} \ddot{\{Y\}} + \{C_s^*\} \dot{\{Y\}} + \alpha \{M^*\} \dot{\{Y\}} + \{K^*\} \{Y\} \\ &= \{ \phi \}^T \{M\} \{-\ddot{x}_g - \alpha \dot{x}_g\} \end{aligned} \quad (3.21)$$

Premultiplying by $\{M^*\}^{-1}$ yields

$$\begin{aligned} & \ddot{\{Y\}} + [2\beta_s \omega] \dot{\{Y\}} + [2\beta_h \omega] \dot{\{Y\}} + [\omega^2] \{Y\} \\ &= \{M^*\}^{-1} \{ \phi \}^T \{M\} \{-\ddot{x}_g - \alpha \dot{x}_g\} \end{aligned} \quad (3.23)$$

where

$$\alpha [I] = [2\beta_h \omega] \quad (3.24)$$

The terms on the right side of Eq. 3.23 can be written as

$$\{M^*\}^{-1} \{ \phi \}^T \{M\} \{-\ddot{x}_g - \alpha \dot{x}_g\} = \{PF\} (-\ddot{x}_g - \alpha \dot{x}_g) \quad (3.25)$$

where

$$\{PF\} = \{M^*\}^{-1} \{ \phi \}^T \{M\} \{I\} \quad (3.26)$$

and PF_i is the participation factor for the i th mode. Substituting Eq. 3.26 into Eq. 3.23

$$\begin{aligned} & \ddot{\{Y\}} + [2\beta_s \omega] \dot{\{Y\}} + [2\beta_h \omega] \dot{\{Y\}} + [\omega^2] \{Y\} \\ &= \{PF\} (-\ddot{x}_g - \alpha \dot{x}_g) \end{aligned} \quad (3.27)$$

For the i th mode, then,

$$\ddot{Y}_i + 2\beta_{s_i}\omega_{ii}\dot{Y}_i + 2\beta_{h_i}\omega_{ii}\dot{Y}_i + \omega_{ii}^2 Y_i = PF_i(-\ddot{x}_g - \alpha\dot{x}_g) \quad (3.28)$$

Since the left side of Eq. 3.28 is linear with respect to the unknown Y , the maximum modal response in the i th mode can be obtained by determining the maximum response of the single degree of freedom equation,

$$\ddot{y}_i + 2\beta_{s_i}\omega_{ii}\dot{y}_i + 2\beta_{h_i}\omega_{ii}\dot{y}_i + \omega_{ii}^2 y_i = -\ddot{x}_g - \alpha\dot{x}_g \quad (3.29)$$

and multiplying this response times the participation factor for the i th mode, PF_i . The nonlinear equations of motion for the multi-degree of freedom system, Eq. 3.1, have now been transformed into a set of linear simultaneous differential equations (Eq. 3.5) by the use of Eqs. 3.18 and 3.22. The linear simultaneous differential equations are transformed into nm uncoupled, single degree of freedom modal equations of the form represented by Eq. 3.28 in the normal coordinate system Y by the use of Eq. 3.2. The total response of the system is the result of a combination of the various modal responses represented by Eq. 3.28.

3.2.5 High Frequency Modes

The existence of a high frequency tail in the response spectrum for a single degree of freedom oscillator was demonstrated and discussed in Chapter 2. Further, the linearization of the nonlinear hydrodynamic drag force was shown to break down when this high frequency tail began to appear. A method for determining the parameters necessary to estimate the magnitude of this tail for each mode in the multi-degree of freedom system is now

developed. Consider the equations of motion for an undamped multi-degree of freedom system

$$[M]\{\ddot{Z}\} + [K]\{Z\} = -[M]\{\ddot{x}_g\} - [K_D]\{\dot{x}_s|\dot{x}_s|\} \quad (3.30)$$

If the system is so stiff that $\{\dot{x}_s\} \approx \{\dot{x}_g\}$, Eq. 3.30 can be written as

$$[M]\{\ddot{Z}\} + [K]\{Z\} = -[M]\{\ddot{x}_g\} - [K_D]\{\dot{x}_g|\dot{x}_g|\} \quad (3.31)$$

Transform Eq. 3.31 into the normal coordinate system by the use of Eq. 3.2 and premultiply by $[\phi]^T$

$$\begin{aligned} [\phi]^T[M][\phi]\{\ddot{Y}\} + [\phi]^T[K][\phi]\{Y\} \\ = -[\phi]^T[M]\{I\}\ddot{x}_g - [\phi]^T[K_D]\{I\}(\dot{x}_g|\dot{x}_g|) \end{aligned} \quad (3.32)$$

or,

$$\begin{aligned} [M^*]\{\ddot{Y}\} + [K^*]\{Y\} \\ = -[\phi]^T[M]\{I\}\ddot{x}_g - [\phi]^T[K_D]\{I\}(\dot{x}_g|\dot{x}_g|) \end{aligned} \quad (3.33)$$

Equation 3.33 represents nm single degree of freedom uncoupled modal equations in normal coordinates for the high frequency multi-degree of freedom system.

Premultiply Eq. 3.33 by $[M^*]^{-1}$, then

$$\{\ddot{Y}\} + [\omega^2]\{Y\} = -\{PF\}\ddot{x}_g - \{K_D^*\}(\dot{x}_g|\dot{x}_g|) \quad (3.34)$$

where

$$\{K_D^*\} = [M^*]^{-1}[\phi]^T[K_D]\{I\} \quad (3.35)$$

For the *i*th mode then,

$$\ddot{Y}_i + \omega_{ii}^2 Y_i = PF_i (-\ddot{x}_g - \frac{K_{Di}^*}{PF_i} \dot{x}_g |\dot{x}_g|) \quad (3.36)$$

Again, since the left side of Eq. 3.36 is linear with respect to the unknown Y , the maximum modal response in the i th mode can be obtained by determining the maximum response of

$$\ddot{y}_i + \omega_{ii}^2 y_i = -\ddot{x}_g - \frac{K_{Di}^*}{PF_i} \dot{x}_g |\dot{x}_g| \quad (3.37)$$

and multiplying this response times the participation factor for the i th mode.

It was shown in Chapter 2 that the quantity $|y_i|_{\max}$ can be estimated for Eq. 3.37 as

$$|y_i|_{\max} \approx \left(\frac{\frac{K_{Di}^*}{PF_i}}{\omega_{ii}^2 M_{ii}^*} \right) (\dot{x}_{g \max})^2 \quad (3.38)$$

and

$$|Y_i|_{\max} = (PF_i)(|y_i|_{\max}) \quad (3.39)$$

3.2.6 Superposition of Modal Responses

The maximum response in any given normal mode of the multi-degree of freedom system can be computed from Eq. 3.28. However, the maximum response in one mode does not necessarily occur at the same time as the maximum response in another mode, and the time of occurrence of the maximum response in the time history of the modal response is not normally known. The actual combination of modal responses in a multi-degree of freedom system is very complex and few generalities can be made about the combination.

An approximation to the actual maximum response of a multi-degree of freedom structure can be made by determining the maximum response in each mode, and then combining the maximum modal responses in some fashion. An upper bound on the maximum response of the structure can be established by assuming that the maximum modal responses occur at the same time in each mode and are additive in nature. In other words, the summation of the absolute values of the maximum response in each mode yields an upper bound to the response of the structure. Another commonly used method of combining the maximum modal responses is to take the square root of the sum of the squares of the modal responses. Other methods of combining modal responses are sometimes used.²² The two most commonly used methods are the summation of the absolute values of the modal maxima (Σ ABS) and the square root of the sum of the squares of the modal maxima (SRSS). These two methods are the only ones used in this thesis for illustrative purposes. Tables 3.28 through 3.33 show the results of the superposition of maximum modal responses applied to three of the five degree of freedom systems. The drag force is linearized in accordance with Eqs. 3.18 and 3.22 (ground velocity linearization), and the amount of linear hydraulic drag β_h in each mode is computed from Eq. 3.24. The maximum modal response in each mode is computed from the response of the single degree of freedom modal equation (Eq. 3.29), and multiplied times the participation factor for the mode. The Σ ABS combination is seen to be higher than the true response (as should be the case) and the SRSS combination is generally less than the true response. No generalizations as to the relative accuracy for different distributions of mass, stiffness, and drag factor can be made, however.¹³ Thus, it is seen that, if the maximum responses of the

single degree of freedom modal equations, Eq. 3.28, can be computed, the maximum response of the structure can be approximated by a combination of the modal maxima.

3.3 Idealized Elastic Deformation Response Spectra

It was seen in the preceding section that the maximum response of a multi-degree of freedom system can be approximated by combining maximum modal responses in some fashion. If the maximum modal responses can be estimated in a way that accounts for the effects of the nonlinear hydrodynamic drag forces in the system, a rapid approximation of the response of the system can be obtained. The principles developed in Chapter 2 for the single degree of freedom oscillator and the method of linearizing the drag forces developed in this chapter can be combined to construct an idealized elastic deformation response spectrum for each mode of the multi-degree of freedom system subjected to strong motion earthquake excitation. The procedure for the construction of the modal elastic deformation response spectra is now set forth.

1. Compute the natural frequencies, $[\omega]$, and mode shapes, $[\phi]$, for the system.
2. Establish the structural damping ratio, β_{s_i} , for each mode. Values of β_{s_i} between 0.005 and 0.05 are reasonable to assume for the type of structure being investigated in this thesis.
3. Determine $x_{g \max}$, $\dot{x}_{g \max}$, $\ddot{x}_{g \max}$, and

$$\frac{\langle \dot{x}_g^2 | \dot{x}_g | \rangle}{\langle \dot{x}_g^2 \rangle}$$

for the earthquake to be used. If the spectra are to be constructed for a hypothetical or "design" earthquake, one-half of the value of $\dot{x}_{g \max}$ is a reasonable value to assume for the quantity

$$\frac{\langle \dot{x}_g^2 | \dot{x}_g | \rangle}{\langle \dot{x}_g^2 \rangle}$$

4. Compute M_{ij}^* , $K_{D_i}^*$, PF_i , α , β_{h_i} , and the high frequency tail estimate from the following expressions:

$$[M^*] = [\phi]^T [M] [\phi]$$

$$\{K_D^*\} = [M^*]^{-1} [\phi]^T [K_D] \{I\} \quad (3.35)$$

$$\{PF\} = [M^*]^{-1} [\phi]^T [M] \{I\} \quad (3.26)$$

$$\alpha = \left(\frac{\sum_{j=1}^{nn} K_{D_{jj}}}{\sum_{j=1}^{nn} M_{jj}} \right) \left(\frac{\langle \dot{x}_g^2 | \dot{x}_g | \rangle}{\langle \dot{x}_g^2 \rangle} \right) \quad (3.22)$$

$$[2\beta_h \omega] = \alpha [I] \quad (3.24)$$

$$\begin{array}{l} \text{High Frequency Tail} \\ \text{Estimate for the } i\text{th} \\ \text{Mode} \end{array} = \left(\frac{K_{D_i}^*}{PF_i} \right) \frac{1}{\omega_{ii}^2 M_{ii}^*} (\dot{x}_{g \max})^2 \quad (3.38)$$

5. With the quantities ω_{ii} , β_{s_i} , β_{h_i} , and the high frequency tail estimate, construct the idealized elastic deformation response

spectrum for the i th mode exactly as described in Section 2.5 for the single degree of freedom system.

It is noted that the idealized response spectrum constructed as outlined above accounts for the fluid-structure interaction in a slightly conservative manner. When an idealized spectrum has been drawn for each mode of the system, the maximum modal responses are obtained from the spectra, multiplied times the appropriate modal participation factor, and combined in some manner to yield an approximate maximum response of the system.

3.4 Hydrodynamic Parameters

An approximate method for computing hydrodynamic parameters for a multi-degree of freedom system by the superposition of normal mode responses is developed in this section. As explained in Chapter 2, these hydrodynamic parameters are absolute displacement and velocity responses of the mass (each node in the multi-degree of freedom system), whose magnitudes are desirable to know in order that the empirical drag and inertia coefficients, C_D and C_I , may be estimated in a reasonable way. The hydrodynamic parameter spectrum amplification factors developed in Chapter 2 may be used to construct idealized spectra from which the response quantity of interest in each mode can be estimated.

Consider again the linear equations of motion,

$$[M]\{\ddot{Z}\} + [C_S]\{\dot{Z}\} + [K]\{Z\} = -[M]\{\ddot{x}_g\} - [K_{DL}]\{\dot{x}_s\} \quad (3.4)$$

Making the substitution $\{Z\} = \{x_s\} - \{x_g\}$, Eq. 3.4 can be written as

$$\begin{aligned}
& [M]\{\ddot{x}_s\} + [C_s]\{\dot{x}_s\} + [K_{DL}]\{\dot{x}_s\} + [K]\{x_s\} \\
& = [K]\{x_g\} + [C_s]\{\dot{x}_g\}
\end{aligned} \tag{3.40}$$

If the velocity force, $[C_s]\{\dot{x}_g\}$, can be dropped from Eq. 3.40 for values of $[C_s]$ up to some magnitude without unreasonable loss of accuracy in the solution (this is discussed in subsequent paragraphs of the section), and the drag factor matrix $[K_{DL}]$ is made to be proportional to the mass matrix $[M]$, then Eq. 3.40 can be written as

$$[M]\{\ddot{x}_s\} + [C_s]\{\dot{x}_s\} + \alpha[M]\{\dot{x}_s\} + [K]\{x_s\} = [K]\{x_g\} \tag{3.41}$$

In order to transform Eq. 3.41 into a "normal" coordinate system, the transformation

$$\{x_s\} = [\phi]\{Q\} \tag{3.42}$$

is made. Substituting 3.42 into Eq. 3.41 and premultiplying the result by $[\phi]^T$,

$$\begin{aligned}
& [M^*]\{\ddot{Q}\} + [C_s^*]\{\dot{Q}\} + \alpha[M^*]\{\dot{Q}\} + [K^*]\{Q\} \\
& = [\phi]^T[K]\{x_g\}
\end{aligned} \tag{3.43}$$

Define

$$\{\gamma\} = [\phi]^T[K]\{I\} \tag{3.44}$$

and Eq. 3.43 can be written as

$$[M^*]\{\ddot{Q}\} + [C_s^*]\{\dot{Q}\} + \alpha[M^*]\{\dot{Q}\} + [K^*]\{Q\} = \{\gamma\}x_g \tag{3.45}$$

Equation 3.45 represents nm uncoupled single degree of freedom modal equations of motion. The equation of motion for the ith mode is

$$M_{ii}^* \ddot{Q}_i + C_{s_{ii}}^* \dot{Q}_i + \alpha M_{ii}^* \dot{Q}_i + K_{ii}^* Q_i = \gamma_i x_g \quad (3.46)$$

or,

$$\ddot{Q}_i + 2\beta_{s_i} \omega_i \dot{Q}_i + 2\beta_{h_i} \omega_{ii} \dot{Q}_i + \omega_{ii}^2 Q_i = \left(\frac{\gamma_i}{M_{ii}^* \omega_{ii}^2} \right) (\omega_{ii}^2 x_g) \quad (3.47)$$

Since the left side of Eq. 3.47 is linear with respect to the unknown Q, the response quantities of interest in the ith mode can be obtained by computing the desired response quantities from

$$\ddot{q} + 2\beta_s \omega \dot{q} + 2\beta_h \omega \dot{q} + \omega^2 q = \omega^2 x_g \quad (3.48)$$

and multiplying the result times the ith mode participation factor for hydrodynamic parameters. The participation factor for hydrodynamic parameters can be seen from Eqs. 3.44 and 3.47 to be

$$\{\text{HDPF}\} = [\Gamma K^*]^{-1} [\phi]^T [K] \{I\} \quad (3.49)$$

Once the modal quantities are obtained in the Q coordinate system, Eq. 3.42 can be used to obtain an approximation of the actual hydrodynamic parameter of interest at each node in much the same manner as an estimate of the maximum deformation of each node is obtained by modal superposition.

To answer the first question raised in this section, the suitability of dropping the velocity force, $[C_s]\{\dot{x}_g\}$, from Eq. 3.40, response calculations were made for the following two equations of motion:

$$\begin{aligned} [\Gamma M] \{\ddot{x}_s\} + [C_s] \{\dot{x}_s\} + [\Gamma K_{DL}] \{\dot{x}_s\} + [K] \{x_s\} \\ = [K] \{x_g\} + [C_s] \{\dot{x}_g\} \end{aligned} \quad (3.40)$$

and

$$[M]\{\ddot{x}_s\} + [C_s]\{\dot{x}_s\} + [K_{DL}]\{\dot{x}_s\} + [K]\{x_s\} = [K]\{x_g\} \quad (3.50)$$

The quantities $\{|x_s|_{\max}\}$, $\{<|x_s|>\}$, $\{|\dot{x}_s|_{\max}\}$, and $\{<|\dot{x}_s|>\}$ for systems 1, 4, and 7 in the mid-frequency range were calculated for the El Centro earthquake from both Eqs. 3.40 and 3.50. The damping matrices $[C_s]$ used in the series of calculations were such that they yielded damping ratios of .02, .05, and .10 in each mode and $[K_{DL}]$ was set to zero. For each structural system and value of $[C_s]$, the hydrodynamic parameters computed from Eq. 3.40 were within 5 percent of the corresponding response quantities computed from Eq. 3.50. The results of the calculations for system 4 and a damping matrix which yields .02 in each mode are shown in Table 3.34. In another set of calculations, the damping matrices $[C_s]$ were made to be proportional to the mass matrix and the numerical values of $[C_s]$ were such that the first mode damping ratios were .02, .05, and .10. Again, for each structural system and value of $[C_s]$, the response quantities computed from Eq. 3.40 were within 5 percent of the corresponding response quantities computed from Eq. 3.50. The numerical results were such that no clear trend resulted that indicated which equation yielded consistently higher or lower results. The hydrodynamic parameters were computed for system 4M in the mid-frequency range, with a structural damping matrix which yielded modal damping ratios of .02 in each mode, for the El Centro earthquake. The drag factor matrix was linearized by using the ground velocity characteristics and made to be proportional to the mass matrix. In one set of computations, the velocity force $[C_s]\{\dot{x}_g\}$ in Eq. 3.40 was included and in another set of computations, the velocity force

$[C_s]\{\dot{x}_g\}$ was neglected. The two sets of numerical results differed by less than 5 percent.

From these calculations, it is concluded that the velocity force $[C_s]\{\dot{x}_g\}$ can be dropped from Eq. 3.40 without sacrificing the accuracy of the results by more than about 5 percent, for values of $[C_s]$ which yield modal damping ratios of up to about .10.

In order to show the similarity of form between Eq. 3.48 and the linear equation of motion for the single degree of freedom oscillator discussed in Chapter 2, it is instructive to recall Eq. 2.7, repeated here for convenience.

$$\ddot{Z} + 2\beta_s \omega \dot{Z} + 2\beta_h \omega \dot{Z} + \omega^2 Z = -\ddot{x}_g - 2\beta_h \omega \dot{x}_g \quad (3.51)$$

Since $Z = x_s - x_g$, Eq. 3.51 can be written

$$\ddot{x}_s + 2\beta_s \omega \dot{x}_s + 2\beta_h \omega \dot{x}_s + \omega^2 x_s = \omega^2 x_g + 2\beta_s \omega \dot{x}_g \quad (3.52)$$

It was seen in Chapter 2 that, for values of β_{total} up to about .10, the hydrodynamic parameters computed from Eq. 3.51 were dependent upon the amount of total damping in the system ($\beta_s + \beta_h$) and not on the distribution of the damping between structural and hydraulic. If all of the damping in Eq. 3.51 is considered to be structural and all of the damping in Eq. 3.52 is considered to be hydraulic, the velocity force on the right side of both equations can be dropped, and Eqs. 3.51 and 3.52 become

$$\ddot{Z} + 2\beta_t \omega \dot{Z} + \omega^2 Z = -\ddot{x}_g \quad (3.51a)$$

and

$$\ddot{x}_s + 2\beta_t \omega \dot{x}_s + \omega^2 x_s = \omega^2 x_g \quad (3.52a)$$

In other words, for values of β_t up to about .10, the hydrodynamic parameters $|x_s|_{\max}$, $\langle |x_s| \rangle$, $|\dot{x}_s|_{\max}$, and $\langle |\dot{x}_s| \rangle$ computed from Eq. 3.51a are within 2 to 4 percent of those which would be computed from Eq. 3.52a for the same system and base disturbance.

It is seen that Eq. 3.48 is of the same form as Eq. 3.52a, so if the hydrodynamic parameters can be calculated, or estimated (as from an idealized response spectrum) for Eq. 3.52a with satisfactory accuracy, then modal hydrodynamic parameters $|q|_{\max}$, $\langle |q| \rangle$, $|\dot{q}|_{\max}$, and $\langle |\dot{q}| \rangle$ can also be calculated or estimated. Once the modal response quantities $|q|_{\max}$, $\langle |q| \rangle$, $|\dot{q}|_{\max}$, and $\langle |\dot{q}| \rangle$ are obtained and multiplied times the appropriate modal hydrodynamic parameter participation factor to obtain $|Q|_{\max}$, $\langle |Q| \rangle$, $|\dot{Q}|_{\max}$, and $\langle |\dot{Q}| \rangle$, the problem arises of how to combine the modal responses.

To obtain an estimate of $\{|x_s|_{\max}\}$ and $\{|\dot{x}_s|_{\max}\}$, the modal responses can be combined in any one of several methods as is the case for obtaining $\{|Z|_{\max}\}$. An upper bound is obtained by summing the absolute values of the modal responses (Σ ABS).

An upper bound on the quantities $\{\langle |x_s| \rangle\}$ and $\{\langle |\dot{x}_s| \rangle\}$ can also be obtained by the Σ ABS method of modal combination, but this is not readily apparent. That the Σ ABS method of modal combination yields an upper bound on the quantity $\{\langle |x_s| \rangle\}$ (or $\{\langle |\dot{x}_s| \rangle\}$) is shown as follows:

$$\{x_s\} = [\phi]\{Q\} \quad (3.42)$$

Assume that the vector $\{Q(t)\}$ has been obtained, then, at the j th node of the system,

$$x_{s_j}(t) = \phi_{j1}Q_1(t) + \phi_{j2}Q_2(t) + \dots + \phi_{j,nm}Q_{nm}(t) \quad (3.53)$$

Taking the absolute value of both sides of Eq. 3.53

$$|x_{s_j}(t)| = |\phi_{j1}Q_1(t) + \phi_{j2}Q_2(t) + \dots + \phi_{j,nm}Q_{nm}(t)| \quad (3.54)$$

An upper bound on $|x_{s_j}(t)|$ is seen from Eq. 3.54 to be

$$|x_{s_j}(t)| \leq |\phi_{j1}||Q_1(t)| + |\phi_{j2}||Q_2(t)| + \dots + |\phi_{j,nm}||Q_{nm}(t)| \quad (3.55)$$

Integrating both sides of Eq. 3.55 over the time of response,

$$\begin{aligned} \frac{1}{t} \int_0^t |x_{s_j}(t)| dt &\leq \frac{1}{t} \int_0^t [|\phi_{j1}||Q_1(t)| + |\phi_{j2}||Q_2(t)| \\ &+ \dots + |\phi_{j,nm}||Q_{nm}(t)|] dt \end{aligned} \quad (3.56)$$

or,

$$\begin{aligned} \langle |x_{s_j}| \rangle &\leq |\phi_{j1}| \langle |Q_1| \rangle + |\phi_{j2}| \langle |Q_2| \rangle \\ &+ \dots + |\phi_{j,nm}| \langle |Q_{nm}| \rangle \end{aligned} \quad (3.57)$$

Which is seen to be the Σ ABS method of modal combination.

Rules for constructing idealized hydrodynamic parameter response spectra from which $|q|_{\max}$, $\langle |q| \rangle$, $|\dot{q}|_{\max}$, and $\langle |\dot{q}| \rangle$ may be estimated for each mode (and then $|Q|_{\max}$, $\langle |Q| \rangle$, $|\dot{Q}|_{\max}$, and $\langle |\dot{Q}| \rangle$ are computed from the q 's and the hydrodynamic parameter participation factors) of the multi-degree of freedom system are discussed in the next section.

3.5 Idealized Elastic Hydrodynamic Parameter Response Spectra

Idealized elastic hydrodynamic parameter response spectra can be constructed for each mode of the multi-degree of freedom system in the following manner:

1. Compute the natural frequencies, $[\omega]$, and mode shapes, $[\phi]$, for the system.
2. Establish the structural damping ratio, β_{s_i} , for each mode.
3. Compute β_{h_i} and HDPF_i from

$$\alpha = \left(\frac{\sum_{j=1}^{nn} K_{D,jj}}{\sum_{j=1}^{nn} M_{jj}} \right) \left(\frac{\langle \ddot{x}_g^2 | \dot{x}_g | \rangle}{\langle \dot{x}_g^2 \rangle} \right) \quad (3.22)$$

$$[2\beta_h \omega] = \alpha [I] \quad (3.24)$$

$$\{\text{HDPF}\} = [K^*]^{-1} [\phi]^T [K] \{I\} \quad (3.49)$$

4. With the quantities ω_{ii} , β_{s_i} , β_{h_i} , $x_{g \max}$ (or $\langle |x_g| \rangle$), $\dot{x}_{g \max}$ (or $\langle |\dot{x}_g| \rangle$), and $\ddot{x}_{g \max}$ (or $\langle |\ddot{x}_g| \rangle$), construct the idealized elastic hydrodynamic parameter response spectrum for the i th mode exactly as described in Section 2.7 for the single degree of freedom system.

When an idealized spectrum has been drawn for each mode of the system, maximum modal hydrodynamic parameters are obtained from the spectra, multiplied times the appropriate modal hydrodynamic parameter participation factor, and combined in some manner to yield an approximate solution of the hydrodynamic parameter of interest.

CHAPTER 4

APPLICATIONS

4.1 General

In Chapters 2 and 3 a method was developed for linearizing the nonlinear hydrodynamic drag force on a single degree of freedom oscillator and a multi-degree of freedom lumped parameter model. The method has been shown to yield satisfactory results for systems subjected to earthquake excitation of the type used in this thesis. Although the method of linearizing employed in the multi-degree of freedom system places a linear damper at the level of the top mass where a nonlinear damper does not exist, it has been shown to yield maximum response quantities which are within a very few percent of the response quantities computed for the nonlinear system. Further, linearizing the drag force by using velocity characteristics of the ground motion has been shown to yield generally conservative results in all but the low frequency range. The linearization technique has been developed in such a manner that the resulting linear simultaneous differential equations of motion for the multi-degree of freedom system possess classical normal modes of response. The existence of classical normal modes permits the use of normal mode superposition, with the modal response quantities determined by response spectrum techniques, as an approximate method of computing the response of multi-degree of freedom systems. The approximate method can be used for displacement response quantities and hydrodynamic parameter response quantities. The research reported in this thesis is not intended to reinvent the method of solution by the superposition of normal mode solutions as determined by

response spectra, but is devoted primarily to developing the linearizing technique which insures the existence of classical normal modes and yields generally conservative results.

This chapter demonstrates the use of the principles and methods developed and discussed in Chapters 2 and 3 in computing the response of a series of actual offshore tower designs and one of the test systems described in Chapter 3.

4.2 Displacement Response

Table 4.1 lists the properties of a series of offshore towers designed for water depths of 400, 600, 800, and 1000 feet.⁴ A structural damping matrix $[C_s]$ which yields modal damping ratios of .01 in each mode is computed for each tower as described in Chapter 3. The structures are subjected to the El Centro earthquake depicted in Fig. 1.2, and various response quantities are computed. In the first set of computations, the equations of motion are numerically integrated and response quantities are found for the case in which there are no hydrodynamic drag forces acting on the structure. The same response quantities are next computed for the case in which the actual nonlinear drag forces are acting on the structure. Finally, the nonlinear drag forces are linearized by using the velocity characteristics of the ground motion, and the response quantities are computed by the combination (Σ ABS and SRSS) of maximum modal responses found from the true response spectrum for each of the first five modes of the structures. The amount of linear hydraulic damping in each mode found from the linearization procedure is shown in Table 4.2. The response quantities of interest in these calculations are

the maximum displacement between the top deck and the ground, the maximum overturning moment, and the maximum base shear expressed as a percent of the total tower weight, including the added mass of the structure. The results of the calculations are shown in Fig. 4.1.

A study of Fig. 4.1 reveals that, for this series of towers subjected to the El Centro earthquake, the nonlinear hydrodynamic drag forces reduce the response of the tallest tower in the top deck displacement and overturning moment quantities by approximately 30 percent from the "no drag" case. The maximum base shear for the tallest tower is reduced only about 8 percent by the nonlinear hydrodynamic drag forces. Exact response calculations were made for the other three earthquake records used in this thesis and the reduction in response due to drag was found to be somewhat lower in magnitude than for the El Centro earthquake. For the tower in 1000 feet of water, the reduction (due to hydrodynamic drag) in the maximum top deck displacement relative to the ground was found to be about 8.5 percent for the Taft earthquake, 11.5 percent for the Ferndale earthquake, and 17 percent for the San Fernando earthquake. In general, the taller, more flexible towers showed more reduction in response due to the hydraulic drag than did the shorter, stiffer towers. No generalizations can be made, however, regarding the magnitude of the reduction in response relative to tower height or stiffness since the actual response is such a complex combination of variables in both the structure and the earthquake.

In the superposition of maximum modal responses computed from the true response spectrum for each of the first five modes of vibration, it was found that the higher modes contributed rather strongly to the maximum base

shear. The contribution of each mode to the maximum base shear computed by the Σ ABS combination of modal responses is shown in Table 4.3. Although the SRSS combination of modal responses appears from Fig. 4.1 to provide a very good estimate of the response of this series of towers to the El Centro earthquake, generalities concerning the accuracy of one method of modal combination relative to another method of modal combination cannot be made.¹³

The response of the towers is computed by the combination of maximum modal responses (Σ ABS and SRSS) found from the idealized deformation response spectrum for each of the first five modes of vibration. The idealized spectra were constructed in accordance with the procedure described in Chapter 3 for ground motion quantities equal to those of the El Centro earthquake. The idealized spectra for the first five modes of tower C are shown in Fig. 4.2. The estimated hydraulic damping ratios in the 3rd, 4th, and 5th modes of the structure are such that the resulting idealized spectra for those modes cannot be shown separately and distinctly on the scale of Fig. 4.2. It is noted that, for the idealized spectra shown in Fig. 4.2, the frequencies of the system are well removed from the high frequency tail region of their respective response spectrum. This was found to be the case for each of the towers A, B, C, and D. The results of the computations using the idealized spectra are shown in Fig. 4.3.

4.3 Hydrodynamic Parameters

To demonstrate the computation of the hydrodynamic parameters $|x_s|_{\max}$, $\langle |x_s| \rangle$, $|\dot{x}_s|_{\max}$, and $\langle |\dot{x}_s| \rangle$ at each node of a multi-degree of freedom system, the five degree of freedom system 4M is used. The properties of this

system, with a structural damping matrix that yields a damping ratio of .02 in each mode, are shown in Table 4.4. The magnitude of $[K]$ was chosen to yield frequencies of the system that fall into the velocity amplification region of the spectrum. The hydrodynamic parameter response quantities are computed by the numerical integration of the equations of motion and by the combination (Σ ABS and SRSS) of maximum modal responses found from the true spectral response in each mode. The results of the computations are shown in Table 4.5. It is seen from Table 4.5 that the combination of modal responses provides results which are, in general, sufficiently close to the exact response at each node to enable the selection of inertia and drag coefficients C_I and C_D with reasonable confidence. In lieu of using the true spectral response quantities, which require the use of a digital computer to obtain for each mode, an idealized spectrum can be constructed for each mode in the manner set forth in Chapter 3.

CHAPTER 5

CONCLUSIONS AND RECOMMENDATIONS FOR FURTHER STUDY

5.1 Conclusions

In this thesis, an approximate method has been developed for computing the response of a multi-degree of freedom system, partially submerged in water, to earthquake excitation. In Chapter 2, the effects of the nonlinear hydrodynamic drag force on a single degree of freedom oscillator are shown, and a generally conservative method of linearizing the drag force is developed. Amplification factors are developed which permit the construction of idealized response spectra for deformation and hydrodynamic parameters. Chapter 3 extends the principles from the single degree of freedom oscillator to multi-degree of freedom systems and develops a generally conservative method of linearizing the drag forces. The method of linearizing insures the existence of classical normal modes in the equations of motion, which in turn permits the response quantities of interest to be obtained by the superposition of normal mode responses. In Chapter 4 the response to the El Centro earthquake of a series of offshore towers is computed using the methods developed in Chapter 3.

Several conclusions may be drawn from the development of principles and methods and the results of sample problems in the preceding three chapters.

1. The maximum relative displacement response of a single degree of freedom oscillator, with drag characteristics described by the parameter $\frac{K_D \ddot{x}_{g \max}}{K}$, approaches a constant value at high frequencies as a result of the nonlinear hydrodynamic drag

force growing very large relative to the inertia force in the equation of motion. The magnitude of this relatively constant high frequency tail can be estimated for earthquake motions by the expression

$$|Z|_{\max} \approx \left(\frac{K_D \ddot{x}_{g \max}}{K} \right) \left(\frac{\dot{x}_{g \max}^2}{\ddot{x}_{g \max}} \right)$$

2. Linearizing the drag force on a single degree of freedom oscillator by using the absolute velocity response of the oscillator yields slightly conservative results for the maximum response to earthquake motions until the high frequency, high drag tail begins.
3. Linearizing the drag force on a single degree of freedom oscillator by using the velocity characteristics of the ground motion yields conservative results for the maximum response to earthquake motions except for low frequency systems and very high frequency systems.
4. The conservatism introduced by using the ground motion velocity characteristics in the linearization of the drag force is reduced as the amount of structural damping in the system is increased.
5. The maximum response of the single degree of freedom oscillator to earthquake motions is sensitive to the total amount of linear, velocity dependent damping in the system, and not to the distribution of this damping between structural and hydraulic, up to linear hydraulic damping ratios of 10 percent of critical.

6. The nonlinear hydrodynamic drag has very little effect on the elasto-plastic deformation response spectrum in the low frequency region.
7. A high frequency tail exists in the elasto-plastic deformation response spectrum for a system with nonlinear hydrodynamic drag forces. Large amounts of drag cause greater reductions in the yield deformation, Z_y , from the maximum elastic deformation for a given ductility factor than do small amounts of drag.
8. The nonlinear hydrodynamic drag force has a damping effect on the elasto-plastic deformation response spectrum in the mid-frequency range. The damping effect of the drag becomes less pronounced as the ductility factor increases.
9. Idealized response spectra which consider the effects of fluid-structure interaction can be constructed as described in this thesis.
10. The linearization of the drag forces on a multi-degree of freedom system by using the absolute velocity response at each node and forcing the linear drag factor matrix $[K_{DL}]$ to be proportional to the mass matrix $[M]$ as described herein is satisfactory.
11. Linearizing the drag forces on a multi-degree of freedom system by using the velocity characteristics of the ground motion and forcing the drag factor matrix to be proportional to the mass matrix as described herein yields generally conservative results except for low frequency systems.
12. For the multi-degree of freedom systems studied in this thesis,

the response to earthquake excitation is relatively insensitive to the spatial distribution of the linear drag forces.

13. The hydrodynamic drag forces can cause a significant reduction in the response of lightly damped systems to earthquake motions.
14. The amount of reduction in response due to hydrodynamic drag varies considerably from one response quantity to another and from one earthquake to another.
15. The reduction in response due to hydrodynamic drag is decreased as the amount of structural damping in the system is increased.
16. Higher modes of a multi-degree of freedom system can contribute appreciably to the total response of the system.

5.2 Recommendations for Further Study

The approximate methods of analysis developed in this thesis are limited by the types of multi-degree of freedom systems used in the investigation and by the inherent limitations in the hydrodynamic force equation used. Further, the study in this thesis is devoted to excitation of the structure in still water, and the ocean is never completely at rest. There are several areas in which further studies should be made of the response of offshore structures to earthquake excitation.

1. The validity of the lumped parameter model should be tested through the use of field measurements of the response of actual offshore structures to strong motion earthquakes.
2. Model tests of single degree of freedom oscillators and multi-degree of freedom structures should be conducted for the types

- of base motion considered in this thesis. Such model tests will be useful in verifying the principles developed herein.
3. Since the ocean is never actually at rest, analytical and experimental studies should be conducted on the response of submerged and partially submerged structures subjected to earthquake motions combined with forces resulting from waves and currents.
 4. The studies in this thesis assume ground motion in one direction only. It is recommended that studies be made of the response when the two orthogonal components of the horizontal ground motion are acting on the structure at the same time.
 5. The earthquake response of the structure in torsion and in the vertical direction should be investigated.
 6. It is recommended that the effects of foundation and soil conditions be included in the model. There are several reasonable approaches to modeling the foundation which should be investigated.²³⁻²⁵
 7. The hydrodynamic force equation used in this thesis (Morison's equation) is based on studies with relatively rigid piles. There is some evidence^{19,20} that the forces on flexible, oscillating structures may be better expressed through the use of different drag and inertia coefficients, or even through the use of a different force expression. Much more information is needed concerning the hydrodynamic forces acting on flexible, oscillating structures.
 8. The linearizing technique should be tested for suitability of

use when the structure has radically different distribution of mass, stiffness, and drag properties from those test structures used in this thesis.

9. It is recommended that the effects of the hydrodynamic forces on the inelastic response of the structure be studied in greater depth. While design for elastic response is satisfactory for earthquakes which may be expected to occur frequently, elastic design for infrequent, severe earthquakes may result in excessively conservative designs. Some response into the inelastic range should be permitted for the occurrence of an unusually strong earthquake, and approximate methods are desirable for the estimation of this inelastic response.
10. It is recommended that approximate methods be developed for the estimation of the response to stochastic representations of the forces resulting from earthquakes, waves, and currents.

LIST OF REFERENCES

1. Hurty, W. C. and Rubinstein, M. F., Dynamics of Structures, Prentice-Hall, Englewood Cliffs, New Jersey, 1965.
2. Morison, J. R., O'Brien, M. P., Johnson, J. W., and Schaaf, S. A., "The Force Exerted by Surface Waves on Piles," Petroleum Transactions, American Institute of Mining, Metallurgical and Petroleum Engineers, Vol. 189, 1950.
3. Murtha, J. P., "The Virtual Mass of Cylindrical Bodies at a Free Surface," Proceedings of the Fifth Midwestern Conference on Fluid Mechanics, University of Michigan Engineering Research Institute, Ann Arbor, Michigan, 1957.
4. Burke, B. G. and Tighe, J. T., "A Time Series Model for Dynamic Behavior of Offshore Structures," Preprints, 1971 Offshore Technology Conference, Vol. 1, Paper No. OTC 1403, 1971.
5. Newmark, N. M., "A Method of Computation for Structural Dynamics," Journal of the Engineering Mechanics Division, American Society of Civil Engineers, Vol. 85, EM3, July 1959.
6. Malhotra, A. K. and Penzien, J., "Response of Offshore Towers to Earthquake Excitation," Proceedings, Civil Engineering in the Oceans II, American Society of Civil Engineers Conference, Miami Beach, Florida, 1969.
7. Penzien, J., Kaul, M. K., and Berge, B., "Stochastic Response of Offshore Towers," National Symposium on Computerized Structural Analysis and Design, George Washington University, Washington, D. C., March 1972.
8. Malhotra, A. K. and Penzien, J., "Response of Offshore Structures to Random Wave Forces," Journal of the Structural Division, American Society of Civil Engineers, Vol. 96, ST10, October 1970.
9. Foster, E. T., Jr., "Statistical Prediction of Wave Induced Responses in Deep Ocean Tower Structures," Ph.D. Thesis, University of California, Berkeley, 1967.
10. Nath, J. H. and Harleman, D.R.F., "The Dynamics of Fixed Towers in Deep Water Random Waves," Proceedings, Civil Engineering in the Oceans, American Society of Civil Engineers Conference, San Francisco, 1967.
11. Blume, J. A., Newmark, N. M., and Corning L. H., Design of Multistory Reinforced Concrete Buildings for Earthquake Motions, Portland Cement Association, Chicago, 1961.

12. Wiegel, R. L., Editor, Earthquake Engineering, Prentice-Hall, Englewood Cliffs, New Jersey, 1970.
13. Newmark, N. M., et al., "Design Procedures for Shock Isolation Systems of Underground Protective Structures," Report RTD-TDR-63-3096, Air Force Weapons Laboratory, Albuquerque, New Mexico, Vol. 3, 1964, and Vol. 5, 1965.
14. Newmark, N. M. and Rosenblueth, E., Fundamentals of Earthquake Engineering, Prentice-Hall, Englewood Cliffs, New Jersey, 1971.
15. Jacobsen, L. S. and Ayre, R. S., Engineering Vibrations, McGraw-Hill, New York, 1958.
16. Amin, M., "A Non-Stationary Stochastic Model for Strong Motion Earthquakes," Ph.D. Thesis, University of Illinois, Urbana, Illinois, 1966.
17. Ippen, A. T., Editor, Estuary and Coastline Hydrodynamics, McGraw-Hill, New York, 1966.
18. Wiegel, R. L., Oceanographical Engineering, Prentice-Hall, Englewood Cliffs, New Jersey, 1964.
19. Keulegan, G. H. and Carpenter, L. H., "Forces on Cylinders and Plates in an Oscillating Fluid," Journal of Research, National Bureau of Standards, Vol. 60, No. 5, May 1958.
20. Laird, A.D.K., "Water Forces on Flexible Oscillating Cylinders," Journal of the Waterways and Harbors Division, American Society of Civil Engineers, Vol. 88, WW3, August 1962.
21. Caughey, T. K., "Classical Normal Modes in Damped Linear Dynamic Systems," Journal of Applied Mechanics, Vol. 27, June 1960.
22. Kassawara, R. P., "Earthquake Response of Light Multiple Degree of Freedom Secondary Systems by Spectrum Techniques," Ph.D. Thesis, University of Illinois, Urbana, Illinois, 1970.
23. Saul, W. E., "Static and Dynamic Analysis of Pile Foundations," Journal of the Structural Division, American Society of Civil Engineers, Vol. 94, ST5, May 1968.
24. Davisson, M. T. and Robinson, K. E., "Bending and Buckling of Partially Embedded Piles," Proceedings, Sixth International Conference on Soil Mechanics and Foundation Engineering, Toronto, Canada, 1965.
25. Ross, H. E., "Dynamic Response of Offshore Piling," Preprints, 1971 Off-shore Technology Conference, Vol. II, Paper No. OTC 1480, 1971.

Table 1.1

Characteristics of Earthquakes Used

Name	\ddot{x}_g max (g)	\dot{x}_g max (in./sec)	x_g max (in.)	Duration of Motion (sec)	$\frac{\langle \dot{x}_g^2 \dot{x}_g \rangle}{\langle \dot{x}_g^2 \rangle}$ (in./sec)	$\frac{\langle \dot{x}_g^2 \dot{x}_g \rangle}{\langle \dot{x}_g^2 \rangle}$ \dot{x}_g max (none)
El Centro, California, 1940, N-S Component	0.312	12.79	8.24	31.20	6.163	0.482
San Fernando, California, 1971, Pacoima Dam Record, S-16-E Component	1.241	43.70	23.18	19.16	22.301	0.510
Ferndale, California, 1954 N-44-E Component	0.167	14.10	8.10	30.16	7.948	0.564
Taft, California, 1952 N-21-E Component	0.178	6.21	3.30	29.84	2.924	0.471

Table 1.1 (Continued)

Name	$\langle x_g \rangle$ (in.)	$\langle \dot{x}_g \rangle$ (in./sec)	$\langle \ddot{x}_g \rangle$ (g)	$\frac{\langle x_g \rangle}{x_{g \text{ max}}}$ (none)	$\frac{\langle \dot{x}_g \rangle}{\dot{x}_{g \text{ max}}}$ (none)	$\frac{\langle \ddot{x}_g \rangle}{\ddot{x}_{g \text{ max}}}$ (none)
El Centro, California, 1940, N-S Component	2.623	2.140	0.0571	0.318	0.167	0.183
San Fernando, California, 1971, Pacoima Dam Record, S-16-E Component	4.993	5.427	0.1037	0.215	0.124	0.084
Ferndale, California, 1954 N-44-E Component	1.573	2.016	0.0246	0.194	0.143	0.147
Taft, California, 1952 N-21-E Component	1.270	0.994	0.0329	0.385	0.160	0.185

Table 2.1

Characteristics of Series Representation
of Base Acceleration

Quantity	Maximum Amplitude	Time of Occurrence
\ddot{x}_g	2.56 g	0.35 t_d
\dot{x}_g	3.85 ft/sec	0.42 t_d
x_g	0.20 ft	0.50 t_d

$$\begin{aligned}\ddot{x}_g = & -0.20401 \cos 2\pi t - 6.87108 \cos 4\pi t + 38.35016 \cos 6\pi t \\ & - 41.35223 \cos 8\pi t - 2.84232 \cos 10\pi t \\ & + 12.91937 \cos 12\pi t\end{aligned}$$

(\ddot{x}_g in ft/sec²)

Table 2.2
Comparison of Estimated $|Z|_{\max}$ With $|Z|_{\max}$ Computed at
High Frequencies by Numerical Integration

Base Disturbance	Frequency (cps)	$K_D \ddot{x}_g \max$ K	$ Z _{\max}$ (inches) Estimated From Eq. 2.4	$ Z _{\max}$ (inches) From Numerical Integration of Eq. 2.1 For		
				$\beta_s = 0.00$	$\beta_s = 0.01$	$\beta_s = 0.02$
Sinusoidal Acceleration	10	0.01	0.04894	--	0.06209	--
	10	0.20	0.97876	--	0.89995	--
	5	0.60	2.93629	--	2.14306	--
Six Term Cosine Series	20	0.20	0.43156	--	0.41365	--
						0.41143
El Centro Earthquake	30	0.006	0.00972	0.01007	--	0.01005
	30	0.08	0.12991	0.12748	--	0.12741
	10	0.50	0.67763	0.63714	--	0.63676
						0.63618

Table 2.3

Distribution of Total Damping Between Structural
and Hydraulic for Comparison Purposes

β_{total}	β_h For			
	$\beta_s = 0$	$\beta_s = .02$	$\beta_s = .05$	$\beta_s = .10$
.02	.02	0		
.05	.05		0	
.07		.05	.02	
.10	.10		.05	0
.12		.10		.02
.15			.10	.05

Table 2.4

Elastic Deformation Spectrum Amplification Factors

$\beta_{\text{total}} (\%)$	Amplification Factor		
	Displacement	Velocity	Acceleration
0	2.5	4.0	6.4
0.5	2.2	3.6	5.8
1	2.0	3.2	5.2
2	1.8	2.8	4.3
5	1.4	1.9	2.6
7	1.2	1.5	1.9
10	1.1	1.3	1.5
20	1.0	1.1	1.2

Table 2.5
Elastic Hydrodynamic Parameter Spectrum
Amplification Factors

β_{total} (%)	$ x_s _{\text{max}}$ Spectrum Amplification Factors	
	Displacement	Velocity
0	2.4	5.2
1	2.2	4.4
2	2.1	3.6
5	1.8	3.1
10	1.6	2.1

β_{total} (%)	$\langle x_s \rangle$ Spectrum Amplification Factors	
	Displacement	Velocity
0	3.8	10.9
1	3.4	8.5
2	3.0	6.8
5	2.3	4.2
10	1.8	3.3

Table 2.5 (Continued)

β_{total} (%)	$ \dot{x}_s _{\text{max}}$ Spectrum Amplification Factors		
	Displacement	Velocity	Acceleration
0	2.2	4.1	7.1
1	1.9	3.1	4.9
2	1.6	2.6	3.7
5	1.4	2.0	3.1
10	1.2	1.8	2.6

β_{total} (%)	$\langle \dot{x}_s \rangle$ Spectrum Amplification Factors		
	Displacement	Velocity	Acceleration
0	3.4	10.1	13.5
1	3.0	6.3	6.2
2	2.7	5.1	4.3
5	2.1	3.0	2.9
10	1.6	2.2	2.2

Table 2.6

Actual and Approximate Reduction Factors for the
High Frequency Region of Inelastic Response
Spectra. El Centro Earthquake

$$\beta_s = 0.02, \frac{K_D \ddot{x}_{g \max}}{K} = 0.50$$

Ductility Factor μ	Z_y (inches)	$ Z _{\max}$ (inches)	Actual Reduction Factor for Z_y	$\frac{\mu}{2\mu - 1}$
1	0.63676	0.63676	1.00	1.00
1.5	0.49526	0.74289	0.77	0.75
2	0.42835	0.85670	0.67	0.67
3	0.35975	1.07925	0.56	0.60
4	0.31523	1.26093	0.49	0.57

Note: All calculations are at a frequency of 10 cps.

Table 3.1

Relative Values of Mass, Stiffness, and Drag Factor for 5 Degree of Freedom Systems

System	1		2		3		4		5		6		7	
	L k_D	M k_D	L k_D	M k_D	L k_D	L k_D	L k_D	M k_D	H k_D	H k_D	M k_D	H k_D	M k_D	H k_D
m_1	2	0	2	0	1	0	1	0	1	0	1	0	1	0
k_1	1		1		1		1		1		1		1	
m_2	1	1	1	1	1	1	1	1	1	1	2	1	2	1
k_2	2		2		2		2		2		2		2	
m_3	1	1	1	1	1	1	1	1	1	2	3	1	3	2
k_3	2		2		2		2		2		2		2	
m_4	1	1	1	1	2	1	2	1	2	3	4	2	4	3
k_4	3		2		3		2		1		2		1	
m_5	1	1	1	1	3	1	3	1	3	4	5	3	5	4
k_5	5		3		5		3		1		3		1	
$\Sigma k_D / \Sigma m$ (inches ⁻¹)	.002	.004	.002	.004	.002	.002	.002	.004	.008	.008	.004	.008	.004	.008
Relative Natural Frequency	f_1		1.00000		1.00000		1.00000		1.00000		1.00000		1.00000	
	f_2	2.70031	2.72831		2.17527		2.25489		2.38174		2.48920		2.58720	
	f_3	4.65410	4.75877		2.27307		3.41382		3.82031		3.55729		3.93241	
	f_4	6.43831	6.63473		4.25580		4.30003		5.23707		4.33114		5.06643	
	f_5	8.30426	7.77067		5.41832		6.16107		6.97167		5.43091		7.01497	
	$f_1 / \sqrt{k_1 / m_1}$	0.08602	0.07855		0.07224		0.06311		0.04166		0.04658		0.03036	

Table 3.2

Response of System 1L to El Centro Earthquake, 1940, N-S Component.
Direct Integration Solution. $\beta_S = .01$

MAXIMUM RELATIVE DISPLACEMENT BETWEEN MASS AND GROUND (INCHES)										COMPARISON OF SOLUTIONS			MODAL PROPERTIES		
FREQ. RANGE	MASS NO.	N) DRAG	ACTUAL ERAG	LINEAR DRAG		ACTUAL DRAG/ NO DRAG	CASE 1/ ACTUAL DRAG		CASE 2/ ACTUAL DRAG	MODE NO.	FREQ. (CPS)	LINEAR HYDRAULIC DAMPING RATIO			
				CASE 1	CASE 2		ACTUAL DRAG	CASE 2							
1	1	8.34376	8.34380	8.34162	8.34185	1.00000	0.99974	0.99977	1	0.02975	0.03694	0.03297			
	2	11.14495	10.13646	10.19525	10.22600	0.90951	1.00580	1.00883	2	0.08033	0.01364	0.01221			
	3	8.33682	8.33675	8.33466	8.33490	0.99999	0.99975	0.99978	3	0.13846	0.00792	0.00708			
	4	10.80862	9.84047	9.76169	9.83508	0.91043	0.99199	0.99945	4	0.19154	0.00572	0.00512			
	5	7.10426	6.72449	6.72896	6.73601	0.94654	1.00066	1.00171	5	0.24705	0.00444	0.00397			
2	1	14.94299	14.66299	14.47408	14.69819	0.98126	0.98712	1.00240	1	0.24705	0.00767	0.00397			
	2	10.34037	10.06055	9.93615	10.12925	0.97294	0.98763	1.00683	2	0.66710	0.00784	0.00147			
	3	8.46221	7.66173	7.28094	7.80763	0.90541	0.95030	1.01904	3	1.14978	0.00165	0.00085			
	4	6.37363	5.81830	5.89662	6.12044	0.91287	1.01346	1.05193	4	1.59056	0.00119	0.00062			
	5	3.73147	3.54765	3.60208	3.66382	0.95074	1.01534	1.03274	5	2.05154	0.00092	0.00048			
3	1	5.95054	5.69982	5.70553	5.79162	0.95787	1.00100	1.01611	1	1.50154	0.00102	0.00065			
	2	4.20023	4.05035	4.04444	4.09924	0.96432	0.99854	1.01207	2	4.05462	0.00028	0.00024			
	3	3.13073	3.02090	3.01867	3.05811	0.96492	0.99926	1.01232	3	6.98833	0.00022	0.00014			
	4	1.76116	1.69931	1.70043	1.72182	0.96488	1.00066	1.01325	4	9.66729	0.00016	0.00010			
	5	0.68853	0.66410	0.66528	0.67354	0.96452	1.00194	1.01422	5	12.46919	0.00012	0.00008			

CASE 1 - VELOCITY OF EACH MASS (COMPUTED IN ACTUAL DRAG PROBLEM) IS USED TO LINEARIZE THE DRAG FORCE

CASE 2 - GROUND VELOCITY IS USED TO LINEARIZE THE DRAG FORCE

Table 3.3

Response of System 1L to El Centro Earthquake, 1940, N-S Component.
Direct Integration Solution. $\beta_s = .05$

MAXIMUM RELATIVE DISPLACEMENT BETWEEN MASS AND GROUND (INCHES)										COMPARISON OF SOLUTIONS				MODAL PROPERTIES			
FREQ. RANGE	MASS NO.	NO DRAG	ACTUAL DRAG	LINEAR DRAG		ACTUAL DRAG/NO DRAG	CASE 1/ACTUAL DRAG		CASE 2/ACTUAL DRAG	MODE NO.	FREQ. (CPS)	LINEAR HYDRAULIC DAMPING RATIO					
				CASE 1	CASE 2		ACTUAL	DRAG				CASE 1	CASE 2				
1	1	8.27668	8.27653	8.27557	8.27526	0.99998	0.99988	0.99985	1	0.02975	0.02578	0.03297					
	2	9.08362	8.88853	8.96776	8.93605	0.97852	1.00891	1.00535	2	0.08033	0.00955	0.01221					
	3	8.21097	8.21106	8.21008	8.20983	1.00001	0.99988	0.99985	3	0.13846	0.00554	0.00708					
	4	7.93429	7.89693	7.89720	7.89726	0.99529	1.00003	1.00004	4	0.19154	0.00400	0.00512					
	5	6.39375	6.32212	6.34960	6.33738	0.98880	1.00435	1.00241	5	0.24705	0.00310	0.00397					
2	1	12.91256	12.72186	12.67997	12.70796	0.98523	0.99671	0.99891	1	0.24705	0.00452	0.00397					
	2	8.19152	8.12225	8.11672	8.12576	0.99154	0.99932	1.00043	2	0.66710	0.00167	0.00147					
	3	5.66697	5.65124	5.62490	5.62997	0.99723	0.99534	0.99624	3	1.14978	0.00097	0.00085					
	4	4.34317	4.27154	4.28118	4.28865	0.98351	1.00226	1.00400	4	1.59056	0.00070	0.00062					
	5	2.11593	2.09029	2.09628	2.09865	0.98788	1.00286	1.00400	5	2.05154	0.00054	0.00048					
3	1	3.39496	3.38702	3.38702	3.38717	0.99766	1.00000	1.00004	1	1.50154	0.00067	0.00065					
	2	2.20938	2.20490	2.20429	2.20439	0.99797	0.99973	0.99977	2	4.05462	0.00025	0.00024					
	3	1.64792	1.63890	1.64080	1.64094	0.99452	1.00116	1.00125	3	6.98833	0.00014	0.00014					
	4	0.93596	0.93059	0.93208	0.93215	0.99426	1.00160	1.00168	4	9.66739	0.00010	0.00010					
	5	0.36560	0.36352	0.36410	0.36413	0.99421	1.00161	1.00169	5	12.46919	0.00008	0.00008					

CASE 1 - VELOCITY OF EACH MASS (COMPUTED IN ACTUAL DRAG PROBLEM) IS USED TO LINEARIZE THE DRAG FORCE

CASE 2 - GROUND VELOCITY IS USED TO LINEARIZE THE DRAG FORCE

Table 3.4

Response of System 1M to El Centro Earthquake, 1940, N-S Component.
Direct Integration Solution. $\beta_s = .01$

FREQ. RANGE	MASS NO.	MAXIMUM RELATIVE DISPLACEMENT BETWEEN MASS AND GROUND (INCHES)					COMPARISON OF SOLUTIONS				MODAL PROPERTIES		
		NO DRAG	ACTUAL DRAG	LINEAR DRAG		ACTUAL DRAG/ NO DRAG	CASE 1/ ACTUAL DRAG		CASE 2/ ACTUAL DRAG	MODE NO.	FREQ. (CPS)	LINEAR HYDRAULIC DAMPING RATIO	
				CASE 1	CASE 2		CASE 1/ ACTUAL DRAG	CASE 2/ ACTUAL DRAG				CASE 1	CASE 2
1	1	8.34376	8.34368	8.33975	8.33993	0.99999	0.99953	0.99955	1	0.02975	0.06903	0.06594	
	2	11.14495	9.84757	9.99678	10.01550	0.88359	1.01515	1.01705	2	0.08033	0.02557	0.02442	
	3	8.33682	8.33653	8.33275	8.33294	0.99997	0.99955	0.99957	3	0.13846	0.01483	0.01417	
	4	10.80862	9.46099	9.18203	9.23493	0.87532	0.97052	0.97611	4	0.19154	0.01072	0.01024	
	5	7.10426	6.55079	6.66979	6.67536	0.92209	1.01816	1.01901	5	0.24705	0.00831	0.00794	
2	1	14.94299	14.57212	14.22263	14.45809	0.97518	0.97602	0.99217	1	0.24705	0.01195	0.00794	
	2	10.34037	9.94032	9.71766	9.92237	0.96131	0.97760	0.99819	2	0.66710	0.00443	0.00294	
	3	8.46221	7.48731	6.87241	7.24566	0.88479	0.91787	0.96773	3	1.14978	0.00257	0.00171	
	4	6.37363	5.58471	5.65216	5.88093	0.87622	1.01208	1.05304	4	1.59056	0.00186	0.00123	
	5	3.73147	3.37250	3.53237	3.59768	0.90380	1.04740	1.06677	5	2.05154	0.00144	0.00096	
3	1	5.95054	5.65177	5.65185	5.63967	0.94979	1.00002	0.99786	1	1.50154	0.00125	0.00131	
	2	4.20023	4.02215	4.01024	4.00247	0.95760	0.99704	0.99511	2	4.05462	0.00046	0.00048	
	3	3.13073	2.99998	2.99404	2.99844	0.95824	0.99802	0.99615	3	6.98833	0.00027	0.00028	
	4	1.76116	1.68694	1.68706	1.68402	0.95786	1.00007	0.99827	4	9.66739	0.00019	0.00020	
	5	0.68853	0.65908	0.66028	0.65913	0.95723	1.00183	1.00007	5	12.46919	0.00015	0.00016	

CASE 1 - VELOCITY OF EACH MASS (COMPUTED IN ACTUAL DRAG PROBLEM) IS USED TO LINEARIZE THE DRAG FORCE

CASE 2 - GROUND VELOCITY IS USED TO LINEARIZE THE DRAG FORCE

Table 3.5

Response of System 1M to El Centro Earthquake, 1940, N-S Component.
Direct Integration Solution. $\beta_s = .05$

FREQ. RANGE	MASS NO.	MAXIMUM RELATIVE DISPLACEMENT BETWEEN MASS AND GROUND (INCHES)				COMPARISON OF SOLUTIONS				MODAL PROPERTIES			
		NO DRAG	ACTUAL DRAG	LINEAR CASE 1	CASE 2	ACTUAL NO DRAG	ACTUAL DRAG	CASE 1/ ACTUAL	CASE 2/ ACTUAL	MODE NO.	FREQ. (CPS)	LINEAR HYDRAULIC DAMPING RATIO	
1	1	8.27668	8.27664	8.27443	8.27387	1.00000	0.99973	0.99973	0.99966	1	0.02975	0.05255	0.06594
	2	9.08362	8.65985	8.85112	8.79439	0.95775	1.01739	1.01739	1.01087	2	0.08033	0.01946	0.02442
	3	8.21097	8.21094	8.20917	8.20872	1.00000	0.99978	0.99978	0.99973	3	0.13846	0.01129	0.01417
	4	7.93429	7.85862	7.89744	7.89755	0.99550	0.99985	0.99985	0.99986	4	0.19154	0.00816	0.01024
	5	6.39375	6.17861	6.30429	6.28184	0.96635	1.02034	1.02034	1.01671	5	0.24705	0.00633	0.00794
2	1	12.91256	12.65838	12.52315	12.50722	0.98032	0.98932	0.98932	0.98806	1	0.24705	0.00762	0.00794
	2	8.19152	8.09426	8.06589	8.06071	0.98813	0.99649	0.99649	0.99585	2	0.66710	0.00282	0.00294
	3	5.66697	5.64506	5.59642	5.59353	0.99613	0.99138	0.99138	0.99087	3	1.14978	0.00164	0.00171
	4	4.34317	4.24070	4.23927	4.23500	0.97641	0.99966	0.99966	0.99866	4	1.59056	0.00118	0.00123
	5	2.11593	2.07038	2.08257	2.08161	0.97547	1.00608	1.00608	1.00542	5	2.05154	0.00092	0.00096
3	1	3.39496	3.38500	3.38356	3.37940	0.99706	0.99957	0.99957	0.99835	1	1.50154	0.00096	0.00131
	2	2.20938	2.20415	2.20207	2.19941	0.99763	0.99906	0.99906	0.99785	2	4.05462	0.00035	0.00048
	3	1.64792	1.63635	1.63770	1.63399	0.99298	1.00082	1.00082	0.99855	3	6.98833	0.00021	0.00028
	4	0.93596	0.92906	0.93039	0.92836	0.99263	1.00142	1.00142	0.99924	4	9.66739	0.00015	0.00020
	5	0.36560	0.36293	0.36345	0.36267	0.99270	1.00145	1.00145	0.99930	5	12.46919	0.00012	0.00016

CASE 1 - VELOCITY OF EACH MASS (COMPUTED IN ACTUAL DRAG PROBLEM) IS USED TO LINEARIZE THE DRAG FORCE

CASE 2 - GROUND VELOCITY IS USED TO LINEARIZE THE DRAG FORCE

Table 3.6

Response of System 2L to E1 Centro Earthquake, 1940, N-S Component.
Direct Integration Solution. $\beta_s = .01$

FREQ. RANGE	MASS NO.	MAXIMUM RELATIVE DISPLACEMENT BETWEEN MASS AND GROUND (INCHES)					COMPARISON OF SOLUTIONS				MODAL PROPERTIES		
		NO DRAG	ACTUAL DRAG	CASE 1	LINEAR DRAG	CASE 2	ACTUAL DRAG/ NO DRAG	CASE 1/ ACTUAL DRAG	CASE 2/ ACTUAL DRAG	MODE NO.	FREQ. (CPS)	LINEAR HYDRAULIC DAMPING RATIO	
1	1	5.49950	9.17185	8.92827	8.91966		0.96551	0.97344	0.97250	1	0.03179	0.03037	0.03085
	2	11.09532	10.35364	10.27146	10.25914		0.93315	0.99206	0.99087	2	0.08674	0.01113	0.01131
	3	12.14936	10.74920	10.47053	10.44627		0.88475	0.97408	0.97182	3	0.15129	0.00638	0.00648
	4	9.42407	8.91512	8.85665	8.84814		0.94599	0.99344	0.99249	4	0.21093	0.00458	0.00465
	5	7.00801	6.46727	6.47506	6.47209		0.92284	1.00120	1.00074	5	0.24705	0.00391	0.00397
2	1	13.72973	13.63457	13.56307	13.61465		0.99307	0.99476	0.99854	1	0.24705	0.00577	0.00397
	2	10.51359	10.42611	10.37374	10.41697		0.99168	0.99498	0.99912	2	0.67402	0.00211	0.00146
	3	7.93934	7.68045	7.66379	7.74862		0.96739	0.99783	1.00888	3	1.17564	0.00121	0.00083
	4	6.04372	5.75649	5.84254	5.90446		0.95247	1.01495	1.02570	4	1.63909	0.00087	0.00060
	5	3.39892	3.25892	3.30242	3.33213		0.95881	1.01335	1.02246	5	1.91972	0.00074	0.00051
3	1	3.48998	3.46740	3.47053	3.47571		0.99353	1.00090	1.00240	1	1.50154	0.00089	0.00065
	2	2.96016	2.94425	2.94479	2.94888		0.99463	1.00018	1.00157	2	4.09666	0.00033	0.00024
	3	2.24834	2.23509	2.23660	2.23973		0.99410	1.00068	1.00207	3	7.14549	0.00019	0.00014
	4	1.14667	1.13901	1.14056	1.14218		0.99332	1.00135	1.00278	4	9.96233	0.00013	0.00010
	5	0.47725	0.47405	0.47463	0.47532		0.99330	1.00122	1.00269	5	11.66800	0.00011	0.00008

CASE 1 - VELOCITY OF EACH MASS (COMPUTED IN ACTUAL DRAG PROBLEM) IS USED TO LINEARIZE THE DRAG FORCE

CASE 2 - GROUND VELOCITY IS USED TO LINEARIZE THE DRAG FORCE

Table 3.7

Response of System 2L to El Centro Earthquake, 1940, N-S Component.
Direct Integration Solution. $\beta_s = .05$

MAXIMUM RELATIVE DISPLACEMENT BETWEEN MASS AND GROUND (INCHES)										COMPARISON OF SOLUTIONS				MODAL PROPERTIES			
FREQ. RANGE	MASS NO.	NO DRAG	ACTUAL CRAG	LINEAR DRAG		ACTUAL DRAG/ NO DRAG		CASE 1/ ACTUAL DRAG		CASE 2/ ACTUAL DRAG	MODE NO.	FREQ. (CPS)	LINEAR HYDRAULIC DAMPING RATIO				
				CASE 1	CASE 2	ACTUAL DRAG	NO DRAG	ACTUAL DRAG	ACTUAL DRAG				CASE 1	CASE 2			
1	1	8.27048	8.27058	8.26955	8.26909	1.00001	0.99988	0.99988	0.99982	1	0.03179	0.02050	0.03085				
	2	8.24486	8.24466	8.24403	8.24361	0.99998	0.99992	0.99992	0.99987	2	0.08674	0.00751	0.01131				
	3	9.20546	9.07775	9.12939	9.09189	0.98613	1.00569	1.00156	1.00156	3	0.15129	0.00431	0.00648				
	4	7.97655	7.97706	7.97646	7.97642	1.00006	0.99992	0.99992	0.99992	4	0.21093	0.00309	0.00465				
	5	6.16006	6.10351	6.12152	6.10220	0.99082	1.00295	0.99978	0.99978	5	0.24705	0.00264	0.00397				
2	1	12.24895	12.18088	12.15051	12.14900	0.99444	0.99751	0.99751	0.99738	1	0.24705	0.00391	0.00397				
	2	8.79445	8.74997	8.72222	8.72112	0.99494	0.99683	0.99683	0.99670	2	0.67402	0.00143	0.00146				
	3	6.67160	6.63372	6.61492	6.61406	0.99432	0.99717	0.99717	0.99704	3	1.17564	0.00082	0.00083				
	4	4.53572	4.49195	4.49734	4.49675	0.99035	1.00120	1.00120	1.00107	4	1.63909	0.00059	0.00060				
	5	2.04375	1.99533	2.00788	2.00734	0.97631	1.00629	1.00629	1.00602	5	1.91972	0.00050	0.00051				
3	1	3.12015	3.10551	3.10868	3.11096	0.99531	1.00102	1.00102	1.00176	1	1.50154	0.00081	0.00065				
	2	2.64754	2.63400	2.63701	2.63910	0.99488	1.00115	1.00115	1.00194	2	4.09666	0.00030	0.00024				
	3	1.86243	1.85306	1.85489	1.85639	0.99497	1.00099	1.00099	1.00180	3	7.14549	0.00017	0.00014				
	4	0.86184	0.85733	0.85767	0.85850	0.99476	1.00040	1.00040	1.00137	4	9.96233	0.00012	0.00010				
	5	0.35558	0.35335	0.35365	0.35403	0.99372	1.00084	1.00084	1.00193	5	11.66800	0.00010	0.00008				

CASE 1 - VELOCITY OF EACH MASS (COMPUTED IN ACTUAL DRAG PROBLEM) IS USED TO LINEARIZE THE DRAG FORCE

CASE 2 - GROUND VELOCITY IS USED TO LINEARIZE THE DRAG FORCE

Table 3.8

Response of System 2M to El Centro Earthquake, 1940, N-S Component.
Direct Integration Solution. $\beta_s = .01$

FREQ. RANGE	MASS NO.	MAXIMUM RELATIVE DISPLACEMENT BETWEEN MASS AND GROUND (INCHES)				COMPARISON OF SOLUTIONS				MODAL PROPERTIES			
		NO DRAG	ACTUAL DRAG	LINEAR CASE 1	DRAG CASE 2	ACTUAL NO DRAG	DRAG ACTUAL	CASE 1/ ACTUAL	CASE 2/ ACTUAL	MODE NO.	FREQ. (CPS)	CASE 1	CASE 2
1	1	9.49950	9.01258	8.49229	8.38407	0.94874	0.94227	0.93026	0.93179	1	0.03179	0.05519	0.06170
	2	11.09532	9.91122	9.65295	9.50095	0.89328	0.97394	0.95861	0.08674	2	0.08674	0.02023	0.02262
	3	12.14936	10.03294	10.16300	10.12984	0.82580	1.01296	1.00966	0.15129	3	0.15129	0.01160	0.01297
	4	9.42407	8.43952	8.43270	8.32606	0.89553	0.9919	0.98656	0.21093	4	0.21093	0.00832	0.00930
	5	7.00801	6.30414	6.41335	6.39964	0.89956	1.01732	1.01515	0.24705	5	0.24705	0.00710	0.00794
2	1	13.72973	13.61662	13.45621	13.50120	0.99176	0.98822	0.99152	0.24705	1	0.24705	0.00953	0.00794
	2	10.51359	10.39743	10.28440	10.32201	0.98895	0.98913	0.99275	0.67402	2	0.67402	0.00349	0.00291
	3	7.93934	7.64308	7.57108	7.59907	0.96268	0.99058	0.99424	1.17564	3	1.17564	0.00200	0.00167
	4	6.04372	5.62495	5.71536	5.76875	0.93071	1.01607	1.02557	1.63909	4	1.63909	0.00144	0.00120
	5	3.39892	3.09184	3.24131	3.26698	0.90965	1.04834	1.05664	1.91972	5	1.91972	0.00121	0.00102
3	1	3.48998	3.46175	3.46366	3.46150	0.99191	1.00055	0.99993	1.50154	1	1.50154	0.00121	0.00131
	2	2.96016	2.93989	2.93937	2.93766	0.99315	0.99982	0.99924	4.09666	2	4.09666	0.00044	0.00048
	3	2.24834	2.23060	2.23246	2.23116	0.99211	1.00083	1.00025	7.14549	3	7.14549	0.00025	0.00027
	4	1.14667	1.13640	1.13840	1.13772	0.99104	1.00176	1.00116	9.96233	4	9.96233	0.00018	0.00020
	5	0.47725	0.47307	0.47370	0.47341	0.99126	1.00133	1.00071	11.66800	5	11.66800	0.00016	0.00017

CASE 1 - VELOCITY OF EACH MASS (COMPUTED IN ACTUAL DRAG PROBLEM) IS USED TO LINEARIZE THE DRAG FORCE

CASE 2 - GROUND VELOCITY IS USED TO LINEARIZE THE DRAG FORCE

Table 3.9

Response of System 2M to El Centro Earthquake, 1940, N-S Component.
Direct Integration Solution. $\beta_s = .05$

MAXIMUM RELATIVE DISPLACEMENT BETWEEN MASS AND GROUND (INCHES)										COMPARISON OF SOLUTIONS				MODAL PROPERTIES		
FREQ. RANGE	MASS NO.	NO DRAG	ACTUAL DRAG	LINEAR DRAG		ACTUAL DRAG/NO DRAG	CASE 1/ACTUAL DRAG		CASE 2/ACTUAL DRAG	MODE NO.	FREQ. (CPS)	LINEAR HYDRAULIC DAMPING RATIO				
				CASE 1	CASE 2		ACTUAL DRAG	CASE 1/ACTUAL DRAG				CASE 1	CASE 2			
1	1	8.27048	8.27043	8.26856	8.26773	0.99999	0.99977	0.99967	1	0.03179	0.04284	0.06170				
	2	8.24486	8.24491	8.24313	8.24238	1.00001	0.99978	0.99969	2	0.08674	0.01570	0.02262				
	3	9.20546	8.92633	9.04888	8.98247	0.96968	1.01373	1.00629	3	0.15125	0.00900	0.01297				
	4	7.97655	7.97752	7.97637	7.97630	1.00012	0.99986	0.99985	4	0.21093	0.00646	0.00930				
	5	6.16006	5.96267	6.07996	6.04524	0.96796	1.01967	1.01385	5	0.24705	0.00551	0.00794				
2	1	12.24895	12.16705	12.07789	12.05043	0.99332	0.99267	0.99041	1	0.24705	0.00683	0.00794				
	2	8.79445	8.74442	8.66907	8.64899	0.99431	0.99138	0.98909	2	0.67402	0.00250	0.00291				
	3	6.67160	6.61798	6.57320	6.55743	0.99196	0.99323	0.99085	3	1.17564	0.00143	0.00167				
	4	4.53572	4.45668	4.46907	4.45838	0.98257	1.00278	1.00038	4	1.63909	0.00103	0.00120				
	5	2.04375	1.94971	1.98161	1.97172	0.95399	1.01636	1.01129	5	1.91972	0.00088	0.00102				
3	1	3.12015	3.10209	3.10330	3.10164	0.99421	1.00039	0.99986	1	1.50154	0.00119	0.00131				
	2	2.64754	2.63035	2.63212	2.63061	0.99351	1.00067	1.00010	2	4.09666	0.00044	0.00048				
	3	1.86243	1.85064	1.85137	1.85029	0.99367	1.00040	0.99981	3	7.14549	0.00025	0.00027				
	4	0.86184	0.85639	0.85576	0.85517	0.99367	0.99926	0.99857	4	9.96233	0.00020	0.00020				
	5	0.35558	0.35275	0.35275	0.35248	0.99204	1.00000	0.99922	5	11.66800	0.00015	0.00017				

CASE 1 - VELOCITY OF EACH MASS (COMPUTED IN ACTUAL DRAG PROBLEM) IS USED TO LINEARIZE THE DRAG FORCE

CASE 2 - GROUND VELOCITY IS USED TO LINEARIZE THE DRAG FORCE

Table 3.10

Response of System 3L to El Centro Earthquake, 1940, N-S Component.
Direct Integration Solution. $\beta_s = .01$

FREQ. RANGE	MASS NO.	MAXIMUM RELATIVE DISPLACEMENT BETWEEN MASS AND GROUND (INCHES)				COMPARISON OF SOLUTIONS				MODAL PROPERTIES			
		NO DRAG	ACTUAL DRAG	CASE 1	LINEAR DRAG CASE 2	ACTUAL DRAG/ NO DRAG	CASE 1/ ACTUAL DRAG	CASE 2/ ACTUAL DRAG	MODE NO.	FREQ. (CPS)	CASE 1	CASE 2	LINEAR HYDRAULIC DAMPING RATIO
1	1	13.20448	12.78873	12.71447	12.58725	0.96851	0.99419	0.98425	1	0.04559	0.01684	0.02151	0.00989
	2	11.24453	10.49355	10.58399	10.43800	0.93321	1.00862	0.99471	2	0.09918	0.00774	0.00657	0.00505
	3	11.39191	11.06992	10.98039	10.86893	0.97174	0.99191	0.98184	3	0.14923	0.00514	0.00396	0.00397
	4	8.89067	8.59288	8.54009	8.50500	0.96650	0.99386	0.98977	4	0.19404	0.00396	0.00311	0.00397
	5	7.26278	6.78631	6.68180	6.53252	0.93440	0.98460	0.96260	5	0.24705	0.00311	0.00397	0.00397
2	1	17.01196	16.51581	16.46686	16.62172	0.97083	0.99704	1.00641	1	0.24705	0.00744	0.00397	0.00397
	2	15.48386	14.87991	15.01287	15.22820	0.96099	1.00893	1.02341	2	0.53739	0.00342	0.00183	0.00183
	3	11.23426	10.16669	10.30785	10.72609	0.90497	1.01388	1.05502	3	0.80860	0.00227	0.00121	0.00121
	4	7.73713	7.01679	7.06955	7.37145	0.90690	1.00752	1.05054	4	1.05138	0.00175	0.00093	0.00093
	5	5.02086	4.53132	4.58887	4.78466	0.90250	1.01270	1.05591	5	1.33858	0.00137	0.00073	0.00073
3	1	7.20725	6.44290	6.45566	6.99750	0.89395	1.00198	1.08608	1	1.50154	0.00263	0.00065	0.00065
	2	5.64242	5.05489	5.08636	5.49006	0.89587	1.00622	1.08609	2	3.26626	0.00121	0.00030	0.00030
	3	4.49212	3.99474	4.03318	4.37030	0.88928	1.00962	1.09401	3	4.91465	0.00080	0.00020	0.00020
	4	2.78515	2.48328	2.49853	2.70901	0.89165	1.00626	1.09086	4	6.39027	0.00062	0.00015	0.00015
	5	1.15390	1.05874	1.05471	1.12768	0.91753	0.99619	1.06511	5	8.13584	0.00049	0.00012	0.00012

CASE 1 - VELOCITY OF EACH MASS (COMPUTED IN ACTUAL DRAG PROBLEM) IS USED TO LINEARIZE THE DRAG FORCE

CASE 2 - GROUND VELOCITY IS USED TO LINEARIZE THE DRAG FORCE

Table 3.11

Response of System 3L to El Centro Earthquake, 1940, N-S Component.
Direct Integration Solution. $\beta_s = .05$

MAXIMUM RELATIVE DISPLACEMENT BETWEEN MASS AND GROUND (INCHES)				COMPARISON OF SOLUTIONS				MODAL PROPERTIES					
FREQ. RANGE	MASS NO.	NO DRAG	ACTUAL DRAG	LINEAR DRAG		ACTUAL DRAG/ NO DRAG	CASE 1/ ACTUAL DRAG		CASE 2/ ACTUAL DRAG	MODE NO.	FREQ. (CPS)	LINEAR HYDRAULIC DAMPING RATIO	
				CASE 1	CASE 2		ACTUAL DRAG	CASE 1				CASE 2	
1	1	10.03302	9.79899	9.80135	9.60027	0.97667	1.00024	0.97972	1	0.04559	0.01136	0.02151	
	2	8.52236	8.24617	8.31121	8.22573	0.96759	1.00789	0.99752	2	0.09918	0.00522	0.00989	
	3	9.13552	8.94046	8.92954	8.75196	0.9865	0.99878	0.97892	3	0.14923	0.00347	0.00657	
	4	8.03778	8.03792	8.03754	8.03733	1.00002	0.99995	0.99993	4	0.19404	0.00267	0.00505	
	5	6.23784	6.23875	6.24016	6.24224	1.00015	1.00023	1.00056	5	0.24705	0.00210	0.00397	
2	1	15.23825	14.92703	14.93779	15.00962	0.97958	1.00072	1.00553	1	0.24705	0.00531	0.00397	
	2	13.05756	12.63515	12.78419	12.85265	0.96765	1.01180	1.01721	2	0.53739	0.00244	0.00183	
	3	8.89772	8.60162	8.69979	8.74932	0.96672	1.01141	1.01717	3	0.80860	0.00162	0.00121	
	4	5.19395	5.13690	5.16272	5.17058	0.98902	1.00502	1.00656	4	1.05138	0.00125	0.00093	
	5	2.75579	2.69515	2.70513	2.71784	0.97800	1.00370	1.00842	5	1.33858	0.00098	0.00073	
3	1	4.22724	4.20123	4.20571	4.21735	0.99385	1.00107	1.00384	1	1.50154	0.00142	0.00065	
	2	3.19186	3.17344	3.17610	3.18462	0.99423	1.00084	1.00352	2	3.26626	0.00065	0.00030	
	3	2.34027	2.32644	2.32925	2.33521	0.99409	1.00121	1.00377	3	4.91465	0.00044	0.00020	
	4	1.61227	1.59351	1.59800	1.60571	0.98836	1.00282	1.00766	4	6.39027	0.00033	0.00015	
	5	0.71128	0.70298	0.70509	0.70844	0.98833	1.00300	1.00776	5	8.13584	0.00026	0.00012	

CASE 1 - VELOCITY OF EACH MASS (COMPUTED IN ACTUAL DRAG PROBLEM) IS USED TO LINEARIZE THE DRAG FORCE

CASE 2 - GROUND VELOCITY IS USED TO LINEARIZE THE DRAG FORCE

Table 3.12

Response of System 4L to El Centro Earthquake, 1940, N-S Component.
Direct Integration Solution. $\beta_s = .01$

MAXIMUM RELATIVE DISPLACEMENT BETWEEN MASS AND GROUND (INCHES)										COMPARISON OF SOLUTIONS				MODAL PROPERTIES		
FREQ. RANGE	MASS NO.	NO DRAG	ACTUAL DRAG	LINEAR DRAG		ACTUAL DRAG/ NO DRAG	CASE 1/ ACTUAL DRAG		CASE 2/ ACTUAL DRAG	MODE NO.	FREQ. (CPS)	LINEAR HYDRAULIC DAMPING RATIO				
				CASE 1	CASE 2		ACTUAL	DRAG				CASE 1	CASE 2			
1	1	13.25834	12.94732	12.92541	12.61753	0.97654	0.99831	0.97453	1	0.04010	0.01261	0.02446				
	2	13.20387	12.50747	12.64050	12.15941	0.94726	1.01064	0.97217	2	0.09042	0.00559	0.01085				
	3	10.63729	10.06772	10.25327	9.90845	0.94645	1.01843	0.98418	3	0.13689	0.00369	0.00717				
	4	8.53037	8.51701	8.48661	8.44743	0.99843	0.99643	0.99183	4	0.17242	0.00293	0.00569				
	5	7.14806	7.14865	7.14991	7.14887	1.00008	1.00018	1.00003	5	0.24705	0.00205	0.00397				
2	1	19.29724	16.05644	16.12639	17.54854	0.83206	1.00436	1.09293	1	0.24705	0.00768	0.00397				
	2	15.53333	14.91803	15.05144	15.28166	0.96039	1.00894	1.02437	2	0.55706	0.00340	0.00176				
	3	12.50000	11.98740	12.07937	12.27763	0.95899	1.00767	1.02421	3	0.84337	0.00225	0.00116				
	4	9.50951	8.61718	8.64316	9.04816	0.90616	1.00301	1.05001	4	1.06231	0.00179	0.00092				
	5	5.99528	5.33854	5.39362	5.67430	0.89046	1.01032	1.06289	5	1.52207	0.00125	0.00064				
3	1	6.89134	6.12729	6.17839	6.71723	0.88913	1.00834	1.09628	1	1.50154	0.00287	0.00065				
	2	5.73027	5.12490	5.14968	5.58831	0.89435	1.00483	1.09042	2	3.38581	0.00127	0.00029				
	3	4.77685	4.27018	4.28155	4.64747	0.93393	1.00266	1.08835	3	5.12599	0.00084	0.00019				
	4	3.51408	3.10447	3.13517	3.42118	0.88344	1.00989	1.10202	4	6.45668	0.00067	0.00015				
	5	1.61615	1.43335	1.44728	1.57481	0.88690	1.00971	1.09869	5	9.25111	0.00047	0.00011				

CASE 1 - VELOCITY OF EACH MASS (COMPUTED IN ACTUAL DRAG PROBLEM) IS USED TO LINEARIZE THE DRAG FORCE

CASE 2 - GROUND VELOCITY IS USED TO LINEARIZE THE DRAG FORCE

Table 3.13

Response of System 4L to El Centro Earthquake, 1940, N-S Component.
Direct Integration Solution. $\beta_s = .05$

MAXIMUM RELATIVE DISPLACEMENT BETWEEN MASS AND GROUND (INCHES)				COMPARISON OF SOLUTIONS				MODAL PROPERTIES					
FREQ. RANGE	MASS NO.	NO DRAG	ACTUAL CRAG	LINEAR DRAG		ACTUAL DRAG/ NO DRAG	CASE 1/ ACTUAL DRAG		CASE 2/ ACTUAL DRAG	MODE NO.	FREQ. (CPS)	LINEAR HYDRAULIC DAMPING RATIO	
				CASE 1	CASE 2		ACTUAL DRAG	CASE 2/ ACTUAL DRAG				CASE 1	CASE 2
1	1	10.12632	5.95900	9.97244	9.70347	0.98348	1.00135	0.97434	1	0.04010	0.00873	0.02446	
	2	10.19318	9.86070	9.94330	9.52367	0.96738	1.00838	0.96582	2	0.09042	0.00387	0.01085	
	3	8.39142	8.22538	8.22524	8.22460	0.98021	0.99998	0.99991	3	0.13689	0.00256	0.00717	
	4	8.14440	8.14446	8.14405	8.14369	1.00001	0.99995	0.99991	4	0.17242	0.00203	0.00569	
	5	6.90793	6.90846	6.90918	6.91177	1.00008	1.00010	1.00048	5	0.24705	0.00142	0.00397	
2	1	14.36318	14.06873	14.08726	14.14453	0.97950	1.00132	1.00539	1	0.24705	0.00544	0.00397	
	2	13.15307	12.71159	12.87065	12.94620	0.96644	1.01251	1.01846	2	0.55706	0.00241	0.00176	
	3	10.50090	10.14432	10.26855	10.33069	0.96604	1.01225	1.01837	3	0.84337	0.00159	0.00116	
	4	6.60460	6.38047	6.45367	6.49400	0.96607	1.01147	1.01779	4	1.06231	0.00126	0.00092	
	5	3.19568	3.16760	3.17753	3.18241	0.99121	1.00314	1.00468	5	1.52207	0.00088	0.00064	
3	1	4.01204	3.98594	3.99053	4.00291	0.99350	1.00115	1.00426	1	1.50154	0.00154	0.00065	
	2	3.29500	3.27357	3.27725	3.29746	0.99362	1.00100	1.00412	2	3.38581	0.00068	0.00029	
	3	2.65675	2.63956	2.64251	2.65071	0.99353	1.00112	1.00422	3	5.12599	0.00045	0.00019	
	4	1.89554	1.86848	1.87628	1.88737	0.98573	1.00417	1.01011	4	6.45668	0.00036	0.00015	
	5	0.92712	0.91502	0.91841	0.92342	0.98695	1.00370	1.00918	5	9.25111	0.00025	0.00011	

CASE 1 - VELOCITY OF EACH MASS (COMPUTED IN ACTUAL DRAG PROBLEM) IS USED TO LINEARIZE THE DRAG FORCE

CASE 2 - GROUND VELOCITY IS USED TO LINEARIZE THE DRAG FORCE

Table 3.14

Response of System 4M to El Centro Earthquake, 1940, N-S Component.
Direct Integration Solution. $\beta_s = .01$

MAXIMUM RELATIVE DISPLACEMENT BETWEEN MASS AND GROUND (INCHES)										COMPARISON OF SOLUTIONS				MODAL PROPERTIES		
FREQ. RANGE	MASS NO.	NO DRAG	ACTUAL CRAG	LINEAR DRAG		ACTUAL DRAG/NO DRAG	CASE 1/ACTUAL DRAG		CASE 2/ACTUAL DRAG	MODE NO.	FREQ. (CPS)	LINEAR HYDRAULIC DAMPING RATIO				
				CASE 1	CASE 2		ACTUAL	DRAG				CASE 1	CASE 2			
1	1	13.25834	12.63619	12.65945	12.01110	0.95308	1.00184	0.95053	1	0.04010	0.02276	0.04892				
	2	13.20387	12.12951	12.22274	11.25315	0.91863	1.00769	0.92775	2	0.09042	0.01009	0.02170				
	3	10.63729	9.82301	9.95267	9.26554	0.92345	1.01320	0.94325	3	0.13689	0.00667	0.01433				
	4	8.53037	8.42515	8.45530	8.36580	0.98767	1.00358	0.99296	4	0.17242	0.00529	0.01138				
	5	7.14806	7.14785	7.14872	7.15044	0.99997	1.00012	1.00036	5	0.24705	0.00369	0.00794				
2	1	19.29724	15.40078	15.28366	16.03261	0.79808	0.99240	1.04103	1	0.24705	0.01216	0.00794				
	2	15.53333	14.72544	14.77813	15.03528	0.94799	1.00358	1.02104	2	0.55706	0.00539	0.00352				
	3	12.50009	11.81780	11.84438	12.06545	0.94542	1.00225	1.02096	3	0.84337	0.00356	0.00233				
	4	9.50951	8.20310	8.18358	8.61534	0.86262	0.99762	1.05025	4	1.06231	0.00283	0.00185				
	5	5.99528	4.97603	5.07640	5.37438	0.82999	1.02017	1.08005	5	1.52207	0.00197	0.00129				
3	1	6.89134	5.93653	5.99812	6.55030	0.86145	1.01037	1.10339	1	1.50154	0.00368	0.00131				
	2	5.73027	4.97499	5.00320	5.45229	0.86819	1.00567	1.09594	2	3.38581	0.00163	0.00058				
	3	4.77685	4.15454	4.16764	4.52537	0.86972	1.00315	1.08926	3	5.12599	0.00108	0.00038				
	4	3.51408	3.00268	3.04000	3.33222	0.85447	1.01243	1.10978	4	6.45668	0.00086	0.00030				
	5	1.61615	1.38688	1.40477	1.53522	0.85814	1.01289	1.10696	5	9.25111	0.00060	0.00021				

CASE 1 - VELOCITY OF EACH MASS (COMPUTED IN ACTUAL DRAG PROBLEM) IS USED TO LINEARIZE THE DRAG FORCE

CASE 2 - GROUND VELOCITY IS USED TO LINEARIZE THE DRAG FORCE

Table 3.15

Response of System 4M to El Centro Earthquake, 1940, N-S Component.
Direct Integration Solution. $\beta_s = .05$

FREQ. RANGE	MASS NO.	MAXIMUM RELATIVE DISPLACEMENT BETWEEN MASS AND GROUND (INCHES)				COMPARISON OF SOLUTIONS				MODAL PROPERTIES			
		NO DRAG	ACTUAL DRAG	LINEAR DRAG		ACTUAL DRAG/ NO DRAG	CASE 1/ ACTUAL DRAG		MODE NO.	FREQ. (CPS)	LINEAR HYDRAULIC DAMPING RATIO		CASE 2
				CASE 1	CASE 2		ACTUAL DRAG	ACTUAL DRAG			CASE 1	CASE 2	
1	1	10.12632	9.76843	9.83511	9.30323	0.96466	1.00683	0.95238	1	0.04010	0.01671	0.04892	
	2	10.19318	9.66858	9.72661	8.92716	0.94853	1.00600	0.92332	2	0.09042	0.00741	0.02170	
	3	8.39142	8.22560	8.22500	8.22338	0.98024	0.99993	0.99973	3	0.13689	0.00489	0.01433	
	4	8.14440	8.14447	8.14398	8.14281	1.00001	0.99994	0.99980	4	0.17242	0.00389	0.01138	
	5	6.90793	6.90562	6.91064	6.91531	1.00024	1.00015	1.00082	5	0.24705	0.00271	0.00794	
2	1	14.36318	14.02899	14.01218	14.02328	0.97673	0.99880	0.99959	1	0.24705	0.00838	0.00794	
	2	13.15307	12.56993	12.72111	12.74317	0.95566	1.01203	1.01378	2	0.55706	0.00371	0.00352	
	3	10.50090	10.02199	10.14559	10.16373	0.95439	1.01233	1.01414	3	0.84337	0.00245	0.00233	
	4	6.60460	6.29193	6.37390	6.38566	0.95266	1.01303	1.01490	4	1.06231	0.00195	0.00185	
	5	3.19568	3.15504	3.16781	3.16925	0.98728	1.00405	1.00451	5	1.52207	0.00136	0.00129	
3	1	4.01204	3.97792	3.98167	3.99383	0.99150	1.00094	1.00400	1	1.50154	0.00218	0.00131	
	2	3.29500	3.26728	3.26994	3.27997	0.99159	1.00081	1.00388	2	3.38581	0.00097	0.00058	
	3	2.65675	2.63396	2.63664	2.64470	0.99142	1.00102	1.00408	3	5.12599	0.00064	0.00038	
	4	1.89554	1.85937	1.86836	1.87924	0.98092	1.00483	1.01068	4	6.45668	0.00051	0.00030	
	5	0.92712	0.91074	0.91482	0.91974	0.98233	1.00449	1.00989	5	9.25111	0.00035	0.00021	

CASE 1 - VELOCITY OF EACH MASS (COMPUTED IN ACTUAL DRAG PROBLEM) IS USED TO LINEARIZE THE DRAG FORCE

CASE 2 - GROUND VELOCITY IS USED TO LINEARIZE THE DRAG FORCE

Table 3.16

Response of System 4H to El Centro Earthquake, 1940, N-S Component.
Direct Integration Solution. $\beta_s = .01$

MAXIMUM RELATIVE DISPLACEMENT BETWEEN MASS AND GROUND (INCHES)										COMPARISON OF SOLUTIONS				MODAL PROPERTIES		
FREQ. RANGE	MASS NO.	NO DRAG	ACTUAL DRAG	LINEAR DRAG		ACTUAL DRAG/ NO DRAG	CASE 1/ ACTUAL DRAG		CASE 2/ ACTUAL DRAG	MODE NO.	FREQ. (CPS)	LINEAR HYDRAULIC DAMPING RATIO				
				CASE 1	CASE 2		ACTUAL	DRAG								
1	1	13.25834	12.03320	12.17210	10.89858	0.90759	1.01154	0.90571	1	0.04010	0.04237	0.09784				
	2	13.20387	11.28428	11.49053	9.74535	0.85462	1.01828	0.86362	2	0.09042	0.01879	0.04339				
	3	10.63729	9.20542	9.43403	8.32842	0.86539	1.02483	0.90473	3	0.13689	0.01241	0.02866				
	4	8.53037	8.33588	8.38593	8.29086	0.97720	1.00600	0.99460	4	0.17242	0.00985	0.02275				
	5	7.14806	7.14926	7.14990	7.15546	1.00017	1.00009	1.00087	5	0.24705	0.00688	0.01588				
2	1	19.29724	15.15814	15.01744	15.17896	0.78758	0.98811	0.99874	1	0.24705	0.02173	0.01588				
	2	15.53333	14.06545	14.21535	14.55687	0.90550	1.01066	1.03494	2	0.55706	0.00964	0.00704				
	3	12.50009	11.26258	11.36081	11.65424	0.90100	1.00872	1.03477	3	0.84337	0.00637	0.00465				
	4	9.50951	7.23986	7.30467	7.82652	0.76133	1.00895	1.08103	4	1.06231	0.00505	0.00369				
	5	5.99528	4.29734	4.47351	4.83086	0.71679	1.04099	1.12415	5	1.52207	0.00353	0.00258				
3	1	6.89134	5.34785	5.42964	6.23662	0.77602	1.01529	1.16619	1	1.50154	0.00655	0.00261				
	2	5.73027	4.47753	4.54221	5.19702	0.78138	1.01444	1.16069	2	3.38581	0.00291	0.00116				
	3	4.77685	3.76602	3.80878	4.31831	0.79839	1.01135	1.14665	3	5.12599	0.00192	0.00077				
	4	3.51408	2.71582	2.74929	3.16596	0.77398	1.01083	1.16403	4	6.45668	0.00152	0.00061				
	5	1.61615	1.23786	1.27116	1.46103	0.76593	1.02691	1.18028	5	9.25111	0.00106	0.00042				

CASE 1 - VELOCITY OF EACH MASS (COMPUTED IN ACTUAL DRAG PROBLEM) IS USED TO LINEARIZE THE DRAG FORCE

CASE 2 - GROUND VELOCITY IS USED TO LINEARIZE THE DRAG FORCE

Table 3.17

Response of System 4H to El Centro Earthquake, 1940, N-S Component.
Direct Integration Solution. $\beta_s = .05$

MAXIMUM RELATIVE DISPLACEMENT BETWEEN MASS AND GROUND (INCHES)										COMPARISON OF SOLUTIONS				MODAL PROPERTIES			
FREQ. RANGE	MASS NO.	NO DRAG	ACTUAL DRAG	LINEAR		ACTUAL DRAG/ NO DRAG	CASE 1/ ACTUAL DRAG		CASE 2/ ACTUAL DRAG		MODE NO.	FREQ. (CPS)	LINEAR HYDRAULIC DAMPING RATIO				
				CASE 1	DRAG CASE 2		ACTUAL DRAG	ACTUAL DRAG	ACTUAL DRAG	CASE 1			CASE 2				
1	1	10.12632	9.42937	9.57001	8.57170	0.93117	1.01491	0.90904	1	0.04010	0.03248	0.09784					
	2	10.19318	9.22517	9.32068	8.23957	0.90503	1.01035	0.89316	2	0.09042	0.01441	0.04339					
	3	8.39142	8.22449	8.22420	8.22140	0.98011	0.99996	0.99962	3	0.13689	0.00951	0.02866					
	4	8.14440	8.14460	8.14340	8.14156	1.00002	0.99985	0.99963	4	0.17242	0.00755	0.02275					
	5	6.90793	6.91107	6.91293	6.92290	1.00045	1.00027	1.00171	5	0.24705	0.00527	0.01588					
2	1	14.36318	13.85137	13.82229	13.82327	0.96437	0.99790	0.99797	1	0.24705	0.01592	0.01588					
	2	13.15307	12.08113	12.34631	12.34822	0.91850	1.02195	1.02211	2	0.55706	0.00706	0.00704					
	3	10.50090	9.61759	9.83784	9.83941	0.91588	1.02290	1.02306	3	0.84337	0.00466	0.00465					
	4	6.60460	6.01298	6.17445	6.17546	0.91042	1.02685	1.02702	4	1.06231	0.00370	0.00369					
	5	3.19568	3.11046	3.14309	3.14322	0.97333	1.01049	1.01053	5	1.52207	0.00258	0.00258					
3	1	4.01204	3.94658	3.95355	3.97577	0.98369	1.00177	1.00739	1	1.50154	0.00423	0.00261					
	2	3.29500	3.24174	3.24674	3.26507	0.98384	1.00154	1.00720	2	3.38581	0.00188	0.00116					
	3	2.65675	2.61294	2.61802	2.63273	0.98351	1.00194	1.00757	3	5.12599	0.00124	0.00077					
	4	1.89554	1.82704	1.84323	1.86307	0.96386	1.00886	1.01972	4	6.45668	0.00098	0.00061					
	5	0.92712	0.89638	0.90345	0.91243	0.96695	1.00788	1.01791	5	9.25111	0.00069	0.00042					

CASE 1 - VELOCITY OF EACH MASS (COMPUTED IN ACTUAL DRAG PROBLEM) IS USED TO LINEARIZE THE DRAG FORCE

CASE 2 - GROUND VELOCITY IS USED TO LINEARIZE THE DRAG FORCE

Table 3.18

Response of System 5H to El Centro Earthquake, 1940, N-S Component.
Direct Integration Solution. $\beta_s = .01$

MAXIMUM RELATIVE DISPLACEMENT BETWEEN MASS AND GROUND (INCHES)										COMPARISON OF SOLUTIONS				MODAL PROPERTIES			
FREQ. RANGE	MASS NO.	NO DRAG	ACTUAL DRAG	LINEAR DRAG		ACTUAL DRAG/ NO DRAG	CASE 1/ ACTUAL DRAG		CASE 2/ ACTUAL DRAG	MODE NO.	FREQ. (CPS)	LINEAR HYDRAULIC DAMPING RATIO					
				CASE 1	CASE 2		ACTUAL DRAG	CASE 1/ ACTUAL DRAG				CASE 1	CASE 2				
1	1	10.36027	8.89469	8.89756	8.33416	0.85854	1.00032	0.93698	1	0.03544	0.03472	0.11072					
	2	9.00907	8.34053	8.33793	8.33304	0.92579	0.99969	0.99910	2	0.08440	0.01458	0.04649					
	3	9.12568	8.33794	8.33602	8.33114	0.91368	0.99977	0.99918	3	0.13538	0.00909	0.02898					
	4	8.31736	8.31709	8.31445	8.30971	0.99997	0.99968	0.99911	4	0.18558	0.00663	0.02114					
	5	7.57978	7.57587	7.58002	7.58353	1.00001	1.00002	1.00048	5	0.24705	0.00498	0.01588					
2	1	16.40099	14.60540	14.96054	15.30479	0.89052	1.02431	1.04788	1	0.24705	0.02117	0.01588					
	2	14.75754	13.20629	13.50048	13.80246	0.89488	1.02228	1.04514	2	0.58840	0.00889	0.00667					
	3	12.47689	11.19467	11.44645	11.69412	0.89723	1.02249	1.04461	3	0.94379	0.00554	0.00416					
	4	9.57945	8.54578	8.76592	8.95993	0.89209	1.02576	1.04846	4	1.29380	0.00404	0.00303					
	5	6.09854	5.04251	5.01928	5.07686	0.82684	0.99539	1.00681	5	1.72232	0.00304	0.00228					
3	1	6.36212	4.98059	4.91876	5.75734	0.78285	0.98759	1.15596	1	1.50154	0.00741	0.00261					
	2	5.91218	4.58844	4.54116	5.35370	0.77610	0.98969	1.16678	2	3.57628	0.00311	0.00110					
	3	5.10398	3.85125	3.89301	4.59149	0.75456	1.01084	1.19221	3	5.73636	0.00194	0.00068					
	4	3.94160	2.58687	3.02461	3.54090	0.75626	1.01468	1.18787	4	7.86368	0.00142	0.00050					
	5	2.22342	1.68910	1.71275	1.99911	0.75969	1.01400	1.18354	5	10.46825	0.00106	0.00037					

CASE 1 - VELOCITY OF EACH MASS (COMPUTED IN ACTUAL DRAG PROBLEM) IS USED TO LINEARIZE THE DRAG FORCE

CASE 2 - GROUND VELOCITY IS USED TO LINEARIZE THE DRAG FORCE

Table 3.19

Response of System 5H to E1 Centro Earthquake, 1940, N-S Component.
Direct Integration Solution. $\beta_s = .05$

FREQ. RANGE	MASS NO.	MAXIMUM RELATIVE DISPLACEMENT BETWEEN MASS AND GROUND (INCHES)				COMPARISON OF SOLUTIONS				MODAL PROPERTIES			
		NO DRAG	ACTUAL DRAG	LIN. DRAG CASE 1	CASE 2	ACTUAL DRAG/NO DRAG	CASE 1/ACTUAL DRAG	CASE 2/ACTUAL DRAG	MODE NO.	FREQ. (CPS)	LINEAR DAMPING RATIO CASE 1	CASE 2	HYDRAULIC DAMPING RATIO
1	1	8.26603	8.26704	8.26489	8.26073	1.00012	0.99974	0.99924	1	0.03544	0.02501	0.11072	
	2	8.25971	8.25582	8.25861	8.25456	1.00001	0.99985	0.99936	2	0.08440	0.01050	0.04649	
	3	8.24480	8.24387	8.24381	8.23998	0.99989	0.99999	0.99953	3	0.13538	0.00655	0.02898	
	4	8.19189	8.19227	8.19120	8.18811	1.00004	0.99987	0.99949	4	0.18558	0.00478	0.02114	
	5	7.37495	7.37660	7.37705	7.38254	1.00022	1.00006	1.00081	5	0.24705	0.00359	0.01588	
2	1	14.08946	12.88284	13.12515	13.20867	0.91436	1.01881	1.02529	1	0.24705	0.01745	0.01588	
	2	12.84013	11.67611	11.97543	12.05015	0.90935	1.02563	1.03203	2	0.58840	0.00733	0.00667	
	3	10.84391	9.86660	10.12372	10.18617	0.90988	1.02606	1.03239	3	0.94379	0.00457	0.00416	
	4	8.16476	7.39727	7.60971	7.65779	0.90600	1.02872	1.03522	4	1.29380	0.00333	0.00303	
	5	4.43244	4.28068	4.28727	4.29989	0.96576	1.00154	1.00449	5	1.72232	0.00250	0.00228	
3	1	3.68855	3.62051	3.62886	3.65570	0.98155	1.00231	1.00972	1	1.50154	0.00478	0.00261	
	2	3.40973	3.34648	3.35412	3.37912	0.98145	1.00228	1.00975	2	3.57628	0.00201	0.00110	
	3	2.89037	2.82595	2.83286	2.85422	0.98111	1.00245	1.01000	3	5.73636	0.00125	0.00068	
	4	2.15211	2.10969	2.11599	2.13223	0.98029	1.00299	1.01068	4	7.86368	0.00091	0.00050	
	5	1.26380	1.21130	1.22545	1.24267	0.95845	1.01169	1.02590	5	10.46825	0.00069	0.00037	

CASE 1 - VELOCITY OF EACH MASS (COMPUTED IN ACTUAL DRAG PROBLEM) IS USED TO LINEARIZE THE DRAG FORCE

CASE 2 - GROUND VELOCITY IS USED TO LINEARIZE THE DRAG FORCE

Table 3.20

Response of System 6M to El Centro Earthquake, 1940, N-S Component.
Direct Integration Solution. $\beta_s = .01$

FREQ. RANGE	MASS NO.	MAXIMUM RELATIVE DISPLACEMENT BETWEEN MASS AND GROUND (INCHES)				COMPARISON OF SOLUTIONS			MODAL PROPERTIES		
		NO DRAG	ACTUAL DRAG	LINEAR CASE 1	DRAG CASE 2	ACTUAL DRAG/ NO DRAG	CASE 1/ ACTUAL DRAG	CASE 2/ ACTUAL DRAG	MODE NO.	FREQ. (CPS)	LINEAR HYDRAULIC DAMPING RATIO CASE 1 CASE 2
1	1	22.97723	19.77847	20.11722	17.45392	0.86079	1.01713	0.88247	1	0.04549	0.02045 0.04312
	2	10.61729	9.19778	9.54875	8.53971	0.86630	1.03816	0.92845	2	0.11323	0.00821 0.01732
	3	8.33501	8.33490	8.3221	8.33038	0.99999	0.99968	0.99946	3	0.16182	0.00575 0.01212
	4	8.79107	8.53151	8.50088	8.26937	0.97047	0.99641	0.96927	4	0.19702	0.00472 0.00996
	5	10.91731	10.06005	10.02830	9.17255	0.92148	0.99684	0.91178	5	0.24705	0.00376 0.00794
2	1	18.16364	15.42001	15.68618	16.49747	0.84895	1.01726	1.06987	1	0.24705	0.01224 0.00794
	2	15.75949	14.84304	14.97760	15.24662	0.94185	1.00906	1.02719	2	0.61495	0.00492 0.00319
	3	13.75409	12.96810	13.06557	13.30256	0.94285	1.00752	1.02579	3	0.87881	0.00344 0.00223
	4	8.75807	7.55182	7.60292	7.73735	0.86227	1.00677	1.02457	4	1.06999	0.00283 0.00183
	5	5.14138	4.56074	4.56624	4.75615	0.88707	1.00121	1.04284	5	1.34168	0.00225 0.00146
3	1	6.73209	5.65440	5.73768	6.39802	0.83992	1.01473	1.12974	1	1.50154	0.00413 0.00131
	2	6.04711	5.08344	5.14452	5.73298	0.84064	1.01201	1.12777	2	3.73764	0.00166 0.00052
	3	5.16690	4.38879	4.41931	4.89371	0.84941	1.00695	1.11505	3	5.34141	0.00116 0.00037
	4	3.73594	3.19990	3.22416	3.55932	0.85652	1.00758	1.11232	4	6.50338	0.00095 0.00030
	5	1.65158	1.43660	1.42327	1.56916	0.86984	0.99768	1.09157	5	8.15473	0.00076 0.00024

CASE 1 - VELOCITY OF EACH MASS (COMPUTED IN ACTUAL DRAG PROBLEM) IS USED TO LINEARIZE THE DRAG FORCE
CASE 2 - GROUND VELOCITY IS USED TO LINEARIZE THE DRAG FORCE

Table 3.21

Response of System 6M to El Centro Earthquake, 1940, N-S Component.
Direct Integration Solution. $\beta_s = .05$

FREQ. RANGE	MASS NO.	MAXIMUM RELATIVE DISPLACEMENT BETWEEN MASS AND GROUND (INCHES)				COMPARISON OF SOLUTIONS			MODAL PROPERTIES			
		NO DRAG	ACTUAL CRAG	LINEAR CASE 1	DRAG CASE 2	ACTUAL DRAG/ NO DRAG	CASE 1/ ACTUAL DRAG	CASE 2/ ACTUAL DRAG	MODE NO.	FREQ. (CPS)	LINEAR HYDRAULIC DAMPING RATIO	
1	1	12.62777	11.53311	11.62202	10.32109	0.91331	1.00771	0.89491	1	0.04549	0.01516	0.04312
	2	8.23270	8.23225	8.23182	8.23021	0.99995	0.99995	0.99975	2	0.11323	0.00609	0.01732
	3	8.21586	8.21605	8.21501	8.21347	1.00002	0.99987	0.99969	3	0.16182	0.00426	0.01212
	4	8.09758	8.09783	8.09708	8.09619	1.00003	0.99991	0.99980	4	0.19702	0.00350	0.00996
	5	7.28249	6.95114	6.94012	6.47830	0.95450	0.99842	0.93198	5	0.24705	0.00279	0.00794
2	1	13.84424	13.08367	13.28299	13.36749	0.94506	1.01523	1.02169	1	0.24705	0.00941	0.00794
	2	13.45003	12.77434	12.94993	13.02645	0.94976	1.01374	1.01974	2	0.61495	0.00378	0.00319
	3	11.60290	11.03047	11.17153	11.23754	0.95066	1.01279	1.01877	3	0.87881	0.00264	0.00223
	4	7.19391	6.83680	6.92540	6.96646	0.95036	1.01296	1.01896	4	1.06999	0.00217	0.00183
	5	3.75909	3.69295	3.69481	3.70468	0.98241	1.00050	1.00317	5	1.34168	0.00173	0.00146
3	1	3.81961	3.78268	3.78788	3.80241	0.99033	1.00137	1.00521	1	1.50154	0.00242	0.00131
	2	3.45087	3.41775	3.42192	3.43519	0.99040	1.00122	1.00510	2	3.73764	0.00097	0.00052
	3	2.93423	2.90573	2.90938	2.92076	0.99029	1.00125	1.00517	3	5.34141	0.00068	0.00037
	4	2.03215	2.01190	2.01493	2.02282	0.99004	1.00150	1.00543	4	6.50338	0.00056	0.00030
	5	0.98744	0.96580	0.97243	0.97930	0.97808	1.00687	1.01398	5	8.15473	0.00045	0.00024

CASE 1 - VELOCITY OF EACH MASS (COMPUTED IN ACTUAL DRAG PROBLEM) IS USED TO LINEARIZE THE DRAG FORCE

CASE 2 - GROUND VELOCITY IS USED TO LINEARIZE THE DRAG FORCE

Table 3.22

Response of System 6H to El Centro Earthquake, 1940, N-S Component.
Direct Integration Solution. $\beta_s = .01$

FREQ. RANGE	MASS NO.	MAXIMUM RELATIVE DISPLACEMENT BETWEEN MASS AND GROUND (INCHES)					COMPARISON OF SOLUTIONS				MODAL PROPERTIES			
		NO DRAG	ACTUAL CRAG	LINEAR CASE 1	DRAG CASE 2	ACTUAL NO DRAG	ACTUAL CASE 1/	ACTUAL CASE 2/	MODE NO.	FREQ. (CPS)	LINEAR HYDRAULIC DAMPING RATIO		CASE 1	CASE 2
1	1	22.97723	17.55089	18.02159	13.52390	0.76384	1.02682	0.77055	1	0.04549	0.03792	0.08625		
	2	10.61729	8.33527	8.75365	8.32800	0.78507	1.05019	0.90913	2	0.11323	0.01523	0.03465		
	3	8.33501	8.33446	8.33088	8.32711	0.99993	0.99957	0.99912	3	0.16182	0.01066	0.02425		
	4	8.79107	8.31334	8.26984	8.26645	0.94566	0.99477	0.99436	4	0.19702	0.00875	0.01991		
	5	10.91731	9.39155	9.35790	7.83236	0.86024	0.99642	0.83398	5	0.24705	0.00698	0.01588		
2	1	18.16364	14.46257	14.85268	15.32010	0.79624	1.02697	1.05929	1	0.24705	0.02219	0.01588		
	2	15.75949	14.06711	14.37524	14.75378	0.89261	1.02190	1.04881	2	0.61495	0.00891	0.00638		
	3	13.75409	12.28424	12.53471	12.86835	0.89313	1.02039	1.04755	3	0.87881	0.00624	0.00446		
	4	8.75807	7.29010	7.30159	7.49096	0.83239	1.00157	1.02755	4	1.06999	0.00512	0.00367		
	5	5.14138	4.29021	4.25566	4.41544	0.83445	0.99195	1.02919	5	1.34168	0.00409	0.00292		
3	1	6.73209	5.00750	5.11892	6.07248	0.74383	1.02225	1.21268	1	1.50154	0.00738	0.00261		
	2	6.04711	4.53924	4.60949	5.44707	0.75065	1.01548	1.20000	2	3.73764	0.00297	0.00105		
	3	5.16690	3.95468	3.98329	4.66335	0.76539	1.00724	1.17920	3	5.34141	0.00208	0.00073		
	4	3.73594	2.91828	2.90231	3.39694	0.78114	0.99487	1.16402	4	6.50338	0.00170	0.00060		
	5	1.65158	1.33931	1.31753	1.50180	0.81093	0.98374	1.12132	5	8.15473	0.00136	0.00048		

CASE 1 - VELOCITY OF EACH MASS (COMPUTED IN ACTUAL DRAG PROBLEM) IS USED TO LINEARIZE THE DRAG FORCE

CASE 2 - GROUND VELOCITY IS USED TO LINEARIZE THE DRAG FORCE

Table 3.23

Response of System 6H to El Centro Earthquake, 1940, N-S Component.
Direct Integration Solution. $\beta_s = .05$

FREQ. RANGE	MASS NO.	MAXIMUM RELATIVE DISPLACEMENT BETWEEN MASS AND GROUND (INCHES)				COMPARISON OF SOLUTIONS			MODAL PROPERTIES			
		NO DRAG	ACTUAL DRAG	LINEAR DRAG CASE 1	LINEAR DRAG CASE 2	ACTUAL DRAG/ NO DRAG	CASE 1/ ACTUAL DRAG	CASE 2/ ACTUAL DRAG	MODE NO.	FREQ. (CPS)	LINEAR HYDRAULIC DAMPING RATIO	
1	1	12.62777	10.69964	10.81974	9.29144	0.84731	1.01122	0.86839	1	0.04549	0.02896	0.08625
	2	8.23270	8.23271	8.23102	8.22819	1.00000	0.99979	0.99945	2	0.11323	0.01164	0.03465
	3	8.21586	8.21590	8.21425	8.21159	1.00000	0.99980	0.99948	3	0.16182	0.00814	0.02425
	4	8.09758	8.09815	8.09664	8.09537	1.00007	0.99981	0.99966	4	0.19702	0.00669	0.01991
	5	7.28249	6.67069	6.65622	6.48942	0.91599	0.99783	0.97283	5	0.24705	0.00533	0.01588
2	1	13.84424	12.65445	12.80832	12.91801	0.91406	1.01216	1.02083	1	0.24705	0.01786	0.01588
	2	13.45003	12.19061	12.51956	12.61912	0.90636	1.02698	1.03515	2	0.61495	0.00717	0.00638
	3	11.60290	10.52691	10.80028	10.88621	0.90727	1.02597	1.03413	3	0.87881	0.00502	0.00446
	4	7.19391	6.51737	6.69450	6.74802	0.90596	1.02718	1.03539	4	1.06999	0.00412	0.00367
	5	3.75909	3.64067	3.63910	3.65196	0.96850	0.99957	1.00310	5	1.34168	0.00329	0.00292
3	1	3.81961	3.74720	3.75810	3.78537	0.98104	1.00291	1.01019	1	1.50154	0.00473	0.00261
	2	3.45087	3.38596	3.39474	3.41563	0.98119	1.00259	1.00994	2	3.73764	0.00190	0.00105
	3	2.93423	2.87858	2.88604	2.90741	0.98104	1.00259	1.01001	3	5.34141	0.00133	0.00073
	4	2.03215	1.99230	1.99875	2.01356	0.98039	1.00323	1.01067	4	6.50338	0.00109	0.00060
	5	0.58744	0.94621	0.95836	0.97124	0.95825	1.01284	1.02646	5	8.15473	0.00097	0.00048

CASE 1 - VELOCITY OF EACH MASS (COMPUTED IN ACTUAL DRAG PROBLEM) IS USED TO LINEARIZE THE DRAG FORCE

CASE 2 - GROUND VELOCITY IS USED TO LINEARIZE THE DRAG FORCE

Table 3.24

Response of System 7M to El Centro Earthquake, 1940, N-S Component.
Direct Integration Solution. $\beta_s = .01$

MAXIMUM RELATIVE DISPLACEMENT BETWEEN MASS AND GROUND (INCHES)										COMPARISON OF SOLUTIONS				MODAL PROPERTIES			
FREQ. RANGE	MASS NO.	NO DRAG	ACTUAL DRAG	LINEAR DRAG		ACTUAL DRAG/ NO DRAG	CASE 1/ ACTUAL DRAG		CASE 2/ ACTUAL DRAG	MODE NO.	FREQ. (CPS)	LINEAR HYDRAULIC DAMPING RATIO					
				CASE 1	CASE 2		ACTUAL DRAG	CASE 2/ ACTUAL DRAG				CASE 1	CASE 2				
1	1	11.53662	11.07492	11.14485	10.36873	0.95998	1.00631	0.93623	1	0.03522	0.01756	0.05570					
	2	8.79195	8.48914	8.52121	8.33660	0.96556	1.00378	0.98203	2	0.09111	0.00679	0.02153					
	3	8.74150	8.33995	8.33855	8.33494	0.95406	0.99983	0.99940	3	0.13849	0.00447	0.01416					
	4	8.31702	8.31767	8.31618	8.31253	1.00008	0.99982	0.99938	4	0.17842	0.00347	0.01099					
	5	7.49576	7.49770	7.49709	7.49718	1.00026	0.99992	0.99993	5	0.24705	0.00250	0.00794					
2	1	16.87407	15.79905	16.00208	16.28996	0.93629	1.01285	1.03107	1	0.24705	0.01198	0.00794					
	2	15.53401	14.56654	14.73950	15.00188	0.93772	1.01187	1.02989	2	0.63916	0.00463	0.00307					
	3	12.73625	12.00641	12.12985	12.32941	0.94270	1.01028	1.02690	3	0.97149	0.00305	0.00202					
	4	9.28915	8.76966	8.85074	8.99591	0.94408	1.00924	1.02580	4	1.25164	0.00237	0.00157					
	5	5.56005	5.42408	5.42271	5.46826	0.97554	0.99975	1.00815	5	1.73302	0.00171	0.00113					
3	1	6.32278	5.27365	5.35251	5.99697	0.83407	1.01495	1.13716	1	1.50154	0.00429	0.00131					
	2	6.06495	5.05694	5.13148	5.75144	0.83380	1.01474	1.13733	2	3.88479	0.00166	0.00050					
	3	5.31912	4.42956	4.49183	5.04124	0.83276	1.01406	1.13809	3	5.90468	0.00109	0.00033					
	4	4.07065	3.46703	3.49216	3.87697	0.85171	1.00725	1.11824	4	7.60746	0.00085	0.00026					
	5	2.28051	1.94430	1.96086	2.17363	0.85345	1.00748	1.11680	5	10.53327	0.00061	0.00019					

CASE 1 - VELOCITY OF EACH MASS (COMPUTED IN ACTUAL DRAG PROBLEM) IS USED TO LINEARIZE THE DRAG FORCE

CASE 2 - GROUND VELOCITY IS USED TO LINEARIZE THE DRAG FORCE

Table 3.25

Response of System 7M to El Centro Earthquake, 1940, N-S Component.
Direct Integration Solution. $\beta_s = .05$

FREQ. RANGE	MASS NO.	MAXIMUM RELATIVE DISPLACEMENT BETWEEN MASS AND GROUND (INCHES)				COMPARISON OF SOLUTIONS				MODAL PROPERTIES			
		NO DRAG	ACTUAL DRAG	LINEAR CASE 1	DRAG CASE 2	ACTUAL NO DRAG	ACTUAL DRAG	CASE 1/ ACTUAL	CASE 2/ ACTUAL	MODE NO.	FREQ. (CPS)	LINEAR DAMPING RATIO CASE 1	HYDRAULIC DAMPING RATIO CASE 2
1	1	9.20059	8.90487	8.98263	8.36590	0.96786	1.00873	0.93947	0.93522	1	0.03522	0.01373	0.05570
	2	8.26157	8.26107	8.26084	8.25887	0.99994	0.99997	0.99973	0.99111	2	0.09111	0.00531	0.02153
	3	8.24953	8.24964	8.24883	8.24695	1.00001	0.99990	0.99967	0.13849	3	0.13849	0.00349	0.01416
	4	8.19265	8.19263	8.19207	8.19060	1.00000	0.99993	0.99975	0.17842	4	0.17842	0.00271	0.01099
	5	7.29806	7.29877	7.29902	7.30228	1.00010	1.00003	1.00048	0.24705	5	0.24705	0.00196	0.00794
2	1	14.10097	13.34390	13.54459	13.64235	0.94631	1.01504	1.02237	0.24705	1	0.24705	0.00967	0.00794
	2	13.21584	12.51573	12.70052	12.79106	0.94733	1.01444	1.02167	0.63916	2	0.63916	0.00374	0.00307
	3	11.18000	10.62262	10.76368	10.83691	0.95015	1.01328	1.02017	0.97149	3	0.97149	0.00246	0.00202
	4	8.16444	7.76271	7.85898	7.91284	0.95080	1.01240	1.01934	1.25164	4	1.25164	0.00191	0.00157
	5	4.72101	4.62491	4.63815	4.65274	0.97965	1.00286	1.00602	1.73302	5	1.73302	0.00138	0.00113
3	1	3.61243	3.57591	3.58035	3.59581	0.98989	1.00124	1.00556	1.50154	1	1.50154	0.00253	0.00131
	2	3.45452	3.41568	3.42387	3.43864	0.98991	1.00122	1.00554	3.88479	2	3.88479	0.00098	0.00050
	3	3.00506	2.97488	2.97858	2.99135	0.98996	1.00124	1.00553	5.90468	3	5.90468	0.00064	0.00033
	4	2.21156	2.18931	2.19225	2.20156	0.98994	1.00134	1.00560	7.60746	4	7.60746	0.00050	0.00026
	5	1.26513	1.23485	1.24416	1.25427	0.97606	1.00754	1.01573	10.53327	5	10.53327	0.00036	0.00019

CASE 1 - VELOCITY OF EACH MASS (COMPUTED IN ACTUAL DRAG PROBLEM) IS USED TO LINEARIZE THE DRAG FORCE

CASE 2 - GROUND VELOCITY IS USED TO LINEARIZE THE DRAG FORCE

Table 3.26

Response of System 7H to E1 Centro Earthquake, 1940, N-S Component.
Direct Integration Solution. $\beta_s = .01$

MAXIMUM RELATIVE DISPLACEMENT BETWEEN MASS AND GROUND (INCHES)										COMPARISON OF SOLUTIONS				MODAL PROPERTIES			
FREQ. RANGE	MASS NO.	NO DRAG	ACTUAL CRAG	LINEAR DRAG		ACTUAL DRAG/ NO DRAG	CASE 1/ ACTUAL DRAG		CASE 2/ ACTUAL DRAG	MODE NO.	FREQ. (CPS)	LINEAR HYDRAULIC DAMPING RATIO					
				CASE 1	CASE 2		CASE 1/ ACTUAL DRAG	CASE 2/ ACTUAL DRAG				CASE 1	CASE 2				
1	1	11.53662	10.69211	10.82391	9.36642	0.92680	1.01233	0.87601	1	0.03522	0.03296	0.11140					
	2	8.79195	8.34064	8.33835	8.33331	0.94867	0.99973	0.99912	2	0.09111	0.01274	0.04306					
	3	8.74150	8.33909	8.33670	8.33167	0.95397	0.99971	0.99911	3	0.13849	0.00838	0.02833					
	4	8.31702	8.31672	8.31426	8.30937	0.99996	0.99970	0.99912	4	0.17842	0.00651	0.02199					
	5	7.49576	7.49621	7.49627	7.50082	1.00006	1.00001	1.00062	5	0.24705	0.00470	0.01588					
2	1	16.87407	14.88133	15.32588	15.72965	0.88191	1.02987	1.05700	1	0.24705	0.02190	0.01588					
	2	15.53401	13.74930	14.12855	14.49455	0.88511	1.02758	1.05420	2	0.63916	0.00846	0.00614					
	3	12.73625	11.37957	11.65568	11.94081	0.89348	1.02426	1.04932	3	0.97149	0.00557	0.00404					
	4	9.28915	8.29898	8.50588	8.71320	0.89341	1.02493	1.04991	4	1.25164	0.00432	0.00313					
	5	5.56005	5.31157	5.31422	5.37949	0.95531	1.00050	1.01279	5	1.73302	0.00312	0.00226					
3	1	6.32278	4.66290	4.74543	5.69930	0.73748	1.01770	1.22227	1	1.50154	0.00771	0.00261					
	2	6.06495	4.47967	4.54771	5.46506	0.73862	1.01519	1.21997	2	3.88479	0.00298	0.00101					
	3	5.31912	3.98382	3.99531	4.78719	0.74896	1.00288	1.20166	3	5.90468	0.00196	0.00066					
	4	4.07065	3.06605	3.12761	3.69939	0.75321	1.02008	1.20656	4	7.60746	0.00152	0.00052					
	5	2.28051	1.72457	1.75894	2.07547	0.75622	1.01993	1.20347	5	10.53327	0.00110	0.00037					

CASE 1 - VELOCITY OF EACH MASS (COMPUTED IN ACTUAL DRAG PROBLEM) IS USED TO LINEARIZE THE DRAG FORCE

CASE 2 - GROUND VELOCITY IS USED TO LINEARIZE THE DRAG FORCE

Table 3.27

Response of System 7H to El Centro Earthquake, 1940, N-S Component.
Direct Integration Solution. $\beta_s = .05$

FREQ. RANGE	MASS NO.	MAXIMUM RELATIVE DISPLACEMENT BETWEEN MASS AND GROUND (INCHES)				COMPARISON OF SOLUTIONS				MODAL PROPERTIES			
		NO DRAG	ACTUAL DRAG	LIN. DRAG CASE 1	LIN. DRAG CASE 2	ACTUAL DRAG/NO DRAG	ACTUAL DRAG	CASE 1/ACTUAL DRAG	CASE 2/ACTUAL DRAG	MODE NO.	FREQ. (CPS)	LINEAR HYDRAULIC DAMPING RATIO	
1	1	9.20059	8.66416	8.78683	8.25961	0.94170	1.01416	0.99987	0.95331	1	0.03522	0.02633	0.11140
	2	8.26157	8.26124	8.26016	8.25615	0.99996	0.99987	0.99987	0.99938	2	0.09111	0.01018	0.04306
	3	8.24953	8.24930	8.24818	8.24434	0.99997	0.99986	0.99986	0.99940	3	0.13849	0.00670	0.02833
	4	8.19265	8.19263	8.19153	8.19847	1.00000	0.99987	0.99987	0.99949	4	0.17842	0.00520	0.02199
	5	7.29806	7.29945	7.29988	7.30625	1.00019	1.00006	1.00006	1.00093	5	0.24705	0.00375	0.01588
2	1	14.10097	12.67736	13.06475	13.20081	0.89904	1.03056	1.03056	1.04129	1	0.24705	0.01839	0.01588
	2	13.21584	11.90823	12.25607	12.38211	0.90106	1.02921	1.02921	1.03979	2	0.63916	0.00711	0.00614
	3	11.18000	10.13237	10.40380	10.50591	0.90629	1.02679	1.02679	1.03687	3	0.97149	0.00468	0.00404
	4	8.16444	7.39763	7.59492	7.66986	0.90608	1.02667	1.02667	1.03680	4	1.25164	0.00363	0.00313
	5	4.72101	4.54460	4.56615	4.58664	0.96263	1.00474	1.00474	1.00925	5	1.73302	0.00262	0.00226
3	1	3.61243	3.54046	3.54987	3.57934	0.98008	1.00266	1.00266	1.01098	1	1.50154	0.00498	0.00261
	2	3.45452	3.38588	3.39473	3.42290	0.98013	1.00261	1.00261	1.01093	2	3.88479	0.00192	0.00101
	3	3.00506	2.94568	2.95340	2.97774	0.98024	1.00262	1.00262	1.01089	3	5.90468	0.00127	0.00066
	4	2.21156	2.16756	2.17389	2.19164	0.98011	1.00292	1.00292	1.01111	4	7.60746	0.00098	0.00052
	5	1.26513	1.20686	1.22427	1.24350	0.95394	1.01442	1.01442	1.03035	5	10.53327	0.00071	0.00037

CASE 1 - VELOCITY OF EACH MASS (COMPUTED IN ACTUAL DRAG PROBLEM) IS USED TO LINEARIZE THE DRAG FORCE

CASE 2 - GROUND VELOCITY IS USED TO LINEARIZE THE DRAG FORCE

Table 3.28

Response of System 1L to E1 Centro Earthquake, 1940, N-S Component.
 Modal Superposition and Direct Integration Solutions. $\beta_s = .01$

FREQ. RANGE	MASS NO.	MAXIMUM RELATIVE DISPLACEMENT BETWEEN MASS AND GROUND (INCHES)				MAXIMUM SPRING DISTORTION BETWEEN ADJACENT MASSES (INCHES)			
		DIRECT INTEGRATION		MODAL SUPERPOSITION		DIRECT INTEGRATION		MODAL SUPERPOSITION	
		LINEAR DRAG	SRSS	LINEAR DRAG	SRSS	LINEAR DRAG	SRSS	LINEAR DRAG	SRSS
1	1	8.34185		15.08467	10.93828	12.54587		20.57635	11.76669
	2	10.22600		20.45833	11.30387	10.33805		15.54370	9.02642
	3	8.33490		13.73722	7.71750	11.01051		15.64782	9.90172
	4	9.83508		17.52200	9.31015	7.08456		9.68657	4.69050
	5	6.73601		12.32122	6.35126	6.73601		12.32122	6.35126
2	1	14.69819		16.03511	13.93484	7.34972		11.41472	6.28902
	2	10.12925		15.02598	10.35346	5.10225		7.67957	4.17624
	3	7.80763		10.75790	7.56924	5.55146		8.02049	4.47387
	4	6.12044		9.46959	5.14182	3.99024		5.32313	2.88460
	5	3.66382		5.40267	2.61464	3.66382		5.40367	2.61464
3	1	5.79162		5.94679	5.73038	1.99849		2.20694	1.73134
	2	4.09924		4.36883	4.06120	1.19696		1.32892	1.13888
	3	3.05811		3.27362	2.94000	1.34976		1.52312	1.35007
	4	1.72182		1.90736	1.59680	1.05120		1.15270	0.98445
	5	0.67354		0.77399	0.61311	0.67354		0.77399	0.61311

GROUND VELOCITY IS USED TO LINEARIZE THE DRAG FORCE

Table 3.29

Response of System 1L to El Centro Earthquake, 1940, N-S Component.
 Modal Superposition and Direct Integration Solutions. $\beta_s = .05$

FREQ. RANGE	MASS NO.	MAXIMUM RELATIVE DISPLACEMENT BETWEEN MASS AND GROUND (INCHES)			MAXIMUM SPRING DISTORTION BETWEEN ADJACENT MASSES (INCHES)		
		DIRECT INTEGRATION LINEAR DRAG	MODAL SUPERPOSITION ABS	MODAL SUPERPOSITION LINEAR DRAG	DIRECT INTEGRATION LINEAR DRAG	MODAL SUPERPOSITION ABS	MODAL SUPERPOSITION LINEAR DRAG
1	1	8.27526	14.35508	10.71628	8.11978	17.48552	9.65981
	2	8.93605	17.88124	9.83471	7.44992	12.90578	7.16681
	3	8.20983	13.04081	7.40634	7.80829	13.05072	6.98705
	4	7.89726	14.78235	7.46724	5.99827	8.39300	4.00853
	5	6.33738	10.35737	5.11801	6.33738	10.35737	5.11801
2	1	12.70796	13.74028	12.15223	5.62778	8.76679	4.93640
	2	8.12576	12.17334	8.84661	3.77043	5.75078	3.14961
	3	5.62997	9.06310	6.53702	4.00460	6.04579	3.44985
	4	4.28865	7.24784	4.07063	3.03109	4.16073	2.37613
	5	2.09865	3.99096	1.92387	2.09865	3.99096	1.92387
3	1	3.38717	3.41661	3.25601	1.19643	1.35155	1.00654
	2	2.20439	2.54055	2.30951	0.69961	0.79550	0.64976
	3	1.64094	1.92399	1.67720	0.74399	0.90233	0.76876
	4	0.93215	1.14672	0.91546	0.56819	0.68951	0.56241
	5	0.36413	0.47556	0.35293	0.36413	0.47556	0.35293

GROUND VELOCITY IS USED TO LINEARIZE THE DRAG FORCE

Table 3.30

Response of System 4M to El Centro Earthquake, 1940, N-S Component.
 Modal Superposition and Direct Integration Solutions. $\beta_s = .01$

FREQ. RANGE	MASS NO.	MAXIMUM RELATIVE DISPLACEMENT BETWEEN MASS AND GROUND (INCHES)			MAXIMUM SPRING DISTORTION BETWEEN ADJACENT MASSES (INCHES)		
		DIRECT INTEGRATION LINEAR DRAG	MODAL SUPERPOSITION LINEAR DRAG ABS	SRSS	DIRECT INTEGRATION LINEAR DRAG	MODAL SUPERPOSITION LINEAR DRAG ARS	SRSS
1	1	12.01110	25.54959	15.09422	12.56363	19.82863	11.45512
	2	11.25315	17.67328	11.19245	3.56035	7.47721	4.29392
	3	9.26554	16.10133	9.96429	6.35624	11.09561	5.62987
	4	8.36580	13.59613	7.97605	6.90115	12.68011	7.23481
	5	7.15044	11.94400	6.64669	7.15044	11.94400	6.64669
2	1	16.03261	22.88118	16.73178	7.61181	10.69806	5.66384
	2	15.03528	16.63190	13.53978	3.17865	5.53258	3.35427
	3	12.06545	14.37894	11.30306	4.82063	7.22274	3.97335
	4	8.61534	12.20533	8.57431	5.14392	8.18220	4.99812
	5	5.37438	7.85466	4.54791	5.37438	7.85466	4.54791
3	1	6.55030	7.20478	6.53395	1.19255	1.82879	1.14496
	2	5.45229	5.79671	5.49254	1.01799	1.24670	0.97306
	3	4.52537	4.87442	4.55092	1.34943	1.69406	1.32184
	4	3.33232	3.65092	3.26003	1.85904	2.17294	1.82654
	5	1.53522	1.86775	1.46268	1.53522	1.86775	1.46268

GROUND VELOCITY IS USED TO LINEARIZE THE DRAG FORCE

Table 3.31

Response of System 4M to El Centro Earthquake, 1940, N-S Component.
 Modal Superposition and Direct Integration Solutions. $\beta_s = .05$

FREQ. RANGE	MASS NO.	MAXIMUM RELATIVE DISPLACEMENT BETWEEN MASS AND GROUND (INCHES)			MAXIMUM SPRING DISTORTION BETWEEN ADJACENT MASSES (INCHES)		
		DIRECT INTEGRATION LINEAR DRAG	MODAL SUPERPOSITION		DIRECT INTEGRATION LINEAR DRAG	MODAL SUPERPOSITION	
			ABS	SRSS		ABS	SRSS
1	1	9.30323	23.13303	14.18194	9.58280	16.25786	9.23642
	2	8.92716	15.86557	10.61650	2.91609	6.55498	3.85185
	3	8.22338	14.40306	9.26064	3.82236	9.31435	4.70026
	4	8.14281	12.31717	7.49671	5.75090	10.47891	5.88514
	5	6.91531	10.16987	5.61206	6.91531	10.16987	5.61206
2	1	14.02328	18.32761	14.29579	3.54136	7.36096	3.87512
	2	12.74317	13.75961	11.78033	2.80165	4.09805	2.55429
	3	10.16373	11.74648	9.79390	4.00847	5.35497	3.16633
	4	6.38566	9.68469	7.24083	4.47605	6.23125	4.12746
	5	3.16925	5.79979	3.56586	3.16925	5.79979	3.56586
3	1	3.99383	4.34189	3.82377	0.72597	1.15689	0.71402
	2	3.27997	3.39175	3.20252	0.64890	0.79293	0.58941
	3	2.64470	2.97311	2.65447	0.85665	1.01957	0.77922
	4	1.87924	2.21838	1.91283	1.08046	1.26452	1.06429
	5	0.91574	1.15300	0.86795	0.91974	1.15300	0.86795

GROUND VELOCITY IS USED TO LINEARIZE THE DRAG FORCE

Table 3.32

Response of System 7H to El Centro Earthquake, 1940, N-S Component.
 Modal Superposition and Direct Integration Solutions. $\beta_s = .01$

FREQ. RANGE	MASS NO.	MAXIMUM RELATIVE DISPLACEMENT BETWEEN MASS AND GROUND (INCHES)		MAXIMUM SPRING DISTORTION BETWEEN ADJACENT MASSES (INCHES)		MODAL SUPERPOSITION		MODAL SUPERPOSITION	
		DIRECT INTEGRATION LINEAR DRAG	MODAL SUPERPOSITION LINEAR DRAG	DIRECT INTEGRATION LINEAR DRAG	MODAL SUPERPOSITION LINEAR DRAG	ABS	SRSS	ABS	SRSS
1	1	9.36642	19.50604	12.42498	3.78456	3.78456	2.18602	3.78456	2.18602
	2	8.33331	15.73490	11.27674	7.96849	7.96849	4.63558	7.96849	4.63558
	3	8.33167	12.41618	9.57736	6.66661	6.66661	4.32820	6.66661	4.32820
	4	8.30937	12.32985	7.97973	8.75144	8.75144	5.42008	8.75144	5.42008
	5	7.50082	10.14439	5.91445	10.14439	10.14439	5.91445	10.14439	5.91445
2	1	15.72965	17.94270	14.20079	1.97602	1.97602	1.06242	1.97602	1.06242
	2	14.49455	15.97205	13.54969	4.53634	4.53634	2.54188	4.53634	2.54188
	3	11.94081	13.16433	11.92834	5.07418	5.07418	3.42412	5.07418	3.42412
	4	8.71320	11.53608	9.28656	6.29101	6.29101	4.42071	6.29101	4.42071
	5	5.37949	7.95274	5.47861	7.95274	7.95274	5.47861	7.95274	5.47861
3	1	5.69930	6.05205	5.58001	0.35267	0.35267	0.22926	0.35267	0.22926
	2	5.46506	5.69945	5.37132	0.93090	0.93090	0.64639	0.93090	0.64639
	3	4.78719	4.88614	4.77080	1.41003	1.41003	1.14899	1.41003	1.14899
	4	3.69939	3.94157	3.66425	1.83372	1.83372	1.65095	1.83372	1.65095
	5	2.07547	2.36821	2.03317	2.36821	2.36821	2.03317	2.36821	2.03317

GROUND VELOCITY IS USED TO LINEARIZE THE DRAG FORCE

Table 3.33

Response of System 7H to El Centro Earthquake, 1940, N-S Component.
 Modal Superposition and Direct Integration Solutions. $\beta_s = .05$

FREQ. RANGE	MASS NO.	MAXIMUM RELATIVE DISPLACEMENT BETWEEN MASS AND GROUND (INCHES)		MAXIMUM SPRING DISTORTION BETWEEN ADJACENT MASSES (INCHES)		MODAL SUPERPOSITION		MODAL SUPERPOSITION	
		DIRECT INTEGRATION LINEAR DRAG	SRSS	DIRECT INTEGRATION LINEAR DRAG	SRSS	DIRECT INTEGRATION LINEAR DRAG	SRSS	DIRECT INTEGRATION LINEAR DRAG	SRSS
1	1	8.25961	11.93466	1.59341	3.24397	1.59341	3.24397	1.59341	3.24397
	2	8.25615	10.97840	3.28493	6.89428	3.28493	6.89428	3.28493	6.89428
	3	8.24434	9.36536	2.51781	6.21027	2.51781	6.21027	2.51781	6.21027
	4	8.18847	11.48842	3.42431	7.64236	3.42431	7.64236	3.42431	7.64236
	5	7.30625	9.18475	7.30625	9.18475	7.30625	9.18475	7.30625	9.18475
2	1	13.20081	15.17476	0.98323	1.52927	0.98323	1.52927	0.98323	1.52927
	2	12.38211	13.64872	2.39682	3.55513	2.39682	3.55513	2.39682	3.55513
	3	10.50591	11.35620	2.97062	4.16325	2.97062	4.16325	2.97062	4.16325
	4	7.66986	9.78277	4.15514	5.19070	4.15514	5.19070	4.15514	5.19070
	5	4.58664	6.57009	4.58664	6.57009	4.58664	6.57009	4.58664	6.57009
3	1	3.57934	3.73614	0.16237	0.21970	0.16237	0.21970	0.16237	0.21970
	2	3.42290	3.51651	0.46046	0.58178	0.46046	0.58178	0.46046	0.58178
	3	2.97774	2.99654	0.80483	0.83994	0.80483	0.83994	0.80483	0.83994
	4	2.19164	2.43095	1.06512	1.11710	1.06512	1.11710	1.06512	1.11710
	5	1.24350	1.46934	1.24350	1.46934	1.24350	1.46934	1.24350	1.46934

GROUND VELOCITY IS USED TO LINEARIZE THE DRAG FORCE

Table 3.34

Hydrodynamic Parameters for System 4, Mid-Frequency Range.
 El Centro Earthquake. $\beta_s = .02$ in Each Mode

Parameter	Node	Including $[C_s]\{x_g\}$	Excluding $[C_s]\{x_g\}$
$\{ x_s _{\max}\}$ (inches)	1	18.95250	18.98743
	2	16.31281	16.37181
	3	13.45125	13.47894
	4	12.30791	12.21299
	5	10.53108	10.50990
$\{< x_s >\}$ (inches)	1	6.28175	6.26993
	2	5.21131	5.20904
	3	4.48454	4.48830
	4	3.75600	3.75798
	5	2.81634	2.81841
$\{ \dot{x}_s _{\max}\}$ (in./sec)	1	32.53683	32.50833
	2	23.84686	24.27509
	3	19.37517	19.68547
	4	21.22523	21.28960
	5	15.38559	15.47496
$\{< \dot{x}_s >\}$ (in./sec)	1	10.26027	10.26663
	2	7.95916	7.94259
	3	6.83778	6.82866
	4	5.61321	5.60034
	5	4.52049	4.51665

Table 4.1

Structural Properties ($\beta_s = .01$ in Each Mode) of Towers A, B, C, and D

Tower A: Water Depth = 400 ft									
$[M]$	=	330.0	160.7	146.5	171.2	213.5	259.3	493.7	kip-sec ² /ft
$[K_D]$	=	0.0	9.3	14.4	15.3	16.6	17.2	32.5	kip-sec ² /ft ²
[K]	=	16499	-19327	636	417	1494	374	1074	
			44574	-23662	- 593	- 1876	1460	- 576	
				48446	-24921	855	- 1436	556	
					53250	-28011	1608	- 1664	kip/ft
			Sym.			60188	-33690	3940	
							68716	-40479	
								91744	
$[C_s]$	=	36.30254	-19.89626	- 4.23742	- 1.72140	0.15371	0.38392	1.02631	
			48.75942	-15.90614	- 3.71944	- 2.40776	0.09008	- 0.49534	
				48.63628	-16.28558	- 2.92469	- 1.85562	- 0.44043	
					55.01339	-18.92170	- 2.80240	- 2.14439	kip-sec/ft
			Sym.			65.04060	-23.13684	- 2.32514	
							77.46720	-29.52320	
								128.17691	
$[\omega]$	=	2.59527	6.07192	10.52559	14.21764	17.95088	21.00869	24.11875	rad/sec
Elevation Above Ocean Floor									
		Node 1	Node 2	Node 3	Node 4	Node 5	Node 6	Node 7	
		475	390	325	260	195	130	65	ft

Table 4.1 (Continued)

Tower B: Water Depth = 600 ft									
$[M]$	=	330.0	220.7	203.6	402.7	708.5	910.1	1068.1	kip-sec ² /ft
$[K_D]$	=	0.0	9.3	14.4	23.6	30.3	36.4	43.8	kip-sec ² /ft ²
$[K]$	=	14039	-16777	233	829	1351	533	264	
			41504	-23733	- 1185	108	137	139	
				49049	-24855	- 888	297	77	
					39992	-14166	- 505	233	kip/ft
			Sym.			30443	-16220	- 200	
							34663	-19357	
								78455	
$[C_s]$	=	34.19497	-20.64983	- 4.34959	- 3.07781	0.46335	0.73357	0.50825	
			54.30686	-19.24839	- 6.96931	- 2.02949	- 0.36377	0.13246	
				57.93790	-23.34279	- 4.49373	- 0.83272	- 0.04627	
					70.62801	-21.70915	- 4.18464	- 0.40070	kip-sec/ft
			Sym.			83.87941	-29.35041	- 3.48209	
							103.95113	-27.86522	
								180.52204	
$[\omega]$	=	1.66846	3.47280	6.26227	8.35677	9.20700	12.83889	18.75695	rad/sec
Elevation Above Ocean Floor		Node 1 675	Node 2 590	Node 3 525	Node 4 460	Node 5 330	Node 6 200	Node 7 70	ft

Table 4.1 (Continued)

Tower C: Water Depth = 800 ft									
$[M]$	=	330.0	158.6	239.8	618.6	765.1	797.4	1144.2	kip-sec ² /ft
$[K_D]$	=	0.0	11.7	27.1	49.6	50.6	52.5	72.8	kip-sec ² /ft ²
$[K]$	=	13954	-16845	422	1510	778	377	134	
			41498	-24122	- 869	250	114	115	
				37343	-13544	- 193	134	382	
			Sym.	23990		-11119	374	- 234	kip/ft
						28566	-18278	678	
							32418	-15465	
								52461	
$[C_s]$	=	32.49534	-18.56393	- 6.89365	- 2.41939	0.53781	0.72679	0.47625	
			46.94816	-19.68617	- 5.02499	- 0.62322	- 0.00576	0.21191	
				53.14490	-18.66401	- 2.49188	- 0.43295	0.36696	
					67.25111	-22.05673	- 3.81089	- 1.13269	kip-sec/ft
			Sym.			83.99149	-33.17556	- 3.38496	
							93.40039	-25.37438	
								151.87234	
$[\omega]$	=	1.42146	2.90480	5.30973	6.80046	8.41763	10.48611	18.88309	rad/sec
Elevation Above Ocean Floor		Node 1 875	Node 2 790	Node 3 725	Node 4 595	Node 5 400	Node 6 270	Node 7 100	ft

Table 4.1 (Continued)

Tower D: Water Depth = 1000 ft										
$[M]$	=	330.0	216.1	333.3	853.9	1293.4	1645.7	2985.8	kip-sec ² /ft	
$[K_D]$	=	0.0	11.7	27.1	47.0	64.8	69.8	88.3	kip-sec ² /ft ²	
[K]	=	13894	-16799	372	1431	821	352	155		
			41354	-24072	- 842	247	123	67		
				37297	-13588	- 161	203	76		
					23939	-11202	330	257		kip/ft
						22200	-11898	356		
			Sym.				23515	-12476		
								27695		
$[C_S]$	=	33.53153	-20.64579	- 7.50804	- 2.63207	0.43698	0.85199	0.66262		
			54.11065	-23.49063	- 6.15587	- 1.04045	0.06142	0.21873		
				62.16421	-22.44448	- 3.61816	- 0.38919	0.10279		
					78.39989	-29.18695	- 4.22089	- 0.71990		kip-sec/ft
						95.77867	-34.76870	- 5.56090		
			Sym.					-40.40622		
								173.31076		
$[\omega]$	=	1.01200	1.91227	3.15342	4.43760	5.64723	9.19385	16.22955	rad/sec	
Elevation Above Ocean Floor										
		Node 1 1075	Node 2 990	Node 3 925	Node 4 795	Node 5 600	Node 6 400	Node 7 200	ft	

Table 4.2

Estimated Linear Hydraulic Damping Ratios
for Towers A, B, C, and D

Mode	Towers			
	A	B	C	D
1	0.00587	0.00632	0.01178	0.01015
2	0.00251	0.00304	0.00576	0.00541
3	0.00145	0.00168	0.00315	0.00328
4	0.00107	0.00126	0.00246	0.00233
5	0.00085	0.00115	0.00199	0.00183

Table 4.3

Contributions of Each Mode to the Maximum
Base Shear. Σ ABS Modal Combination

Tower	Contribution (as % of Total) of Mode				
	1	2	3	4	5
A	32.8	40.2	18.7	6.8	1.5
B	33.0	28.3	24.0	13.6	1.1
C	19.3	24.6	15.6	35.0	5.5
D	38.9	41.8	17.9	1.4	0.0

Table 4.4

Properties of System 4M, Mid-Frequency Range.
 $\beta_s = .02$ in Each Mode

$[M]$:	1	1	1	2	3	lb-sec ² /in.
$[K_D]$:	0	.00457	.00457	.00914	.01371	lb-sec ² /in. ²
$[K]$:	15.32	-15.32	0	0	0	
	-15.32	45.96	-30.64	0	0	
			61.29	-30.64	0	lb/in.
		Sym.		61.29	-30.64	
					76.61	
$[C_s]$:	0.13917	-0.06907	-0.01734	-0.01149	-0.00479	
		0.24264	-0.09762	-0.02638	-0.00830	
			0.28693	-0.10783	-0.01633	lb-sec/in.
		Sym.		0.40007	-0.12933	
					0.58443	

Modal Properties

Mode	Frequency (cps)	β_h (estimated) (none)	Hydrodynamic Parameter Participation Factor (none)
1	0.24705	0.00794	2.49115
2	0.55706	0.00352	1.13695
3	0.84337	0.00233	0.66289
4	1.06231	0.00185	0.25179
5	1.52207	0.00129	0.01573

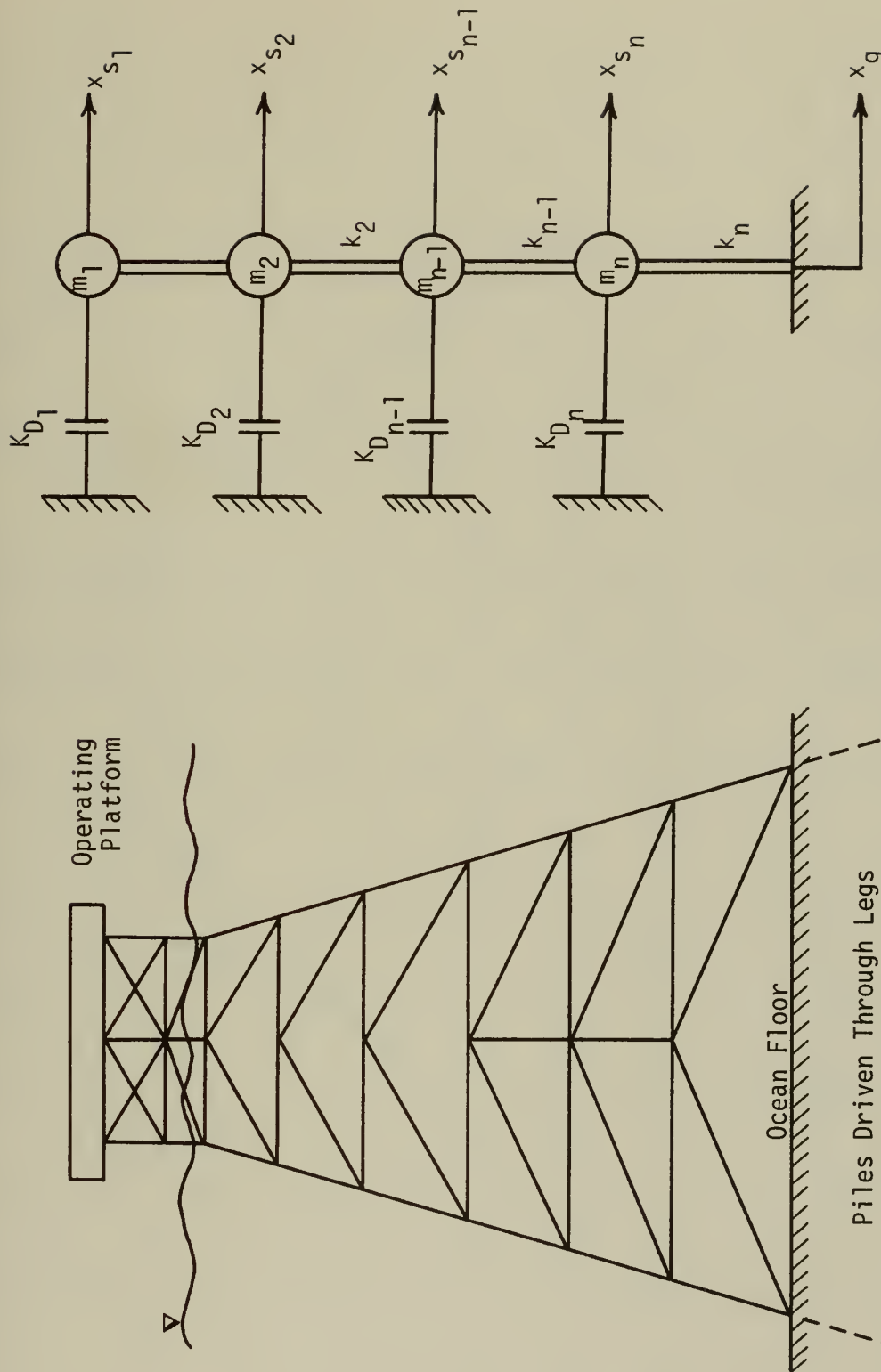
Table 4.4 (Continued)

Spectral Response Quantities (True Spectra)

Mode	$ q _{\max}$ (in.)	$\langle q \rangle$ (in.)	$ \dot{q} _{\max}$ (in./sec)	$\langle \dot{q} \rangle$ (in./sec)
1	12.618	4.044	16.648	5.295
2	13.382	3.197	22.807	7.056
3	9.316	3.096	25.950	10.182
4	10.376	2.926	38.248	9.798
5	10.811	2.712	31.994	9.387

Table 4.5
Hydrodynamic Parameters for System 4M.
El Centro Earthquake

Response Quantity	Node	Exact Value	Modal Superposition - Using True Spectral Response	
			Σ ABS	SRSS
$\{ x_s _{\max}\}$ (inches)	1	17.82343	31.32392	21.00747
	2	16.05878	21.29961	16.04786
	3	13.26795	18.78246	13.53510
	4	11.71001	17.13259	11.14007
	5	10.23945	11.85761	6.68999
$\{< x_s >\}$ (inches)	1	5.09378	9.28465	6.43887
	2	4.08737	6.63971	5.12691
	3	3.44525	5.81354	4.30800
	4	2.63410	4.96109	3.32816
	5	1.45048	3.42885	1.91468
$\{ \dot{x}_s _{\max}\}$ (in./sec)	1	31.62296	50.63429	30.31177
	2	22.94491	35.58812	22.48838
	3	17.93618	30.87149	19.23872
	4	19.32336	26.62459	16.66792
	5	13.95569	22.63737	12.06787
$\{< \dot{x}_s >\}$ (in./sec)	1	8.98920	16.32071	9.69329
	2	6.82424	11.41066	7.21779
	3	5.89449	10.20436	6.32494
	4	4.96801	8.89230	5.18860
	5	4.10293	7.49280	4.08744



(a) Typical Offshore Structure

(b) Lumped Parameter Model of Structure

Fig. 1.1 Schematic Diagram of Typical Offshore Structure and Lumped Parameter Model

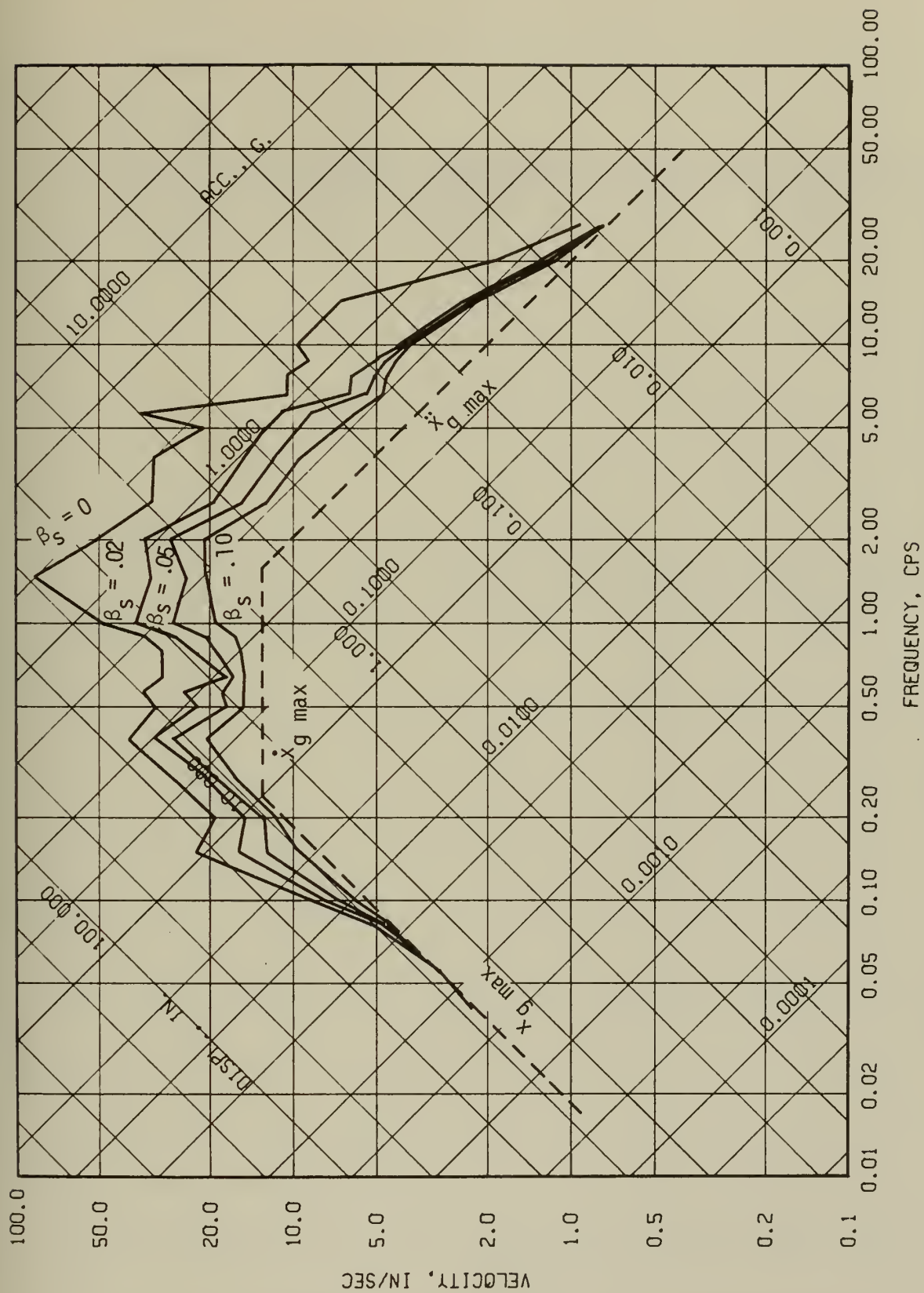


Fig. 1.2 Elastic Deformation Response Spectra for El Centro Earthquake

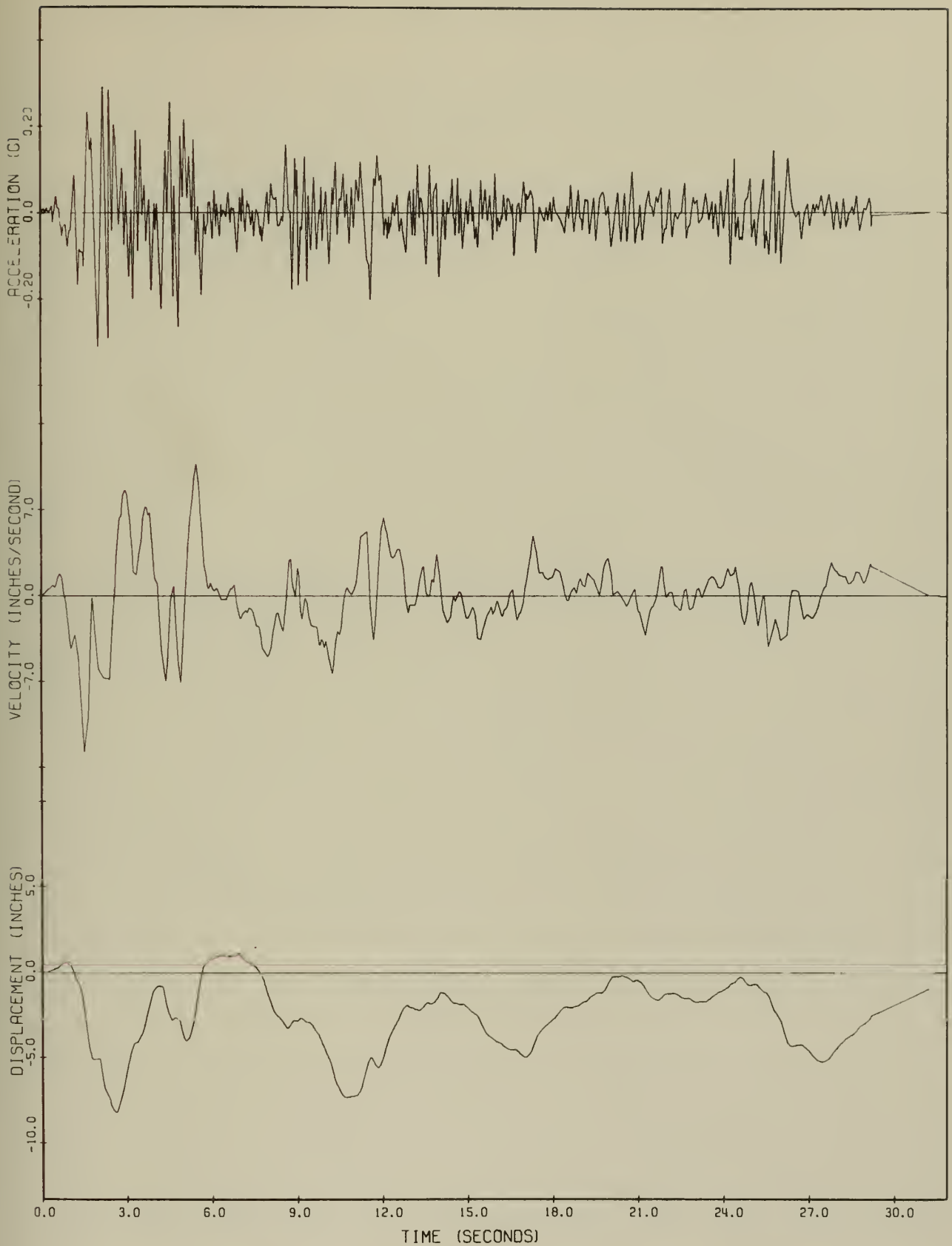


Fig. 1.3 Ground Acceleration, Velocity, and Displacement of El Centro Earthquake, 1940, N-S Component

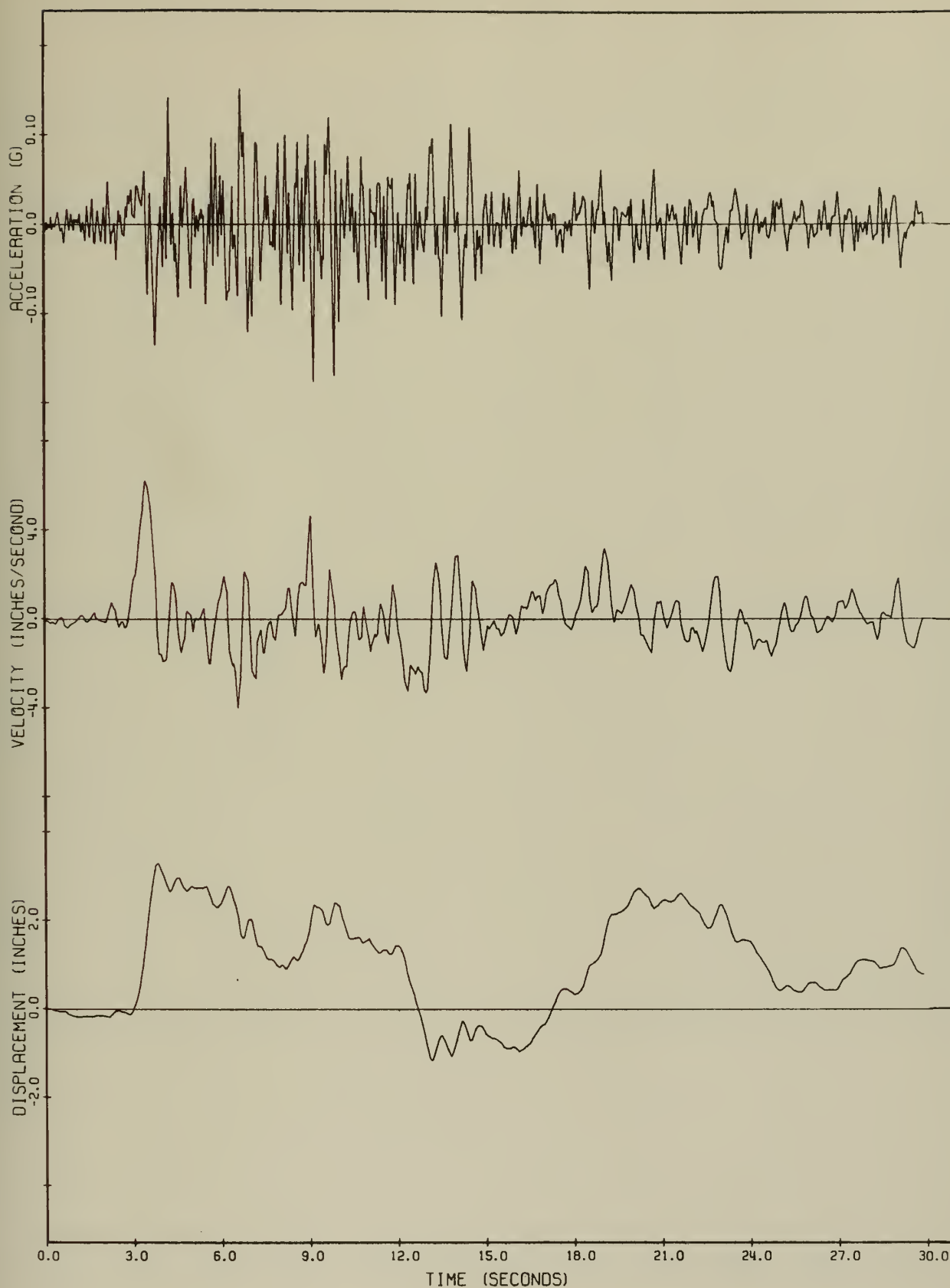


Fig. 1.4 Ground Acceleration, Velocity, and Displacement of Taft Earthquake, 1952, N-21-E Component

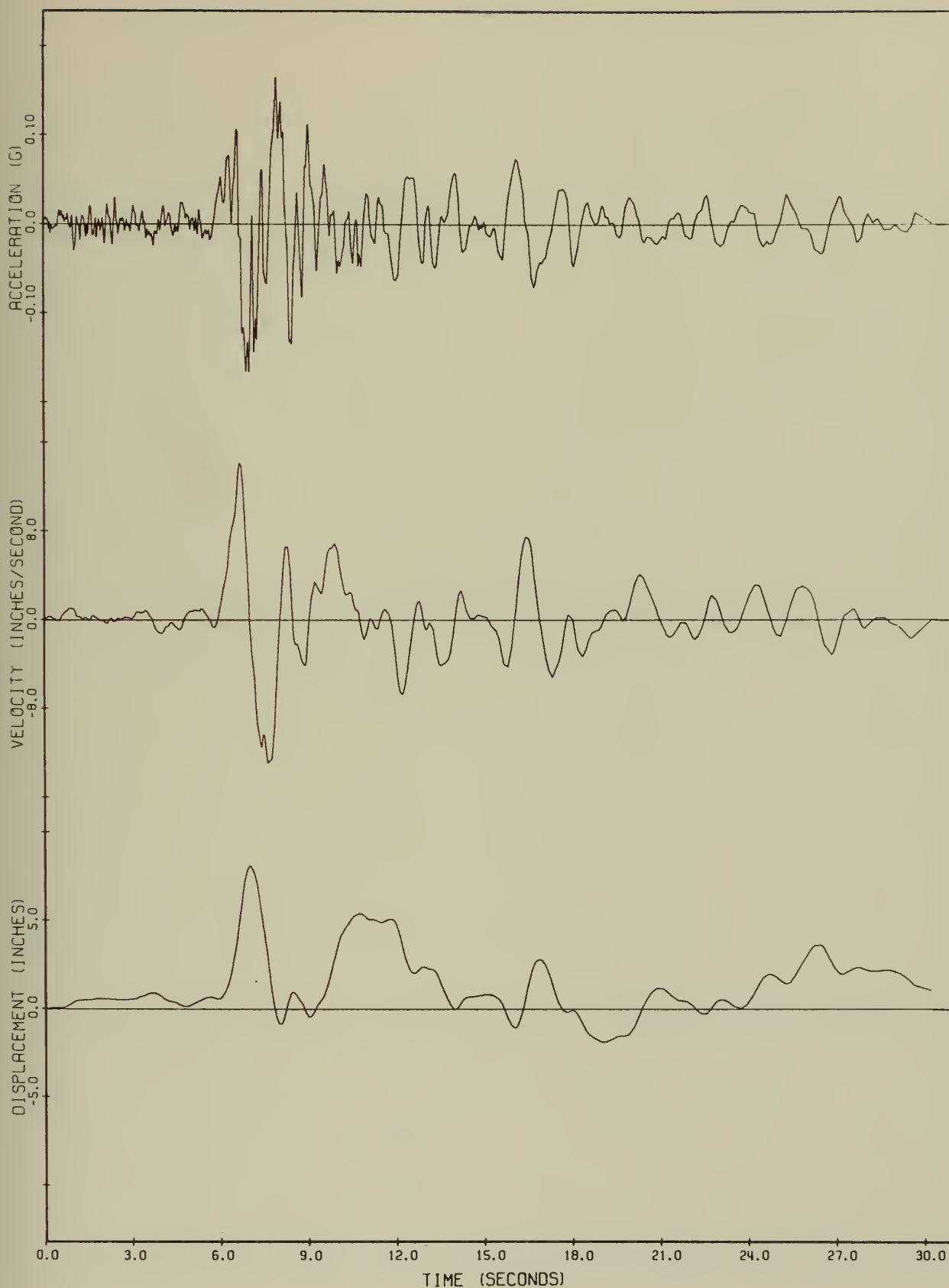


Fig. 1.5 Ground Acceleration, Velocity, and Displacement of Ferndale Earthquake, 1954, N-44-E Component

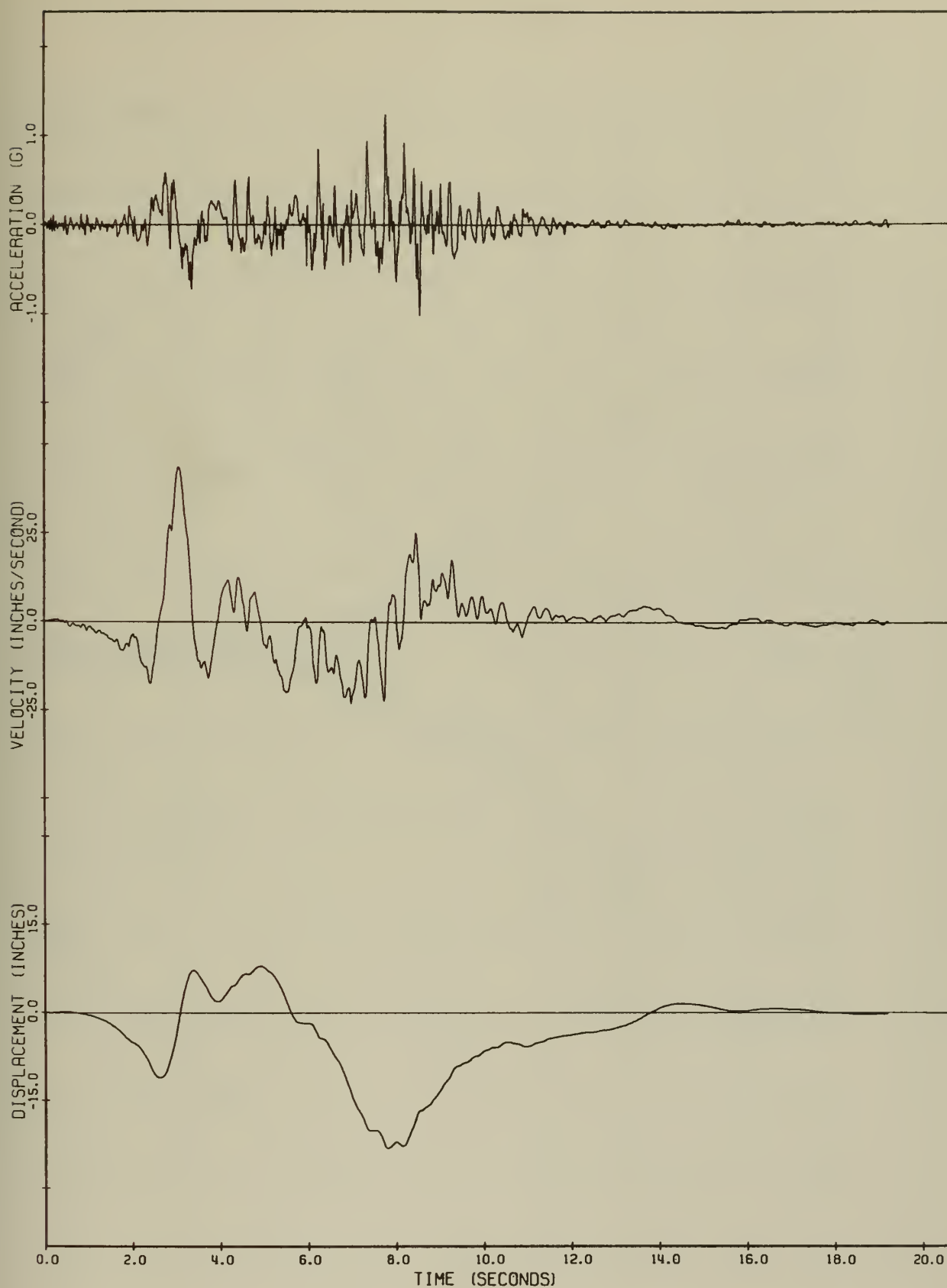


Fig. 1.6 Ground Acceleration, Velocity, and Displacement of San Fernando Earthquake (Pacoima Dam Record), 1971, S-16-E Component

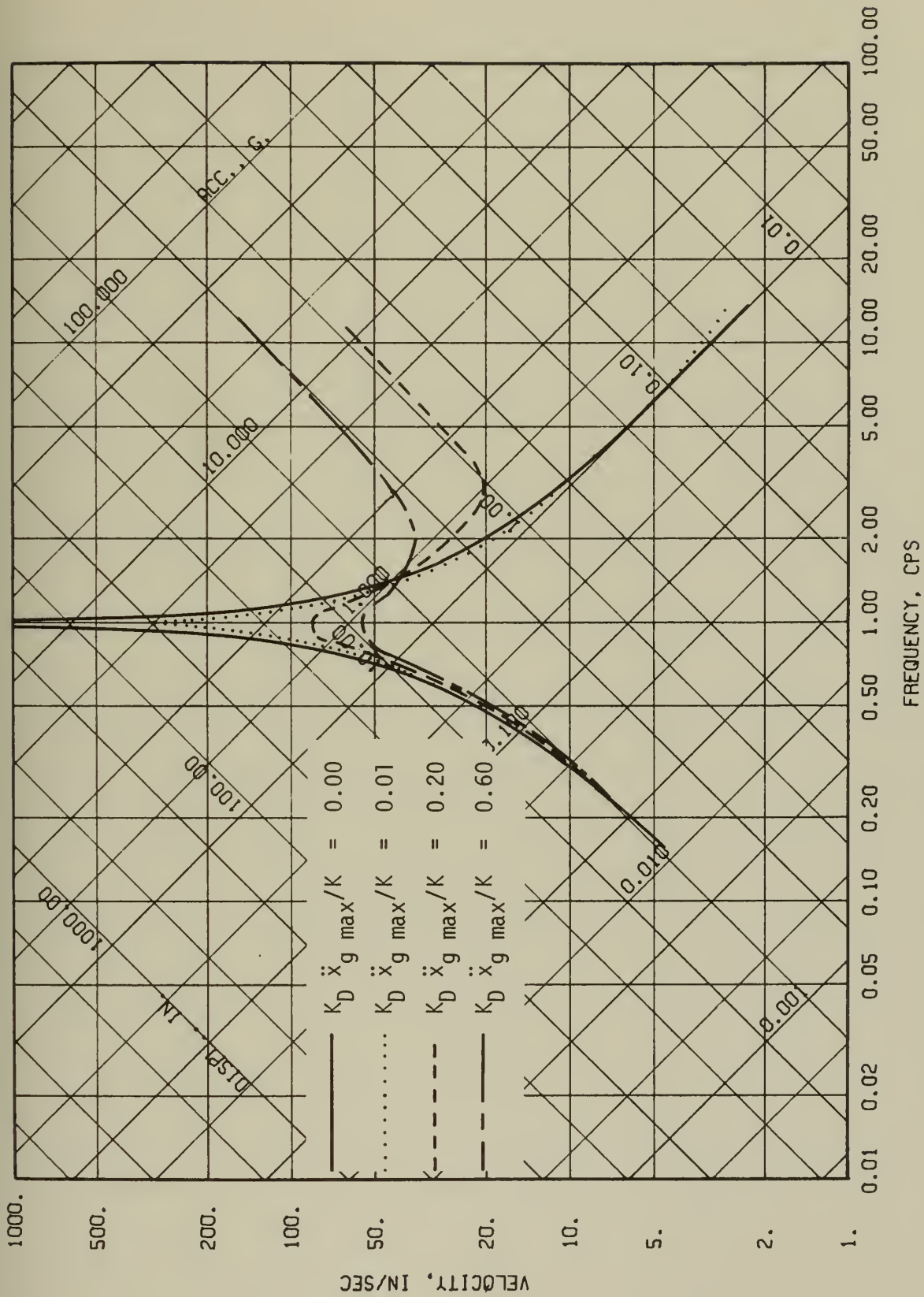


Fig. 2.1 Elastic Deformation Response Spectra for $\ddot{x}_g = 16.1 \sin 2 \pi t$ (ft/sec²). $\beta_s = 0.01$

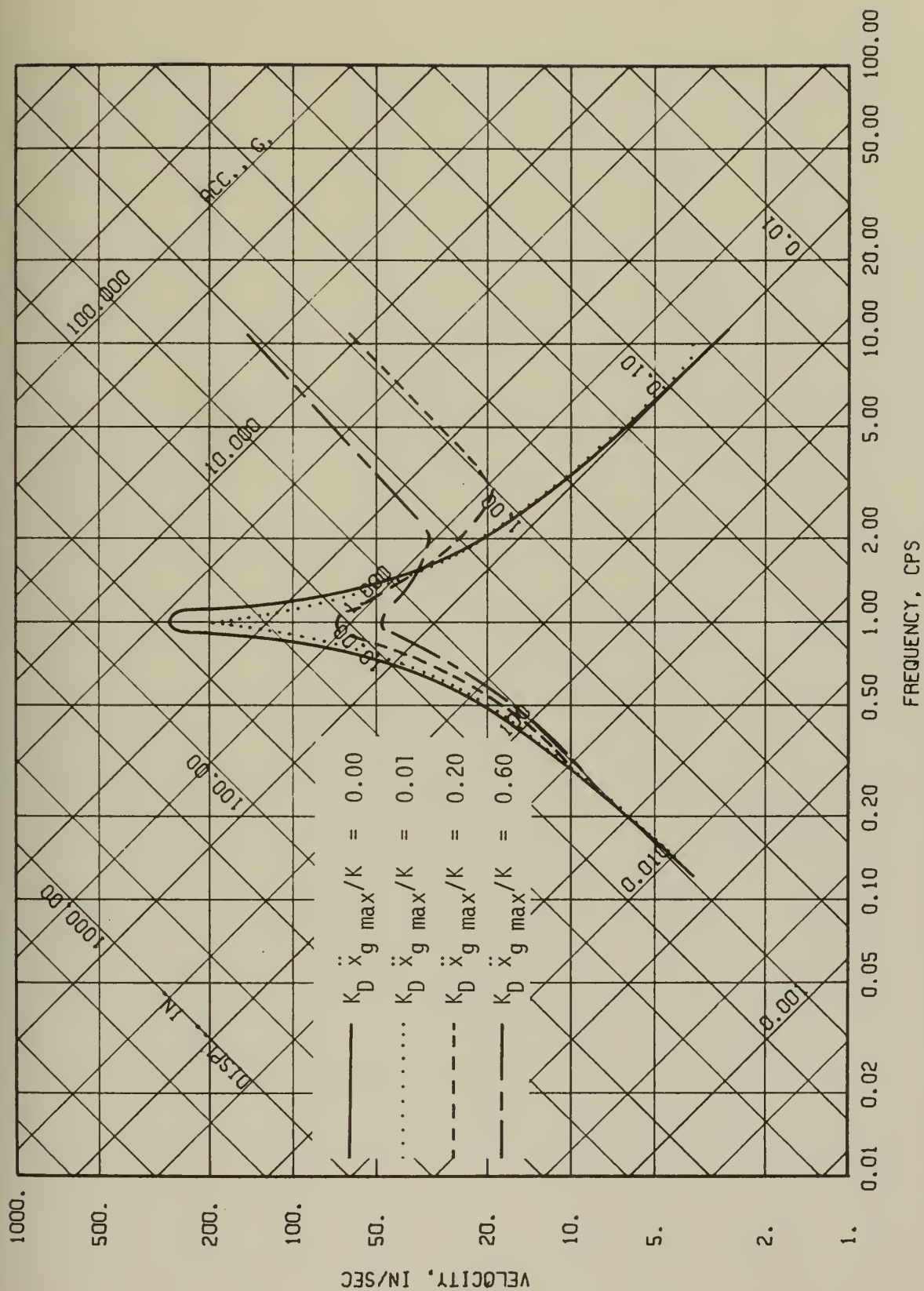


Fig. 2.2 Elastic Deformation Response Spectra for $\ddot{x}_g = 16.1 \sin 2\pi t$ (ft/sec²). $\beta_s = 0.05$

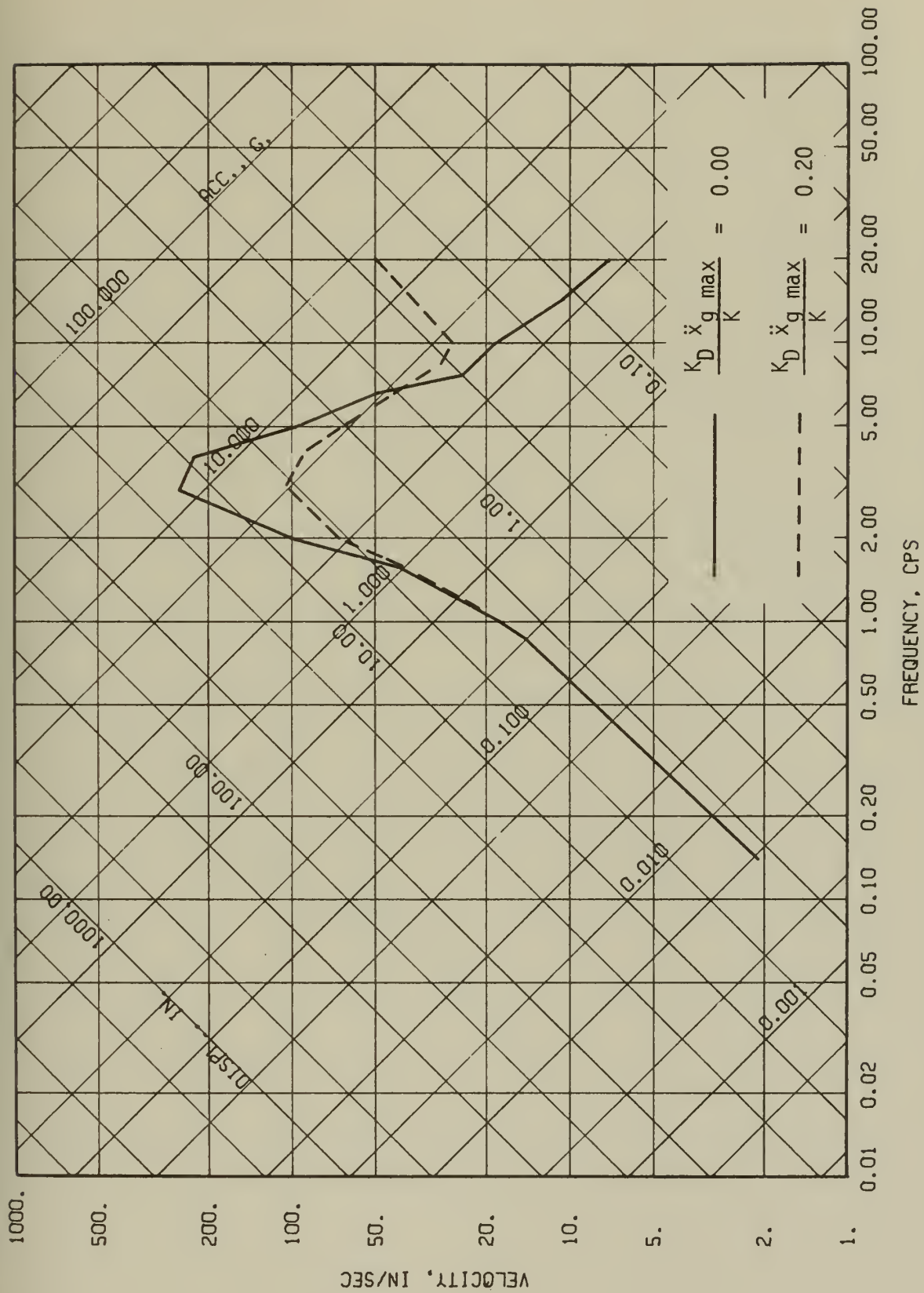


Fig. 2.4 Elastic Deformation Response Spectra for Six Term Series Base Acceleration Record. $\beta_s = 0.05$

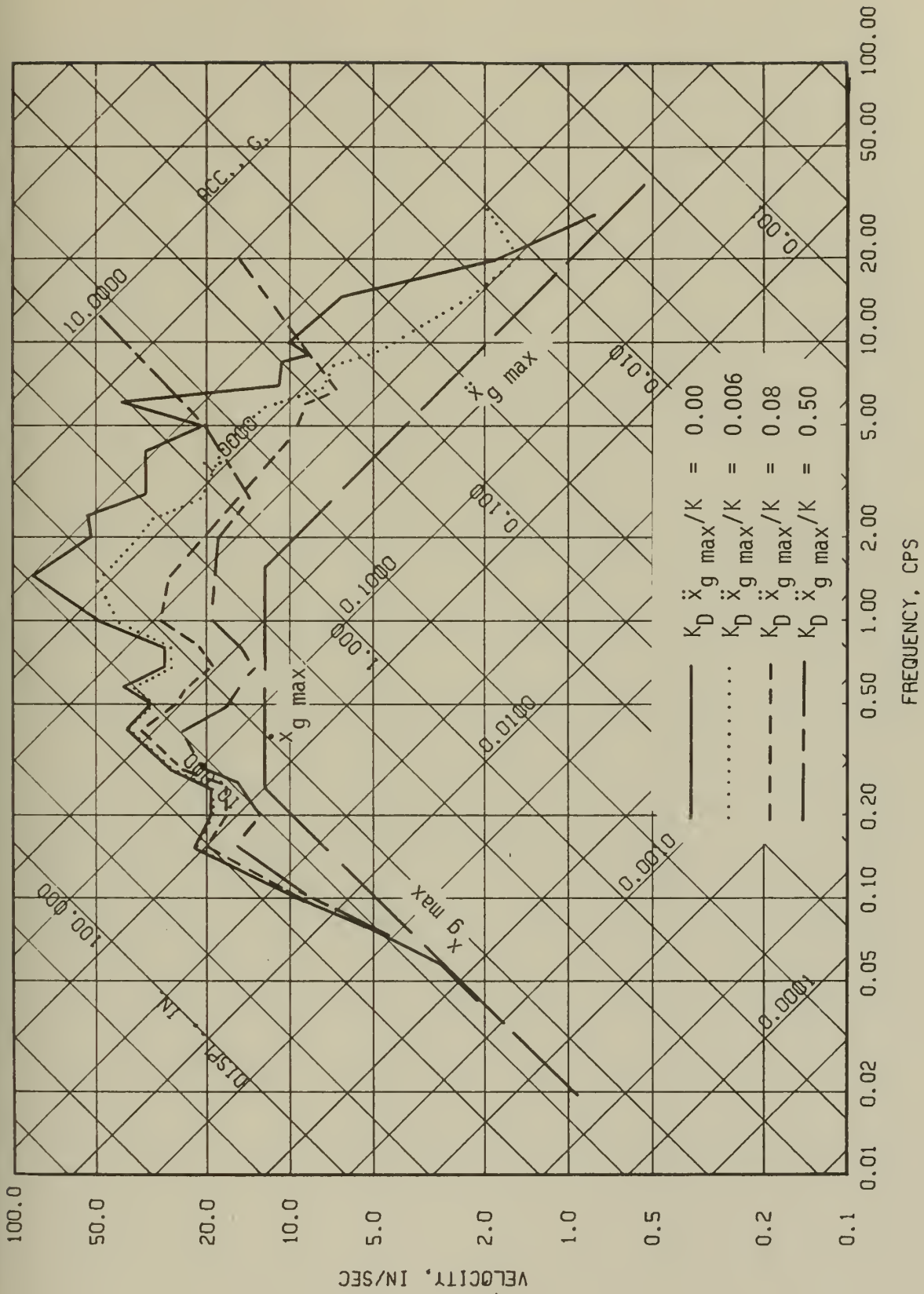


Fig. 2.5 Elastic Deformation Response Spectra.
El Centro Earthquake. $\beta_s = .00$

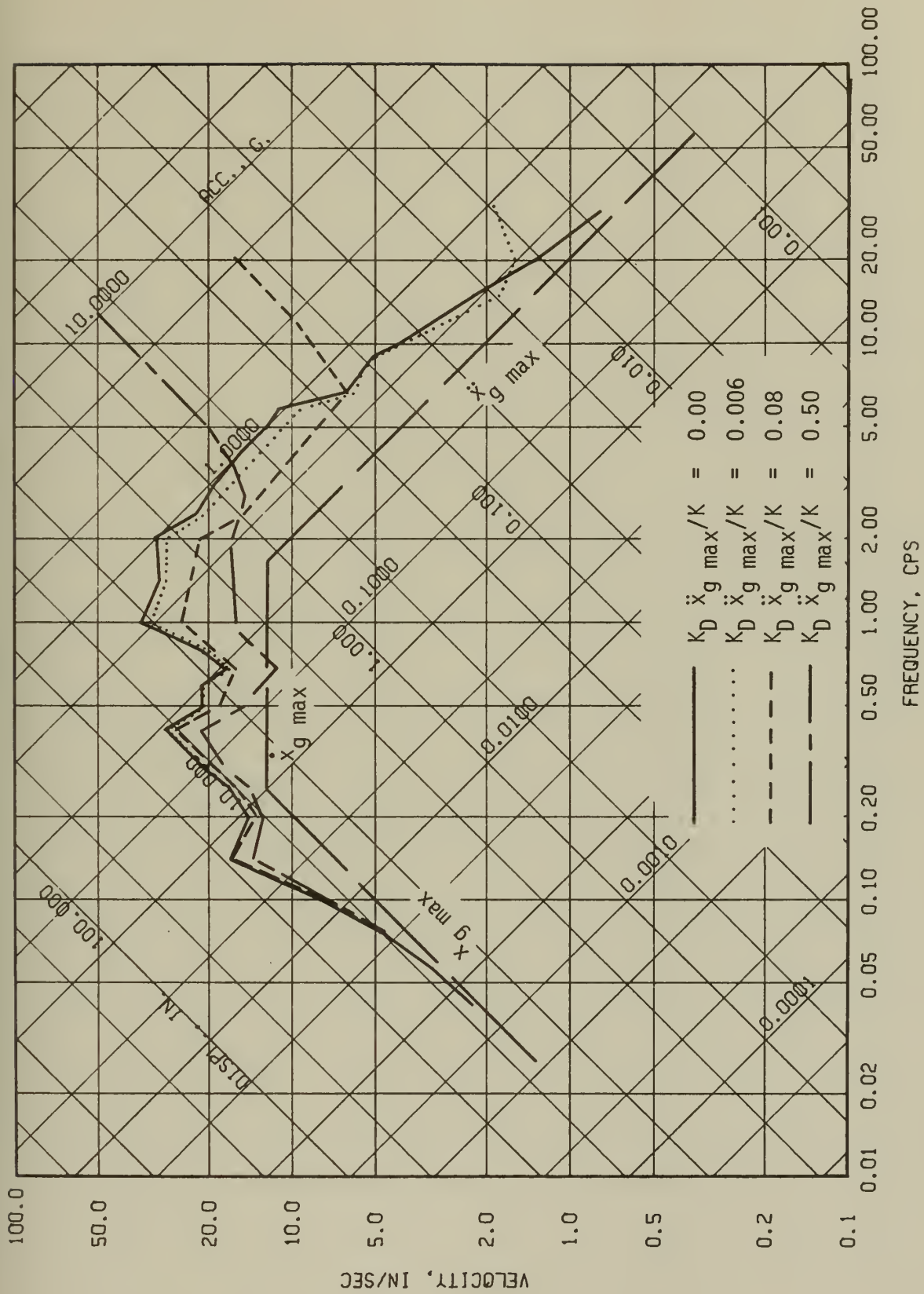


Fig. 2.6 Elastic Deformation Response Spectra.
El Centro Earthquake. $\beta_s = .02$

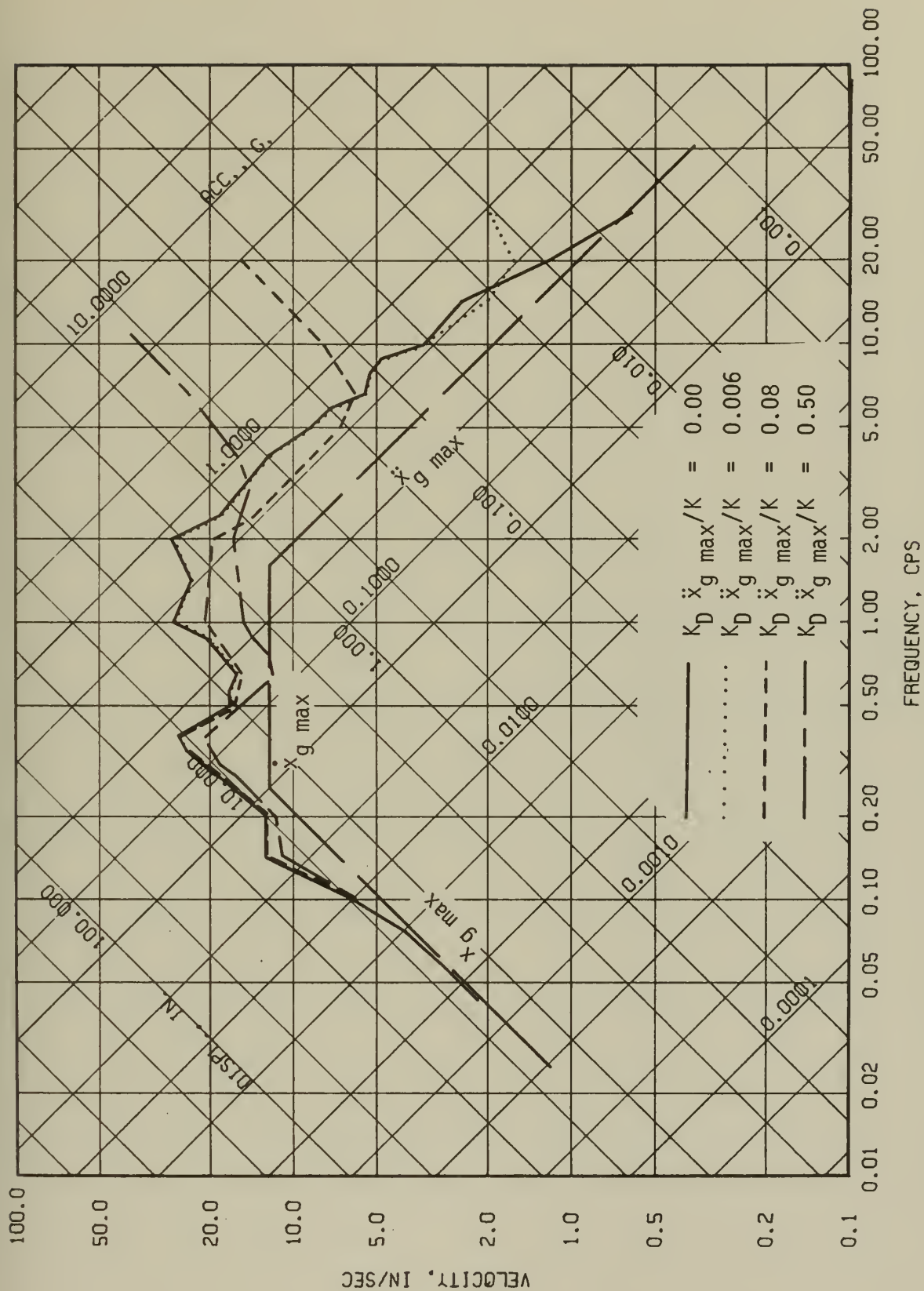


Fig. 2.7 Elastic Deformation Response Spectra.
El Centro Earthquake. $\beta_s = .05$

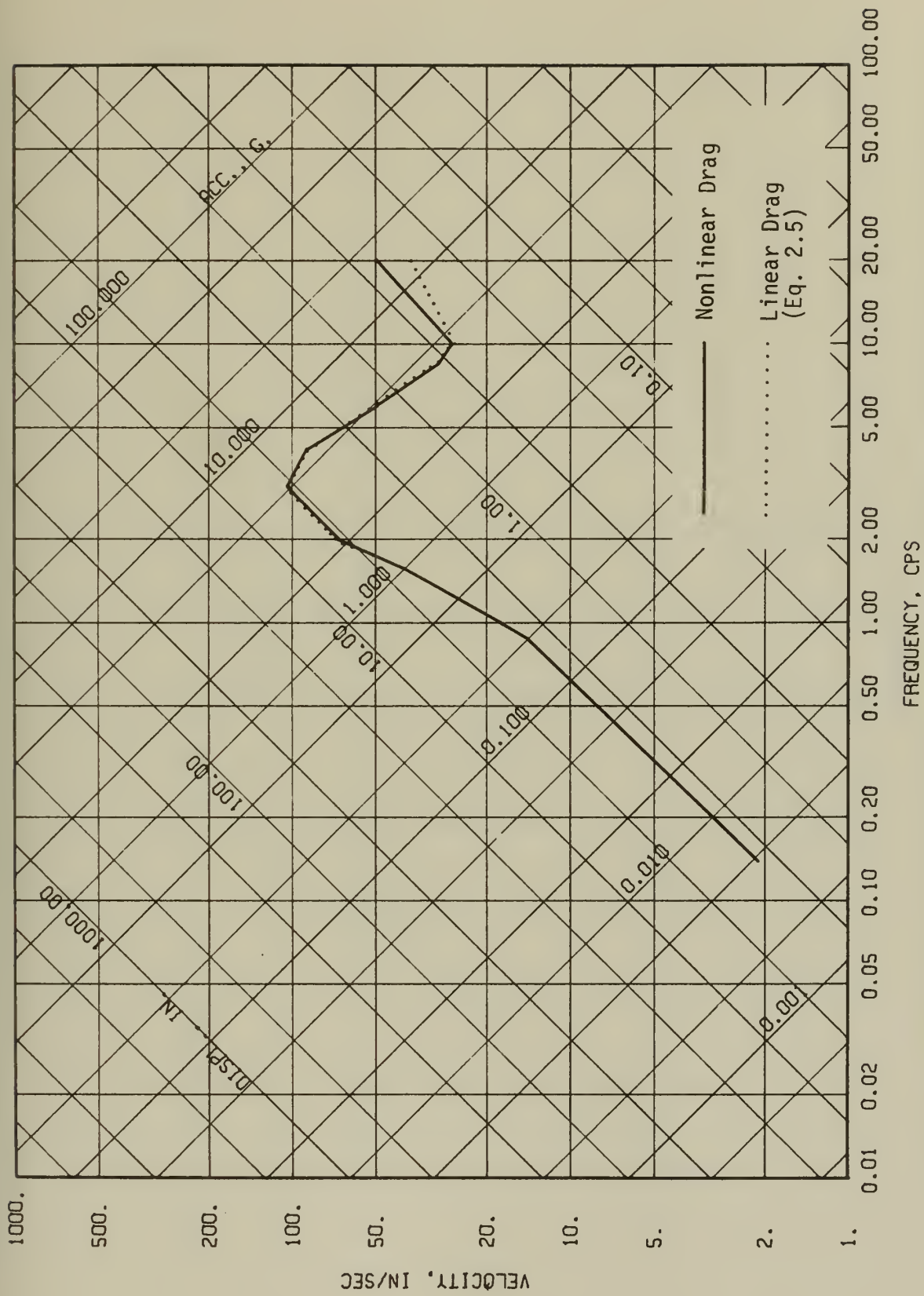


Fig. 2.9 Comparison of Elastic Deformation Response Spectra With Linear and Nonlinear Drag for Series Representation of Base Disturbance. $\beta_s = 0.05$, $K_D \ddot{x}_g \max / K = 0.20$

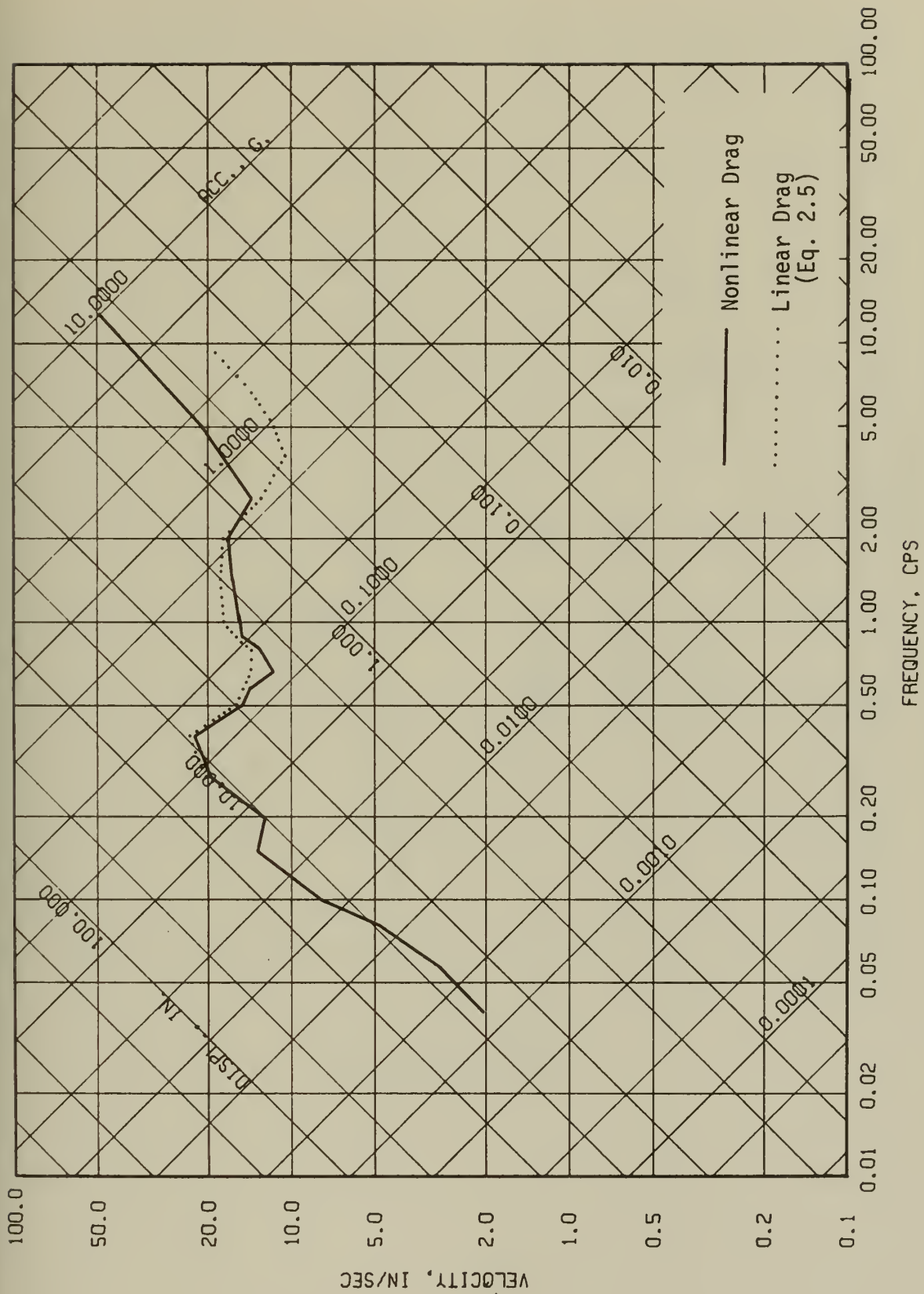


Fig. 2.10 Comparison of Elastic Deformation Response Spectra With Linear and Nonlinear Drag for El Centro Earthquake. $\beta_s = 0.02$, $K_D \ddot{x}_g \max / K = 0.50$

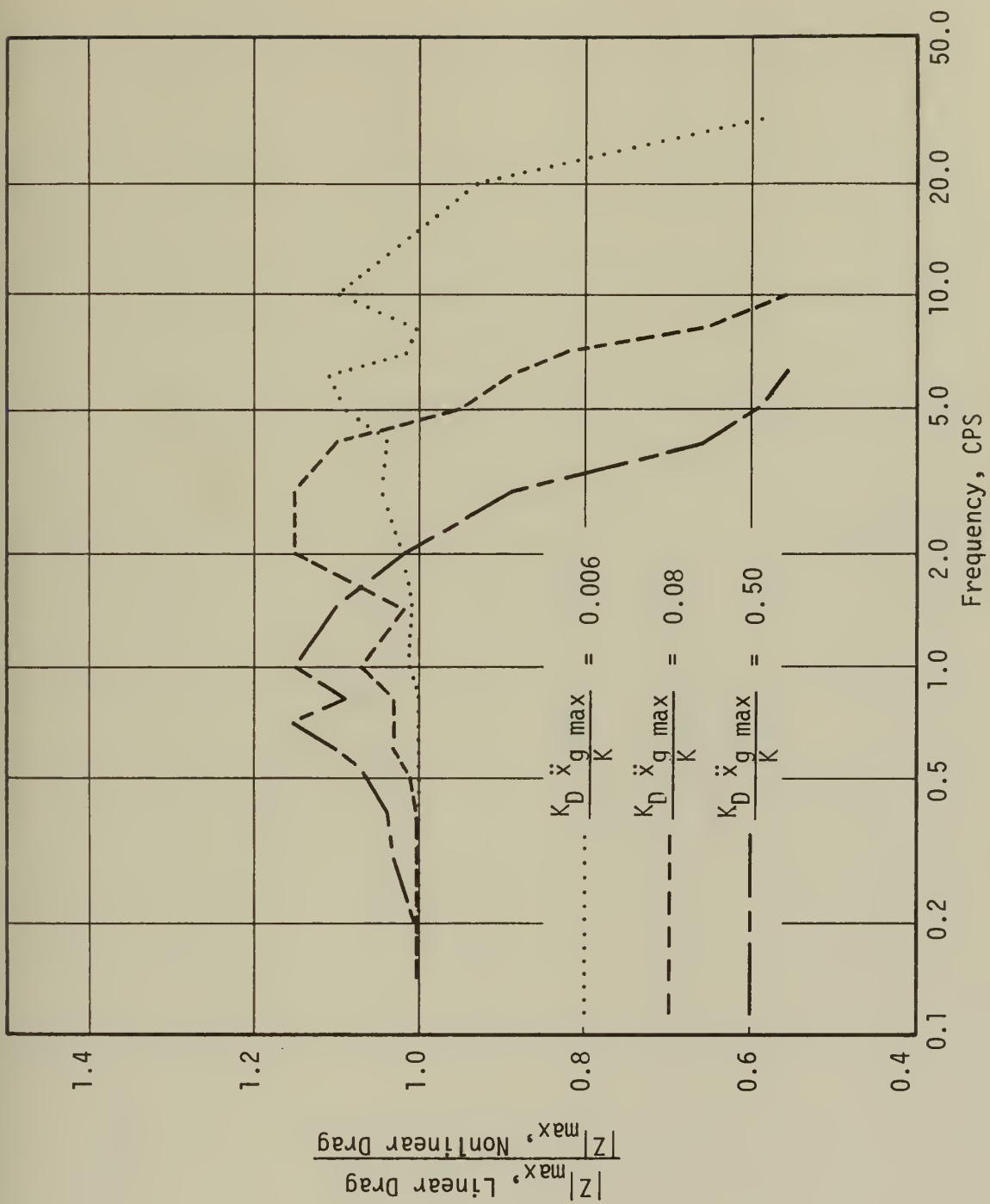


Fig. 2.11 Comparison of Linear and Nonlinear Solution. (Linearized by Oscillator Velocity) El Centro Earthquake. $\beta_s = .00$

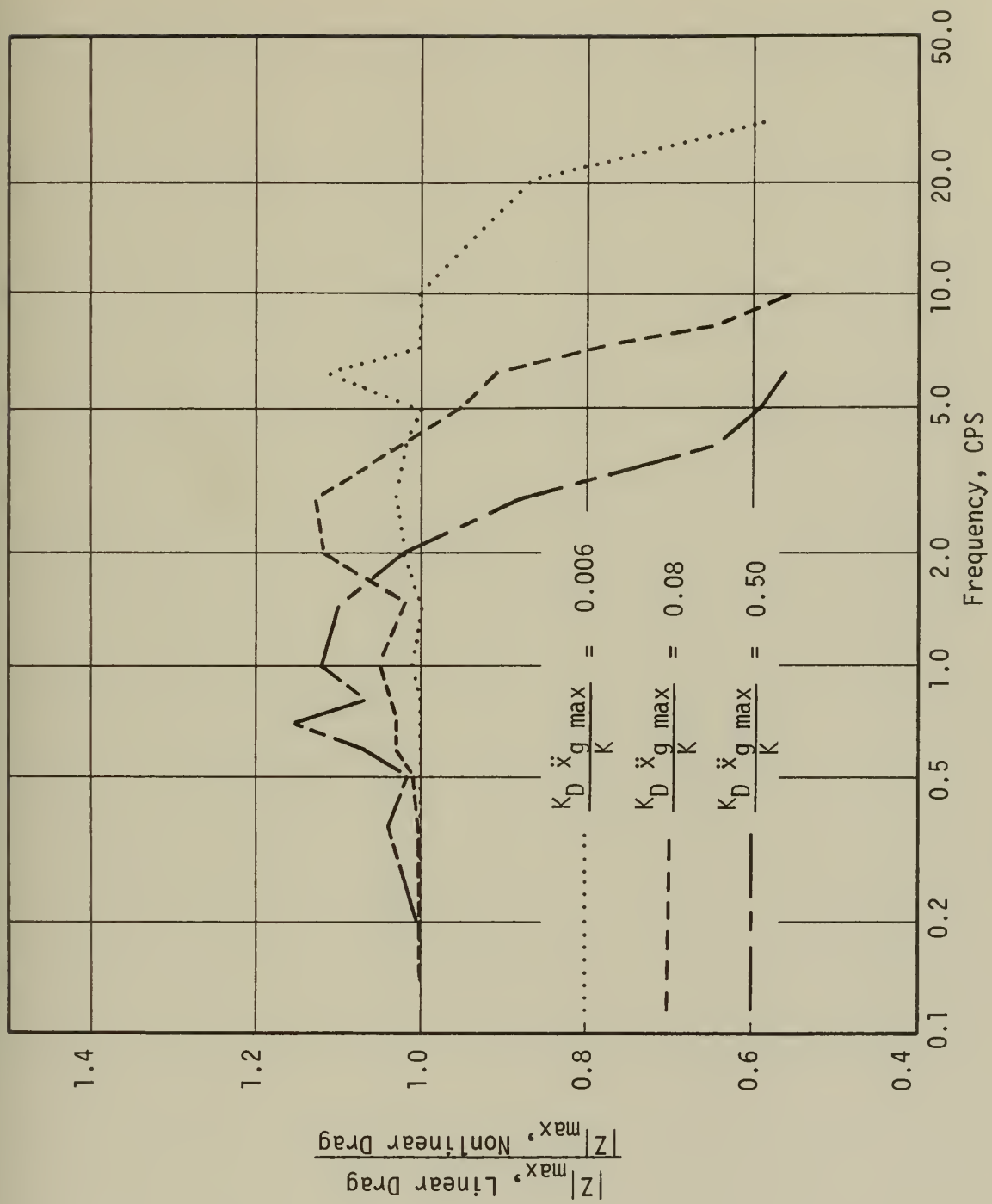


Fig. 2.12 Comparison of Linear and Nonlinear Solution. (Linearized by Oscillator Velocity) El Centro Earthquake. $\beta_s = .02$

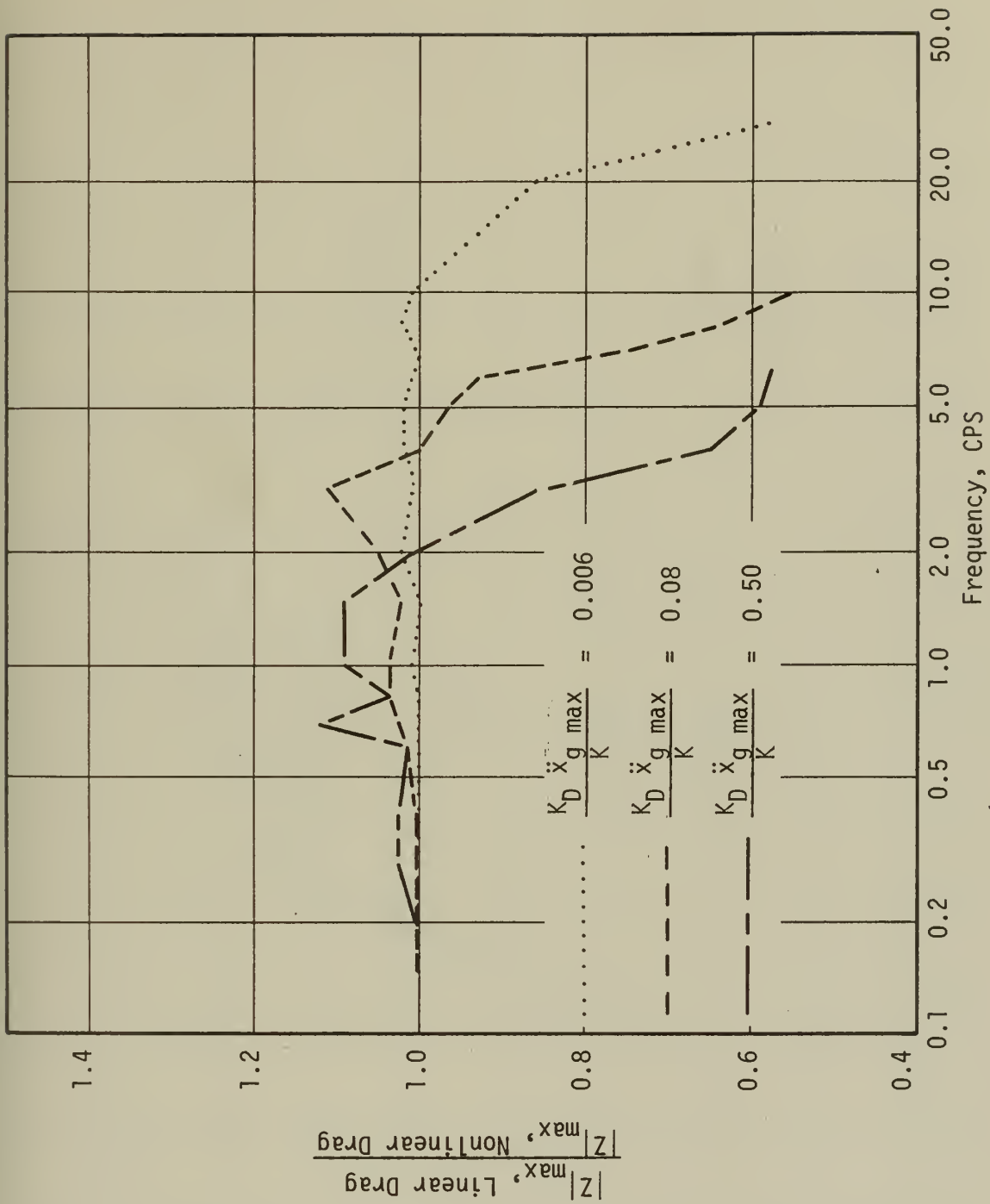


Fig. 2.13 Comparison of Linear and Nonlinear Solution. (Linearized by Oscillator Velocity) El Centro Earthquake. $\beta_s = .05$

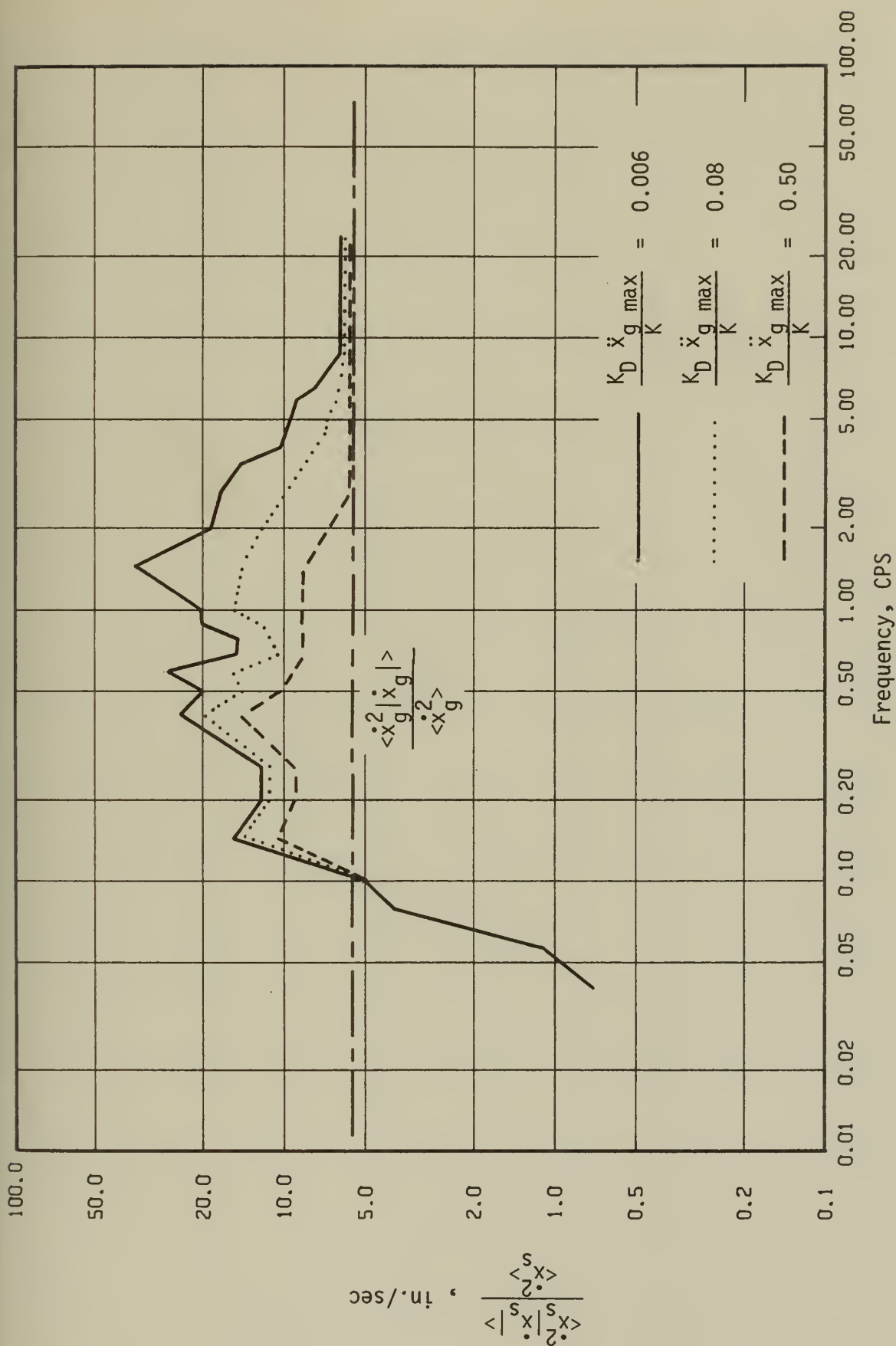


Fig. 2.14 Linearizing Parameter for Single Degree of Freedom Oscillator. El Centro Earthquake. $\beta_s = .00$

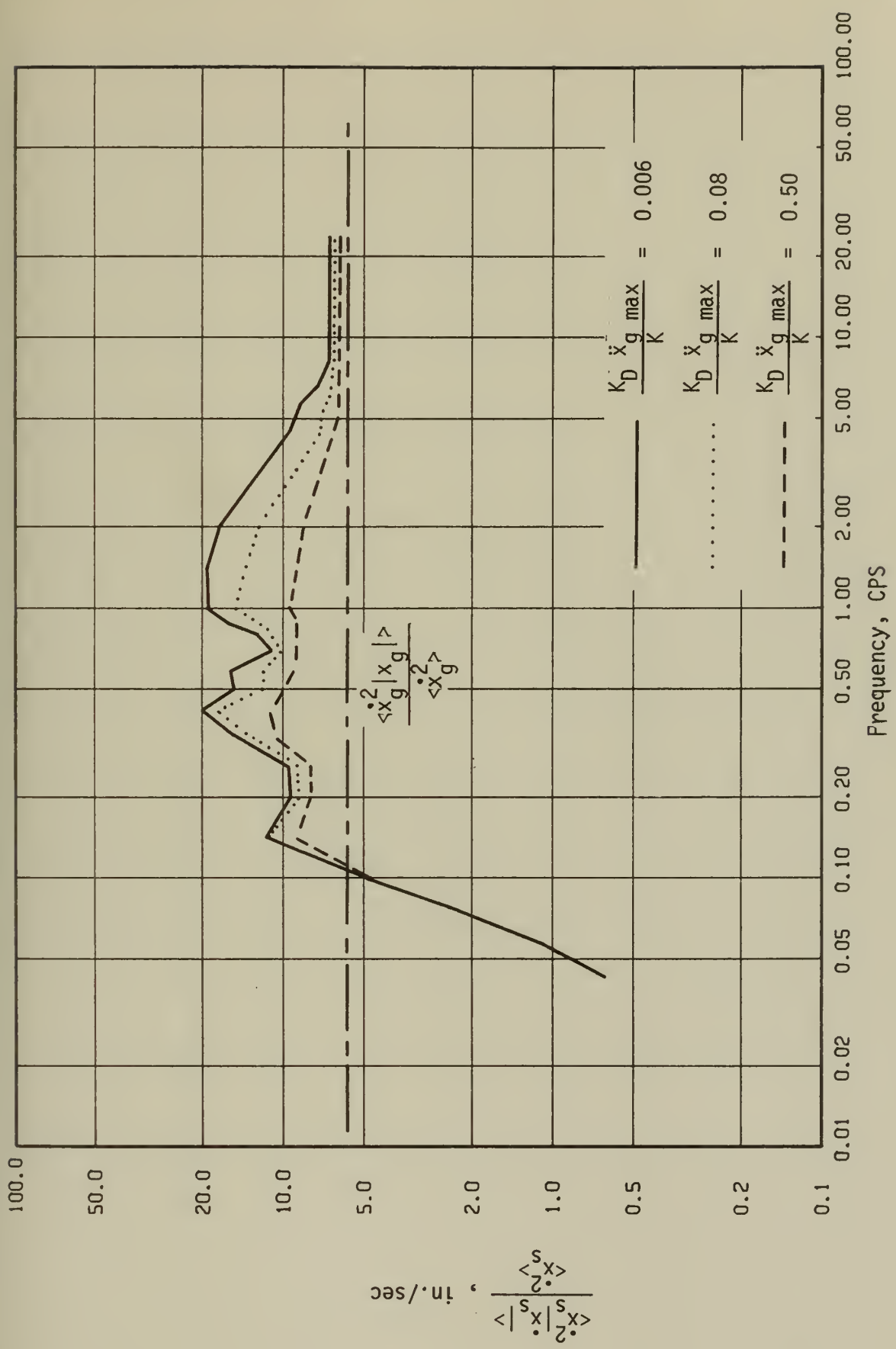


Fig. 2.15 Linearizing Parameter for Single Degree of Freedom Oscillator. El Centro Earthquake. $\beta_s = .02$

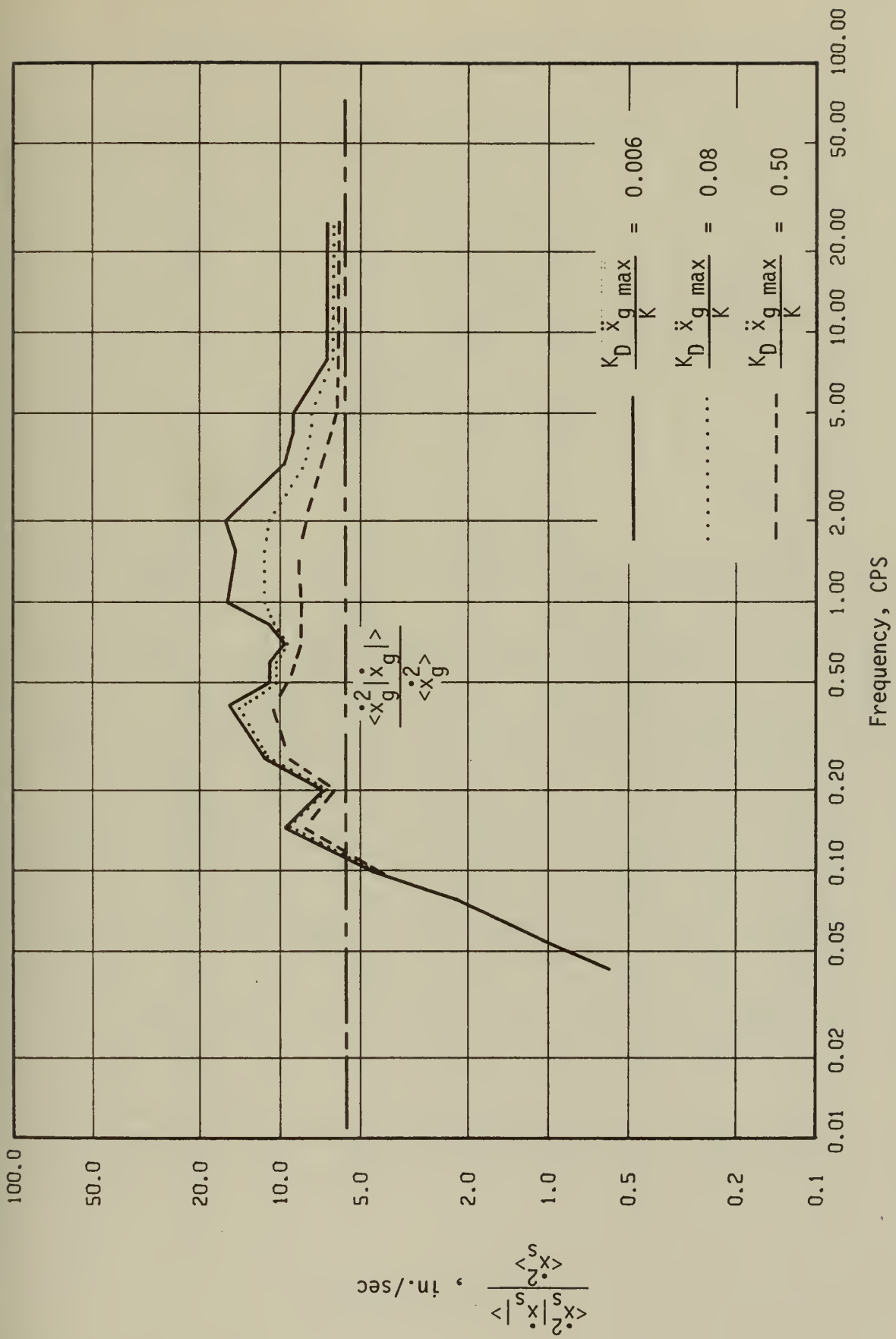


Fig. 2.16 Linearizing Parameter for Single Degree of Freedom Oscillator. El Centro Earthquake. $\beta_s = .05$

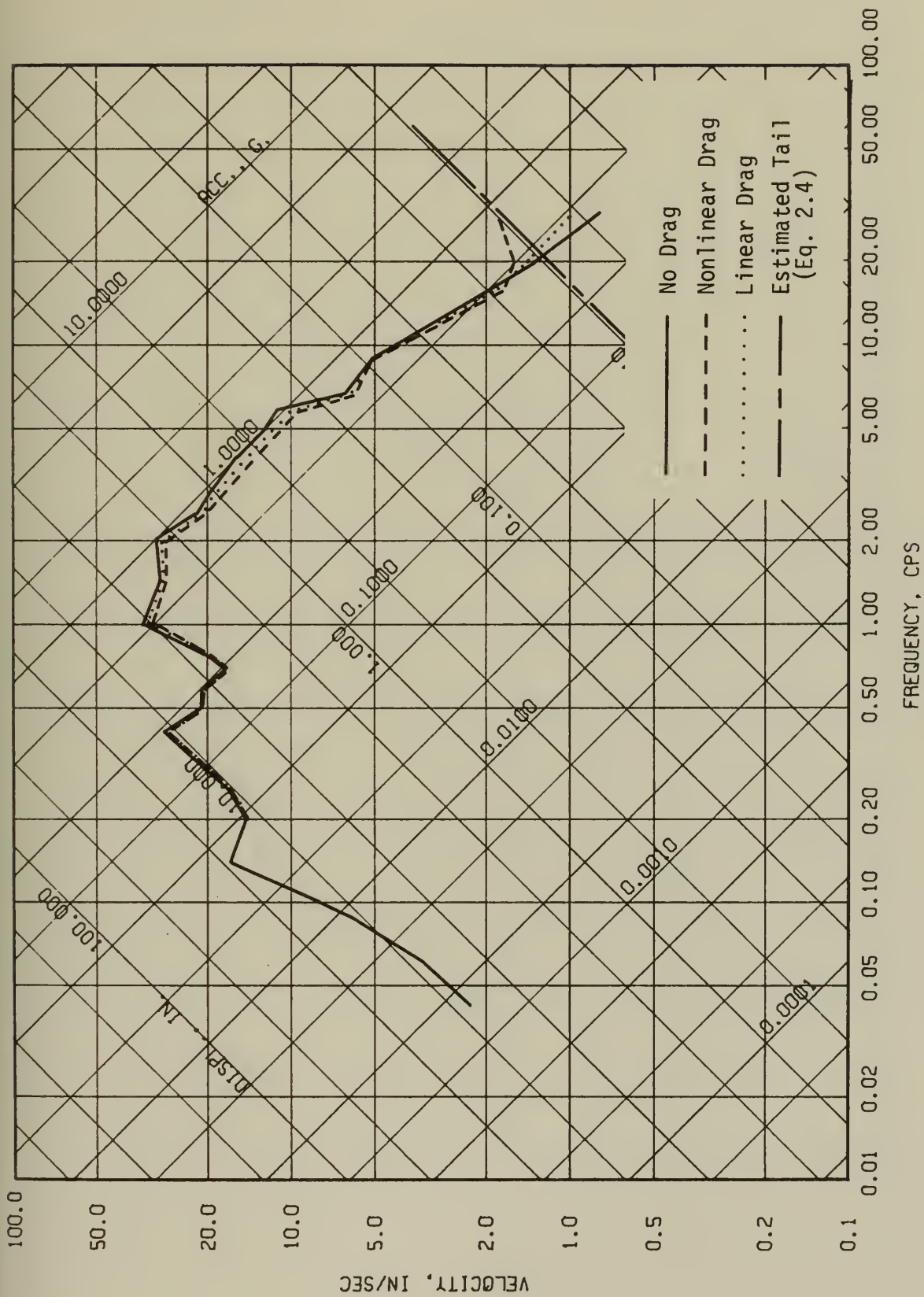


Fig. 2.17 Comparison of Nonlinear Drag Spectrum With Linear Drag Spectrum (Linearized by Ground Velocity). El Centro Earthquake. $\beta_s = 0.02$, $K_D \ddot{x}_g \max / K = 0.006$

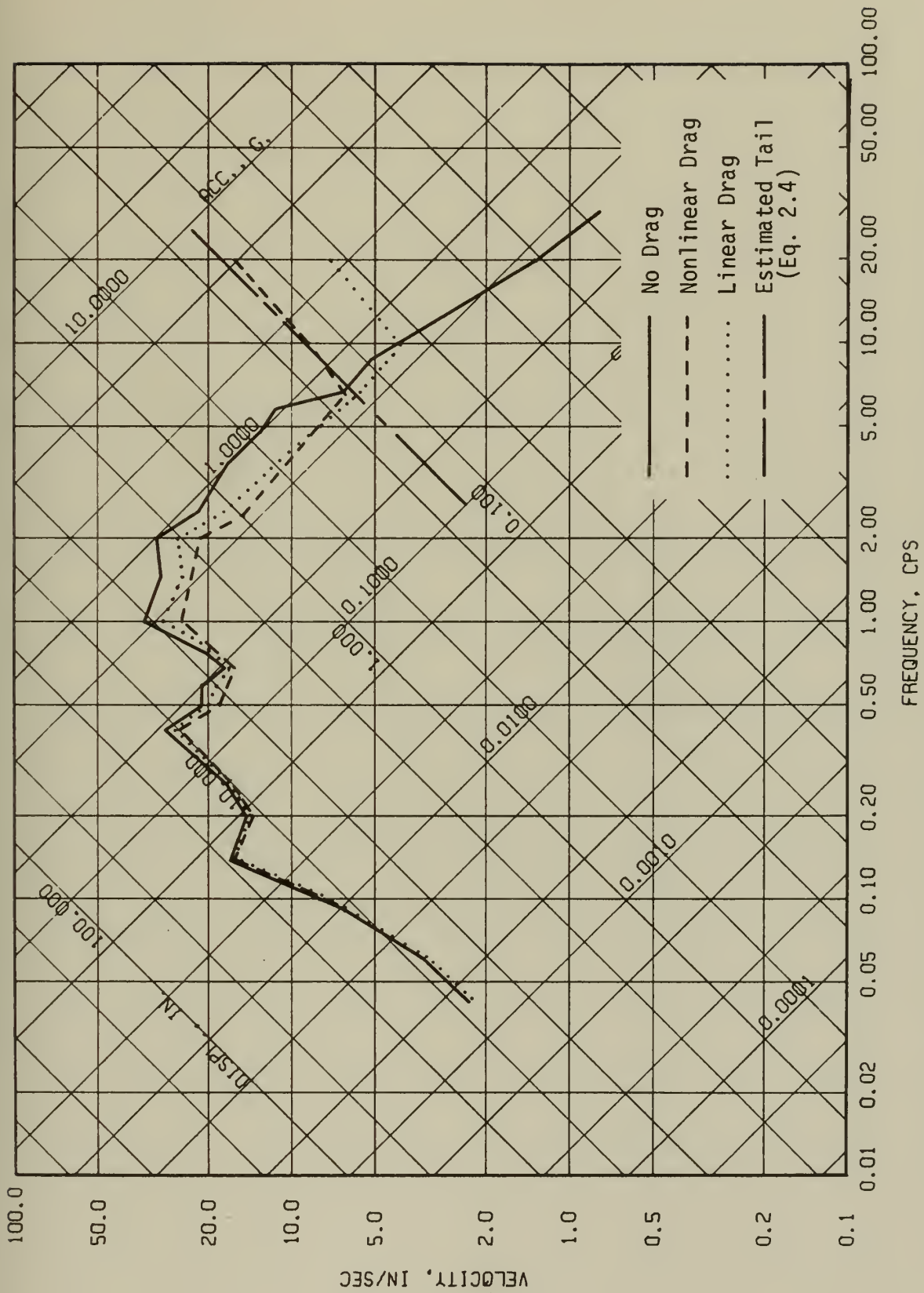


Fig. 2.18 Comparison of Nonlinear Drag Spectrum With Linear Drag Spectrum (Linearized by Ground Velocity). E1 Centro Earthquake. $\beta_s = 0.02$, $K_D \ddot{x}_{g \max} / K = 0.08$

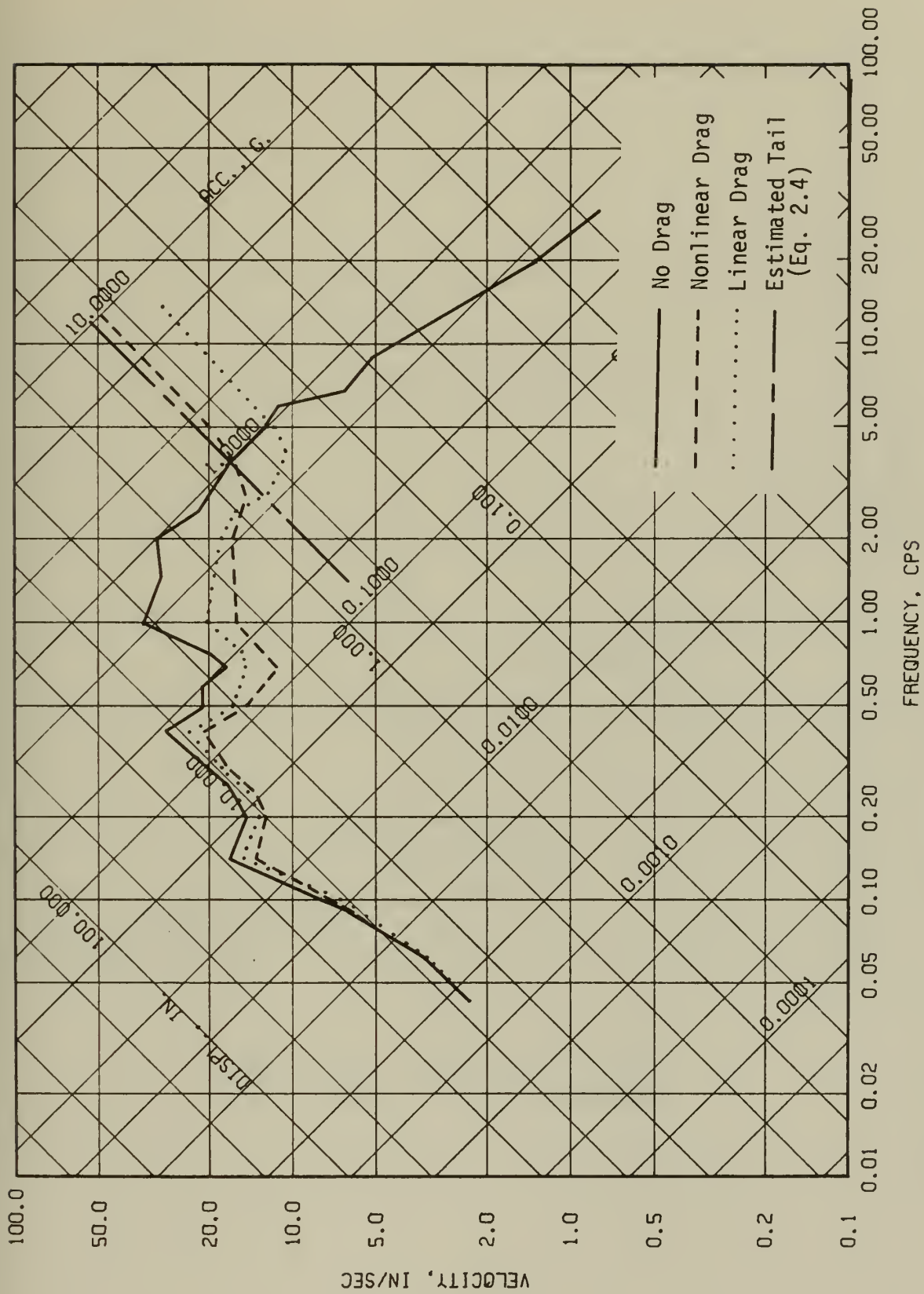


Fig. 2.19 Comparison of Nonlinear Drag Spectrum With Linear Drag Spectrum (Linearized by Ground Velocity). El Centro Earthquake. $\beta_s = 0.02$, $K_D \ddot{x}_g \max / K = 0.50$

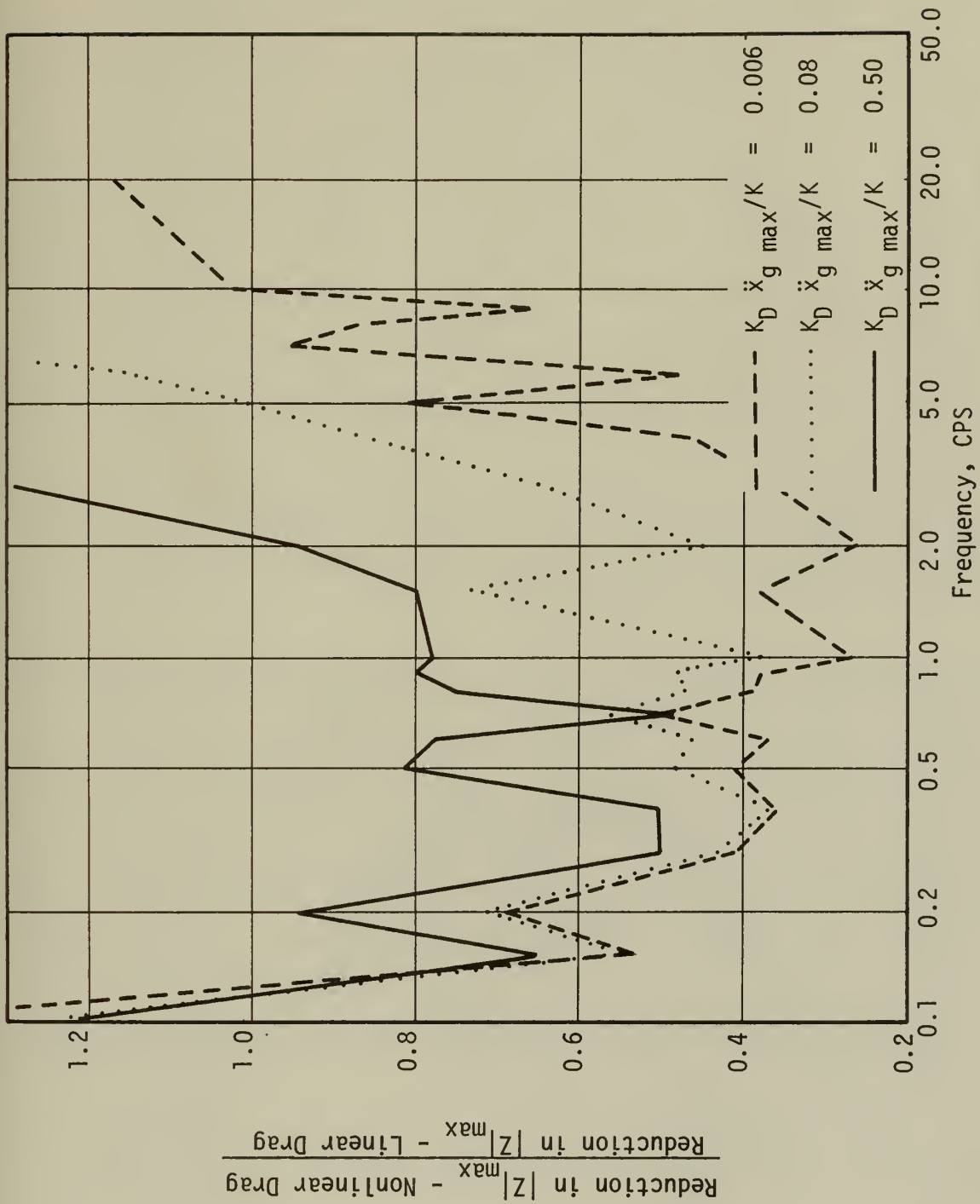
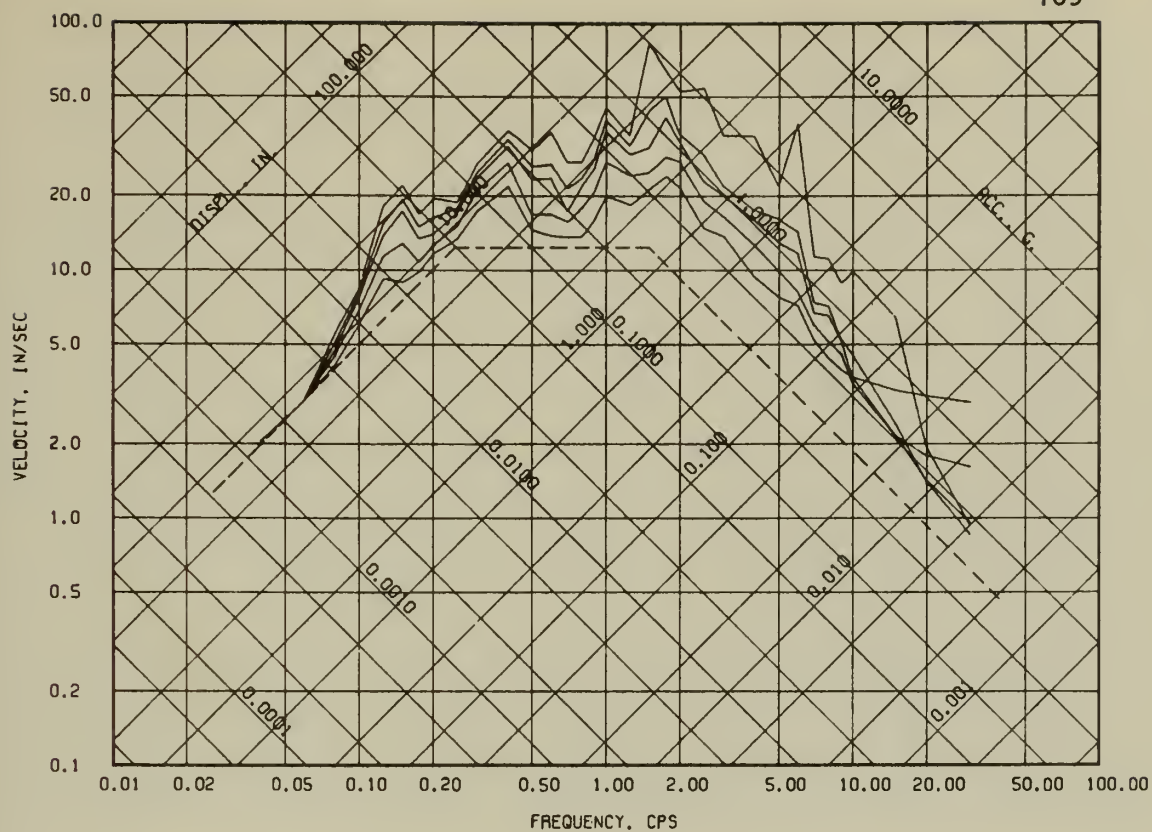
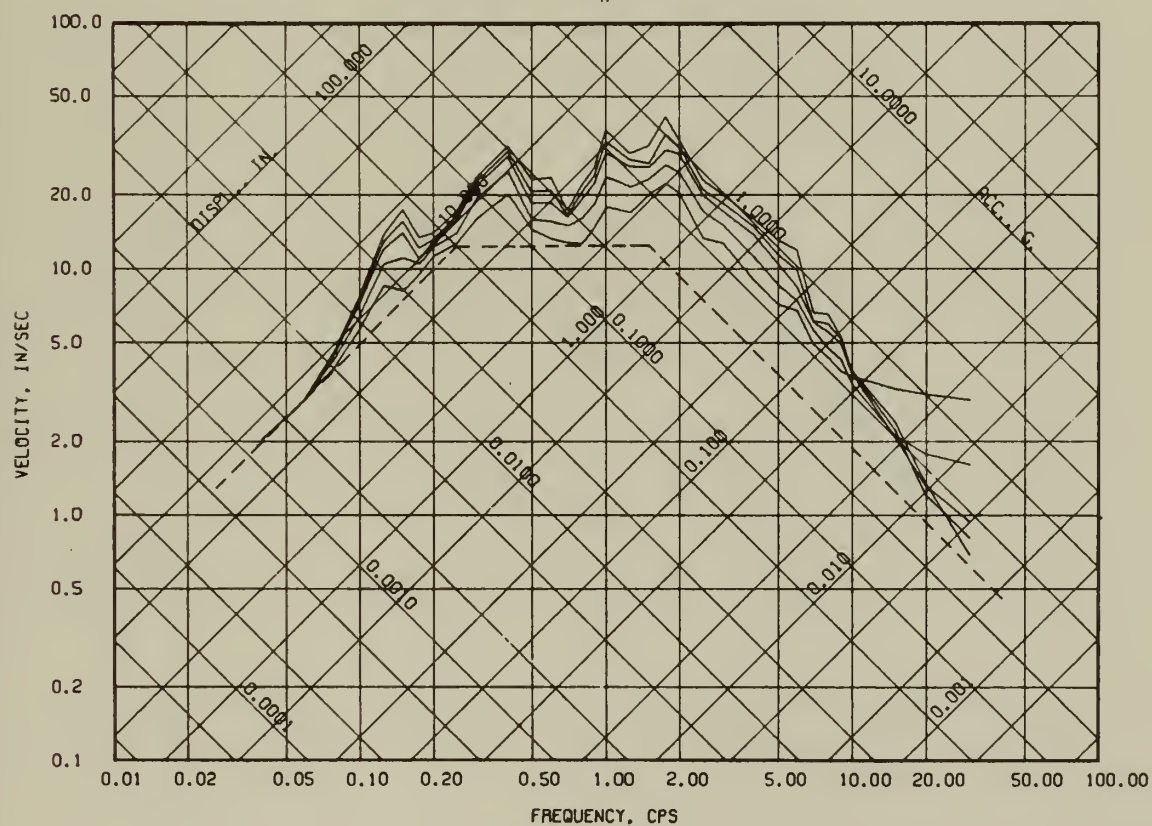


Fig. 2.20 Comparison of Linear and Nonlinear Solution (Linearized by Ground Velocity). E1 Centro Earthquake. $\beta_s = 0.02$

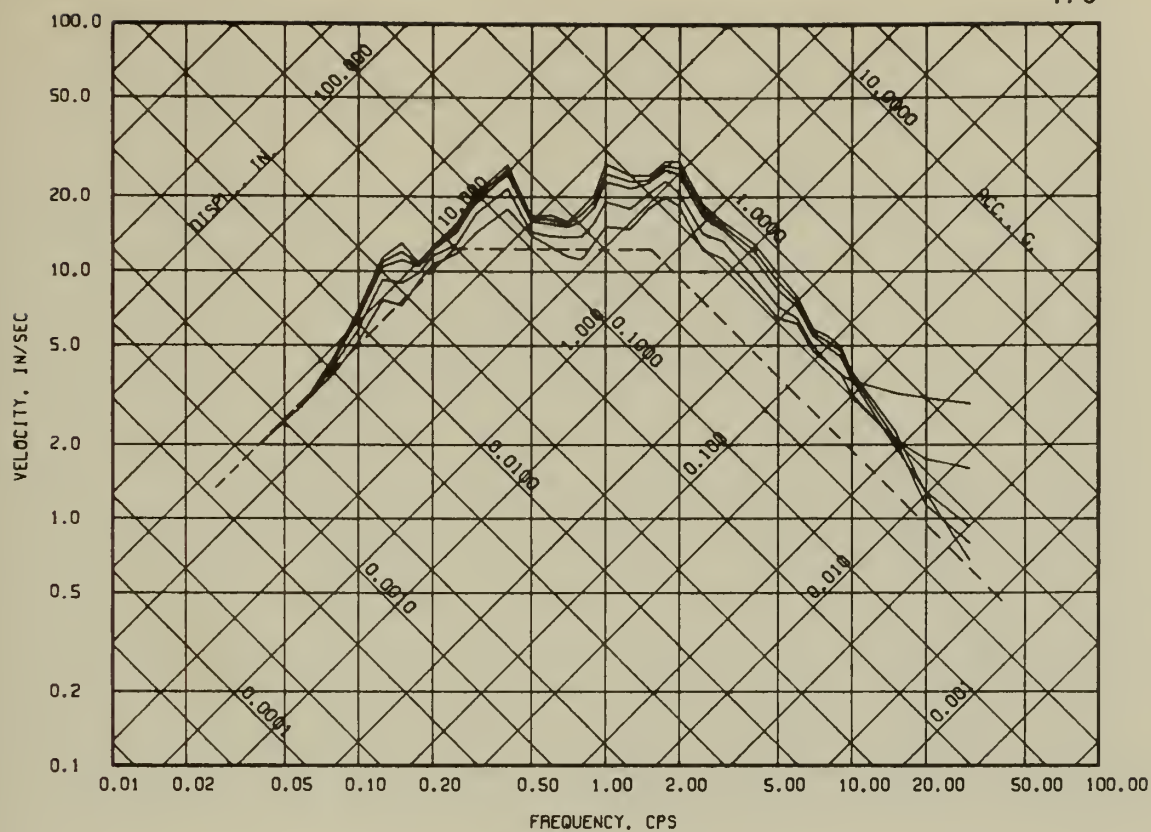


(a) $\beta_s = 0\%$ $\beta_h = 0, 1, 2, 5, 10\%$

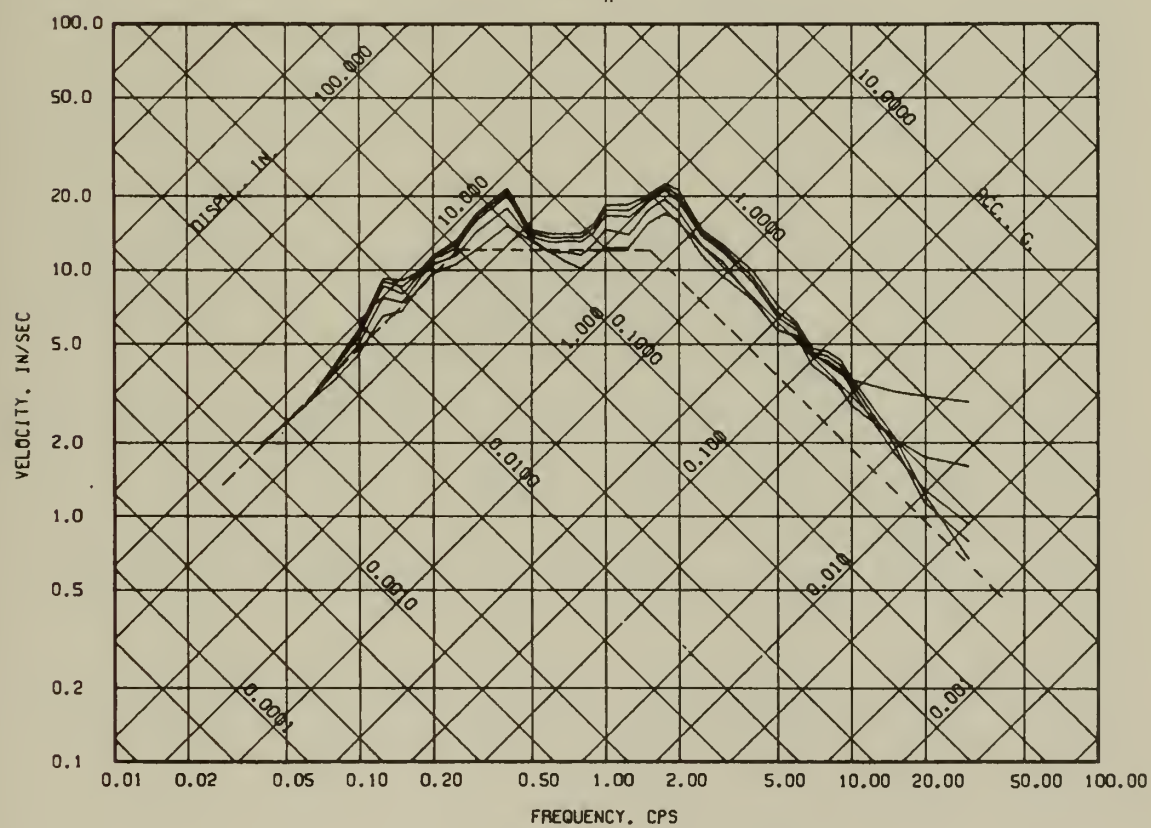


(b) $\beta_s = 2\%$ $\beta_h = 0, 1, 2, 5, 10\%$

Fig. 2.21 Elastic Deformation Response Spectra for El Centro Earthquake

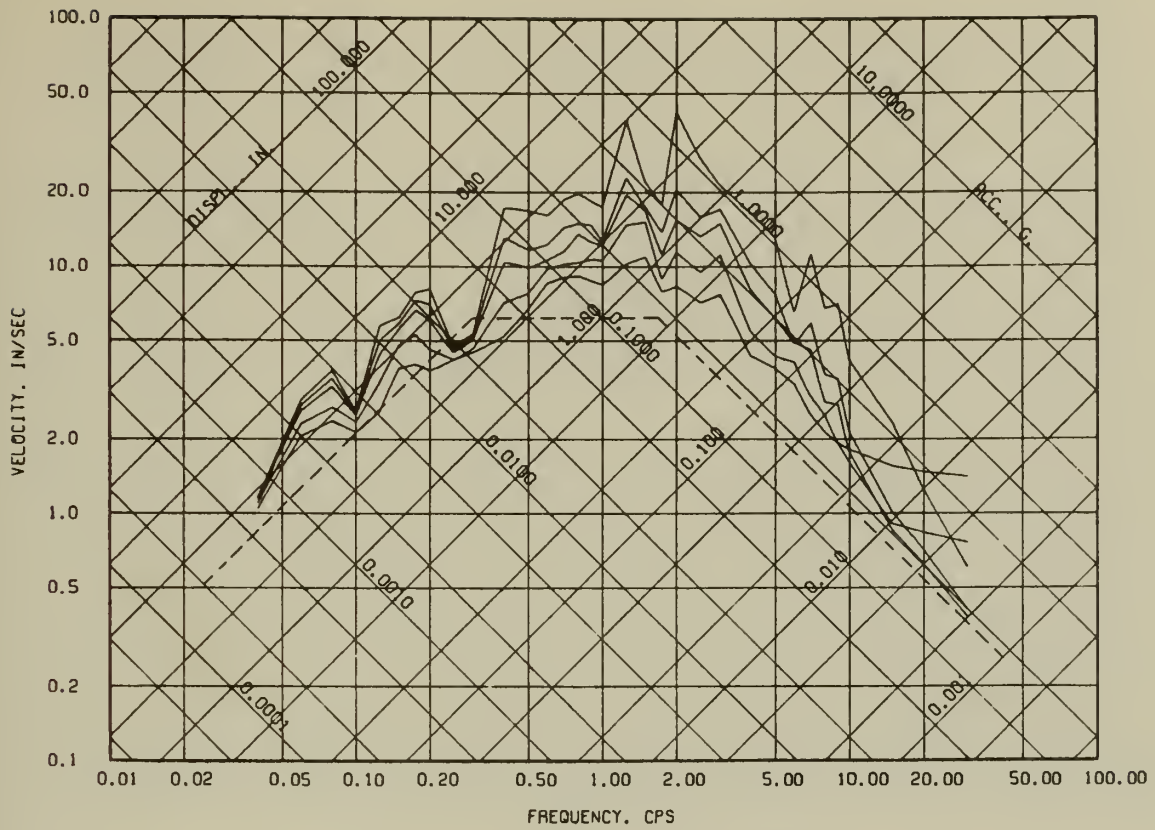


(c) $\beta_s = 5\%$ $\beta_h = 0, 1, 2, 5, 10\%$

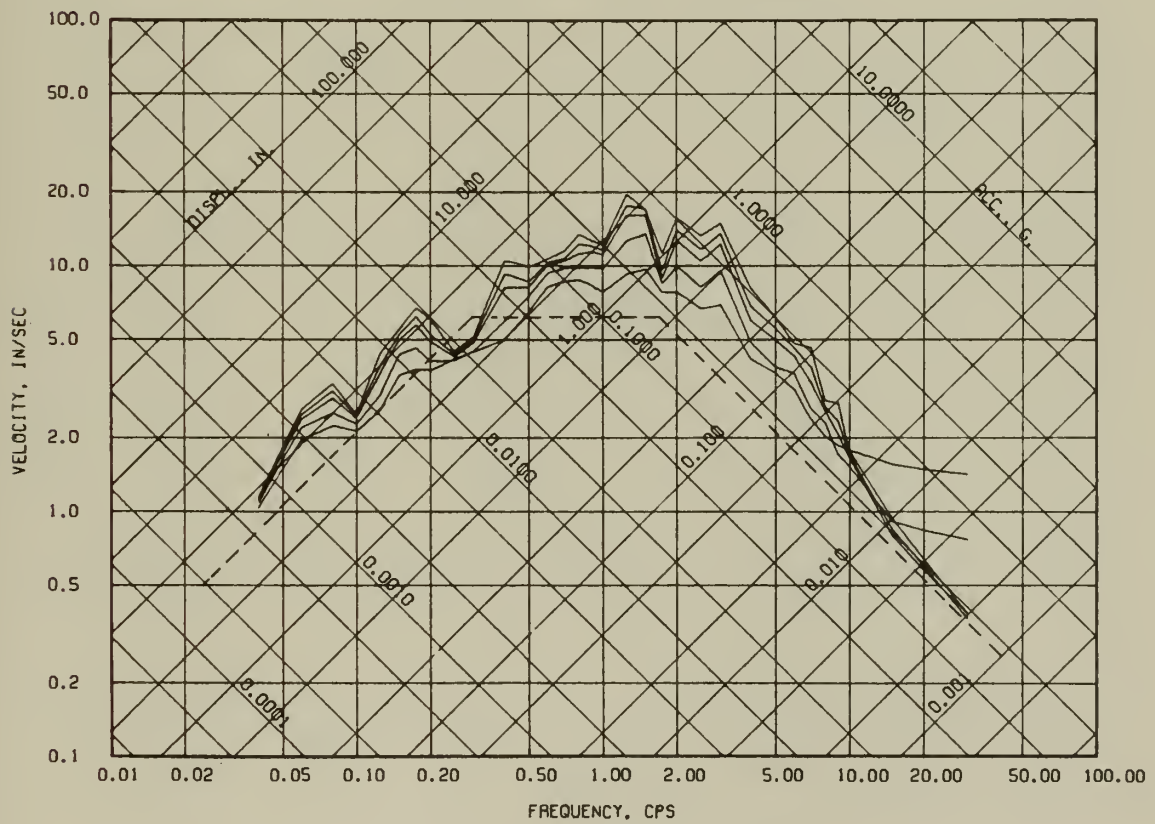


(d) $\beta_s = 10\%$ $\beta_h = 0, 1, 2, 5, 10\%$

Fig. 2.21 (Continued)



(a) $\beta_s = 0\%$ $\beta_h = 0, 1, 2, 5, 10\%$



(b) $\beta_s = 2\%$ $\beta_h = 0, 1, 2, 5, 10\%$

Fig. 2.22 Elastic Deformation Response Spectra for Taft Earthquake

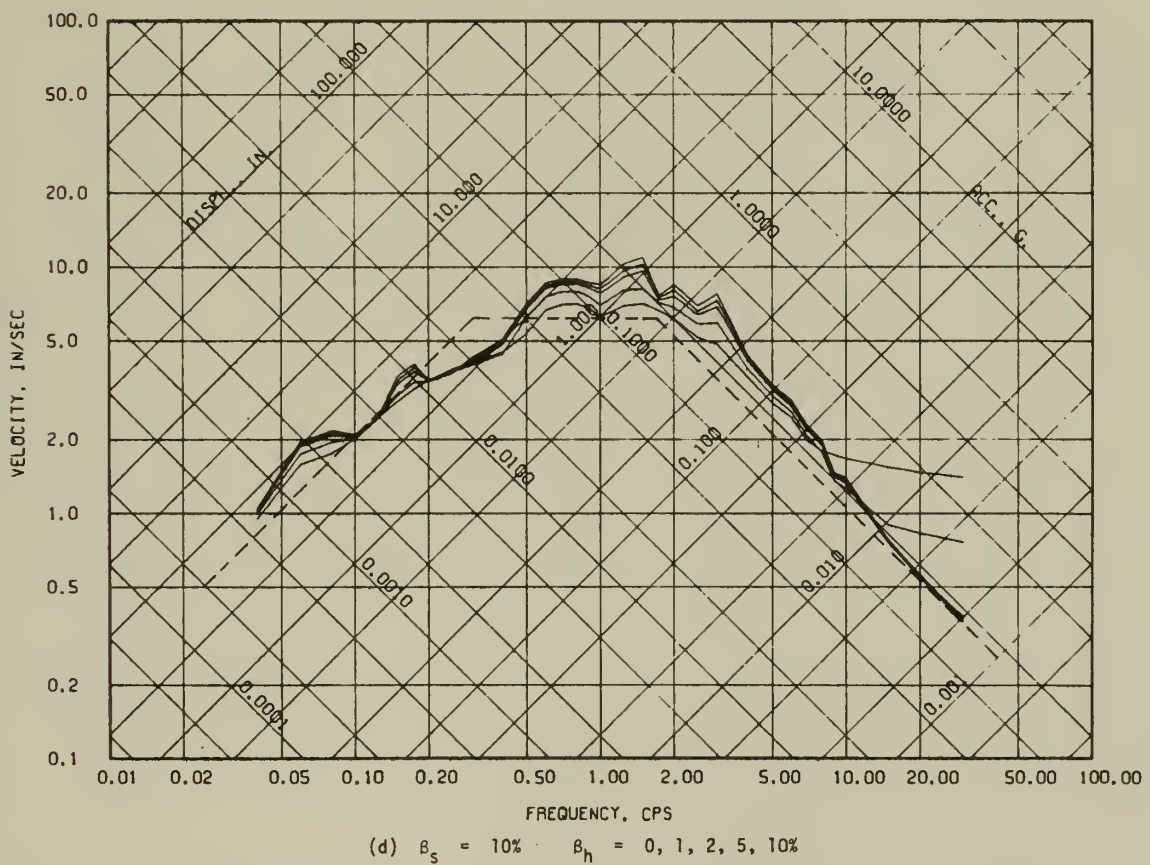
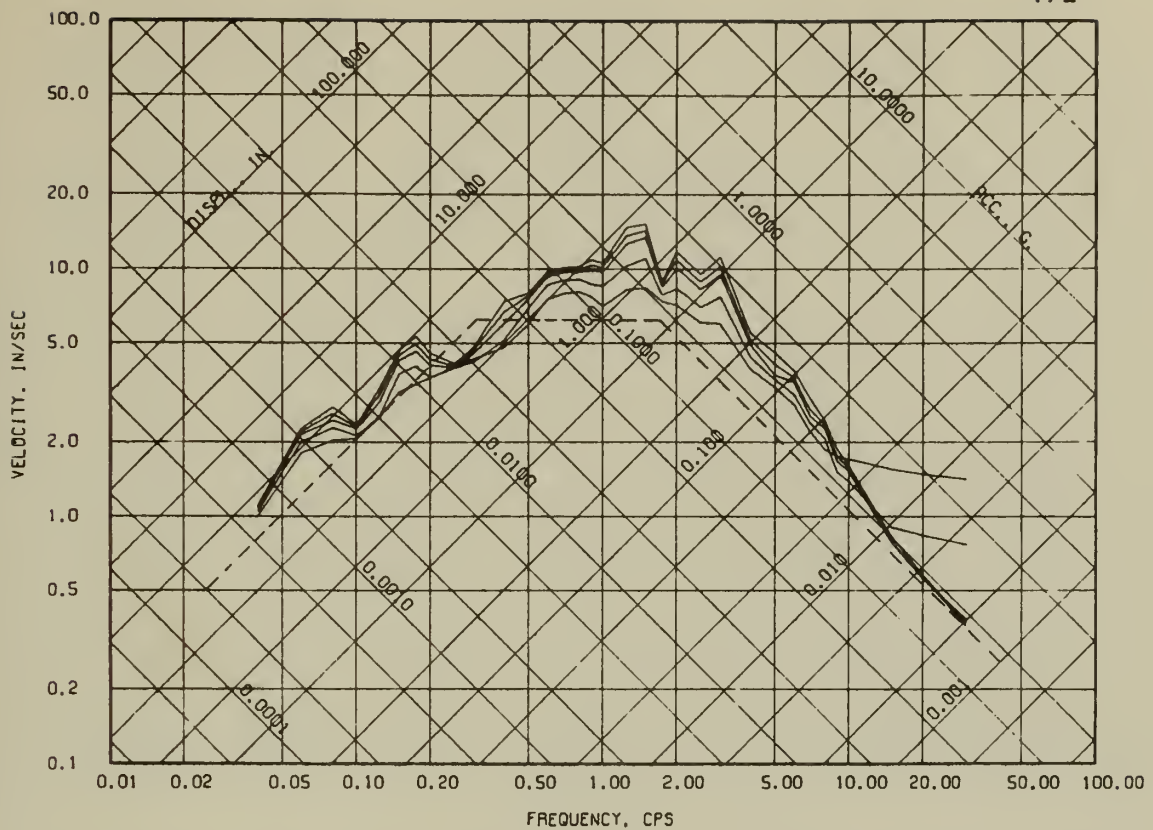
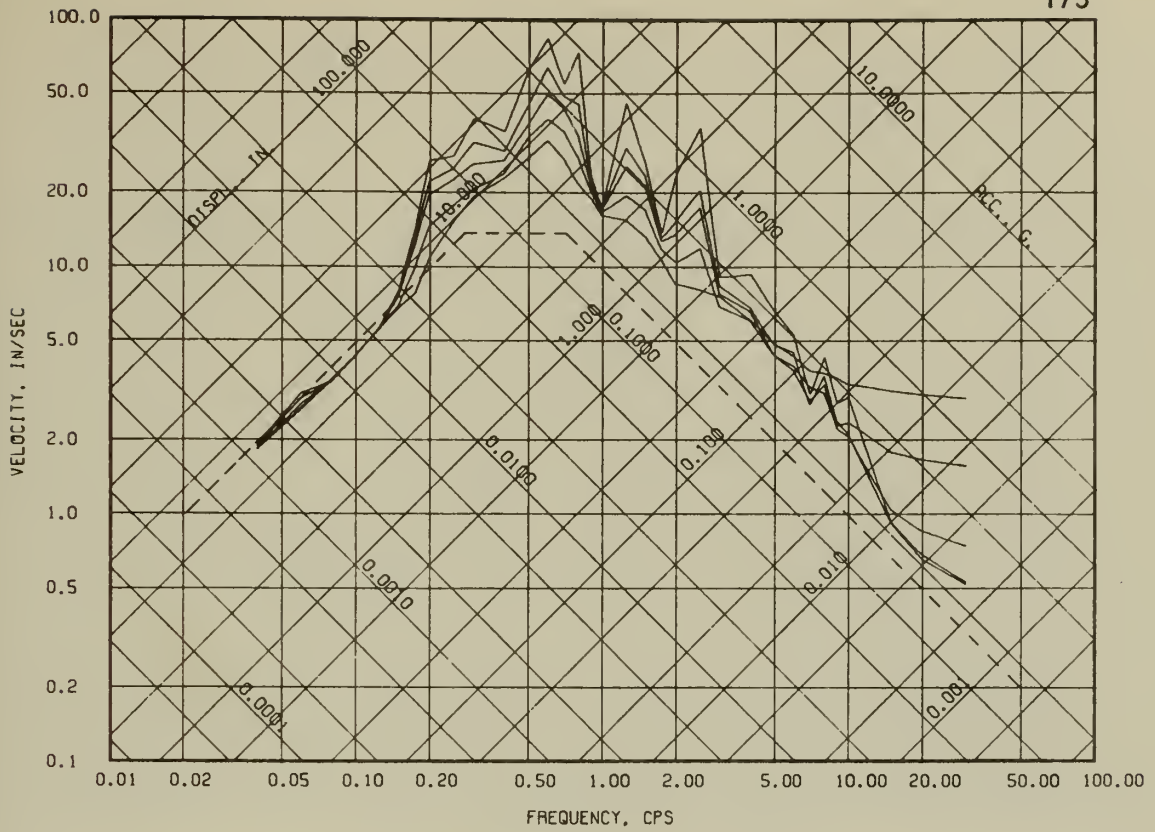
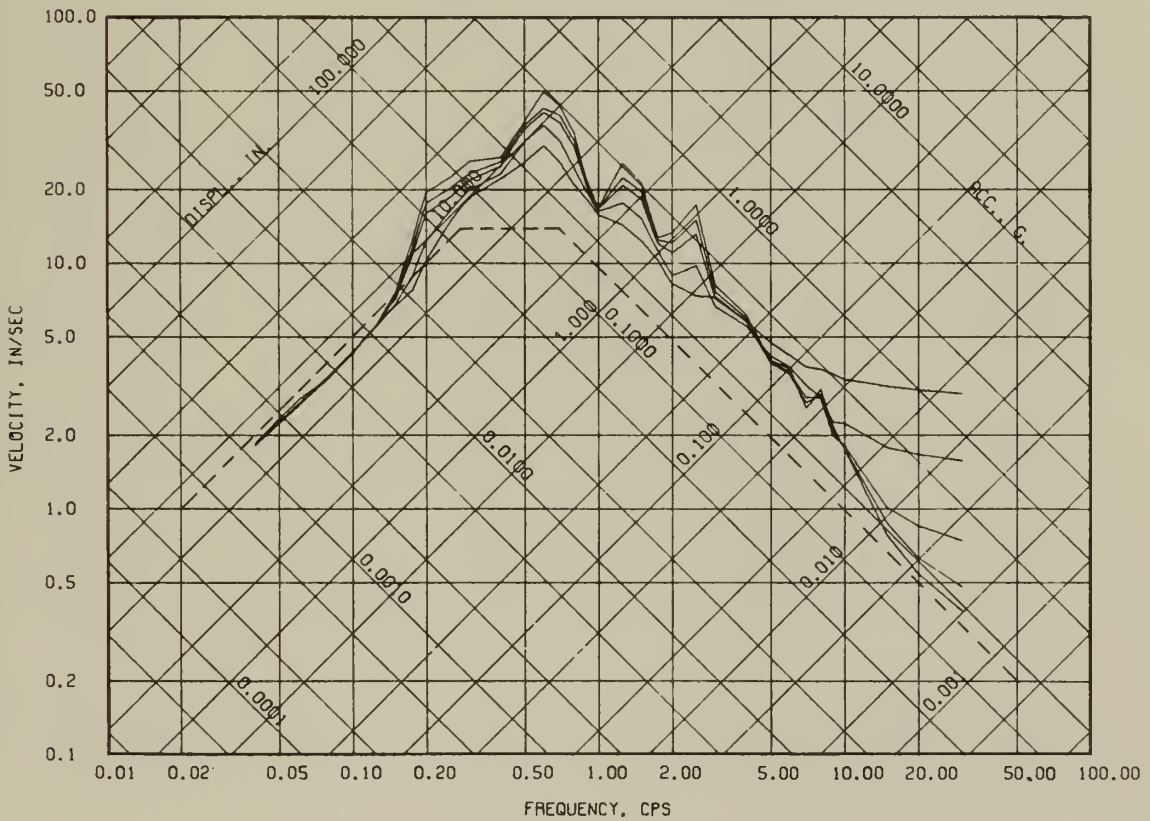


Fig. 2.22 (Continued)



(a) $\beta_s = 0\%$ $\beta_h = 0, 1, 2, 5, 10\%$



(b) $\beta_s = 2\%$ $\beta_h = 0, 1, 2, 5, 10\%$

Fig. 2.23 Elastic Deformation Response Spectra for Ferndale Earthquake

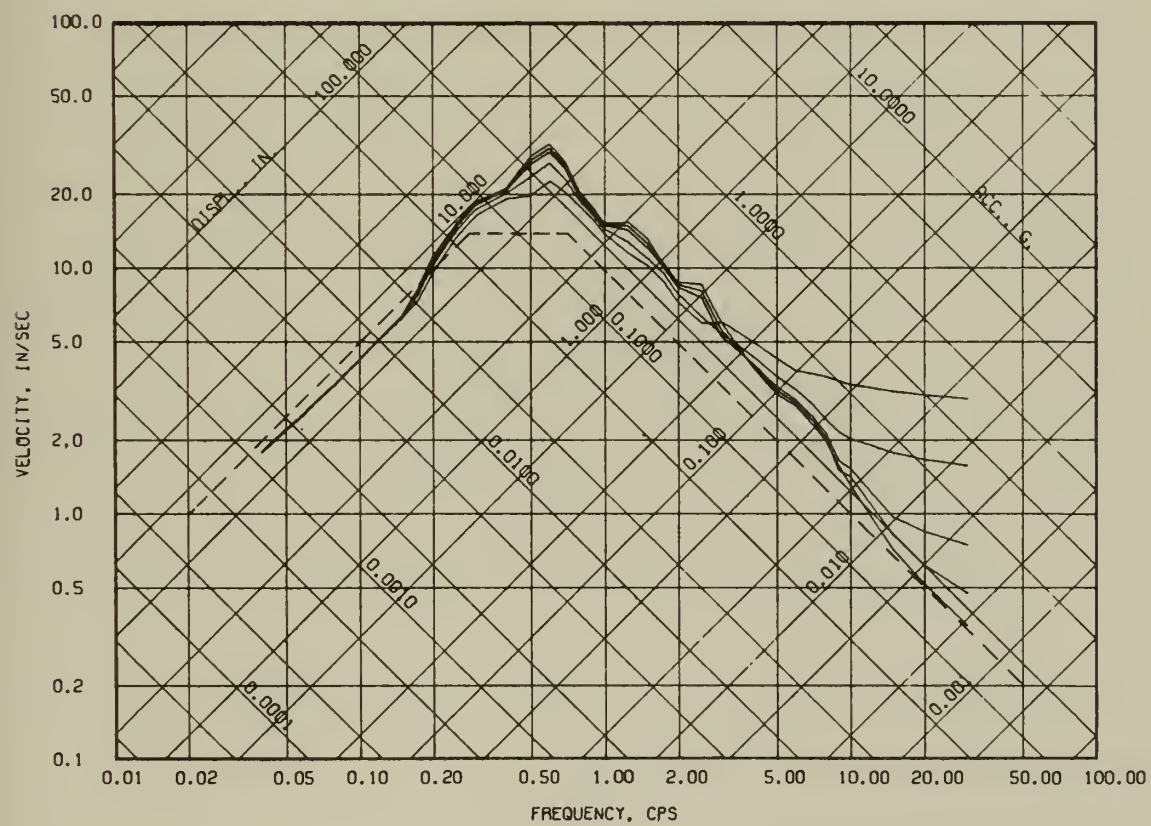
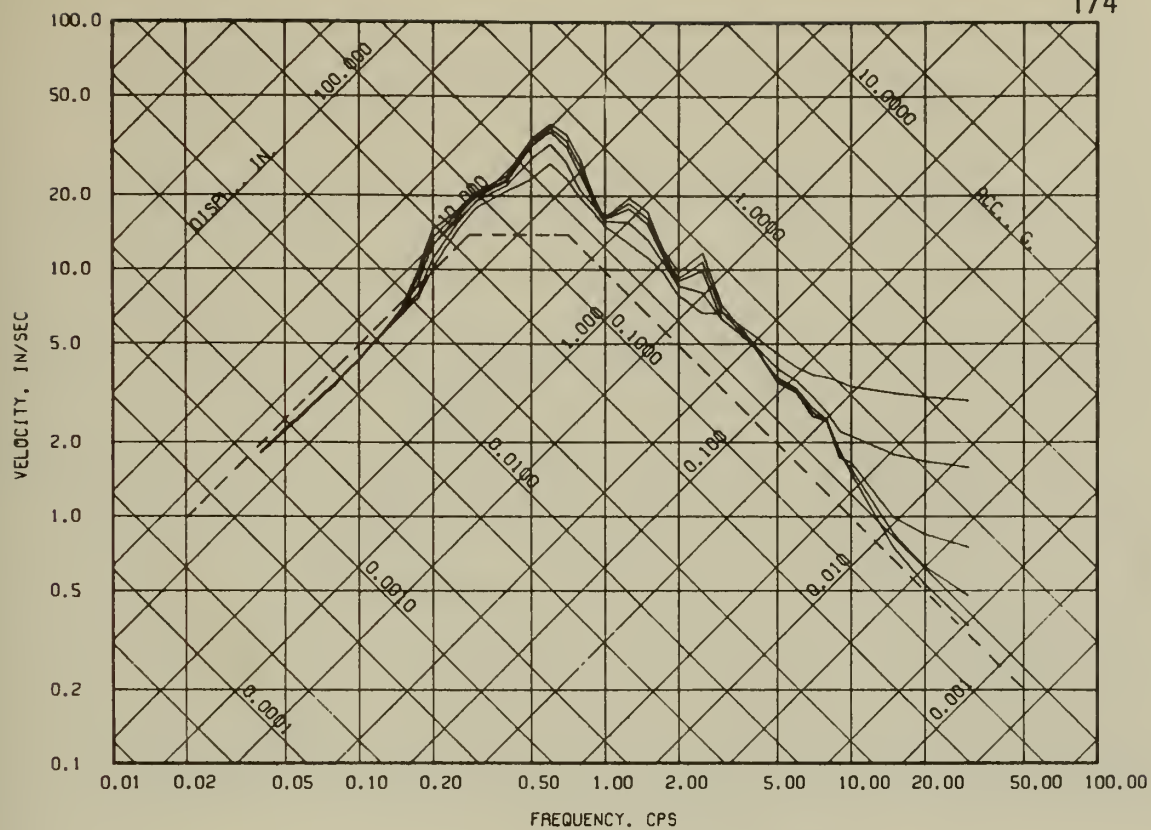


Fig. 2.23 (Continued)

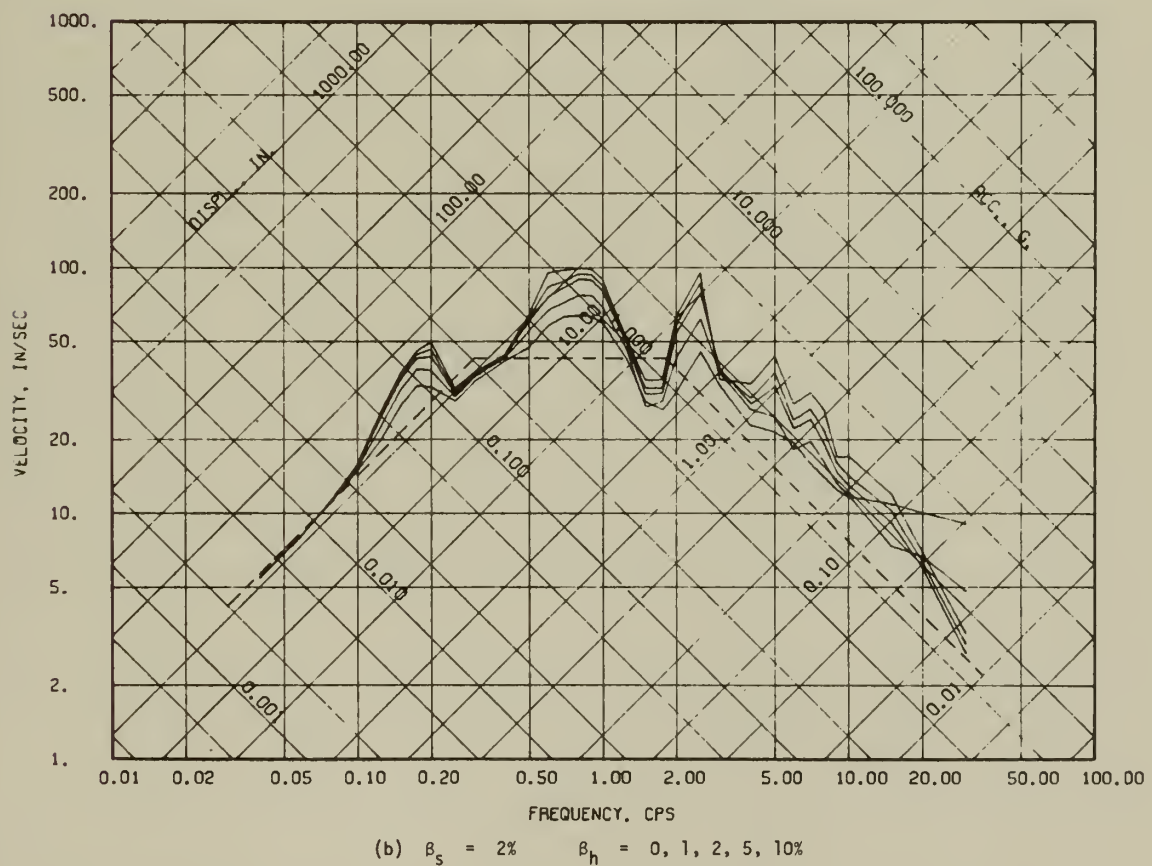
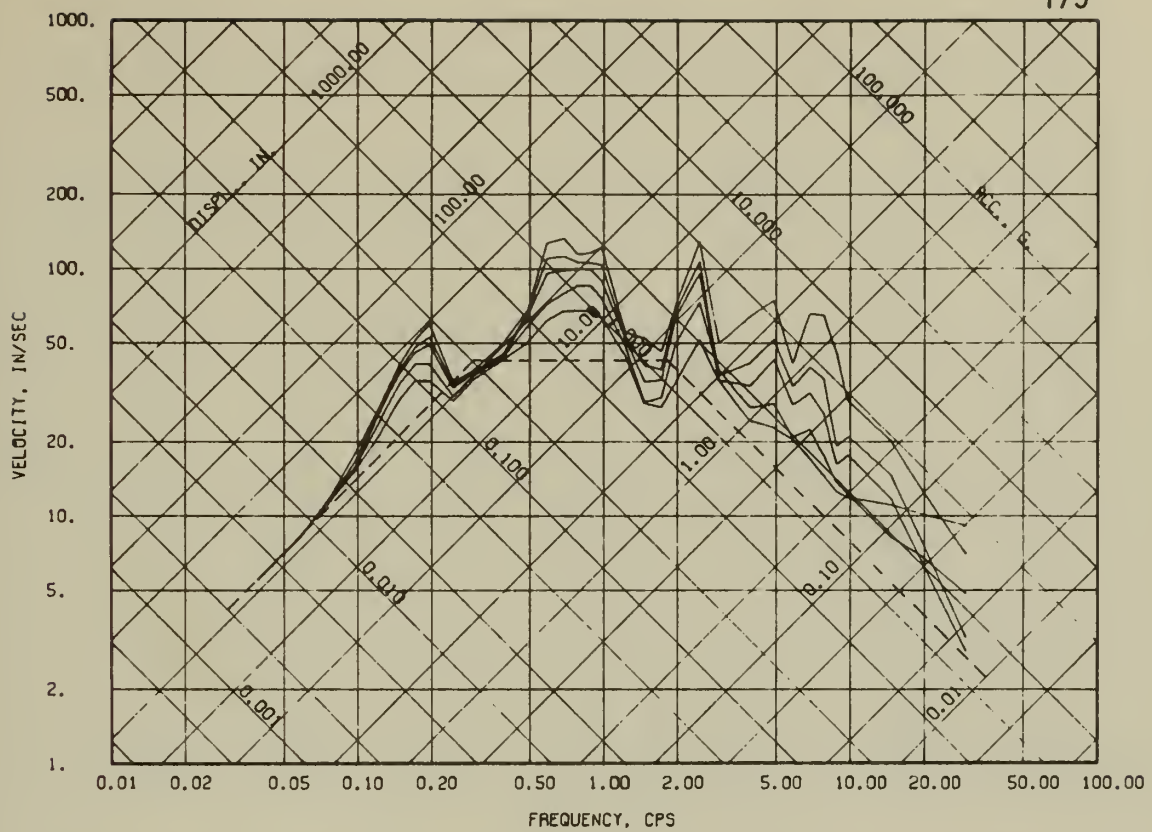
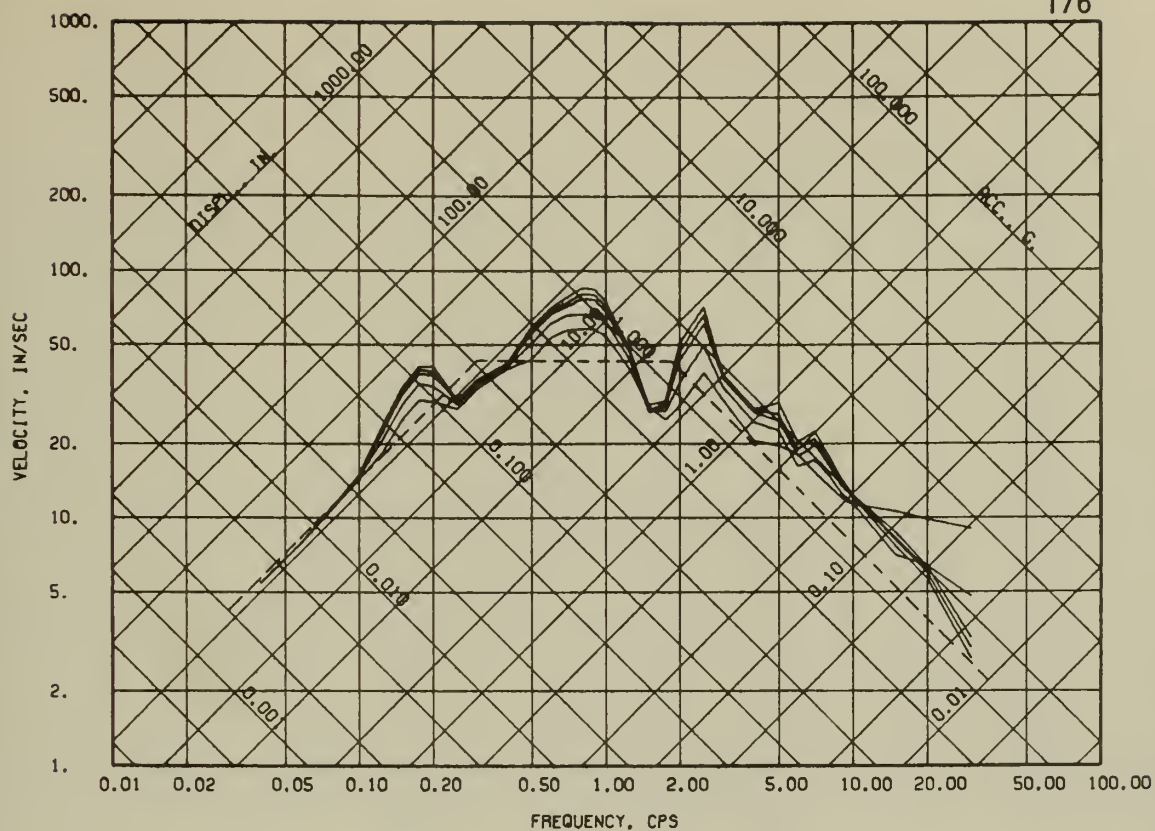
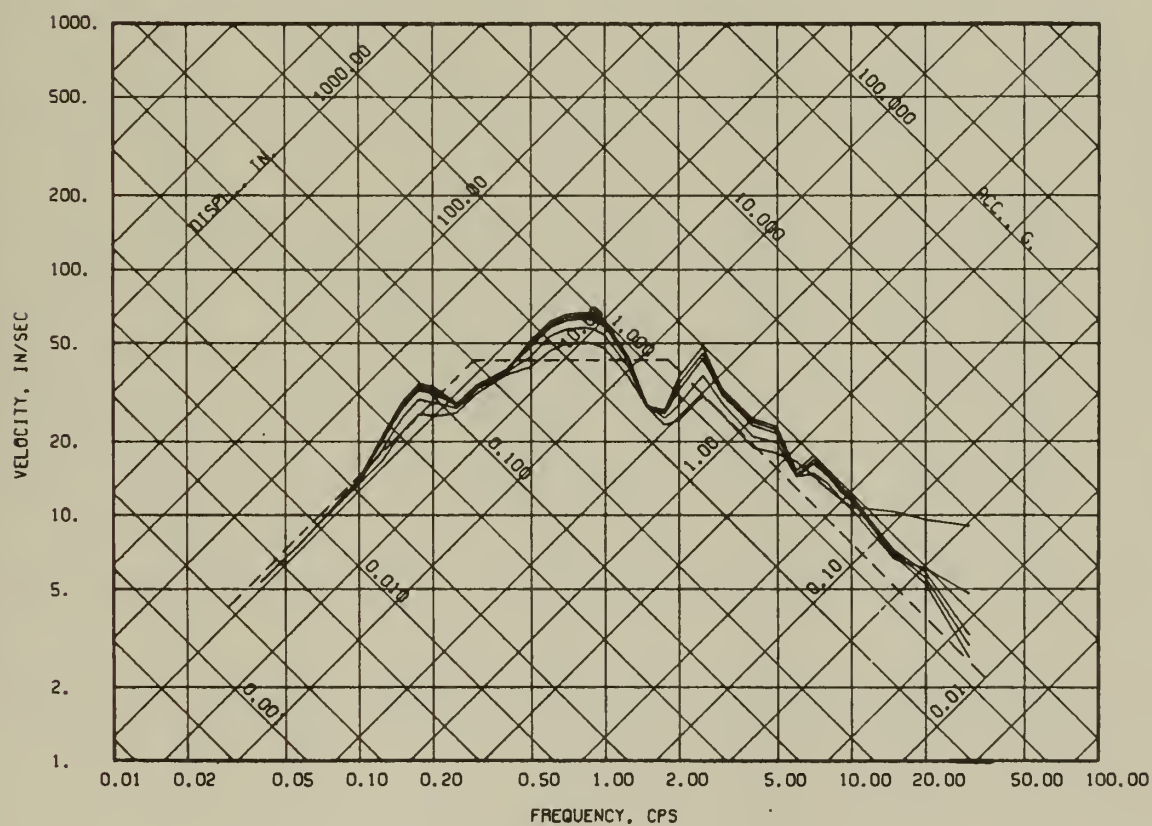


Fig. 2.24 Elastic Deformation Response Spectra for San Fernando Earthquake



(c) $\beta_s = 5\%$ $\beta_h = 0, 1, 2, 5, 10\%$



(d) $\beta_s = 10\%$ $\beta_h = 0, 1, 2, 5, 10\%$

Fig. 2.24 (Continued)

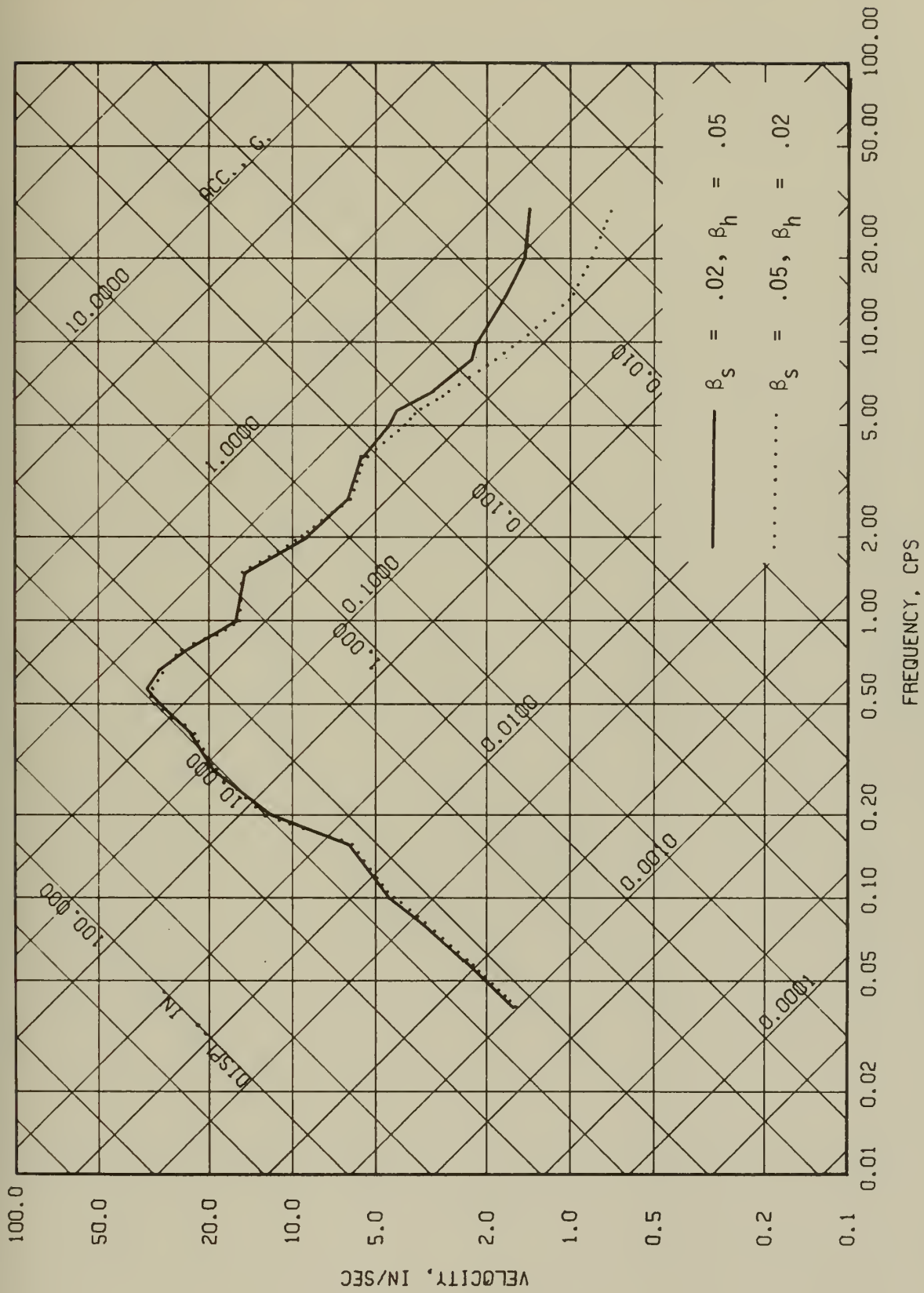
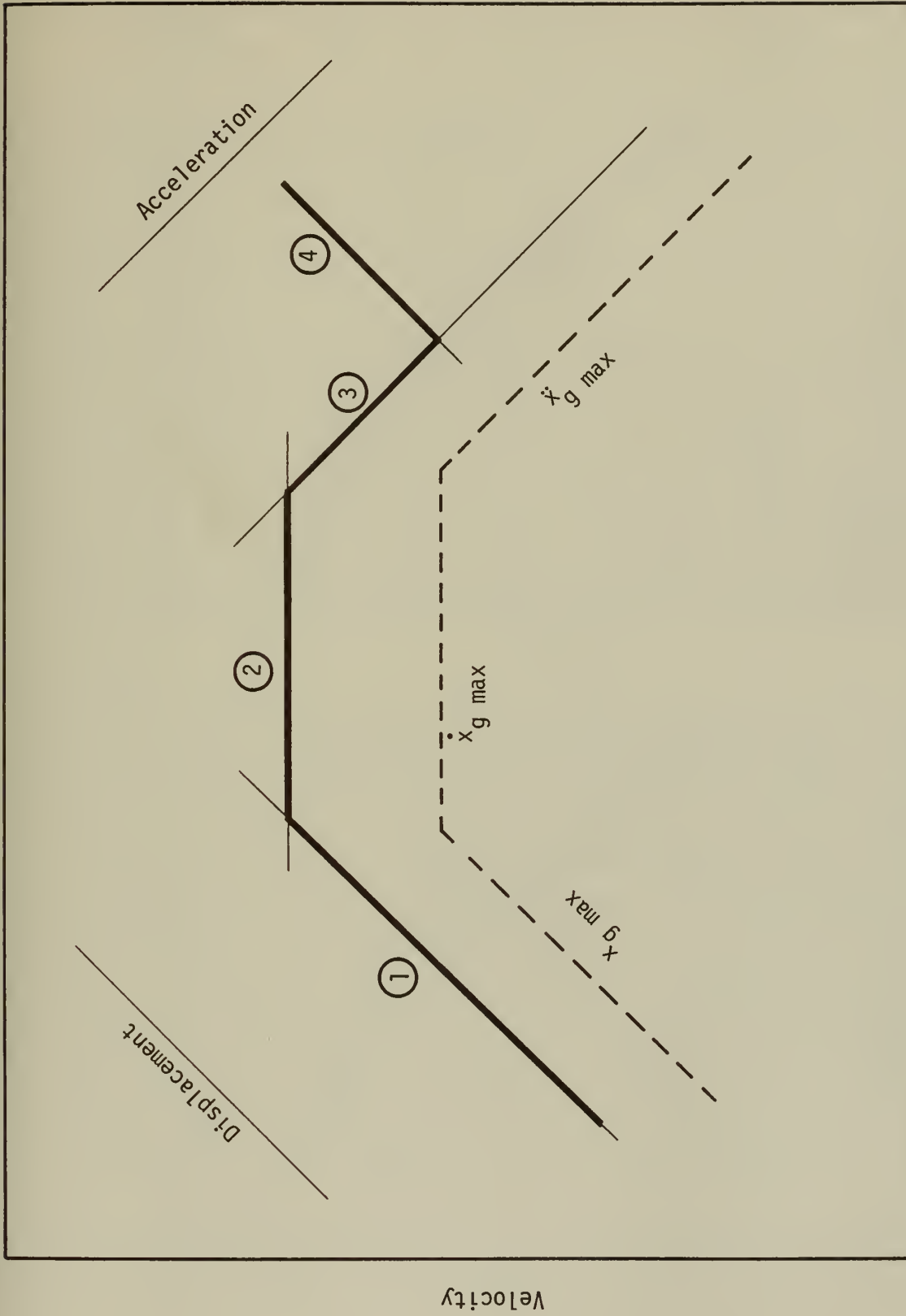


Fig. 2.25 Comparison of Spectra for Two Distributions of Total Damping Ratio. Ferndale Earthquake. $\beta_{total} = .07$



Frequency, CPS

Fig. 2.26 Construction of Idealized Elastic Deformation Response Spectrum

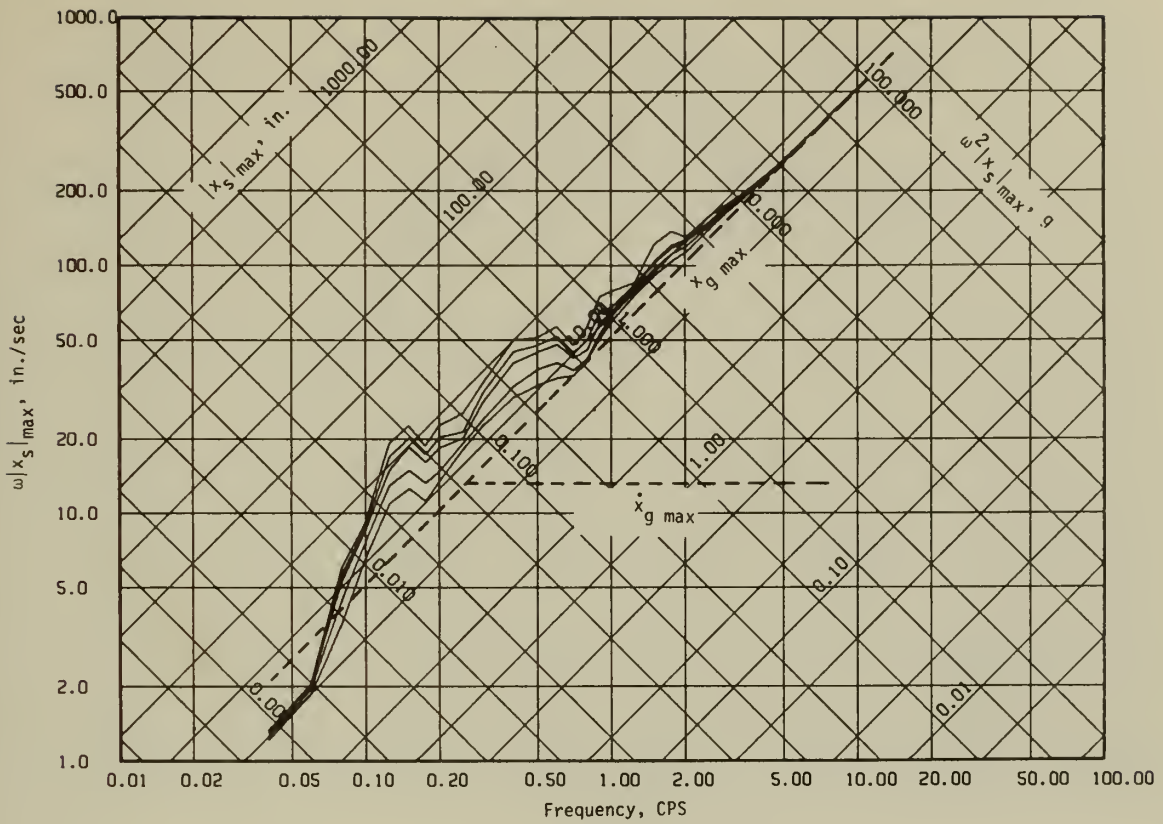
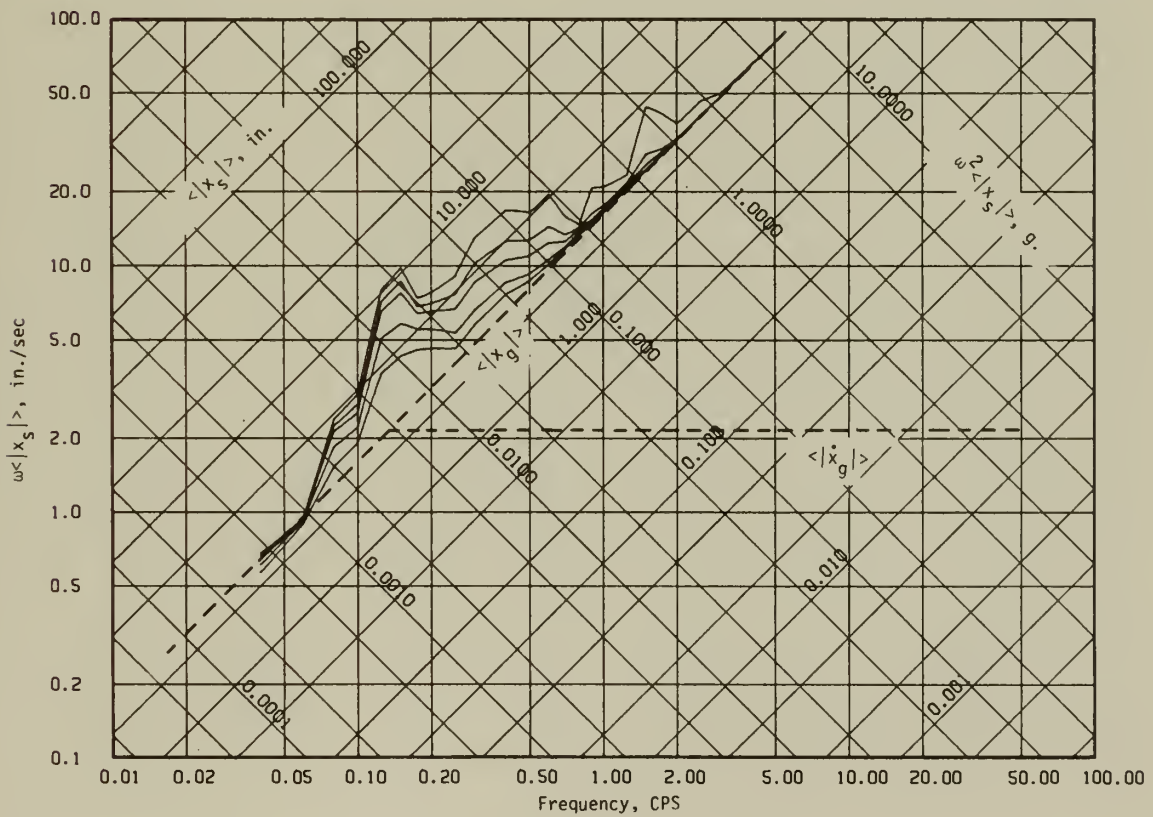
(a) $|x_s|_{\max}$ (b) $\langle |x_s| \rangle$

Fig. 2.27 Elastic Hydrodynamic Parameter Response Spectra.
 El Centro Earthquake. $\beta_{\text{total}} = 0, 1, 2, 5, 10\%$

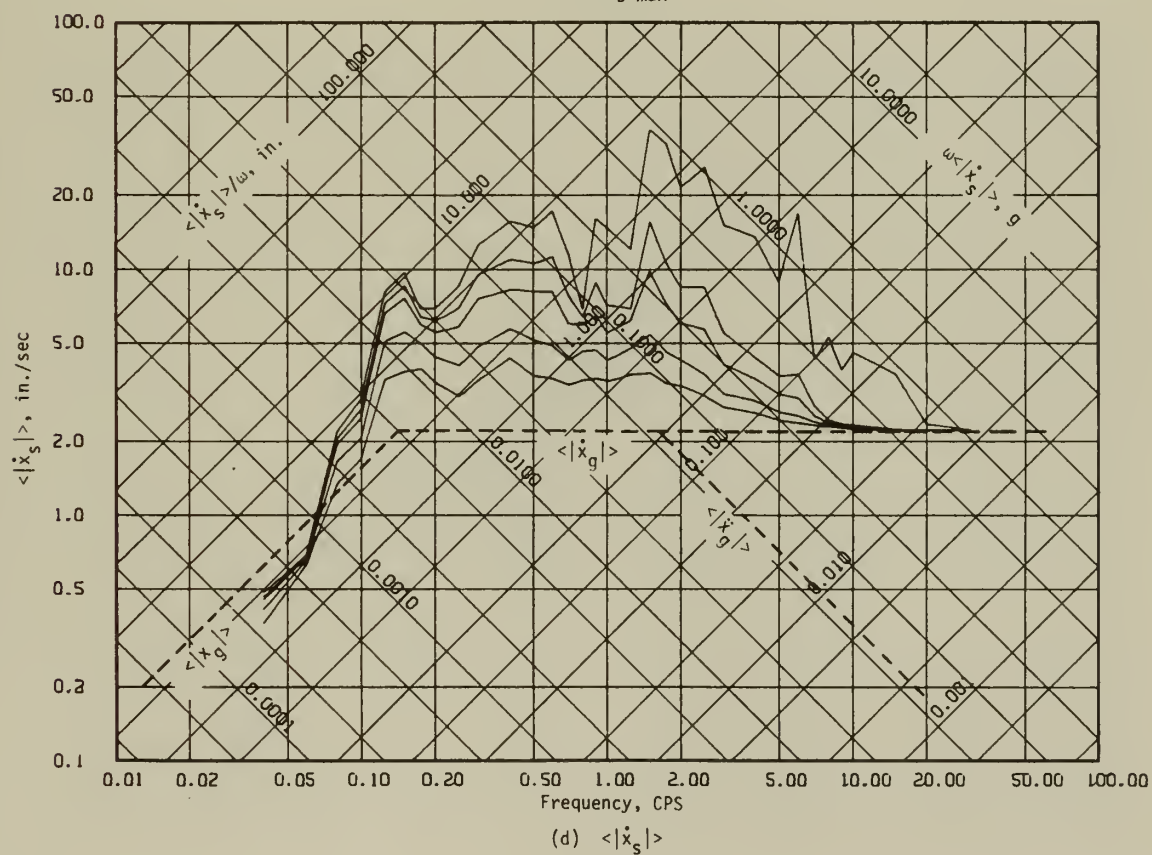
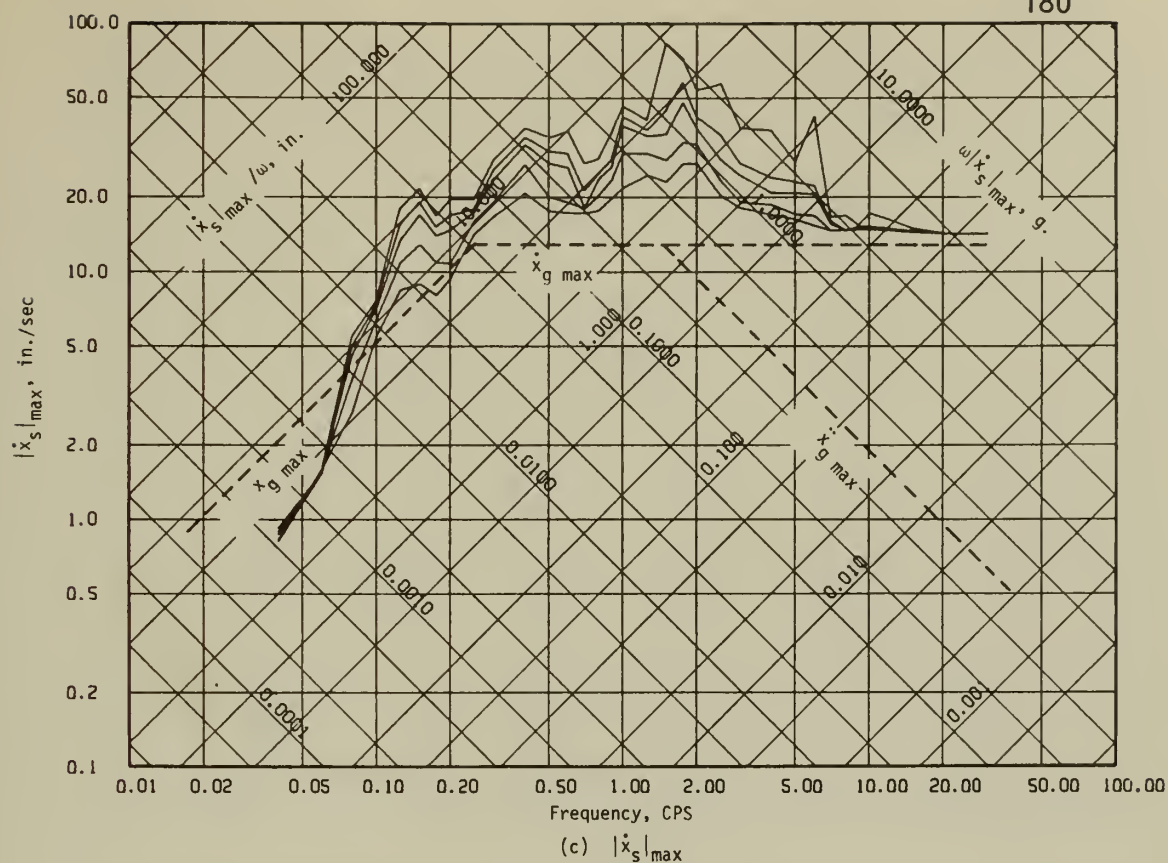


Fig. 2.27 (Continued)

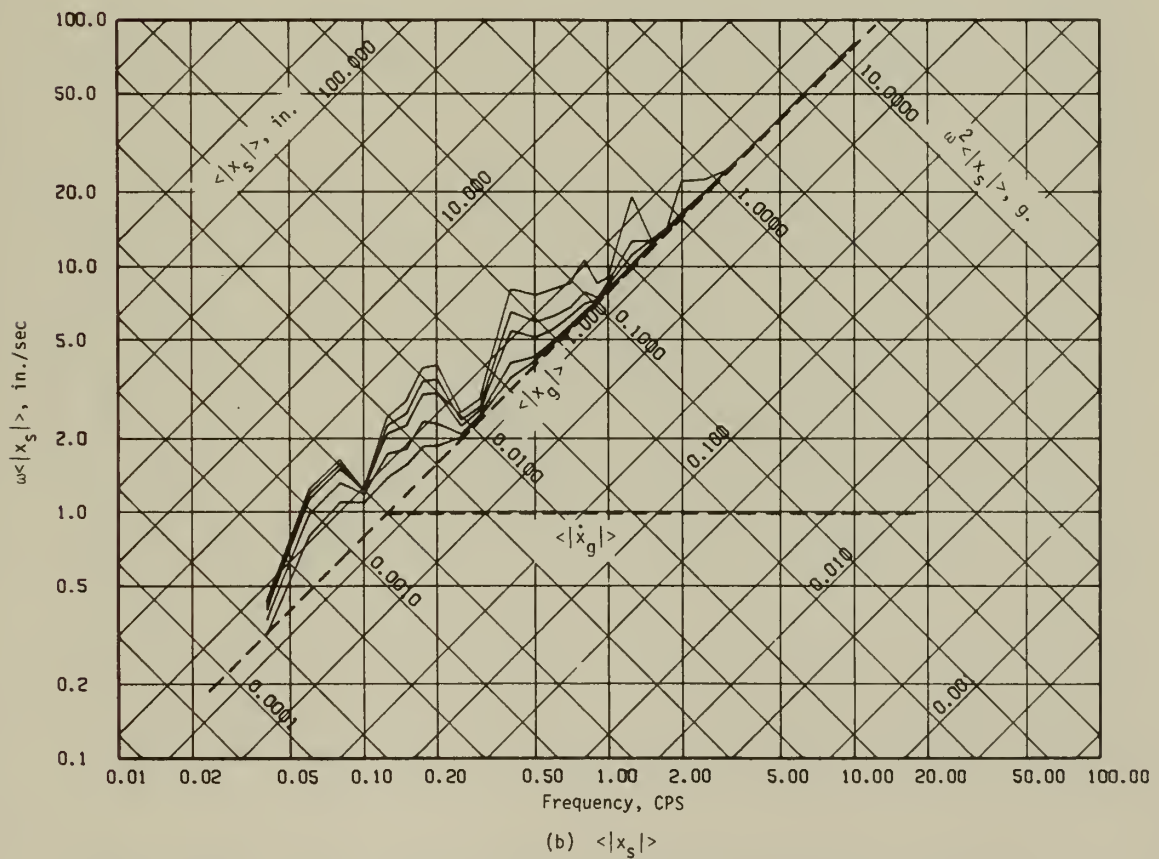
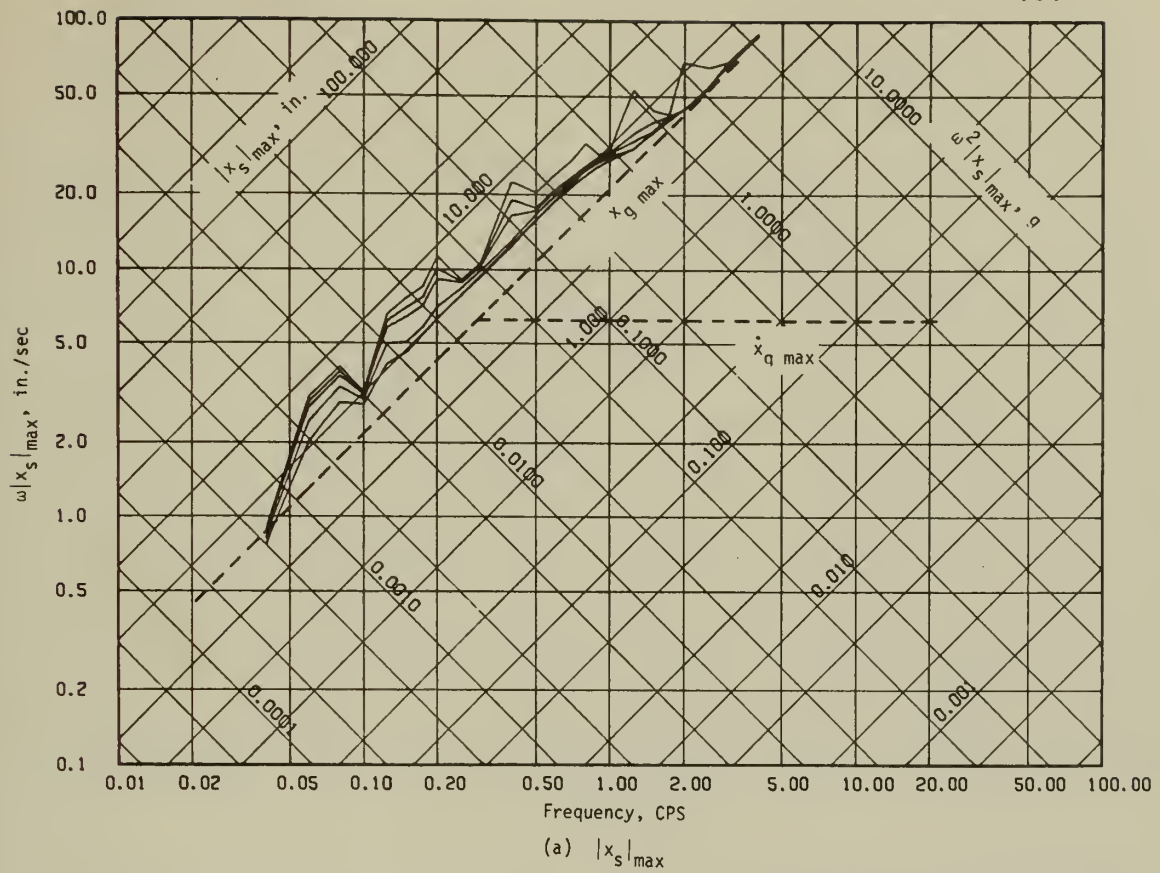


Fig. 2.28 Elastic Hydrodynamic Parameter Response Spectra.
Taft Earthquake. $\beta_{\text{total}} = 0, 1, 2, 5, 10\%$

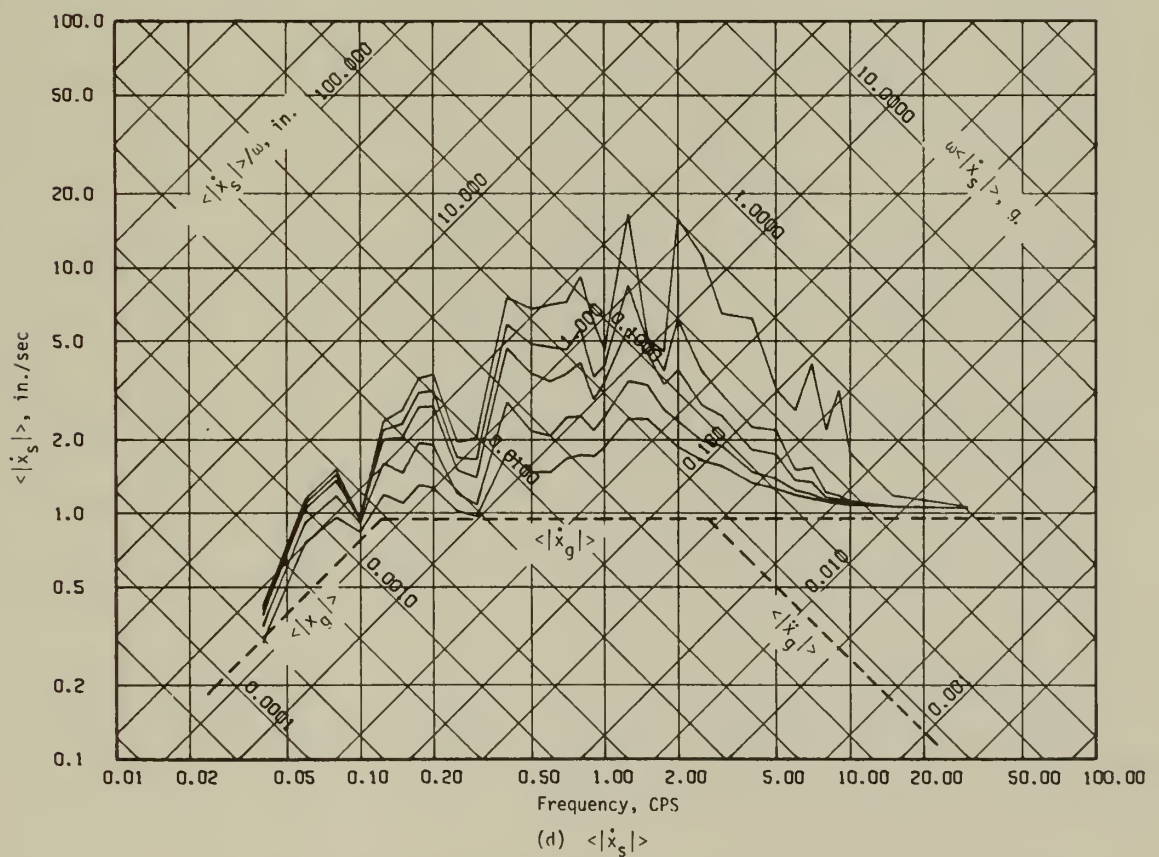
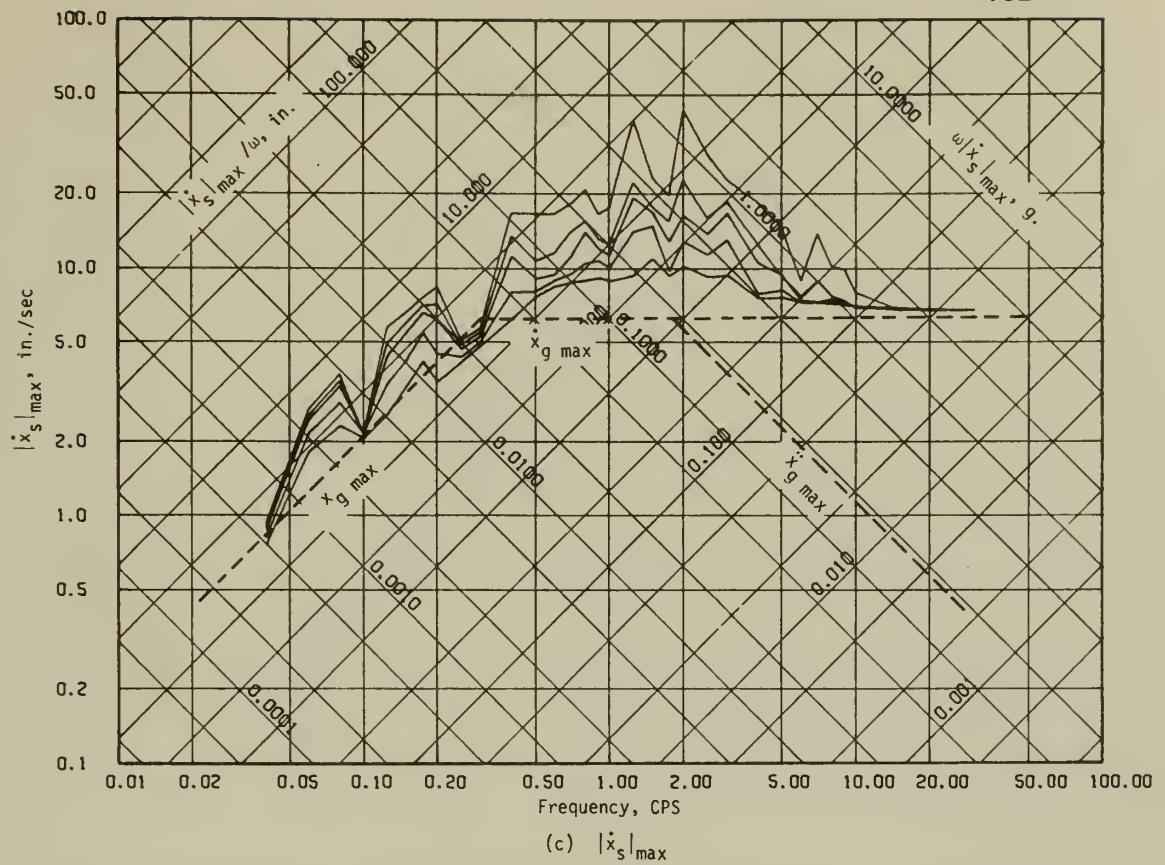


Fig. 2.28 (Continued)

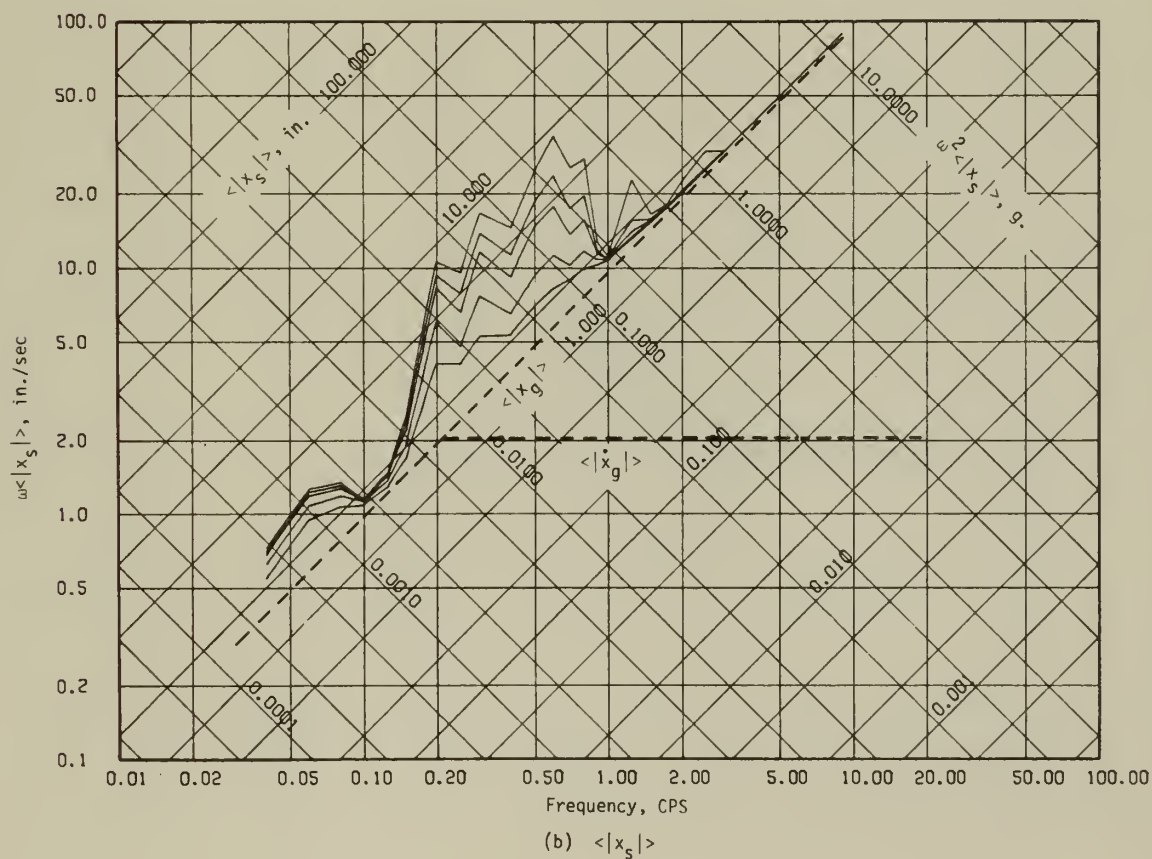
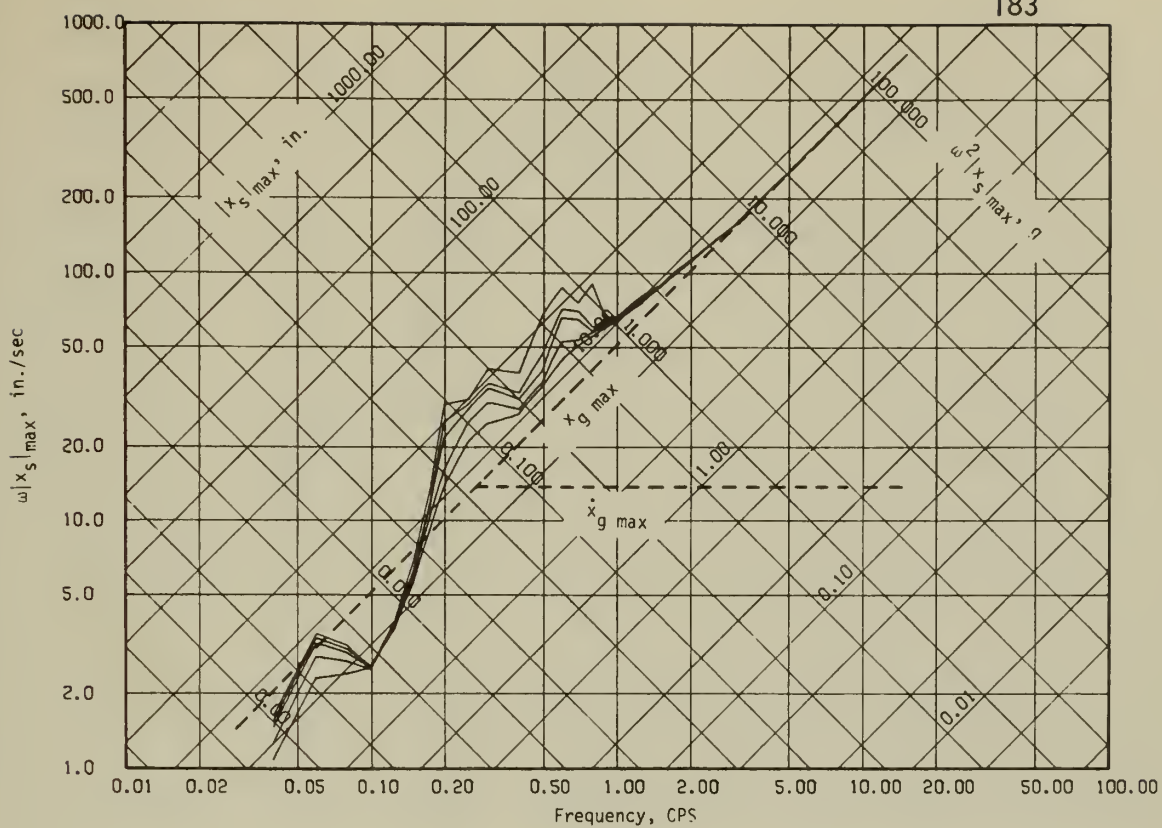


Fig. 2.29 Elastic Hydrodynamic Parameter Response Spectra.
Ferndale Earthquake. $\beta_{\text{total}} = 0, 1, 2, 5, 10\%$

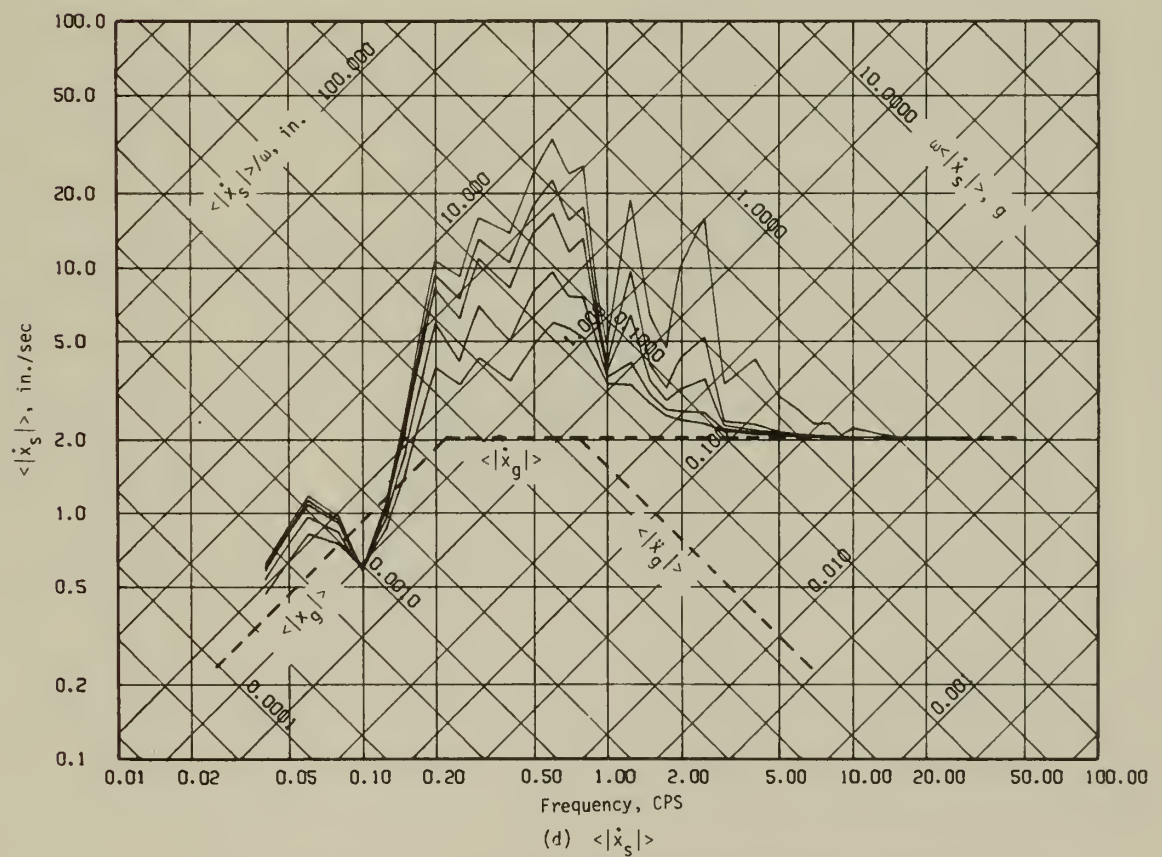
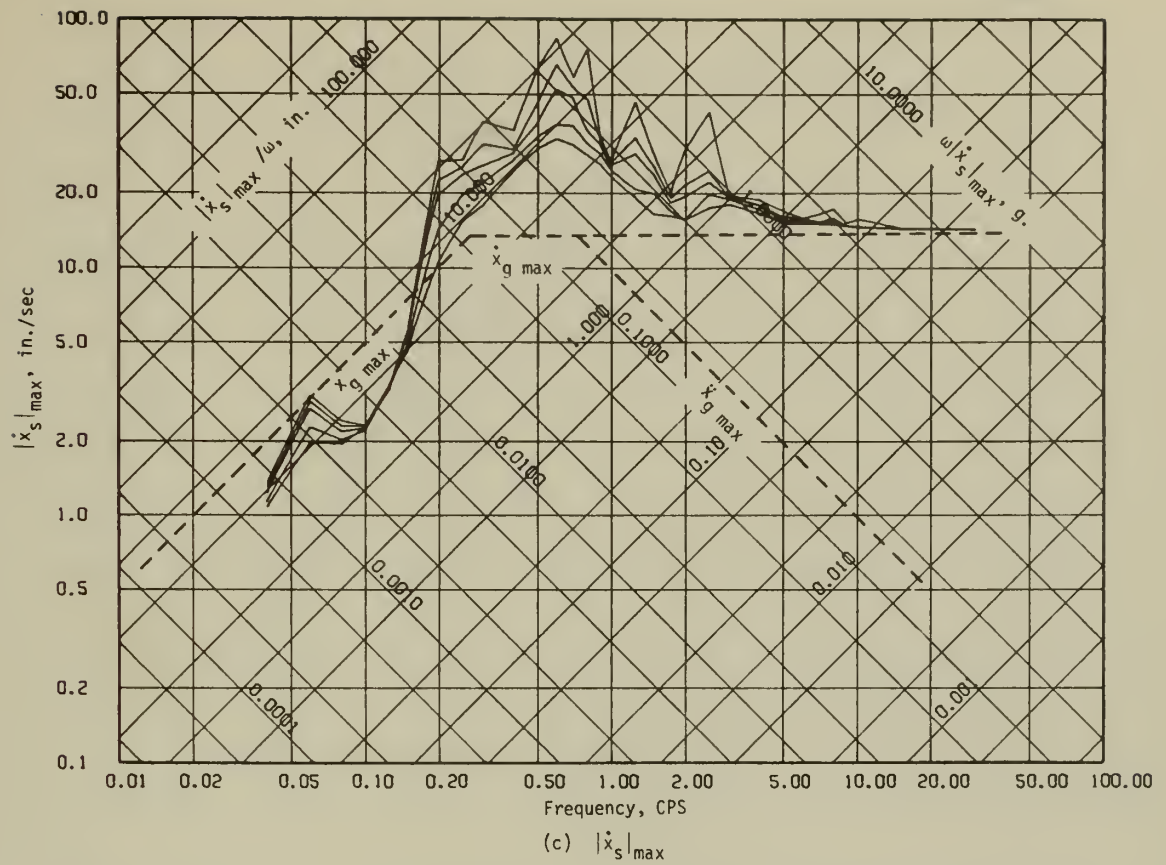


Fig. 2.29 (Continued)

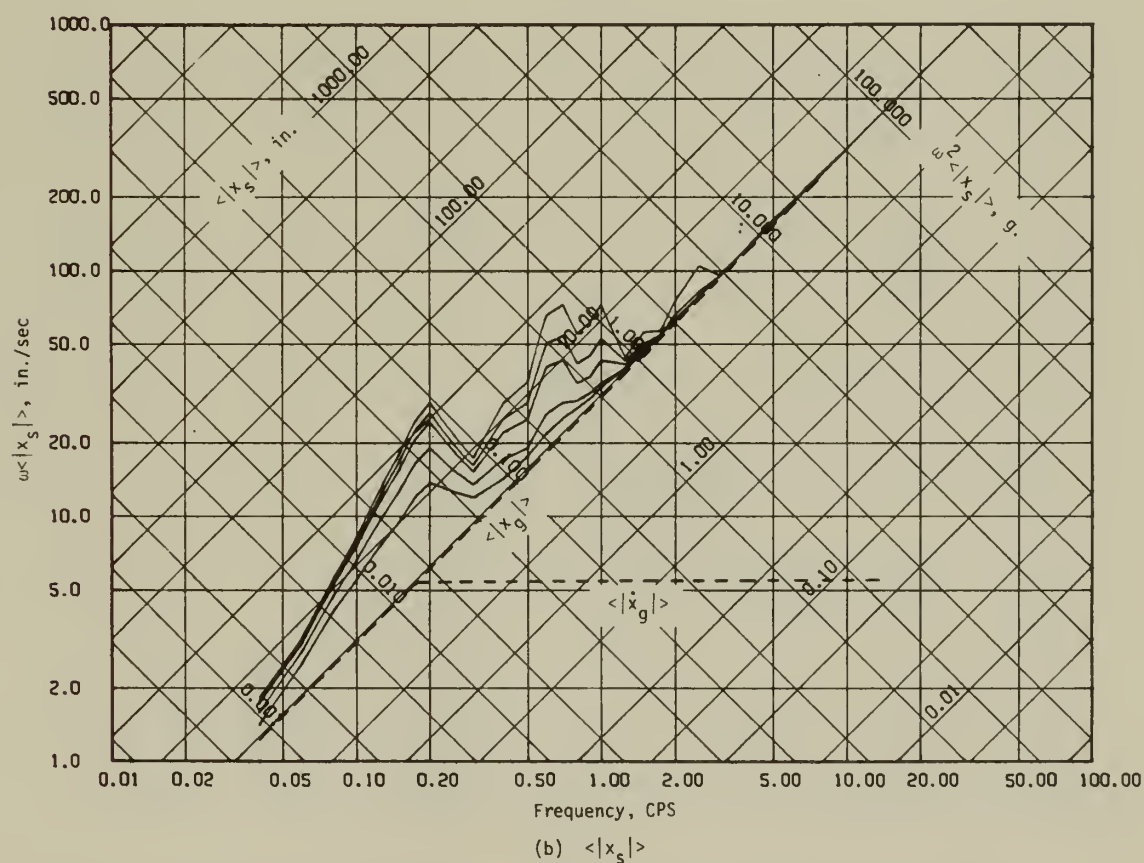
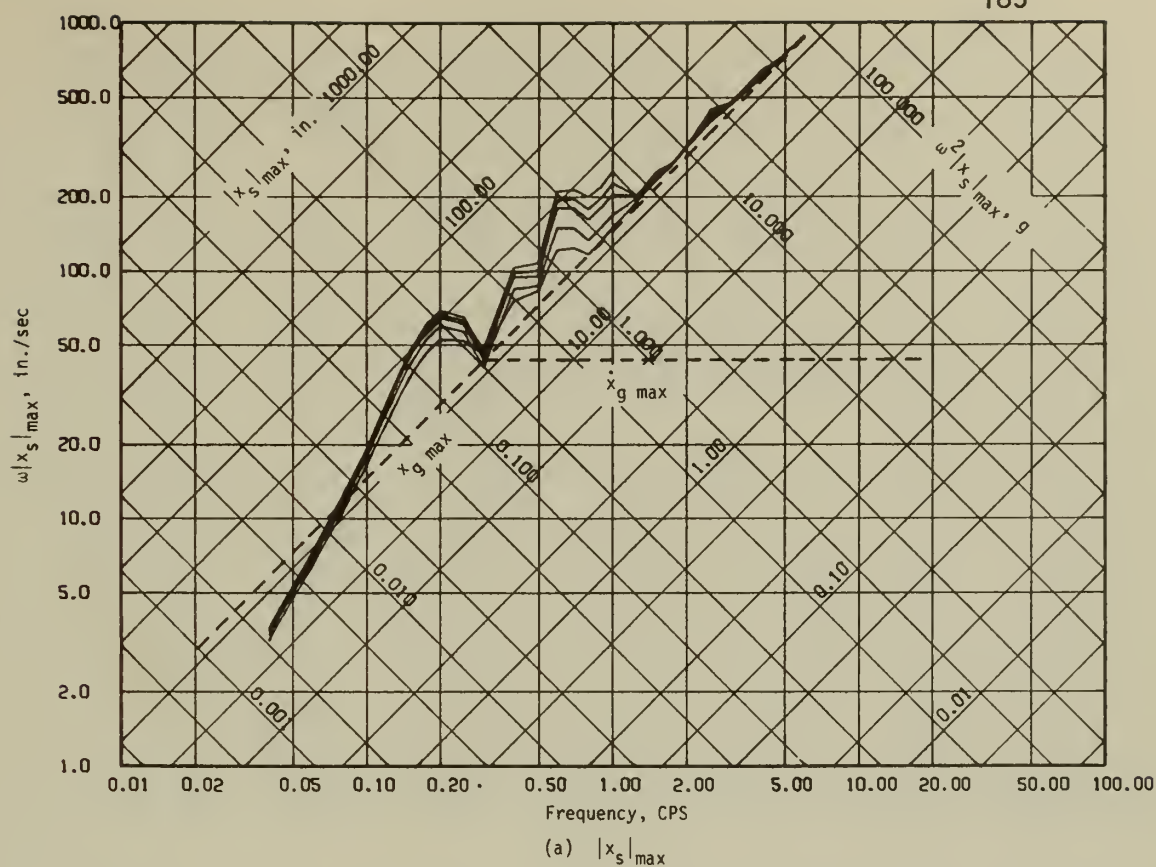


Fig. 2.30 Elastic Hydrodynamic Parameter Response Spectra.
San Fernando Earthquake. $\beta_{\text{total}} = 0, 1, 2, 5, 10\%$

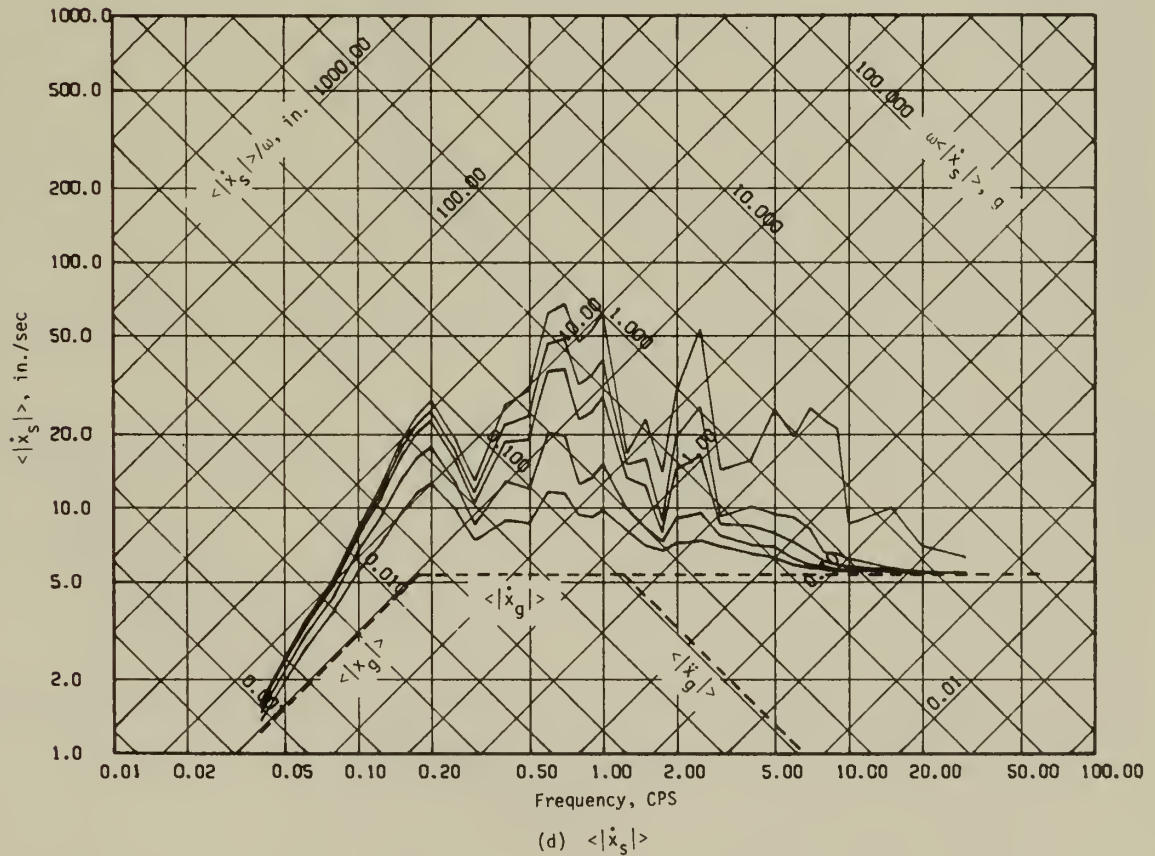
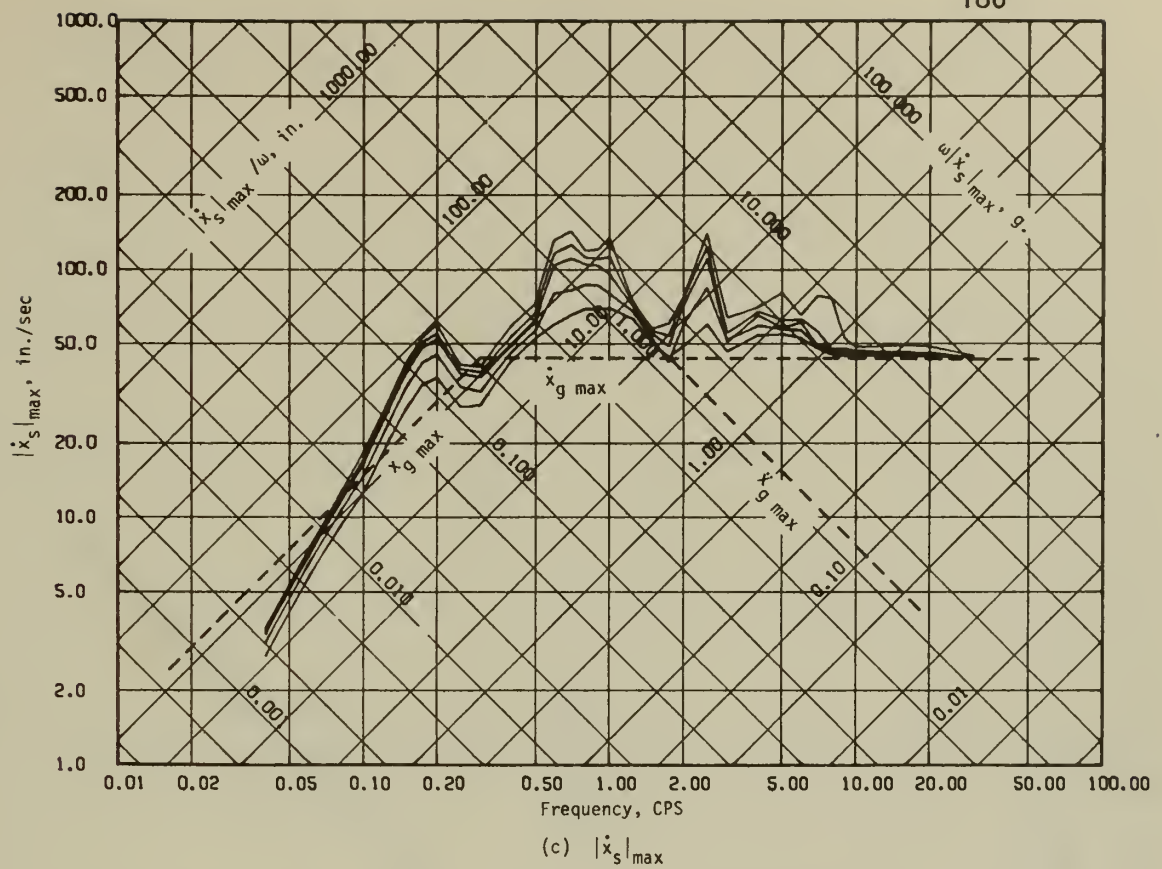


Fig. 2.30 (Continued)

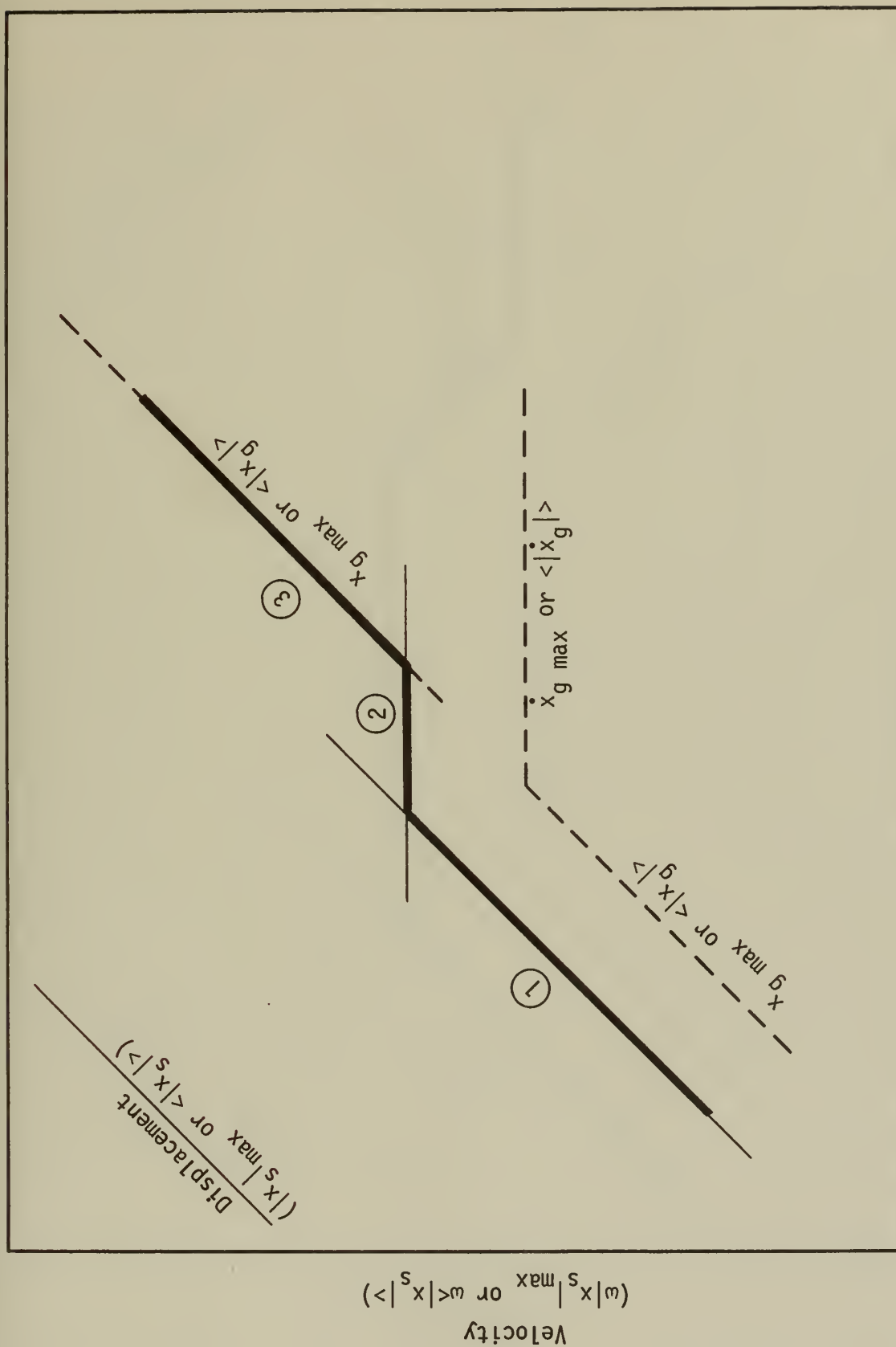


Fig. 2.31 Construction of Idealized Hydrodynamic Parameter Response Spectrum for a Displacement Parameter

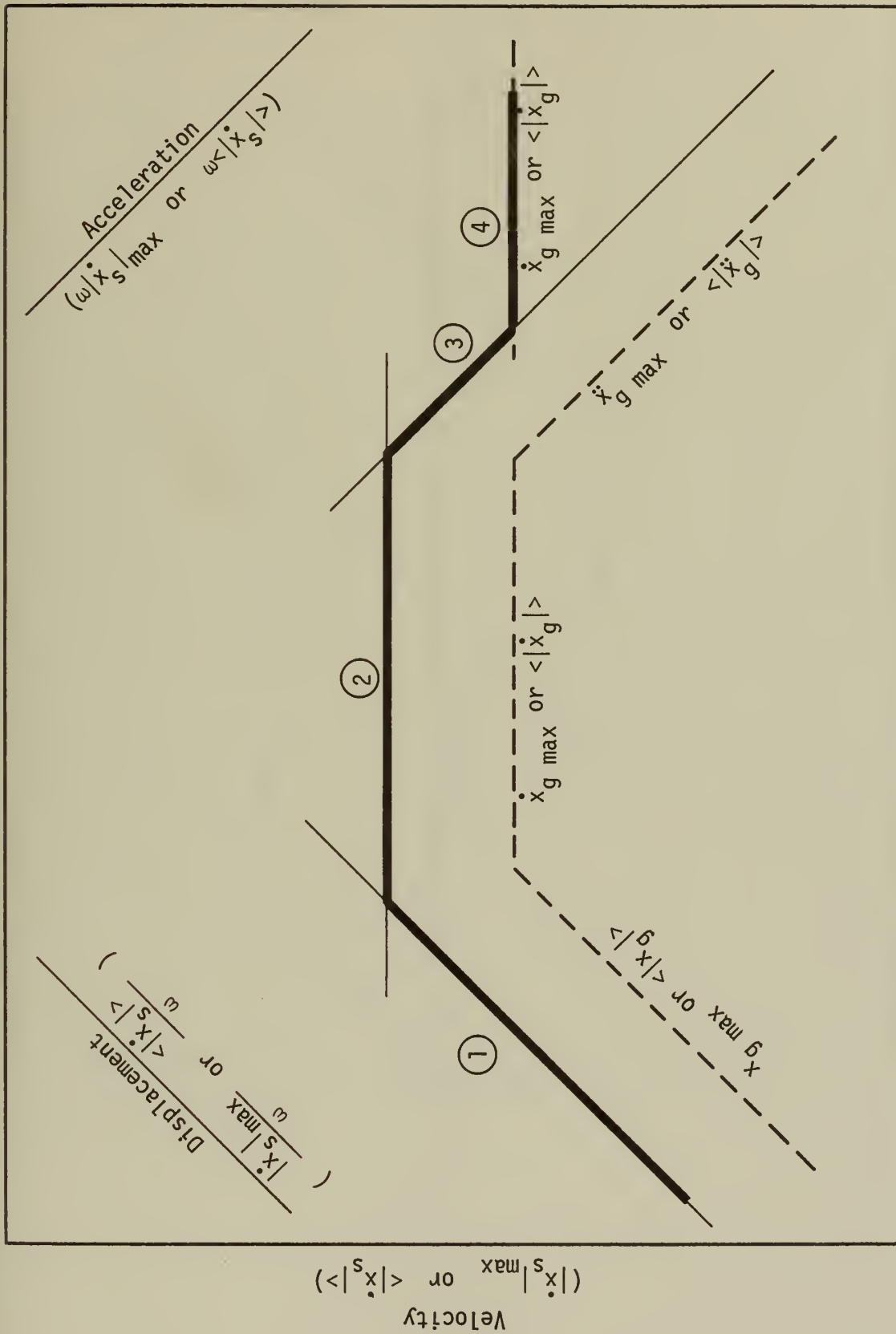


Fig. 2.32 Construction of Idealized Hydrodynamic Parameter Response Spectrum for a Velocity Parameter

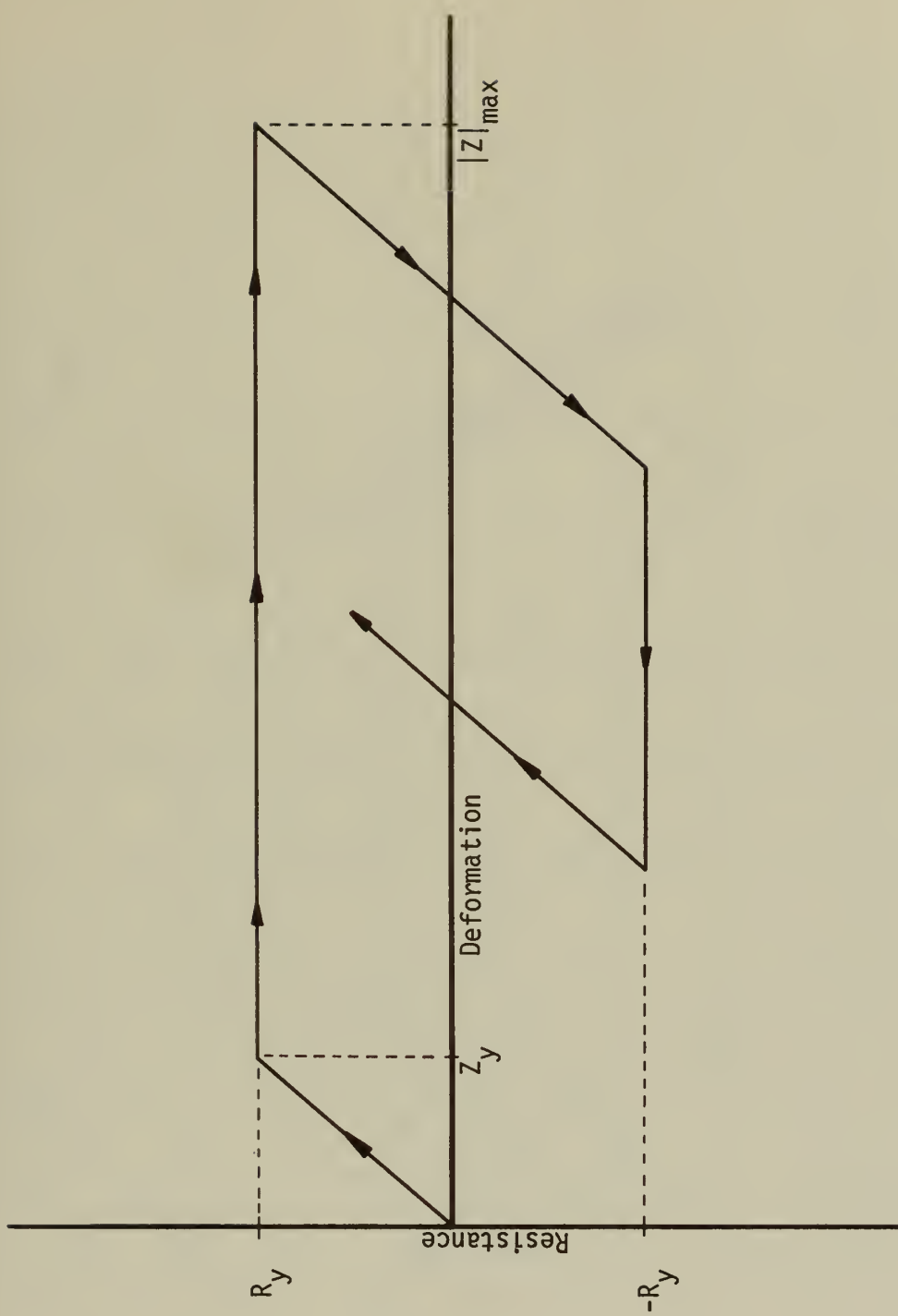


Fig. 2.33 Elasto-Plastic Resistance-Deformation Relationship

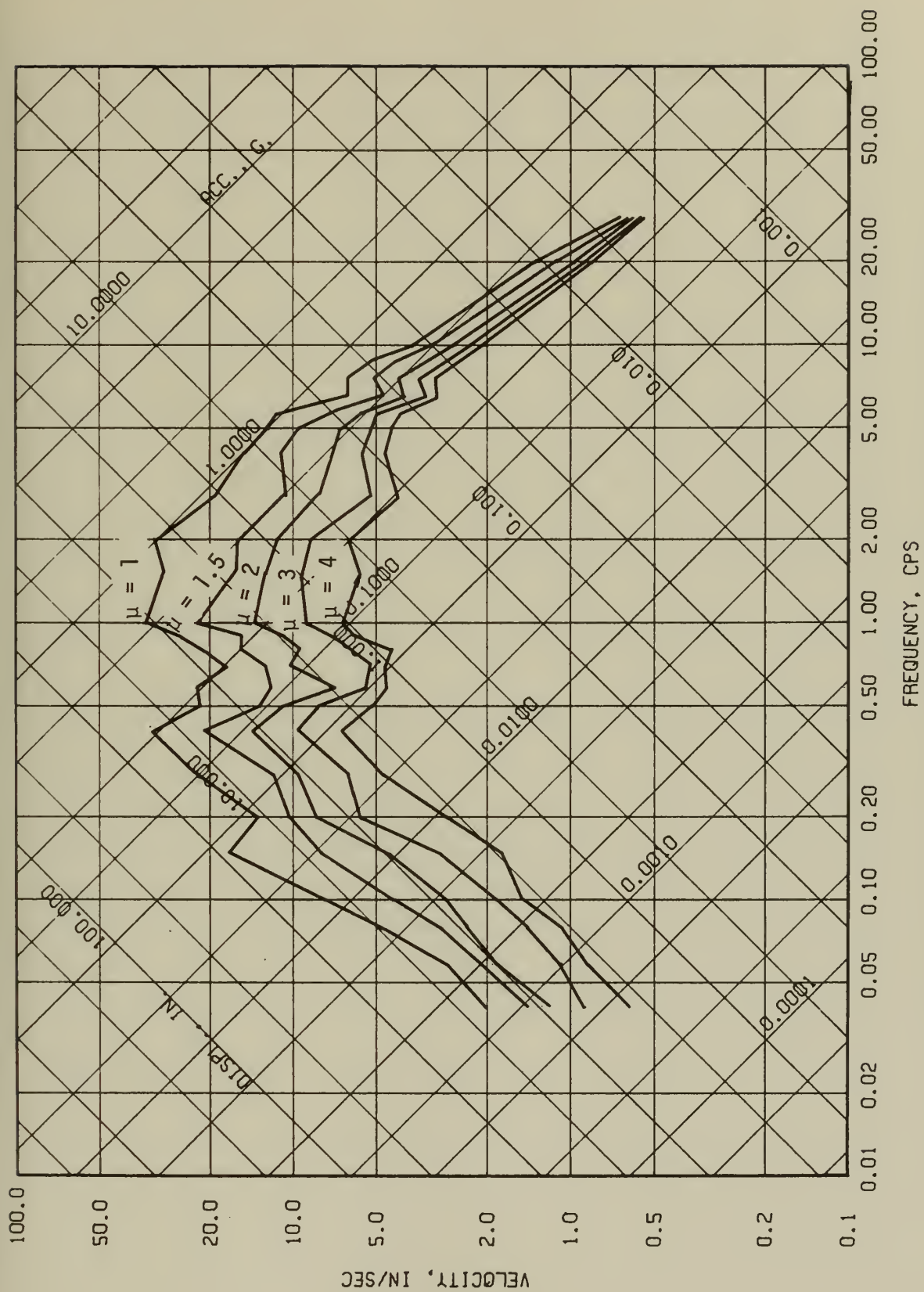


Fig. 2.34 Inelastic (Elasto-Plastic) Response Spectra, El Centro Earthquake,
 $\beta_s = .02$, $K_D \ddot{x}_{\max} / K = 0.00$

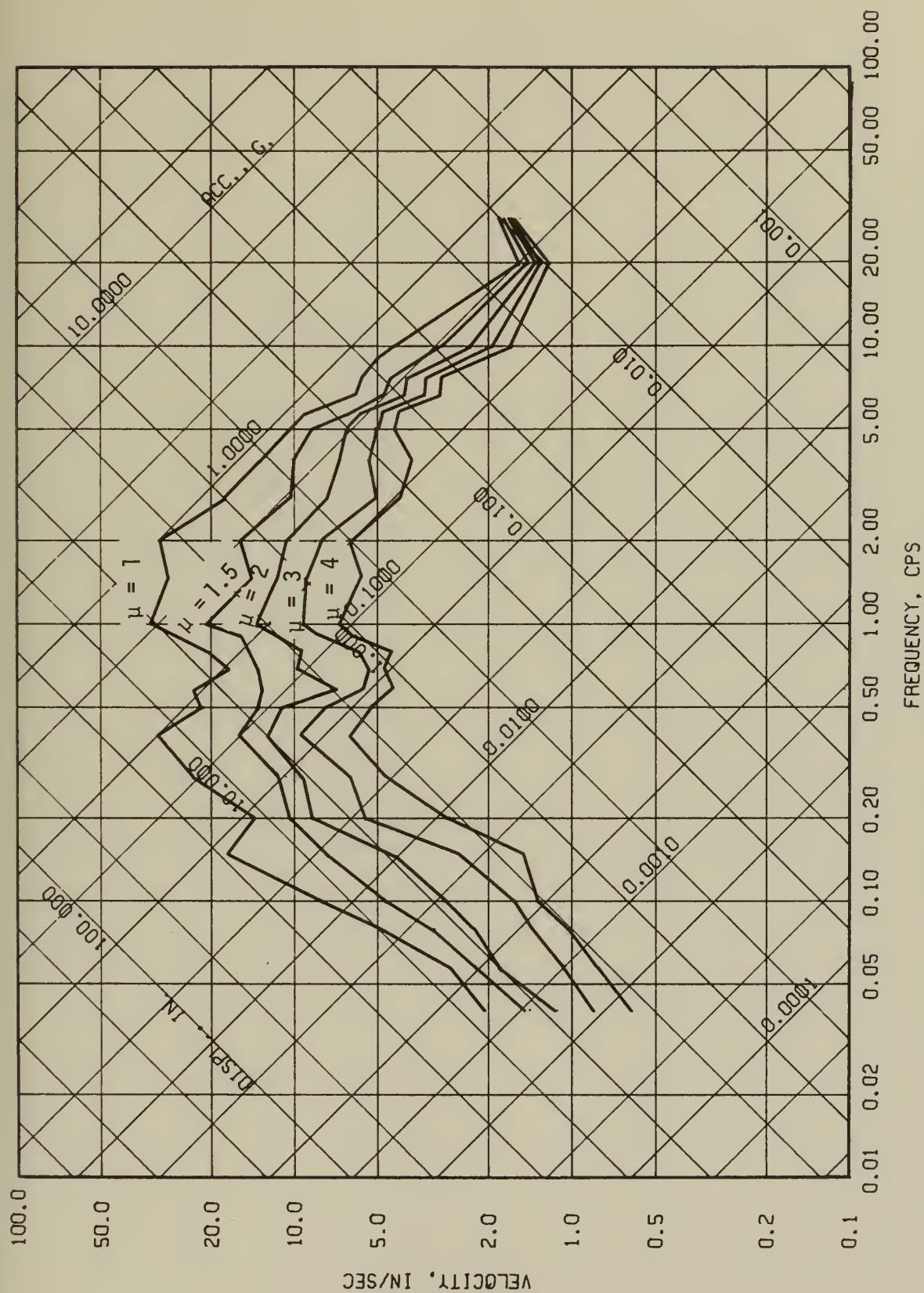


Fig. 2.35 Inelastic (Elasto-Plastic) Response Spectra, El Centro Earthquake,
 $\beta_s = .02, K_D \ddot{x}_{\max} / K = 0.006$

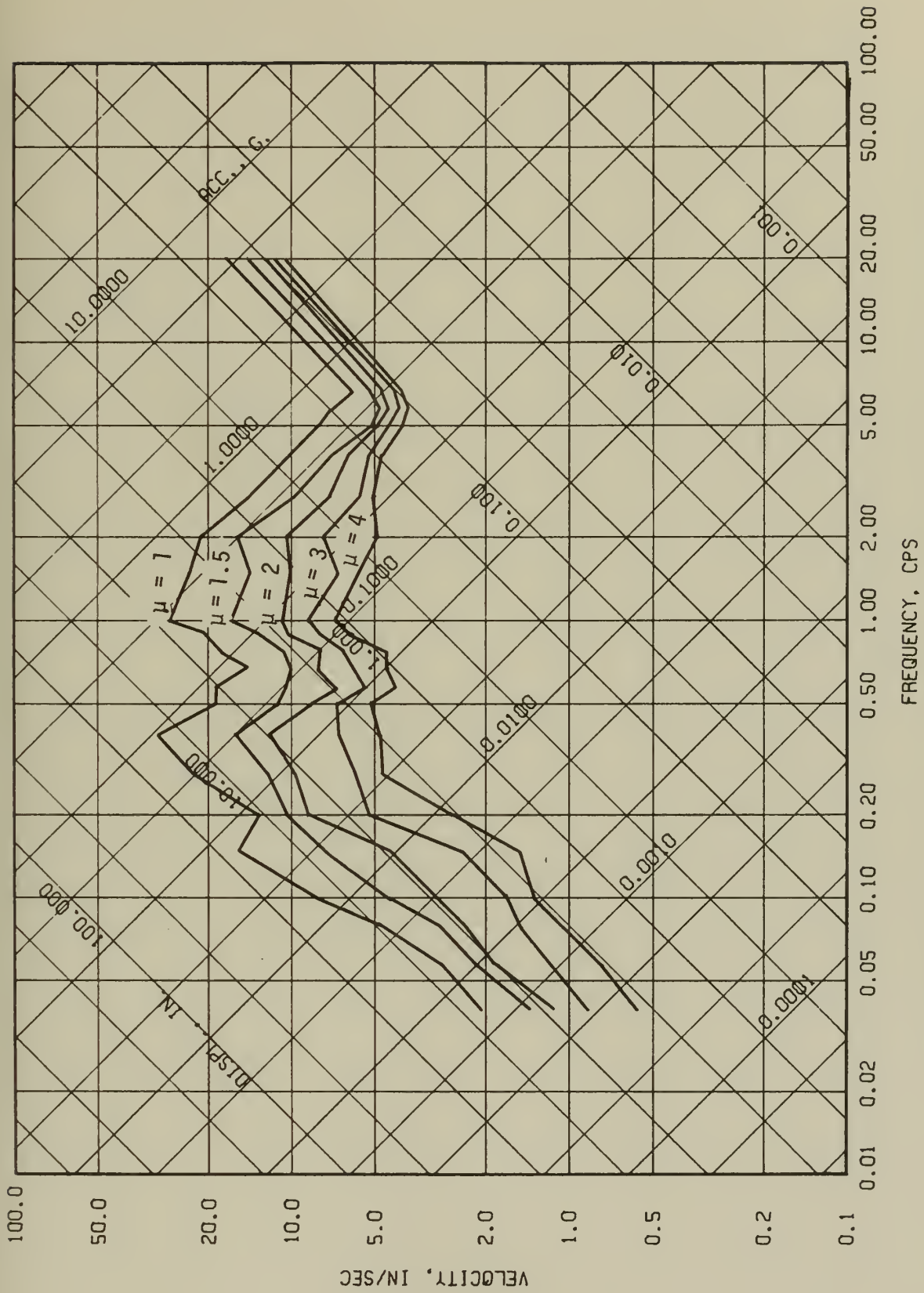


Fig. 2.36 Inelastic (Elasto-Plastic) Response Spectra, El Centro Earthquake,
 $\beta_s = .02, K_D \ddot{x}_{g \max} / K = 0.08$

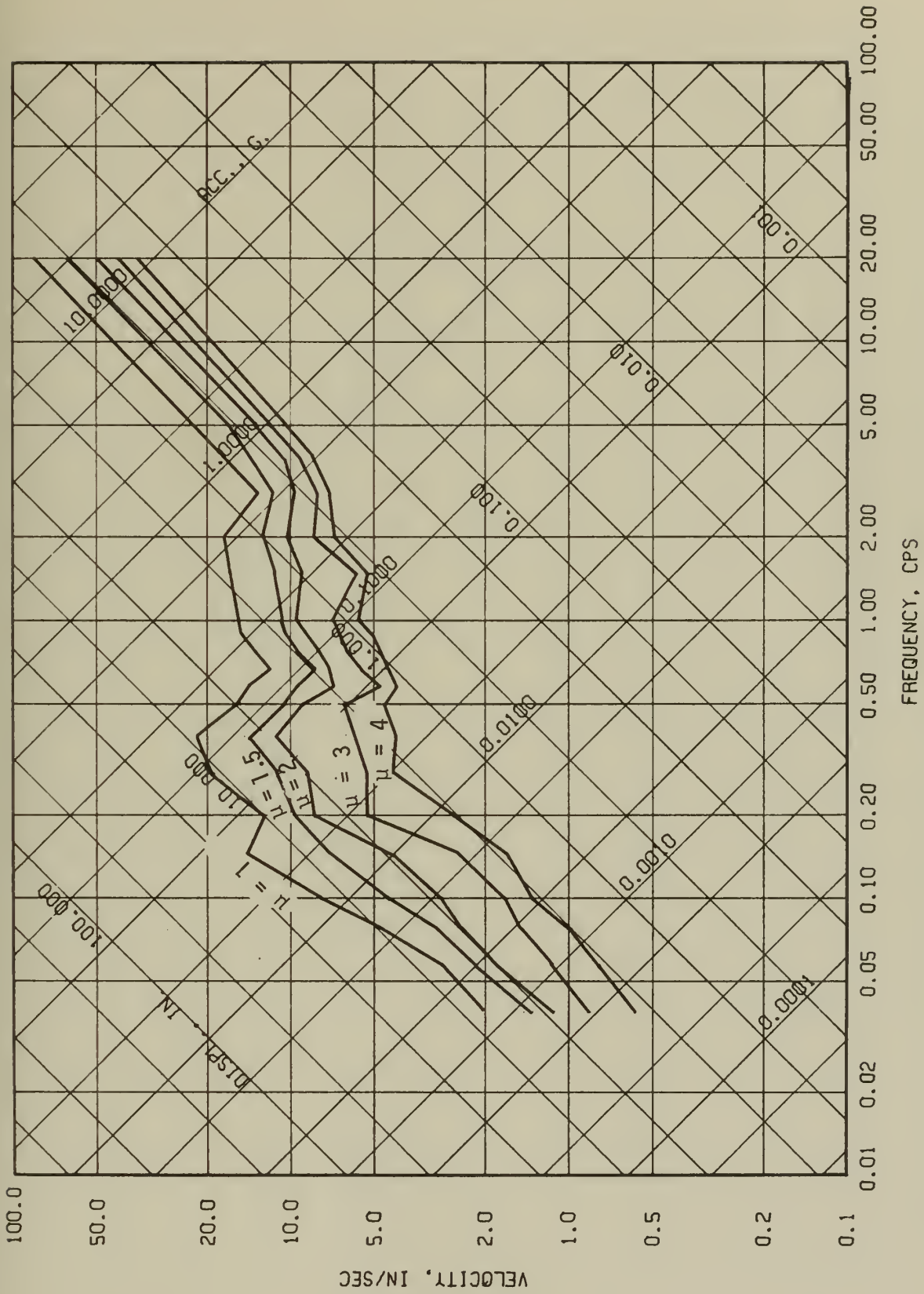


Fig. 2.37 Inelastic (Elasto-Plastic) Response Spectra, El Centro Earthquake,
 $\beta_s = .02, K_D \ddot{x}_g \text{ max} / K = 0.50$

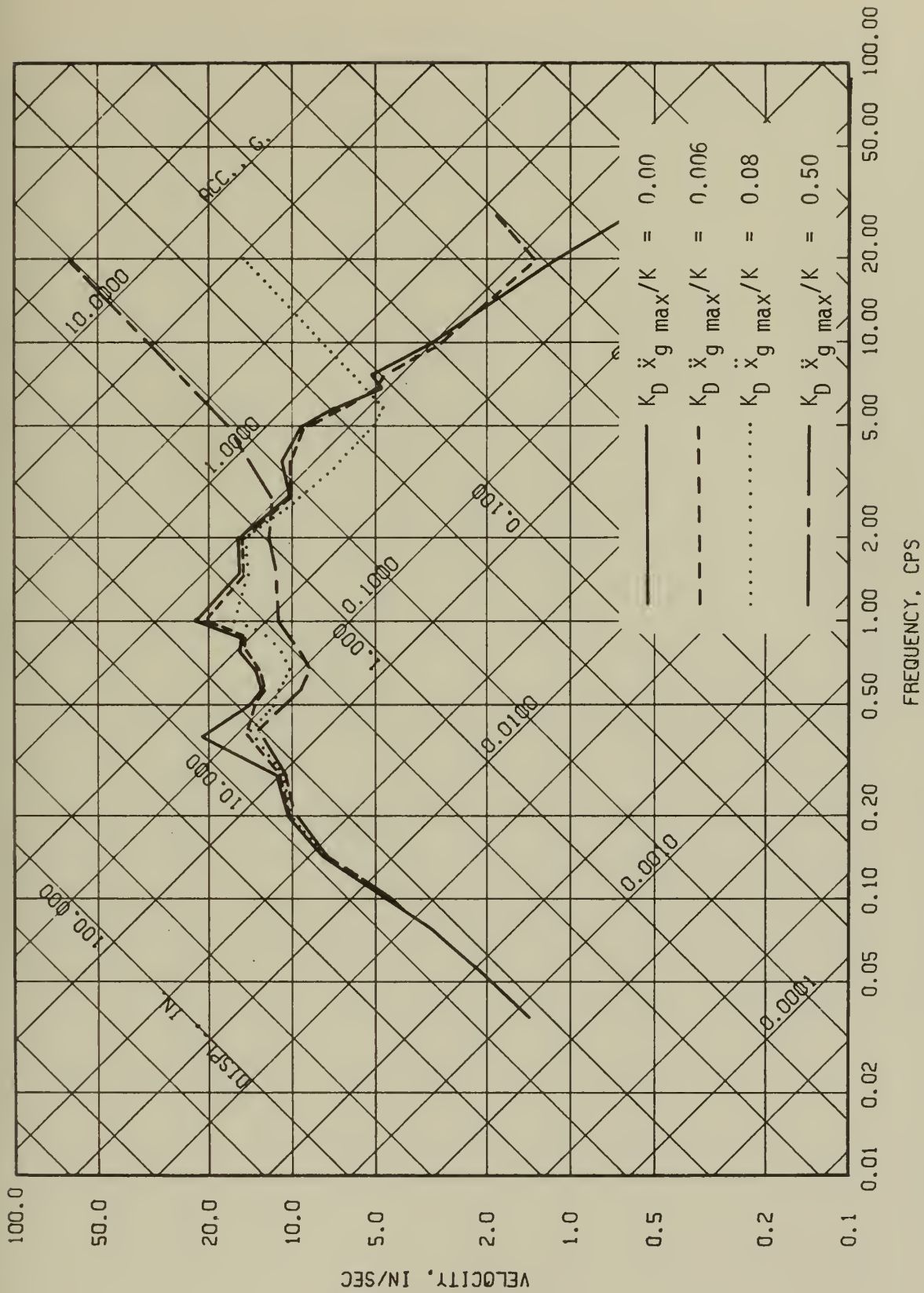


Fig. 2.38 Inelastic (Elasto-Plastic) Response Spectra, El Centro Earthquake, $\beta_s = .02, \mu = 1.5$

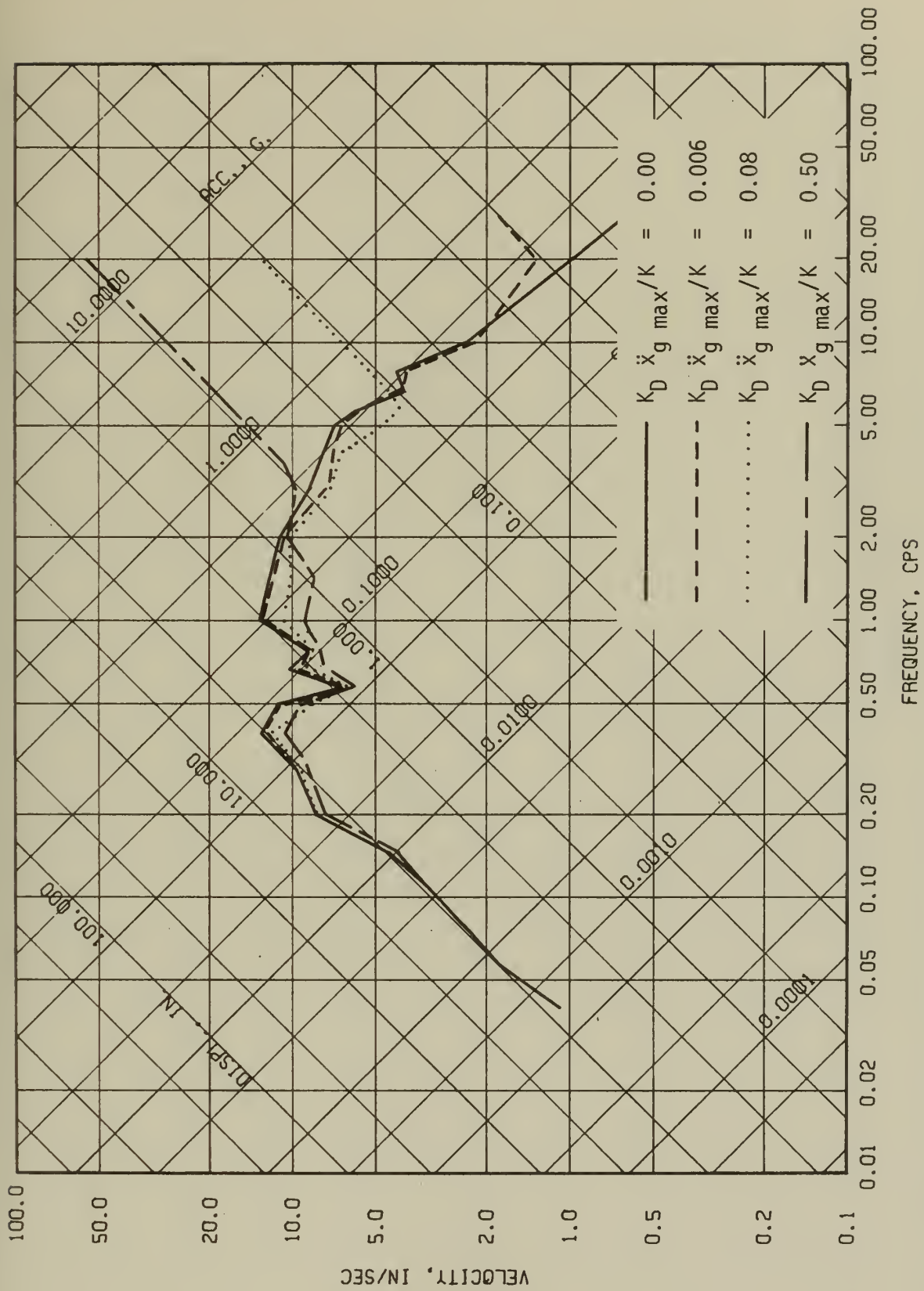


Fig. 2.39 Inelastic (Elasto-Plastic) Response Spectra, El Centro Earthquake, $\beta_s = .02$, $\mu = 2.0$

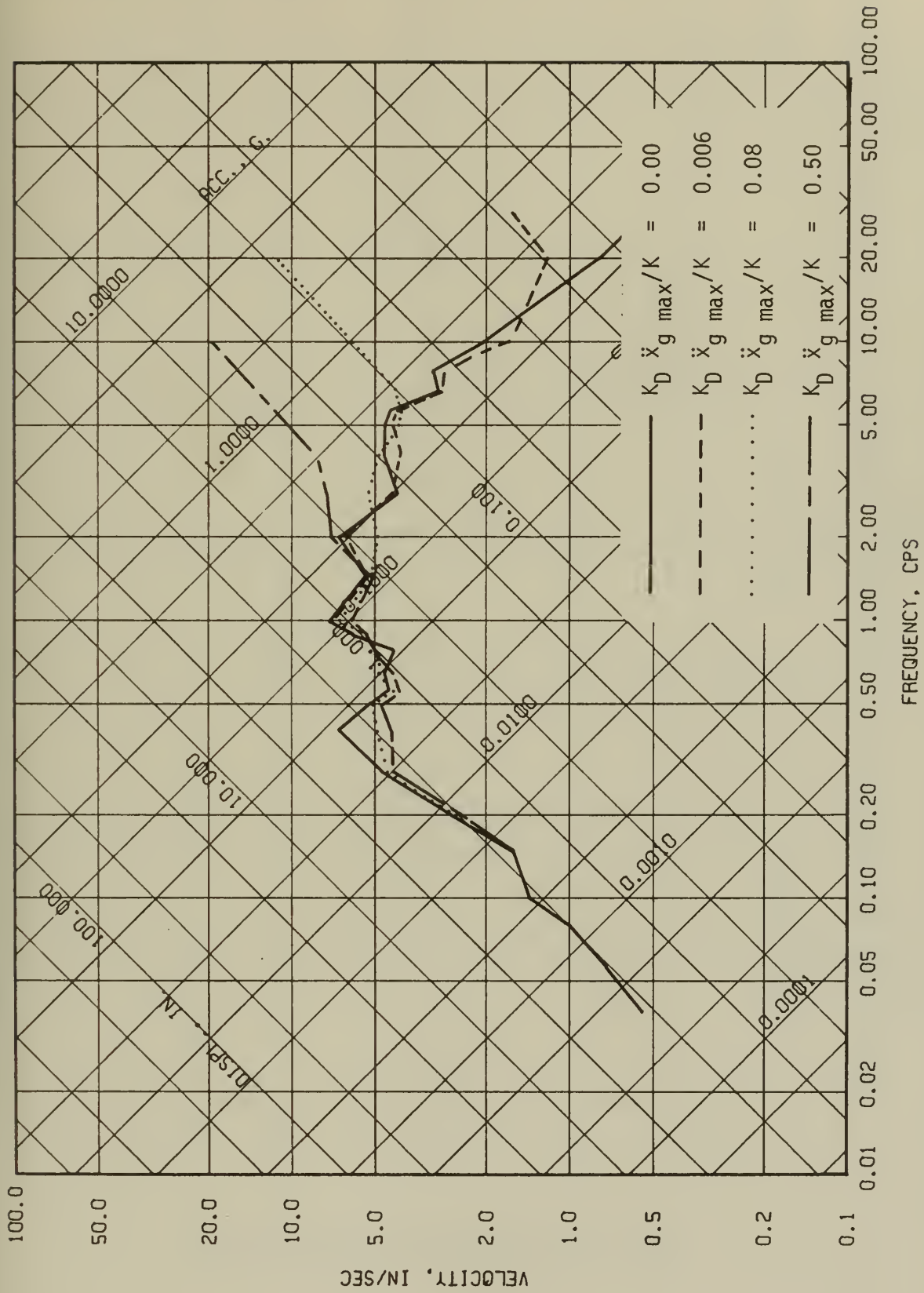


Fig. 2.40 Inelastic (Elasto-Plastic) Response Spectra, El Centro Earthquake, $\beta_s = .02$, $\mu = 4.0$

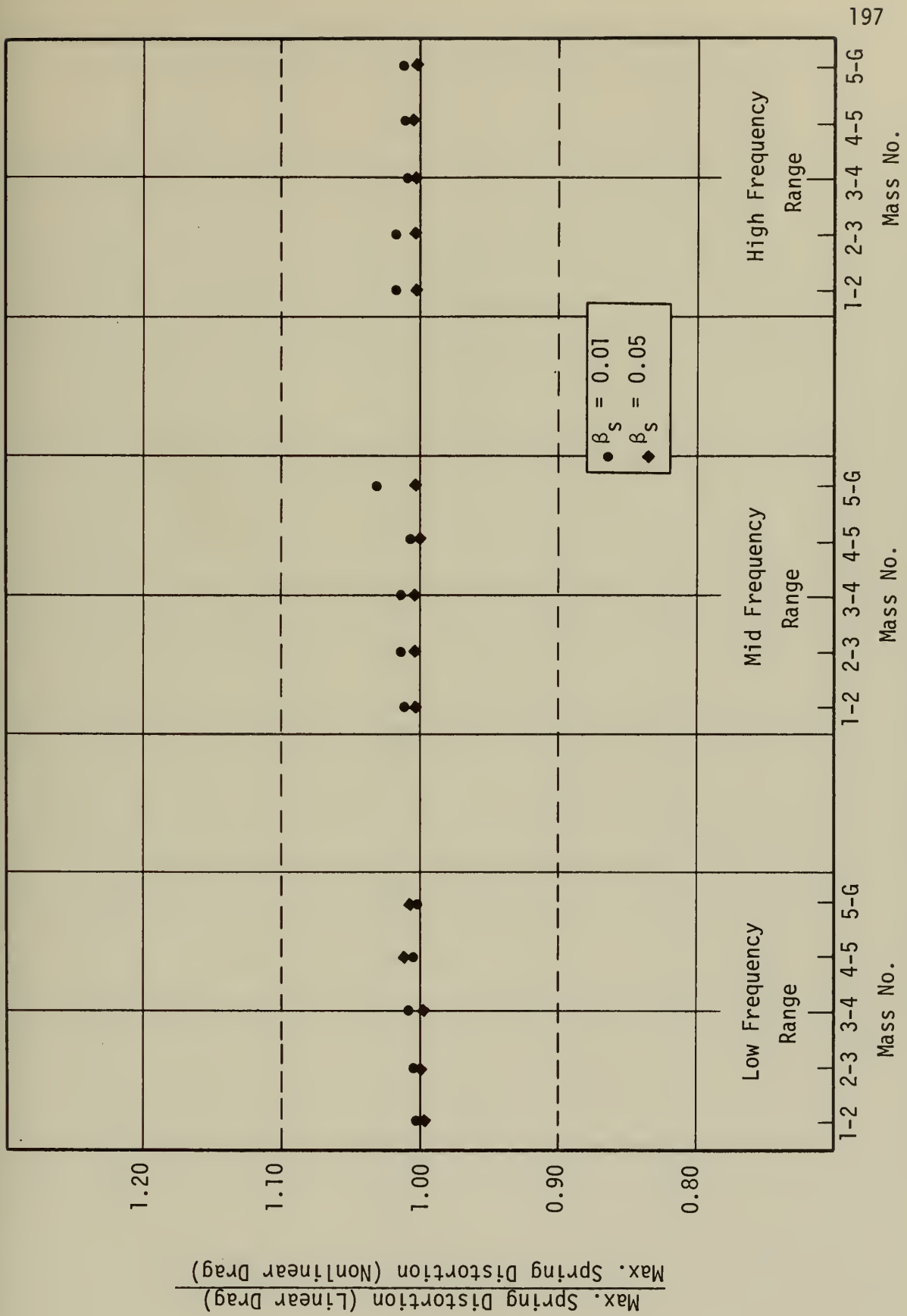


Fig. 3.1 Comparison of Linear Drag Solution (Linearized by Ground Velocity) and Nonlinear Drag Solution. System 1L. El Centro Earthquake, 1940, N-S Component.



Fig. 3.2 Comparison of Linear Drag Solution (Linearized by Ground Velocity) and Non-linear Drag Solution. System 1M. El Centro Earthquake, 1940, N-S Component.

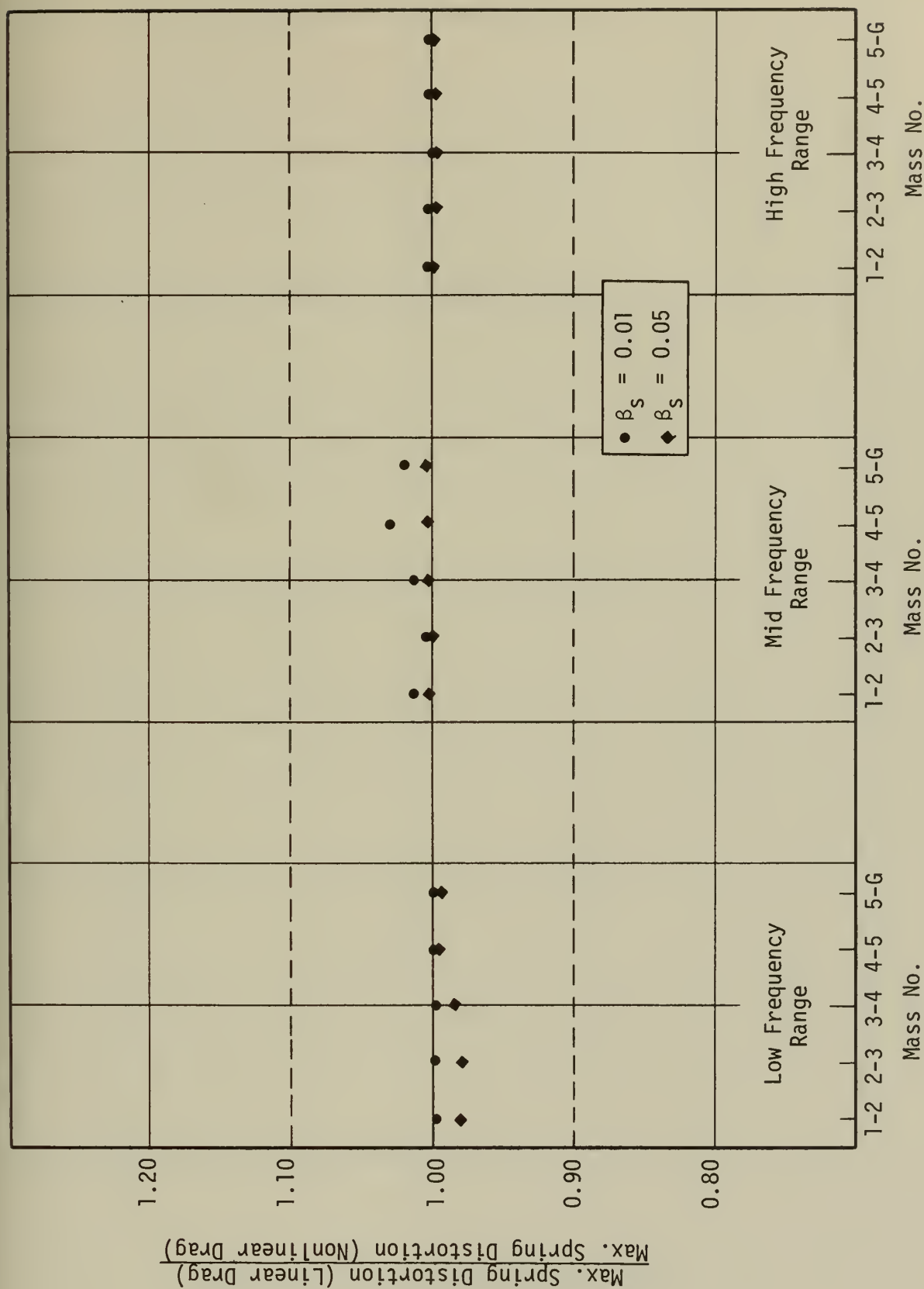


Fig. 3.3 Comparison of Linear Drag Solution (Linearized by Ground Velocity) and Non-Linear Drag Solution. System 2L. El Centro Earthquake, 1940, N-S Component.

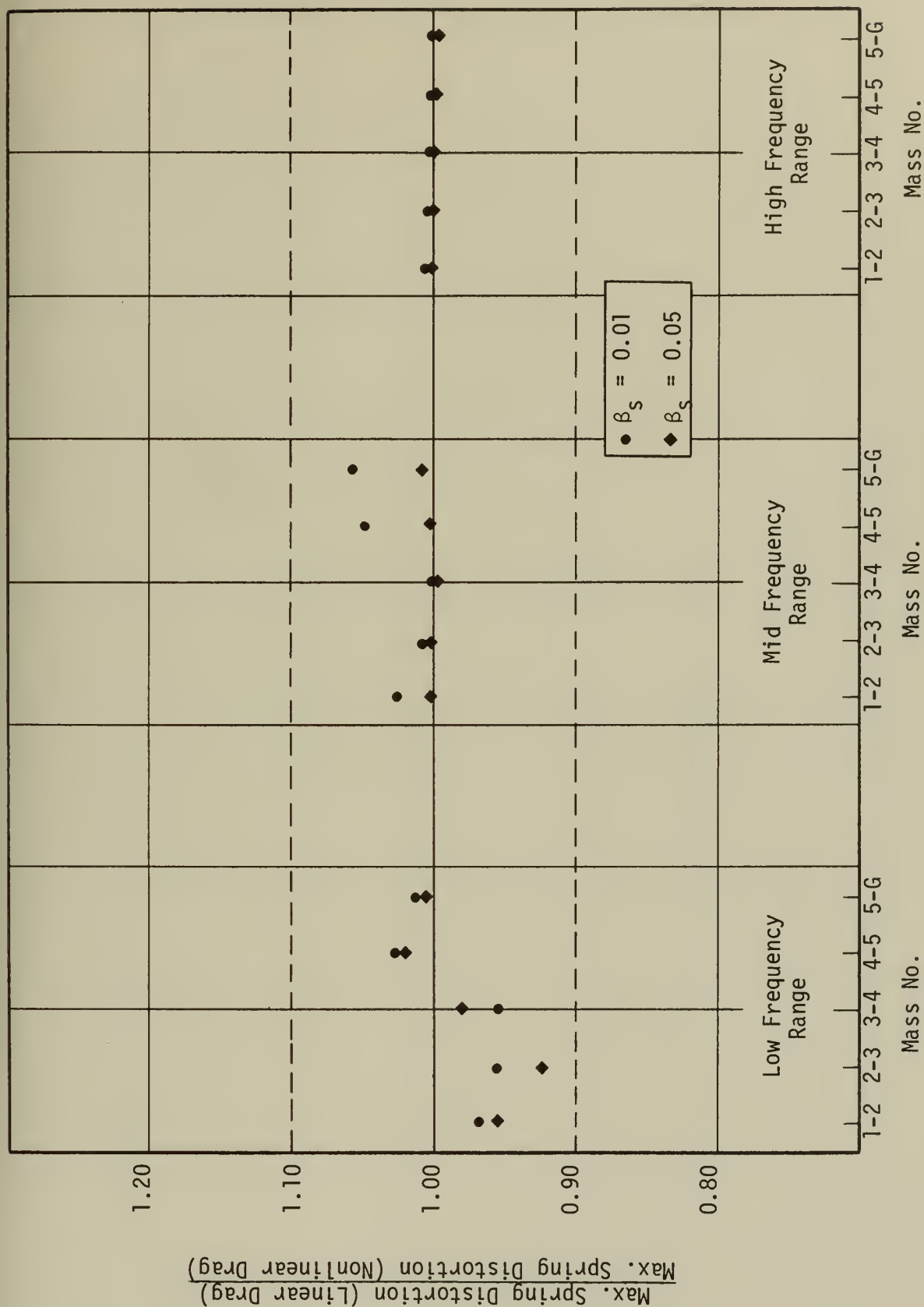


Fig. 3.4 Comparison of Linear Drag Solution (Linearized by Ground Velocity) and Non-linear Drag Solution. System 2M. El Centro Earthquake, 1940, N-S Component.

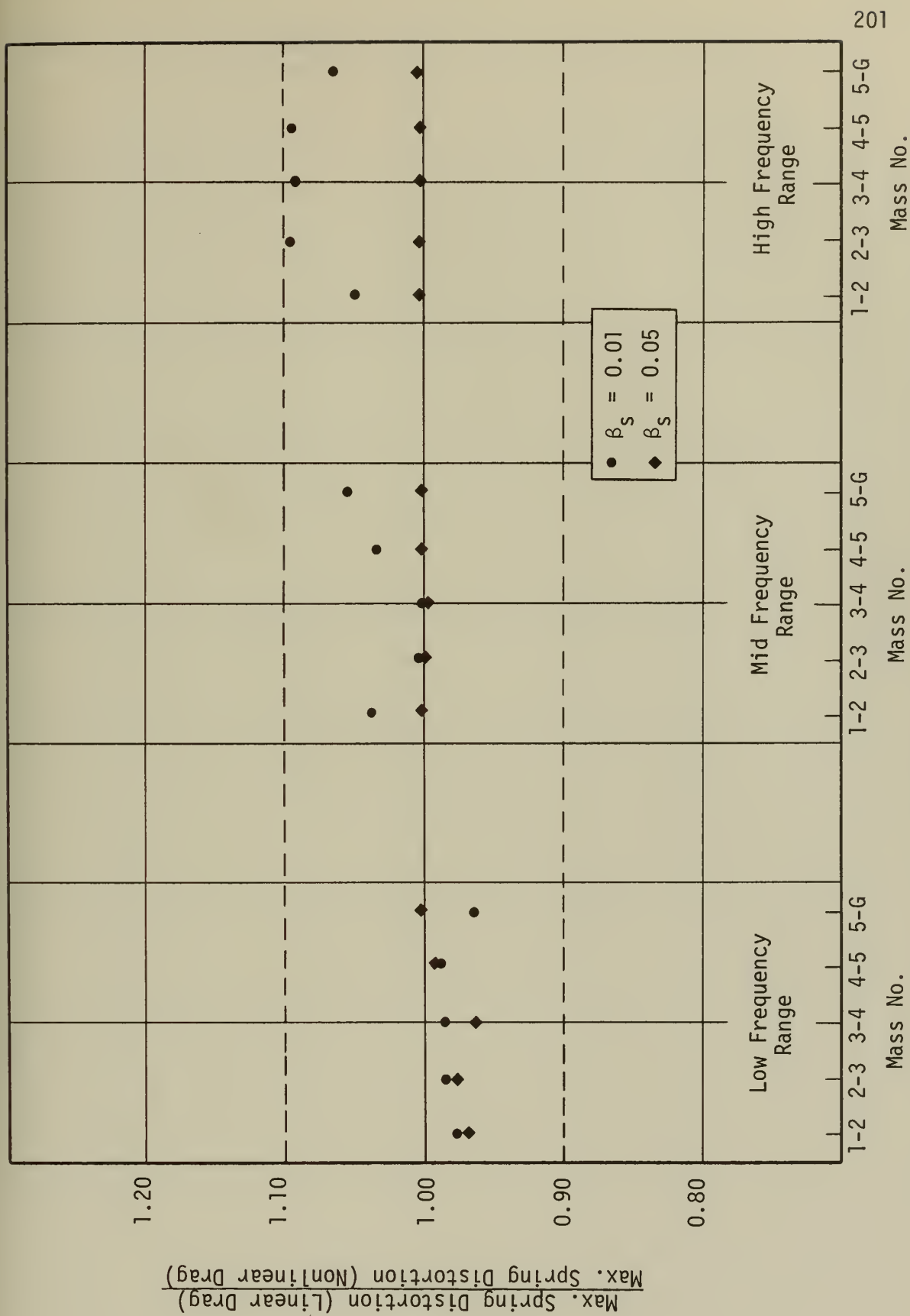


Fig. 3.5 Comparison of Linear Drag Solution (Linearized by Ground Velocity) and Non-linear Drag Solution. System 3L. El Centro Earthquake, 1940, N-S Component.

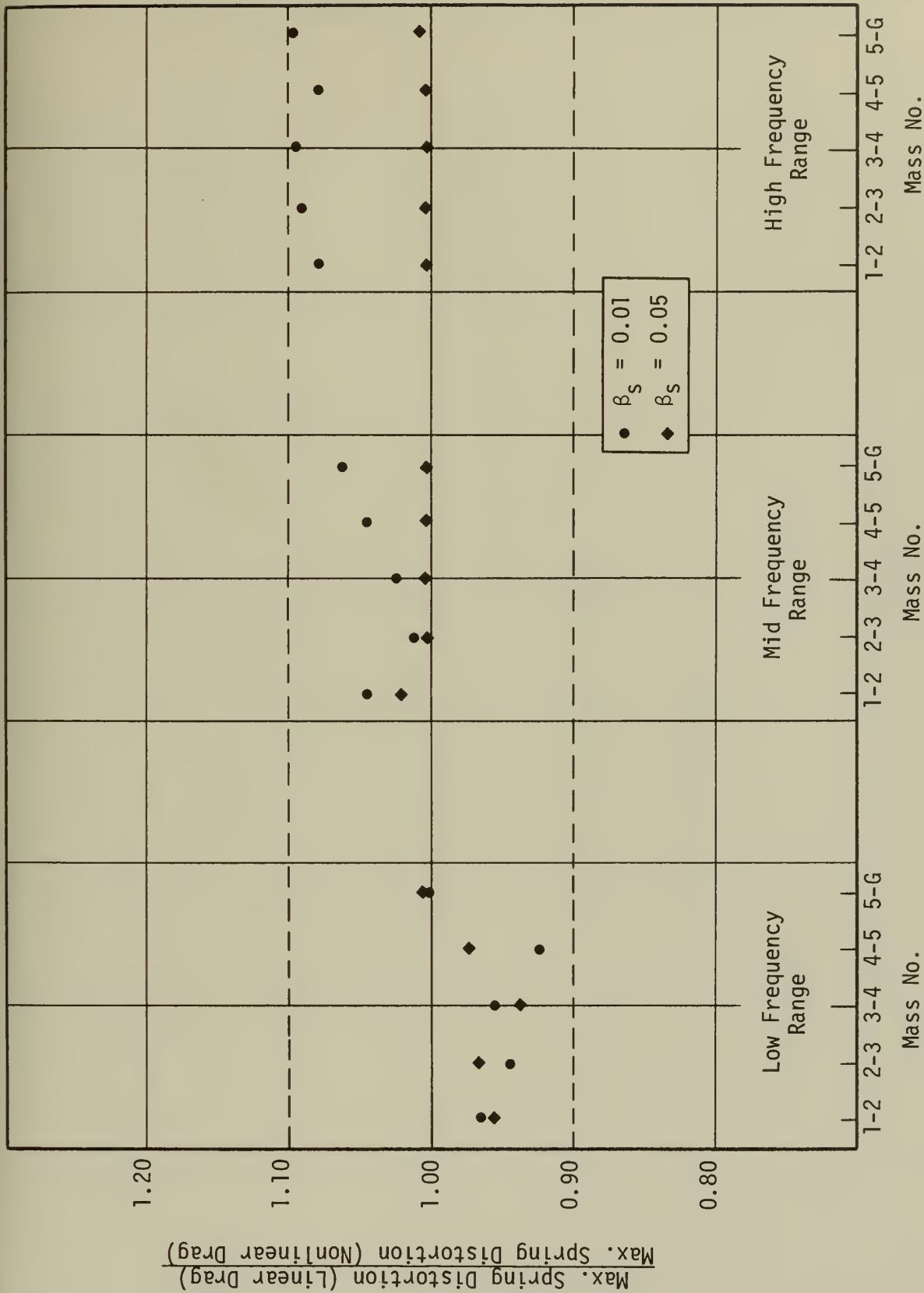


Fig. 3.6 Comparison of Linear Drag Solution (Linearized by Ground Velocity) and Non-linear Drag Solution. System 4L. El Centro Earthquake, 1940, N-S Component.

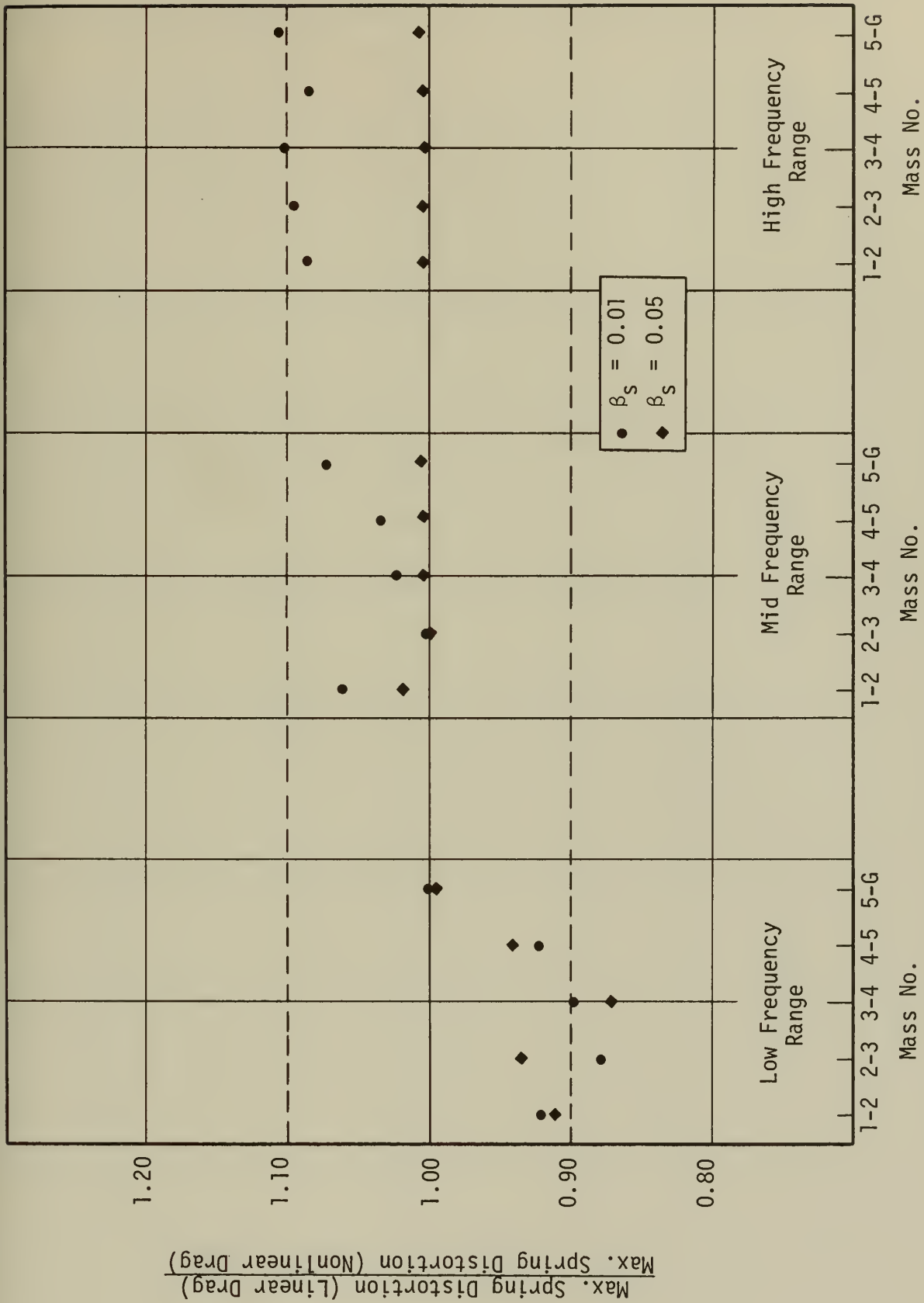


Fig. 3.7 Comparison of Linear Drag Solution (Linearized by Ground Velocity) and Non-linear Drag Solution. System 4M. El Centro Earthquake, 1940, N-S Component.

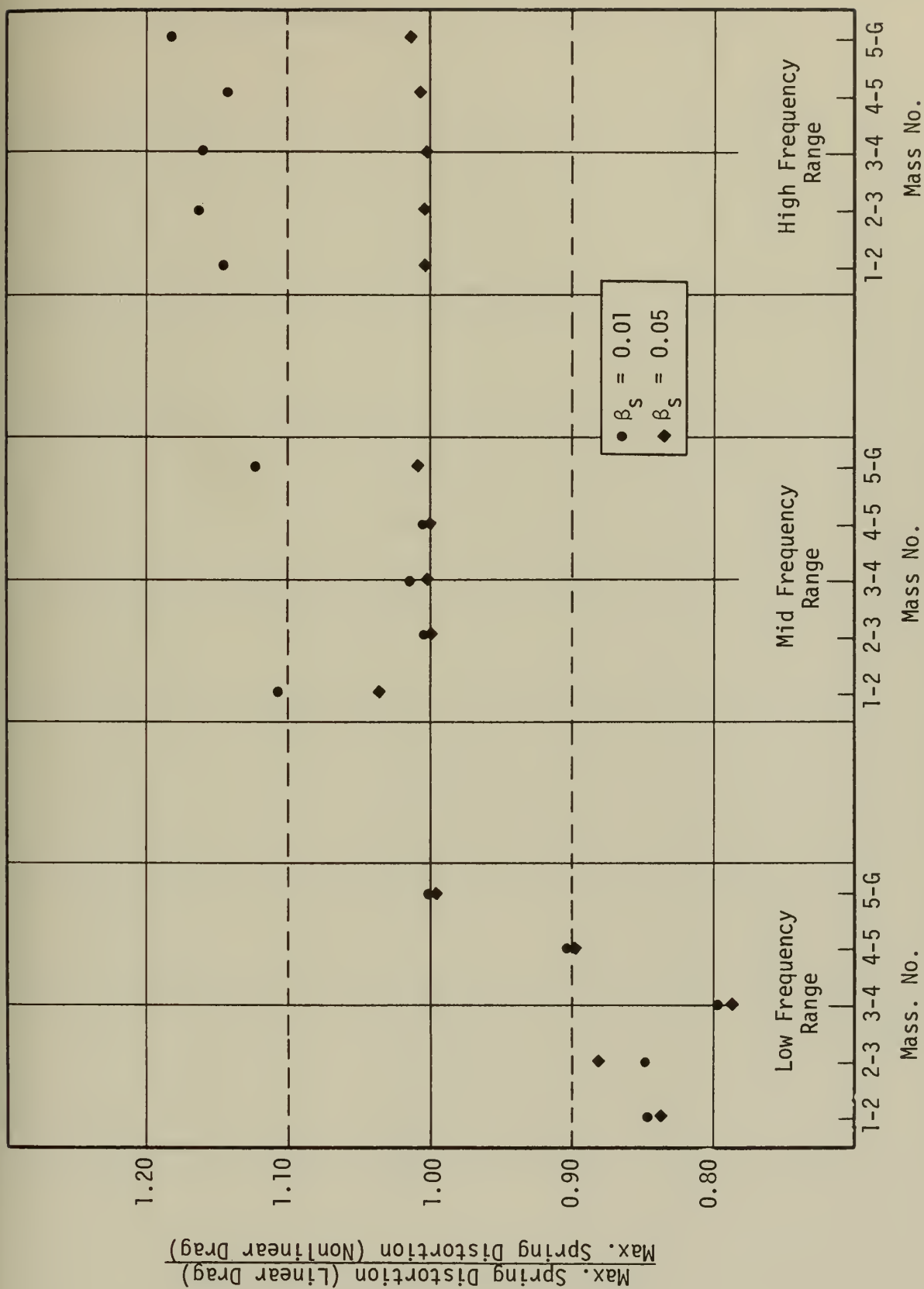


Fig. 3.8 Comparison of Linear Drag Solution (Linearized by Ground Velocity) and Non-linear Drag Solution. System 4H. El Centro Earthquake, 1940, N-S Component.

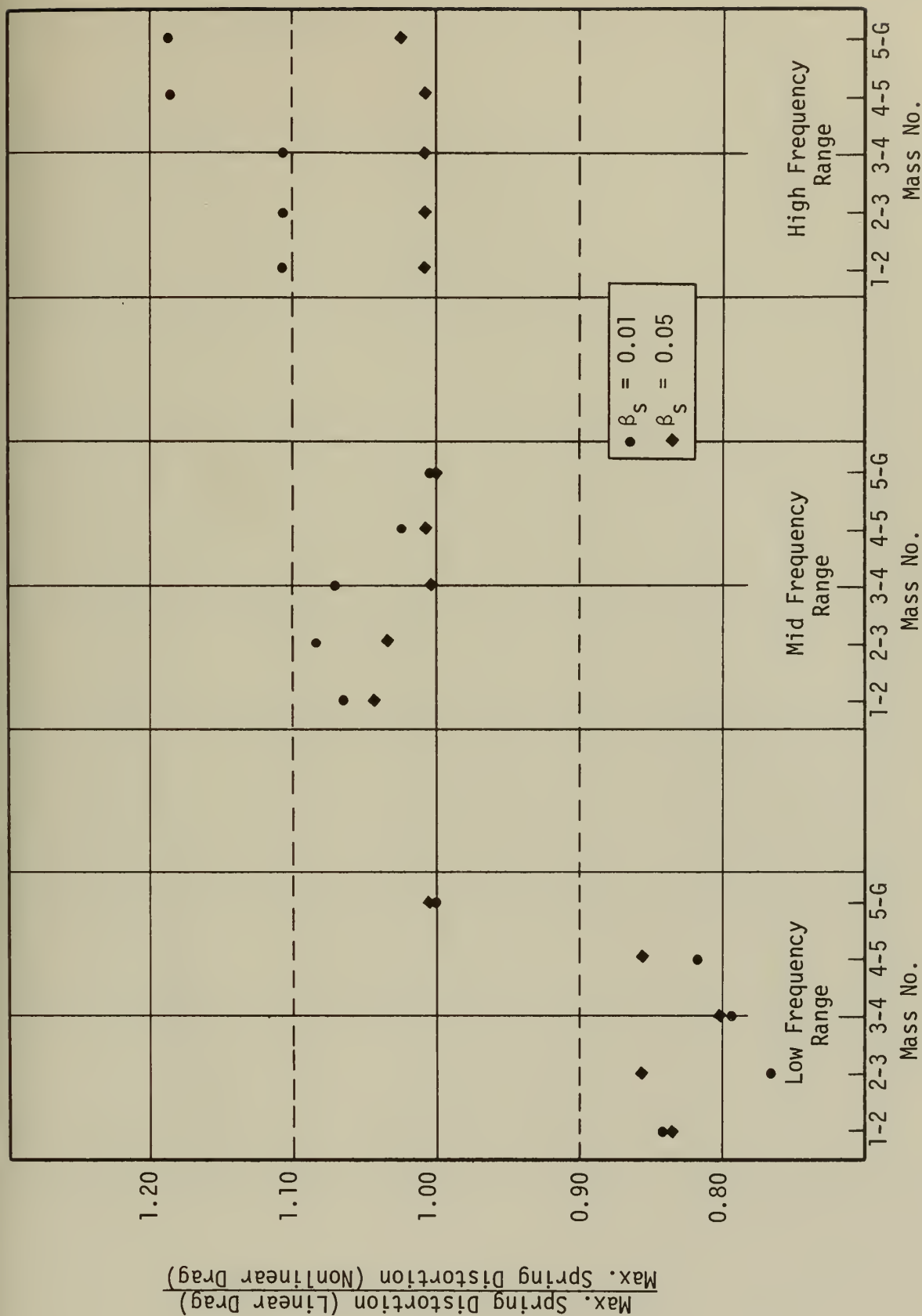


Fig. 3.9 Comparison of Linear Drag Solution (Linearized by Ground Velocity) and Non-Linear Drag Solution. System 5H. El Centro Earthquake, 1940, N-S Component.



Fig. 3.10 Comparison of Linear Drag Solution (Linearized by Ground Velocity) and Non-linear Drag Solution. System 6M. El Centro Earthquake, 1940, N-S Component.

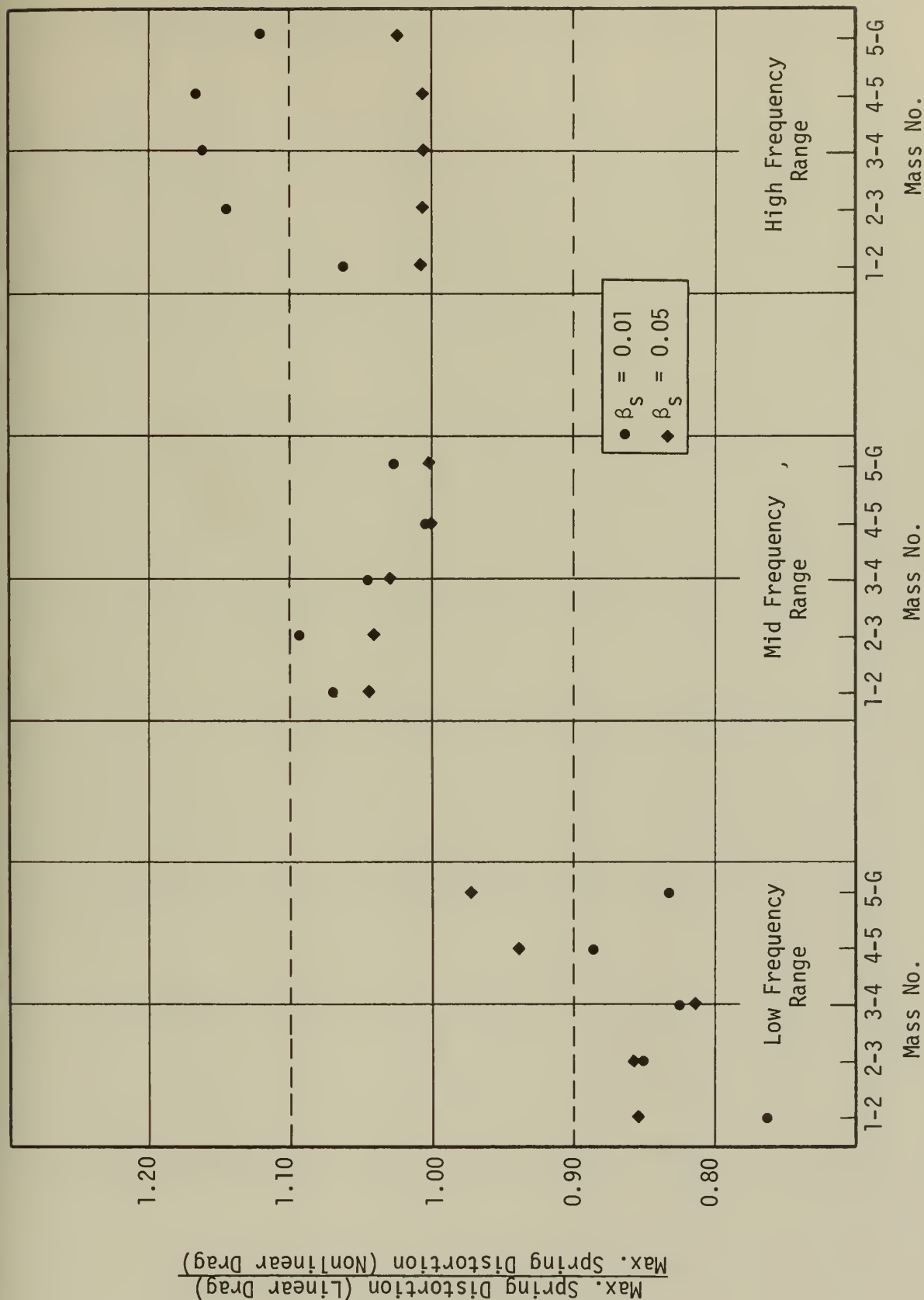


Fig. 3.11 Comparison of Linear Drag Solution (Linearized by Ground Velocity) and Non-linear Drag Solution. System 6H. El Centro Earthquake, 1940, N-S Component.

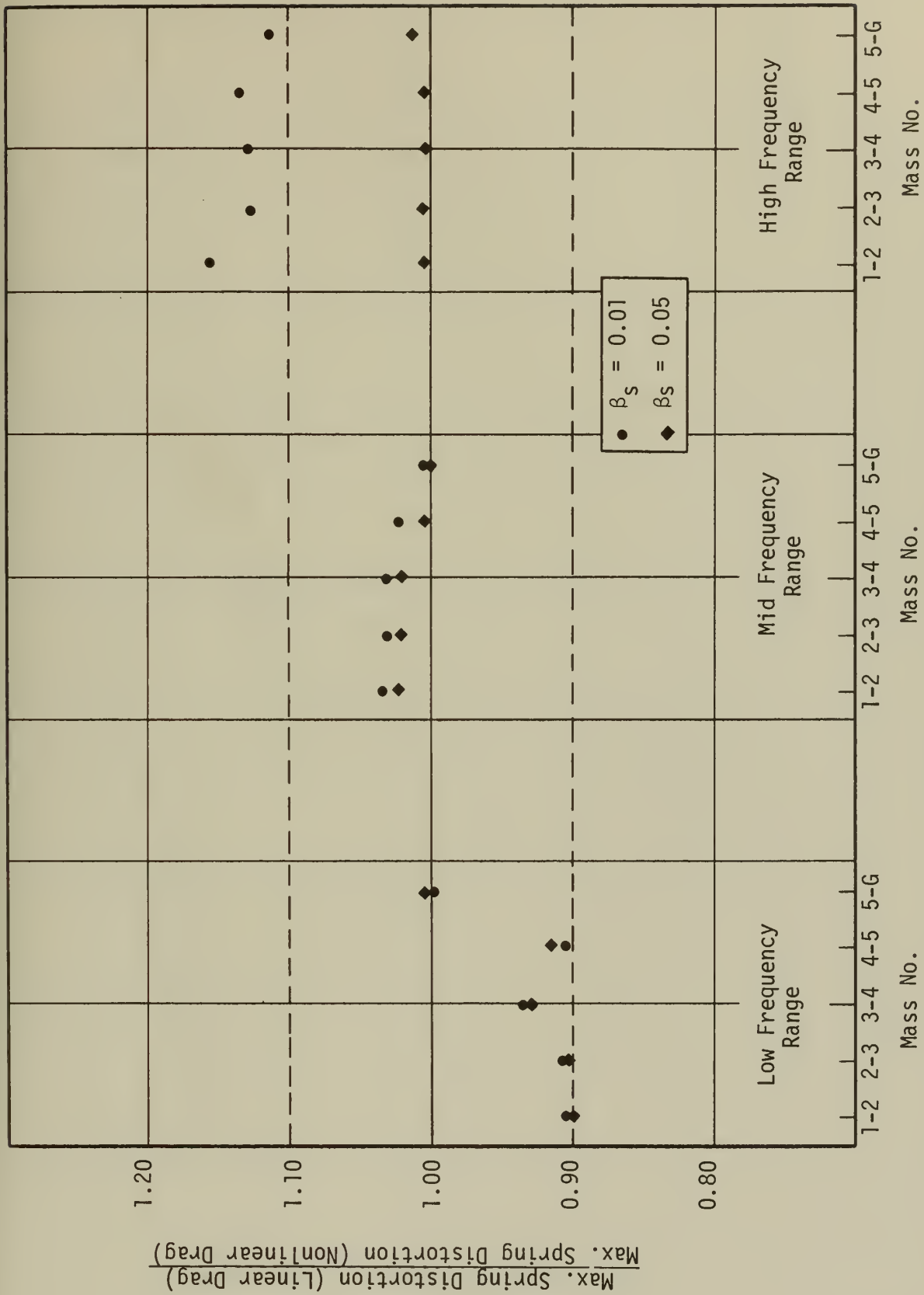


Fig. 3.12 Comparison of Linear Drag Solution (Linearized by Ground Velocity) and Non-linear Drag Solution. System 7M. El Centro Earthquake, 1940, N-S Component.



Fig. 3.13 Comparison of Linear Drag Solution (Linearized by Ground Velocity) and Non-linear Drag Solution. System 7H. El Centro Earthquake, 1940, N-S Component.

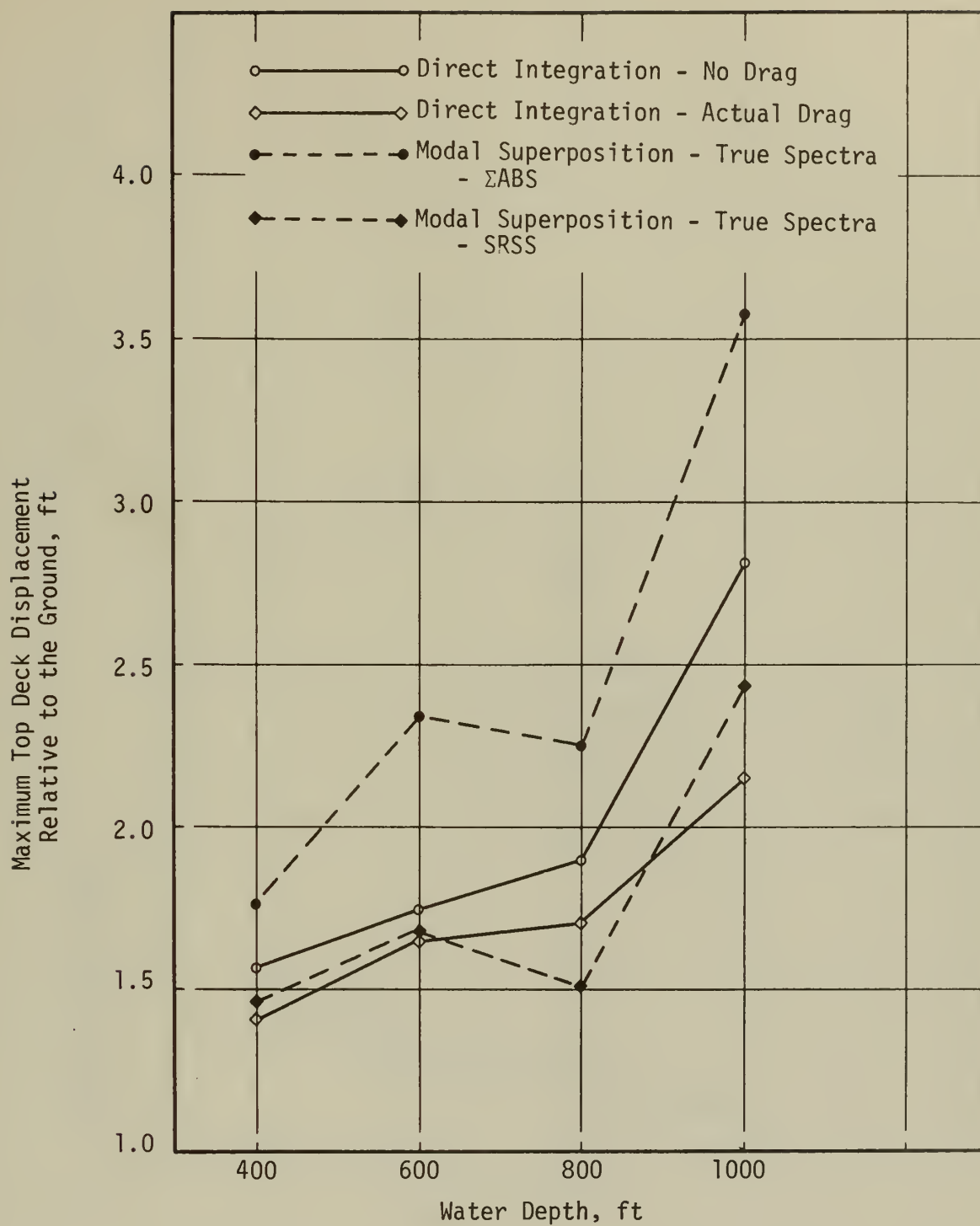


Fig. 4.1 Response of Towers A, B, C, and D to El Centro Earthquake, 1940, N-S Component. $\beta_s = 0.01$

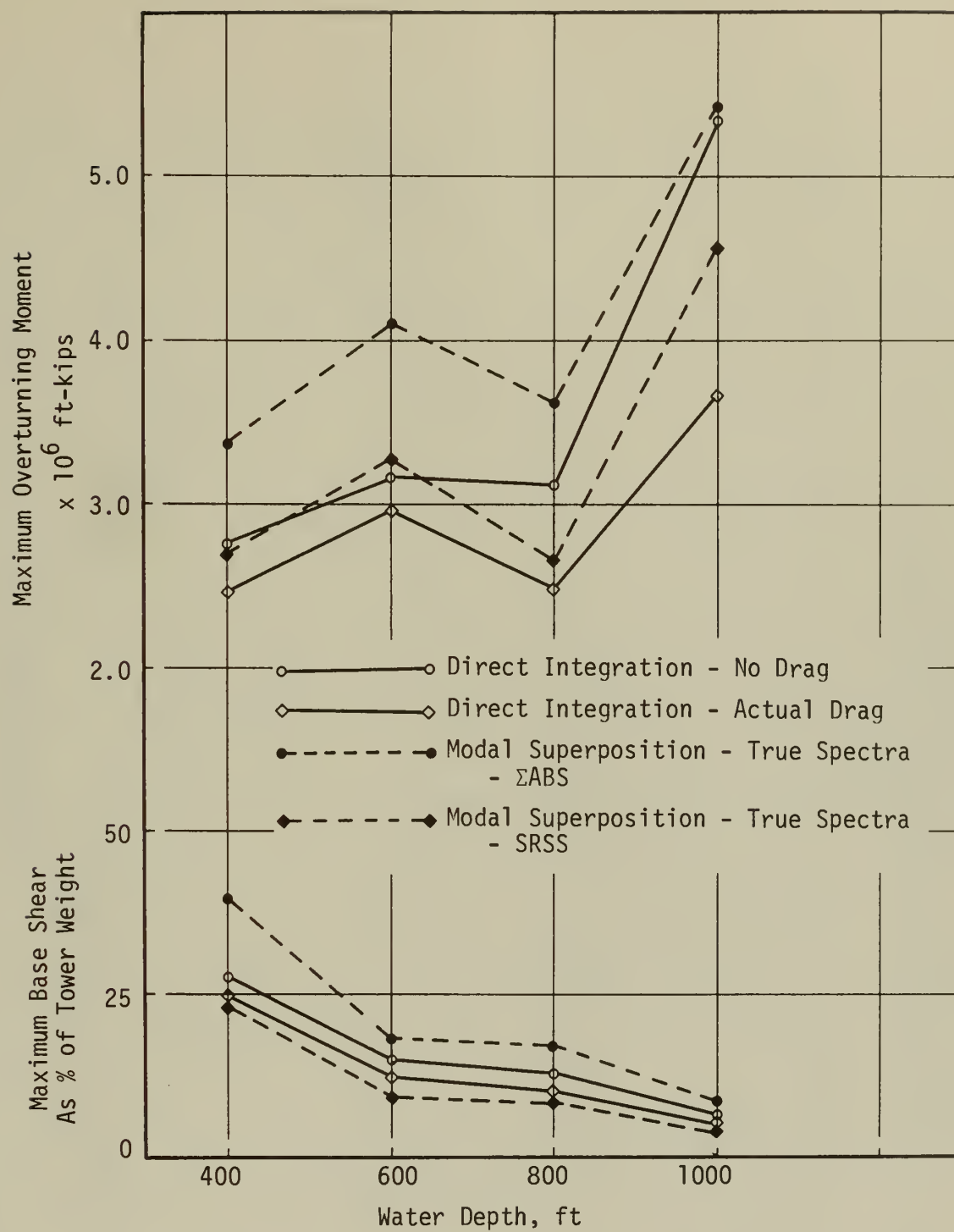


Fig. 4.1 (Continued)

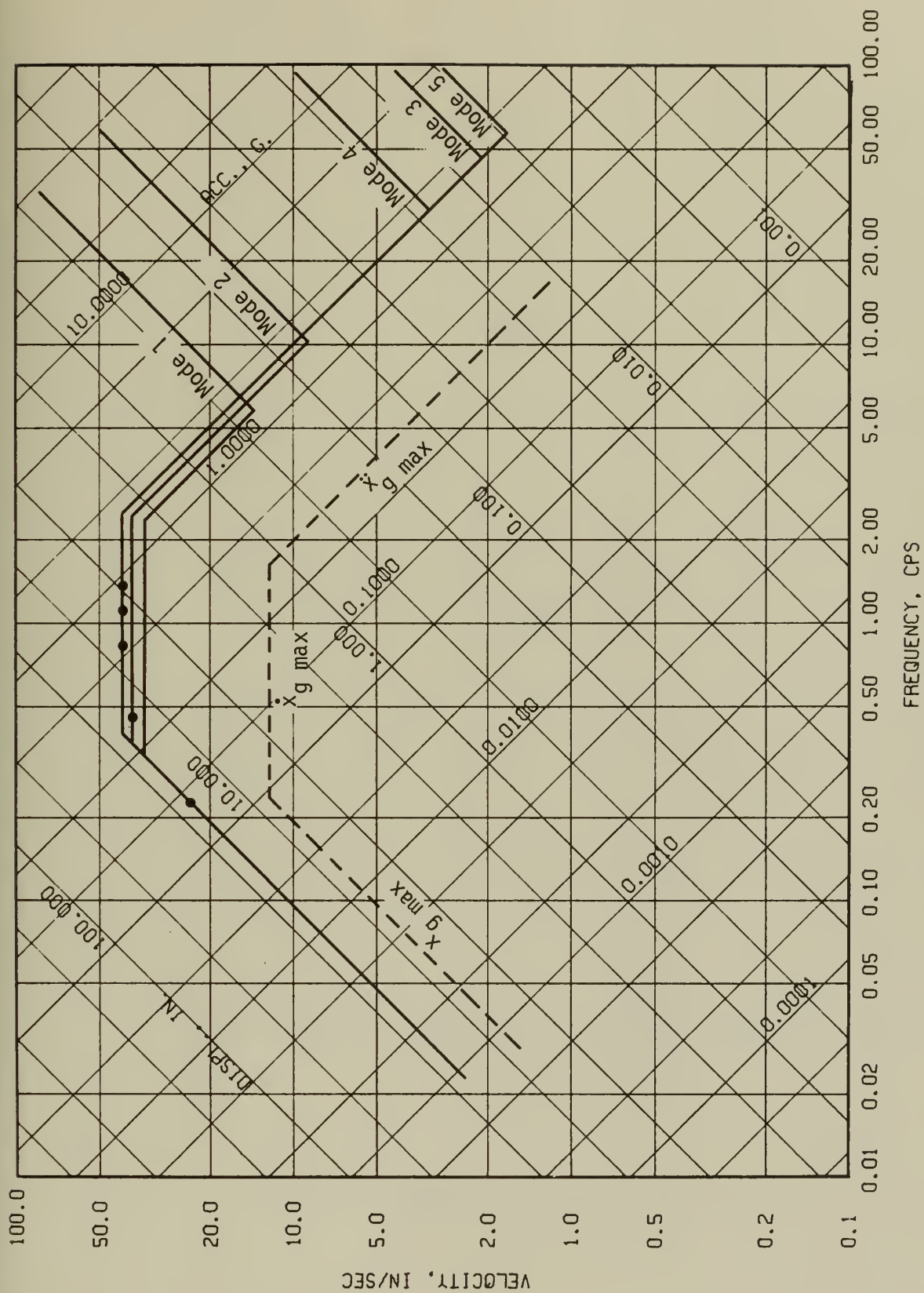


Fig. 4.2 Idealized Elastic Deformation Response Spectra for the First Five Modes of Tower C. $\beta_s = .01$ in Each Mode.

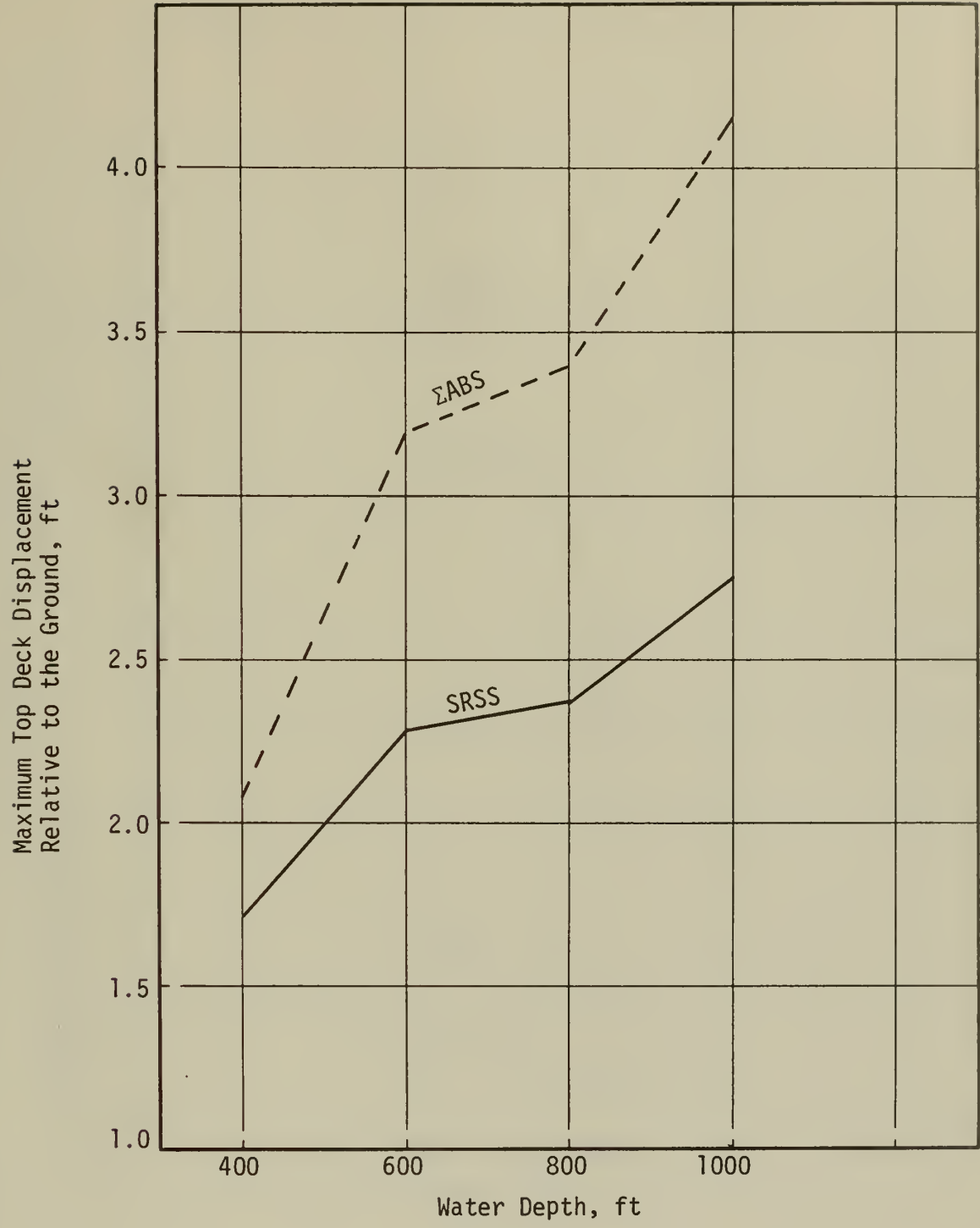


Fig. 4.3 Response of Towers A, B, C, and D Using Idealized Spectra

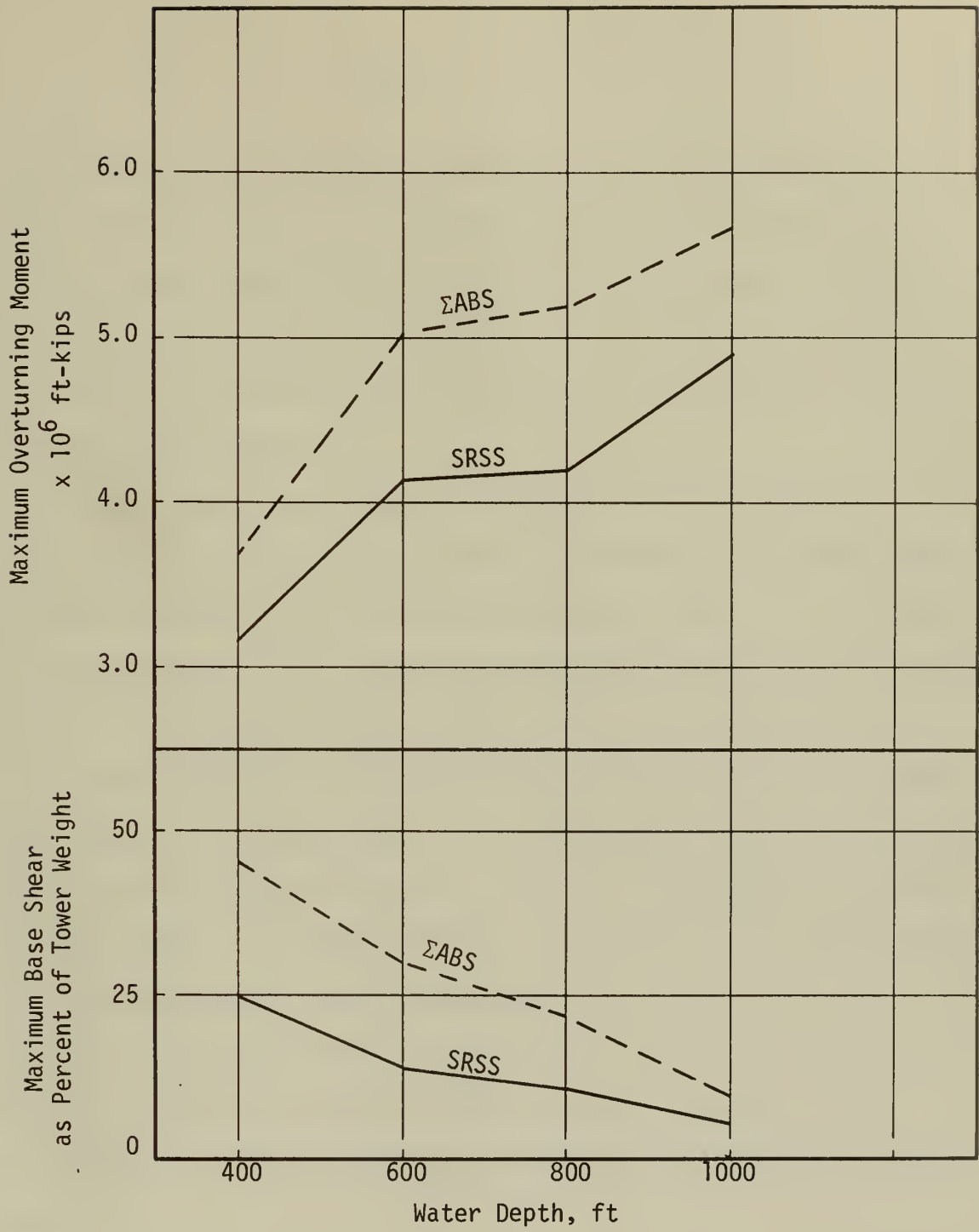


Fig. 4.3 (Continued)

VITA

Owen Major Kirkley was born on 30 March 1936 in Washington, D. C. He attended schools in Texarkana, Arkansas and graduated from Arkansas High School in 1953. After attending the Rice Institute for one year, he entered the United States Naval Academy. He graduated from the Naval Academy in 1958 with a Bachelor of Science degree and was commissioned an Ensign, Civil Engineer Corps, United States Navy.

Following a short tour of duty at the U.S. Naval Air Station, Quonset Point, Rhode Island, he entered Rensselaer Polytechnic Institute and graduated with a Bachelor of Civil Engineering degree in 1960. After serving tours of duty with the U.S. Naval Administrative Unit Annex, Thurmont, Maryland, U.S. Naval Mobile Construction Battalion ONE, and the U.S. Navy Public Works Center, San Diego, California, he entered the University of Illinois in 1967. He received a Master of Science degree in civil engineering from the University of Illinois in 1968, and then served tours of duty with the Officer in Charge of Construction, Republic of Vietnam, Saigon, Vietnam and at the Headquarters, Naval Facilities Engineering Command, Washington, D. C.

He is a registered Professional Engineer in the state of New York, is a member of the American Society of Civil Engineers, Tau Beta Pi, Chi Epsilon, Phi Kappa Phi, and Sigma Xi, and holds the rank of Commander, United States Navy.

7 AUG 73

S10493

Thesis
K516

Kirkley

Earthquake response
of fixed offshore struc-
tures.

142037

2 JUN 73
7 AUG 73

DISPLAY
S10493

Thesis
K516

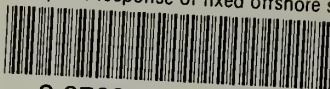
Kirkley

Earthquake response
of fixed offshore struc-
tures.

142037

thesK516

Earthquake response of fixed offshore st



3 2768 002 10912 6

DUDLEY KNOX LIBRARY